FGF signalling in the control of craniofacial and tracheal gland development

May, Alison Judith

Awarding institution:
King's College London

FGF Signalling in the Control of Craniofacial and Tracheal Gland Development

Alison Judith May

A thesis submitted for the degree of Doctor of Philosophy,
University of London

Department of Craniofacial Development and Stem Cell Biology,
King's College London, UK

Abstract

The submucosal glands (SMGs) of the respiratory system are specialized structures essential for maintaining airway homeostasis. The significance of SMGs is highlighted by their involvement in respiratory diseases such as cystic fibrosis and asthma, where their phenotype and function are severely altered. Uncovering the normal development of the airway SMGs is essential to elucidate their role in these disorders, however, very little is known about their morphogenesis.

To begin to understand the mechanisms involved in their arborisation, the development of the nasal SMGs was investigated, with glands being categorised into different subsets based on their locations and methods of development. We also used these heterogeneous nasal glands as a model to investigate the process of lumen formation within gland ducts.

Due to the imperative role of FGF signalling during the development of other branched structures, we investigated the role of *Fgf10* during the branching morphogenesis of the nasal SMGs. In the *Fgf10* null embryo, some nasal SMGs were absent while others showed normal duct elongation but defective branching, indicating that different glands require *Fgf10* for selective stages of development. Furthermore, certain SMGs present in the *Fgf10* homozygote were missing in the *Fgfr2b* mutant, suggesting compensation by another FGF ligand.

In *Fgf10* heterozygous mice the tracheal glands were reduced in size at an early age, with an altered A/P distribution of the SMGs postnatally, a deficit in glands that was not recovered in adults. The functional consequence of the reduction of SMGs in adult heterozygotes was investigated and showed that tracheal SMGs in *Fgf10* mutant mice produce less mucus. Considering this, we assessed the ability of mutant mice to respond to respiratory challenges. We also analysed the defective salivary gland phenotype of *Fgf10* heterozygotes and showed that gland dysplasia gave rise to a reduction in saliva output.

I would like to dedicate this work to all the women in science.
Be the Leslie Knope of whatever you do.

Acknowledgements

First and foremost, I would like to express my deepest appreciation for my supervisor Abigail Tucker. I cannot thank you enough for the guidance, patience and continuous fun we have had over the past three years. I know this is not the end of our scientific collaboration.

Secondly thank you to my second supervisor Alistair Noble. It was an absolute pleasure to work with you and learn so much about another area of science. Your teaching and advice are truly appreciated. I must also express my gratitude to Gordon Proctor, for being a supportive post-graduate coordinator and a great teacher.

Team Tucker! What can I say? It has been so wonderful working with you all. A special thank you to Hannah, Marcia and Neal for their constant help and training. Jen, we've had so many fun times and created amazing memories over these past few years. We made it! Also a big thank you to Cynthia Andoniadou, my number one science sister! Your motivation and support has been wonderful and I can't wait to call you when I start my own lab by 31! I am most grateful to everyone else in the Craniofacial Development and Stem Cell Department, past and present, who have helped me along the way. No matter how big or small your contribution to this work, it has been genuinely appreciated.

My incredible parents. Your unconditional love and support have made it that much easier for me to accomplish my goals and be determined to aim higher. Dad, thank you for always being there. I am so thankful to have someone like you in my life I can rely on no matter what the situation. Mum, my best friend and soul mate. Words cannot describe how you have inspired me. I have no idea where I would be without you. Peter, although I don't get to see you as much as I'd like, your support and encouragement have played a big role in my doctoral accomplishments.

Completing this work would have been all the more difficult were it not for the support and friendship of all the amazing people in Dublin and London. Cazz, you have been the greatest friend a girl could ever ask for. You have been my home here in this crazy city and your constant positive attitude has gotten me through many ups and downs. Thank you so much. Also my Dublin girls! Those late nights and weekends home kept me sane through all of the study.

Table of Contents

List of Figures

List of Tables

1.1 The Mammalian Respiratory System

1.1.1 Structure of the Mammalian Respiratory System

The vertebrate evolutionary transition from water to land moulded a highly complex, interconnecting closed network of organs designed for successful gas exchange. The mammalian respiratory system is made up of a conserved structure consisting of two types of airways: the respiratory airways (RAs), where gas exchange takes place and the conductive airways (CAs), which function in directing air to the RAs. The CAs of the system consist of the nasal and oral cavity, pharynx, larynx, trachea, bronchi, bronchioles and terminal bronchioles (Figure 1.1), while the RAs include the respiratory bronchioles, alveolar ducts and alveoli.

Cells of the body require oxygen from the external environment to produce adenosine triphosphate, the main currency of energy used in metabolic processes. Cellular respiration produces carbon dioxide, which is toxic in large amounts and needs to be expelled from our body. On average the resting human will inhale over 20,000 times a day, taking in over 12,000 litres of air on a daily basis (Rogers, 2007). Considering the composition of the external environment, with every breath, our body takes in a torrent of harmful inhalants and airway irritants (Seaton et al., 1995). Considering this, the soft tissues of our respiratory system are constantly exposed to the effects of the external environment and extremely susceptible to potential infection and damage.

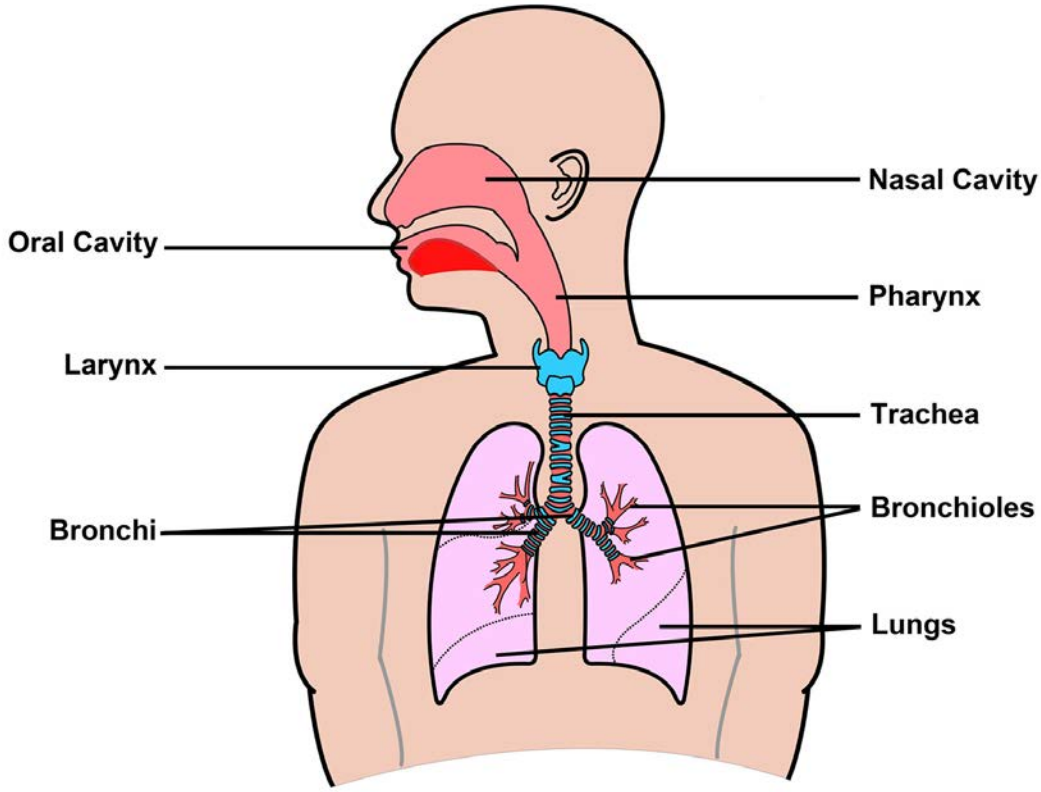

Figure 1.1 Structure of the human respiratory system outlining the conductive airways and the lungs.
The anterior respiratory system consists of both the nasal and oral cavities. It continues into the posterior region of the throat known as the pharynx, leading into the larynx, which additionally plays a role in sound production. The larynx also protects the anterior trachea, or windpipe, which is a long tube held open by C-shaped cartilage rings. The trachea bifurcates into the three-lobed right lung and the two-lobed left lung via two tubes known as the bronchi, which are also held open and protected by cartilage rings. Bronchi branch into an array of smaller tubes called the bronchioles, whose walls are devoid of cartilage. From here the system continues into respiratory airways (RAs) consisting of the respiratory bronchioles, alveolar ducts and small sacs of cells known as alveoli. It is in these RAs in which gas exchange takes place.

1.1.2 Protection of the Mammalian Respiratory System

Not only do the CAs function in directing air to the RAs, they are also required to warm, humidify and filter the air before it reaches the lungs. To carry out this function the walls of the CAs are lined with a specialized respiratory epithelium (RE). The RE is a pseudostratified columnar epithelium whose tight junctions between its epithelial cells render it ideal as a protective and immunological barrier (Xiao, 2013). All of the epithelial cells sit on a basement membrane, or basal lamina, which is a rich matrix sheet of proteins that acts as a structural support, as well as a communication medium for neighbouring epithelial cells (LeBleu et al., 2007). The apical epithelial cell surfaces of the RE are specialized with hair like projections known as cilia. These cilia move in synchronized beats in an anterior direction, moving airway mucus away from the lungs.

Airway mucus plays a vital role in maintaining airway homeostasis as it provides the first line of defence against airborne irritants in the nasal cavity, and is essential in the mucociliary process carried out in all of the CAs, ensuring no foreign particles reach the lungs. Not only does its thick consistency trap foreign particles; its protein constitution additionally contains bactericidal enzymes, hindering any risk of infection.

In humans, 5% of the respiratory mucus is secreted by goblet cells, which are glandular, simple columnar cells that are found scattered within the respiratory epithelium (Reid, 1960). The nucleus of these cells is found basally, while the apex of the cell is rich in mucin secretory granules (Freeman, 1962). The remaining 95% of the mucus secretion is released by the nasal and tracheal submucosal glands (SMGs) that lie in the underlying submucosal layer beneath the RE (Reid, 1960).

1.2 The SMGs of the Respiratory System

1.2.1 Temporal Localisation of the SMGs

The SMGs are hidden in the submucosal connective tissue running along the conductive airways. Nasal SMGs are organised into various named groups that are located in the medial and lateral nasal cavity walls (Grüneberg, 1971; Cuschieri and Bannister, 1974), while in the trachea, SMGs lie in the submucosal layer between the cartilage rings and smooth muscle (Finkbeiner, 1999). In the mouse, SMGS are found

in the upper trachea with the highest volume of tracheal glands found at the anterior boundary between the cricoid cartilage (CC) of the larynx and the first tracheal cartilage ring (C1) and extending no further than the sixth cartilaginous ring (C6) (Borthwick et al., 1999; Rawlins and Hogan, 2005). In humans these glands are also localised more uniformly in the anterior trachea, but are known to spread entirely through the tracheal tube all the way down to the submucosal layer of the bronchi (Sturgess and Imrie, 1982; Borthwick et al., 1999). In the mouse, nasal SMGs begin to develop on embryonic day (E) 12.5 with the appearance of the first lateral nasal gland (or Steno's gland) in the form of a single tube with all subgroups of nasal SMGs being reported to begin their development by E17.5 (Grüneberg, 1971; Michael et al., 1994). In mice, it has been reported that the tracheal SMGs first appear on postnatal day (P) 2 as initial gland buds that then undergo morphogenesis with all tracheal SMGs initiated by postnatal day P21 (Borthwick et al., 1999; Rawlins and Hogan, 2005).

1.2.2 Cellular Composition of the SMGs

The SMGs boast a typical tree-like structure common to all branched organs such as the mammalian lungs, kidney, mammary glands, lacrimal glands and salivary glands. Research has shown that tracheobronchial SMGs consist of three distinct domains in relation to the overlying RE: (A) the secretory region of the distal gland, (B) the medial collecting region and (C) the proximal ciliated duct (Meyrick et al., 1969; Wine and Joo, 2004)(Figure 1.2). The secretory region is made up of two main secretory cell types: serous cells and mucous cells. Glandular acini, "acinus" meaning "berry" in Latin, describes the cluster of serous secretory cells found at the distal gland that forms a closed off sac surrounding a central lumen (Meyrick and Reid, 1970)(Figure 1.2). These distal serous cells make up 61% of the overall secretory cell volume making it the primary defensive cell of the airway mucosa (Basbaum et al., 1990). Serous cells produce a watery solution primarily made up of mucins (MUC2, MUC7), proteoglycans and bactericidal proteins such as lactoferrin and lysozyme (Masson et al., 1966; Klockars and Reitamo, 1975; Finkbeiner, 1999). Serous tubules then lead into more proximal mucous tubules with mucous cells making up 39% of the remaining secretory gland volume (Basbaum et al., 1990) (Figure 1.2). Mucous cells produce a thick gel containing mucins MUC2 and MUC5 and antimicrobial peptide Cathelicidin (Finkbeiner, 1999). The protein consistency of mucus provides

ideal lubrication and acts as a chemical barrier to the exposed epithelium. The serum and mucus secreted by these specialized cells accumulates in a non-ciliated collecting duct and is then passed through a ciliated duct into the airway lumen (Figure 1.2). It is generally believed that mucus is expelled into the airway through the movement of the cilia within the ducts, however no concrete evidence indicates this is the case and it is suggested that the fluid is rather moved through a means of bulk flow (Ballard and Spadafora, 2007). Once secreted into the airway, mucus is swept away from the lungs to the pharynx by RE cilia movement where it is either swallowed and ingested, or is removed from the body by sneezing or coughing.

1.3 The SMGs and Airway Disease

The importance of SMG structure and function is increasingly emphasised as more and more evidence shows their involvement in an array of respiratory diseases. The most common hyper-secretory diseases in which SMGs play a role are cystic fibrosis, asthma and chronic bronchitis.

1.3.1 Cystic Fibrosis

Cystic Fibrosis (CF) (OMIM #219700) is an autosomal recessive disorder seriously affecting the respiratory system as well as the digestive system, due to the overproduction of mucus with a thick viscosity (Rowe et al., 2005). The prevalence of CF in the UK is approximately 1 in 2500 live births, with the highest international rate of 1 in 1461 live births found in the Republic of Ireland (Fitzgerald and Ryan, 2011). The major repercussion of CF is lung disease as high mucus concentration blocks the airways leading to inflammation, atelectasis, and chronic hypoxia (Fitzgerald and Ryan, 2011). Defective mucociliary clearance and the accumulation of thick mucus also provide an ideal moist environment for the proliferation of harmful bacteria, most commonly *Pseudomonas aeruginosa* and *Staphylococcus aureus,* which results in severe pulmonary infection (Oliver et al., 2000; Razvi et al., 2009).

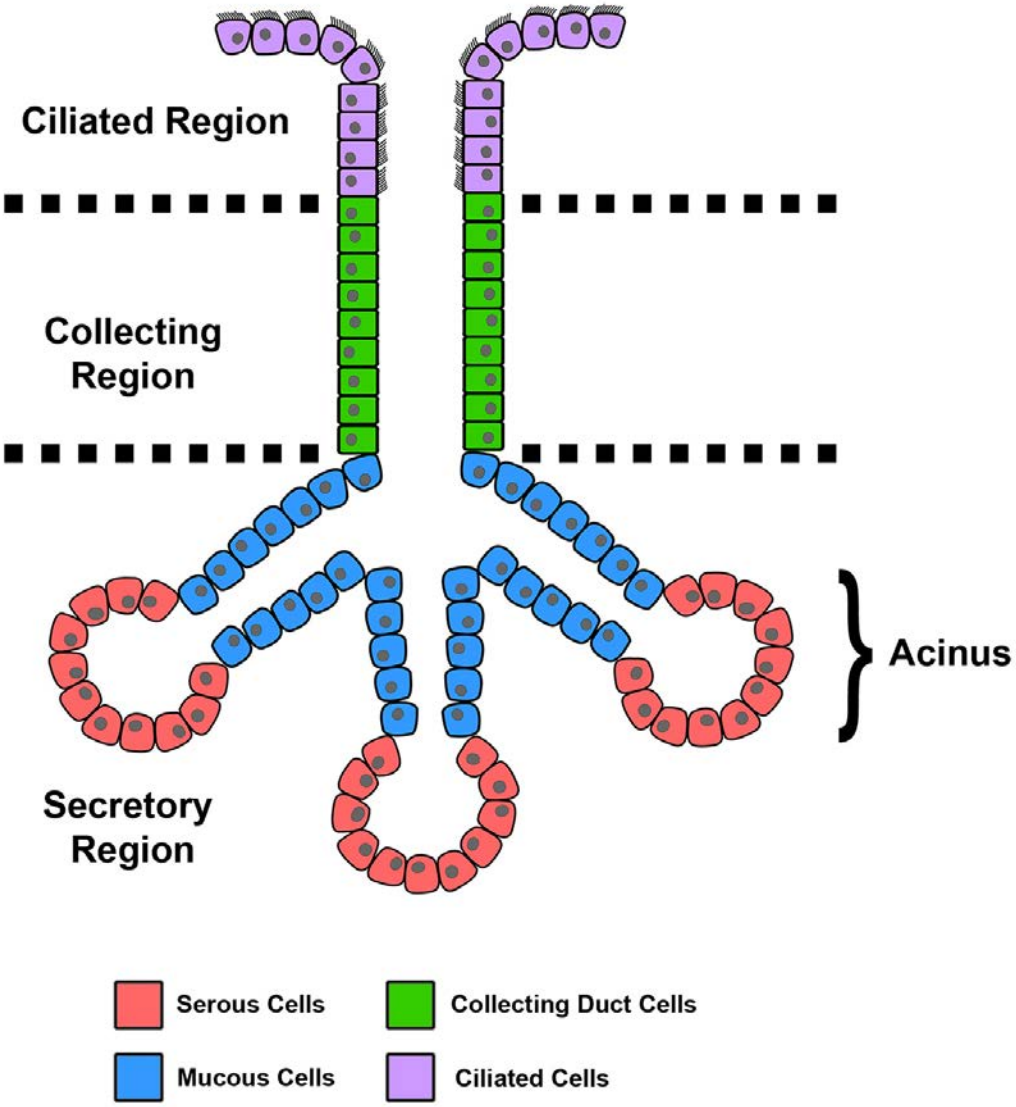

Figure 1.2 Schematic illustration outlining the cellular composition of the submucosal glands.
The distal glands are composed of closed sacs of serous cells, which form acini. These serous cells secrete a watery like secretion rich in bactericidal enzymes. Acini run into tubules of mucous cells, which secrete a thicker gel like substance rich in glycosylated proteins. These two types of secretions are then combined in a collecting duct, whose wall is composed of non-ciliated columnar epithelial cells. The collecting duct then runs into a ciliated duct made of more respiratory epithelial-like cells that possess beating cilia on their apical surfaces. Mucus is secreted through this ciliated duct into the airway lumen where it covers the surface epithelium.

The aetiology of CF lies in a defect of ion channels involved in mucus secretion. In 1989, extensive studies elucidated that one gene, cystic fibrosis transmembrane conductance regulator (*CFTR*) was the main culprit for the disease (Riordan et al., 1989; Kerem et al., 1989; Rommens et al., 1989). The *CFTR* gene is located on chromosome 7 and encodes for a 1480 amino acid CFTR protein (Riordan et al., 1989). In healthy individuals, the membrane bound CFTR protein acts as an ion channel, modulating the hydro-electrolytic flux and controlling osmotic gradients between epithelial cells and airway mucus (Vankeerberghen et al., 2002). In normal conditions, airway mucus is approximately 98% water (H_2O) (Wine and Joo, 2004). This is maintained by CFTR channels allowing the passage of negatively charged chloride ions (Cl^-) out of the epithelial cells into the overlying airway mucus. Following this, positively charged sodium ions (Na^+) follow and pass into the mucus via separate membrane bound sodium channels. This higher ion concentration in the overlying mucus causes the movement of H_2O through osmosis from the epithelial cell and surrounding tissues into the mucus. In sufferers of CF, the CFTR channels are permanently closed, blocking off translocation of Cl^- ions into the mucus. This causes epithelial cells to have a negative charge and leads to the movement of H_2O from the mucus into the epithelial cell, rendering airway mucus a lot thicker due to a severe decrease in water content. This thick mucus then coats the airways, as well as the pancreas and lumens of the digestive system, causing serious respiratory and digestive difficulties and increased susceptibility to bacterial infection.

The airway SMGs are the primary mucus-producing machines of the respiratory system. Engelhardt et al. (1992) showed that the serous cells, and a small percentage of cells of the collecting ducts of human SMGs of the bronchi are predominant sites of *CFTR* expression focusing interest on SMGs as culprits in the pathogenicity of CF. One of the earliest steps in CF pathophysiology is the occlusion and dilation of SMG ducts, evident in third trimester neonates with CF (Ornoy et al., 1987). Infants with CF then show early onset of hyperplasia and hypertrophy of SMGs (Oppenheimer and Esterly, 1975; Sturgess and Imrie, 1982). Later studies elucidated that the distribution of SMGs in two *CFTR*-deficient mouse models is abnormal, with glands extending more posteriorly in homozygous animals indicating that there is not only an ion channel/secretion defect but also suggesting a SMG developmental defect associated with CF (Borthwick et al., 1999).

1.3.2 Asthma

Asthma is a common inflammatory disease of the respiratory system that is characterized by periodic episodes of shortness of breath, wheezing and a recurrent cough. These responses are due to complex processes including airway hyper-responsiveness to irritants, inflammation and reversible structural changes to the airways referred to as "airway remodelling". Bronchoconstriction, the main cause of shortness of breath during an asthma attack, is brought about by airborne stimulants referred to as "asthma triggers". These triggers are irritants such as pollen, house dust mites, cigarette smoke and fungal spores. Upon inhalation, these triggers influence changes within the lower bronchiole tubes. The bronchioles of the respiratory system are not held open by cartilaginous rings unlike the more anterior trachea and bronchi and therefore their walls, made of smooth muscle, can freely change in diameter. This characteristic renders bronchioles susceptible to constriction, leading to breathing difficulties or asthma attacks.

In sensitized individuals, upon inhalation of asthma triggers, the irritants are detected by cell surface receptors of epithelial cells in the bronchioles. This detection stimulates both smooth muscle constriction and an immune response to tackle invasion of foreign stimuli. To date over 100 inflammatory mediators are known, including mast cells, T-cells and eosinophils (Barnes et al., 1998; Barnes, 2004). Constriction of bronchiole smooth muscle causes muscle cells to contract, tightening and decreasing the diameter of the bronchiole tubes. Additionally, the inflammatory response also reduces the size of the bronchiole lumen and thus significantly impairs the volume of air received by the lungs.

While investigation continues into smooth muscle activity and inflammation pathways involved in asthma, research has also begun to focus on the additional pathophysiological feature of mucus hyper-secretion. Increasing evidence shows that airways of asthmatic patients become blocked with mucus plugs, and that the consistency of this mucus changes, becoming more gel like and solidified (Sheehan et al., 1995; Rogers, 2004). Comparison of the mucus occupying ratio (MOR) of airways of asthma sufferers that died of severe asthma attack was significantly greater than the MOR of chronic asthma sufferers and control patients (Aikawa et al., 1992; Rogers, 2004). Goblet cell hyperplasia and an increase in goblet cell mucin stores

contribute to this influx in mucus secretion (Aikawa et al., 1992; Ordoñez et al., 2001). Furthermore, hyperplasia of the bronchial SMGs is a well defined feature of asthma airways with gland:bronchial wall area ratio being significantly increased in both chronic asthma sufferers and those that die of sudden attack, compared to control patients (Aikawa et al., 1992; Rogers, 2004).

1.3.3 Chronic Obstructive Pulmonary Disease

Chronic Obstructive Pulmonary Disease (COPD) is an umbrella term for a collection of airflow limitation respiratory diseases including chronic bronchitis, a disease of the airways, and emphysema, inflammation of the pulmonary parenchyma. It has been estimated to be the fifth-leading cause and the sixth leading cause of death in high-income and low-middle income countries, respectively (Mannino and Buist, 2007). Unlike asthma, COPD progresses slowly and airway obstruction and inflammation is usually irreversible (Barnes, 2004). Cigarette smoke is the most common and lethal COPD trigger, yet others include air pollutants, industrial toxins and chemicals (Baur et al., 2012).

In chronic bronchitis, inhalation and long-term exposure to COPD triggers lead to the inflammation and fibrosis of the bronchiole walls. Similarly to asthma this leads to the reduction of bronchiole diameter, dramatically reducing airflow. Additionally, within the airway lumens, accumulation of mucus leads to plugging, further reducing airflow to the lungs. In sufferers of chronic bronchitis, the bronchial SMGs are hypertrophic, displaying mucus hyper-secretion and an increase in mucous cells compared to serous cell counterparts (Reid, 1960; Rogers, 2008). This mucous:serous cell ratio imbalance leads to an altered protein consistency of the mucus released into the airway lumen and a significant increase in the MUC5A:MUC5B ratio (Rogers, 2004). While mucus plugs are easier to dislodge in patients of COPD compared to sufferers of asthma, mucus plugging and blockage can still lead to terminal infection and mortality (Prescott et al., 1995; Rogers, 2004). Chronic bronchitis sufferers also show an influx of neutrophils and macrophages in their bronchial SMGs (Saetta and Turato, 1997).

Considering the critical involvement of SMGs in the above respiratory conditions, little is known about the developmental and homeostatic mechanisms of the respiratory glands. In order to elucidate if a developmental defect occurs in sufferers

of disease, normal developmental signalling factors, modulators and pathways involved in SMG morphogenesis must be delineated.

1.4 Signalling in SMG Development

1.4.1 Wnt/β-catenin Signalling

The Wnt signalling pathway is an evolutionary conserved pathway, critical for controlling the development of an organism. Many developmental processes such as cell proliferation, migration, polarity and fate determination rely on the regulation of Wnt signalling (Komiya and Habas, 2008). A total of 19 Wnt ligands have been identified in humans and these can trigger one of two categories of Wnt transduction pathways, the canonical Wnt/β-catenin cascade, and the non-canonical Wnt/β-catenin-independent cascades, which include the Wnt/Planar Cell Polarity pathway and the Wnt/Calcium pathway. The former of these, the canonical Wnt signalling pathway, is the most studied and involves the binding of extracellular Wnt ligands to transmembrane bound Frizzled receptors. In the absence of Wnt ligand binding, cytoplasmic β-catenin is constantly broken down by the Axin complex (Figure 1.3, A). This protein compound consists of Axin, a scaffolding protein, glycogen synthase kinase 3 (GSK3), casein kinase 1 (CK1) and the *adenomatous polyposis coli* gene product (APC). Together, GSK3 and CK1 phosphorylate β-catenin, rendering it recognisable to the E3 ubiquitin ligase subunit β-Trcp (Liu et al., 2002; Davidson et al., 2005; Zeng et al., 2005). Subsequent ubiquitin of β-catenin occurs, followed by its proteosomal degradation (He et al., 2004) (Figure 1.3, A). This constant breakdown of β-catenin prevents it from translocating into the nucleus. Following Wnt-ligand binding to Frizzled, along with one of its co-receptors, low-density lipoprotein receptor related protein 5 (LRP5) or LRP6, Dishevelled (Dsh), another scaffolding protein, is recruited to the Frizzled receptor (Wallingford and Habas, 2005)(Figure 1.3). Dsh activation triggers LRP5/6 phosphorylation, which in turn leads to the recruitment of the Axin complex to the LRP receptor (Mao et al., 2001). This receptor binding to the Axin complex prevents the β-catenin inhibitory effects of these proteins, and thus β-catenin degradation (He et al., 2004). β-catenin now accumulates within the cytoplasm and translocates into the nucleus where it can activate Wnt-responsive genes, by regulating the function of specific transcription factors. The most studied nuclear mediators targeted by Wnt signalling belong to the lymphoid

enhancer factor 1/T-cell factor (LEF-1/TCF) family (Eastman and Grosschedl, 1999; Arce et al., 2006).

Using the *Lef1* -/- mouse to study the biological role of this gene, it was shown that knockout mice failed to develop organs such as teeth, hair follicles and mammary glands (van Genderen et al., 1994). As these organs require epithelial-mesenchymal interactions similar to developing SMGs, it was hypothesised that Wnt/β-catenin activity may be involved in the development of the nasal SMGs. Using the β-catenin/Tcf-βgal reporter (TOPGAL) mouse, it has been shown that the canonical Wnt pathway is active during early nasal gland bud formation (Driskell et al., 2007). Additionally, the transcription factor *Lef1*, has been shown to be highly expressed in progenitor cells of early SMG buds in the mouse nose and trachea, and the ferret trachea, and in *Lef1* knockout mice amorphous aggregates of cells develop where nasal SMGs are seen in wildtypes (Duan et al., 1998, 1999; Driskell et al., 2004). *Lef1* promoter expression has been shown to be regulated by the Wnt3-a ligand during SMG morphogenesis, and in the Wnt3-a knockout mouse, SMG *Lef1* expression was lost and cell proliferation of epithelial gland cells was reduced in SMG buds (Driskell et al., 2007). While these studies have given insight into the necessity of Wnt signalling for early SMG bud formation, the involvement of Wnt molecules in later stages of respiratory gland development has not been investigated.

1.4.2 Bone Morphogenetic Protein Signalling

The bone morphogenetic proteins (BMPs) belong to the transforming growth factor β (TGFβ) superfamily (Miyazono et al., 2010). The BMPs play a multitude of roles during early embryonic patterning and morphogenesis such as the regulation of cell proliferation, differentiation, apoptosis and cell-fate determinations (Hogan, 1996; Kishigami and Mishina, 2005). Twenty BMPs have been identified, all having heterogeneous functions during developmental processes such as neurogenesis, bone and cartilage formation, and organogenesis (Hogan, 1996; Zhao, 2003).

In general, the BMP pathway involves the extracellular BMP ligands binding to the cell membrane bound BMP receptors (BMPR). These receptors are serine-threonine kinase receptors that belong to two groups, Type I and Type II (Massagué et al., 1994). BMPs bind to the Type I BMPR with higher affinity to that of Type II (Wrana

et al., 1994; Kirsch et al., 2000). In order for ligand binding to stimulate an intracellular signal, heterodimerization of one Type I and one Type II BMPR is required (Figure 1.4). Upon BMP ligand binding to the Type I receptor, the Type II receptor is recruited (Kirsch et al., 2000; Carreira et al., 2014). The Type II BMPR then catalyses the phosphorylation of the intracellular serine-threonine domain of the Type 1 BMPR, recruiting a cytoplasmic receptor-activated Smad protein (either Smad1, 5 or 8). (Wrana et al., 1994). Phosphorylation of one of these Smads triggers the recruitment of another cytoplasmic Smad, Smad4 (Whitman, 1998). This dimeric Smad complex can now translocate into the nucleus where BMP target genes can be activated. A number of extracellular antagonists also function in regulating the pathway. These include such soluble proteins as Noggin, Gremlin and Chordin, which form complexes with BMP ligands, preventing them from binding to their cell receptors (Yanagita, 2005; Walsh et al., 2010).

It has been previously shown that BMP signalling is critical for the development and patterning of the trachea and lungs (Weaver et al., 1999; Eblaghie et al., 2006; Li et al., 2008). The only investigation into the roles of BMP signalling in respiratory gland development have been shown during that of the tracheal SMGs (Rawlins and Hogan, 2005). Using the *Bmp4*^{lacz} reporter mouse, it was reported that at P2 when tracheal buds were initiating from the respiratory epithelium, *Bmp4* was expressed throughout the underlying mesenchyme. During later development at P7, *Bmp4* detection was reduced and found only in the mesenchyme close to the newly formed gland branches (Rawlins and Hogan, 2005). By P28, *Bmp4* expression had reduced even further, and was only detected in a few mesenchymal cells (Rawlins and Hogan, 2005).

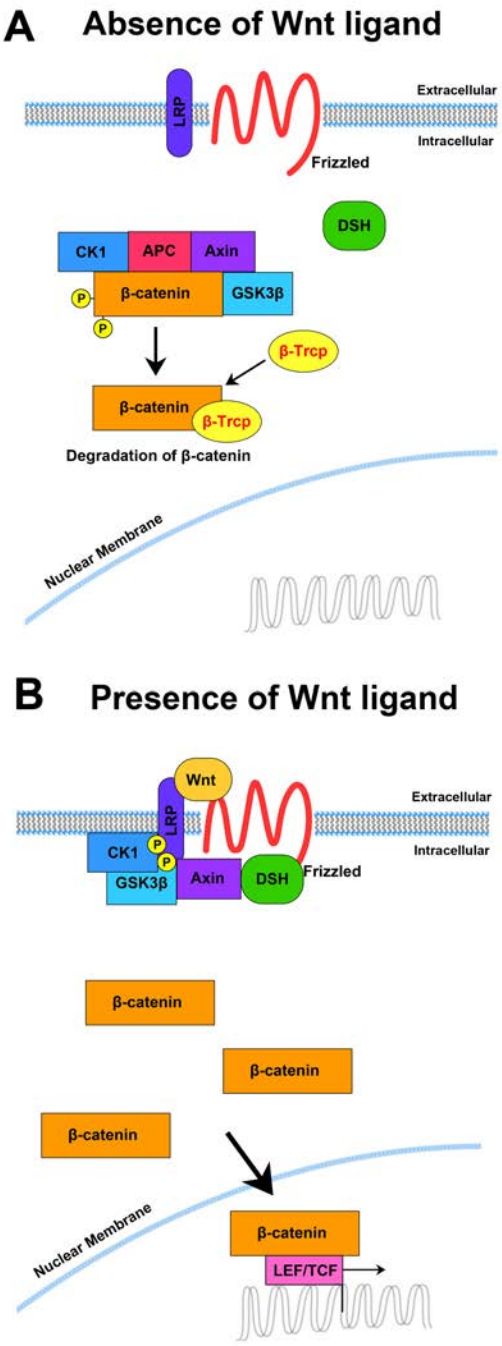

Figure 1.3 The canonical Wnt/β-catenin pathway.
(A) In the absence of Wnt ligand binding to the membrane bound Frizzled receptor and its co-receptor LRP5/6, the Axin complex binds to cytoplasmic β-catenin. This binding leads to the phosphorylation of β-catenin by CK1 and GSK3β, leading to the degradation of β-catenin, and preventing its translocation into the nucleus. (B) Upon extracellular Wnt ligand binding, a Frizzled-LRP receptor complex is formed, leading to the recruitment of Dsh by Frizzled. This phosphorylates LRP5/6, which triggers Axin recruitment to the receptor complex. Recruitment of Axin inhibits the phosphorylation of β-catenin by the Axin complex, and thus prevents its degradation. β-catenin now accumulates within the cell and translocates into the nucleus where it regulates activation of LEF/TCP transcription factors and Wnt-responsive genes, required for developmental processes.

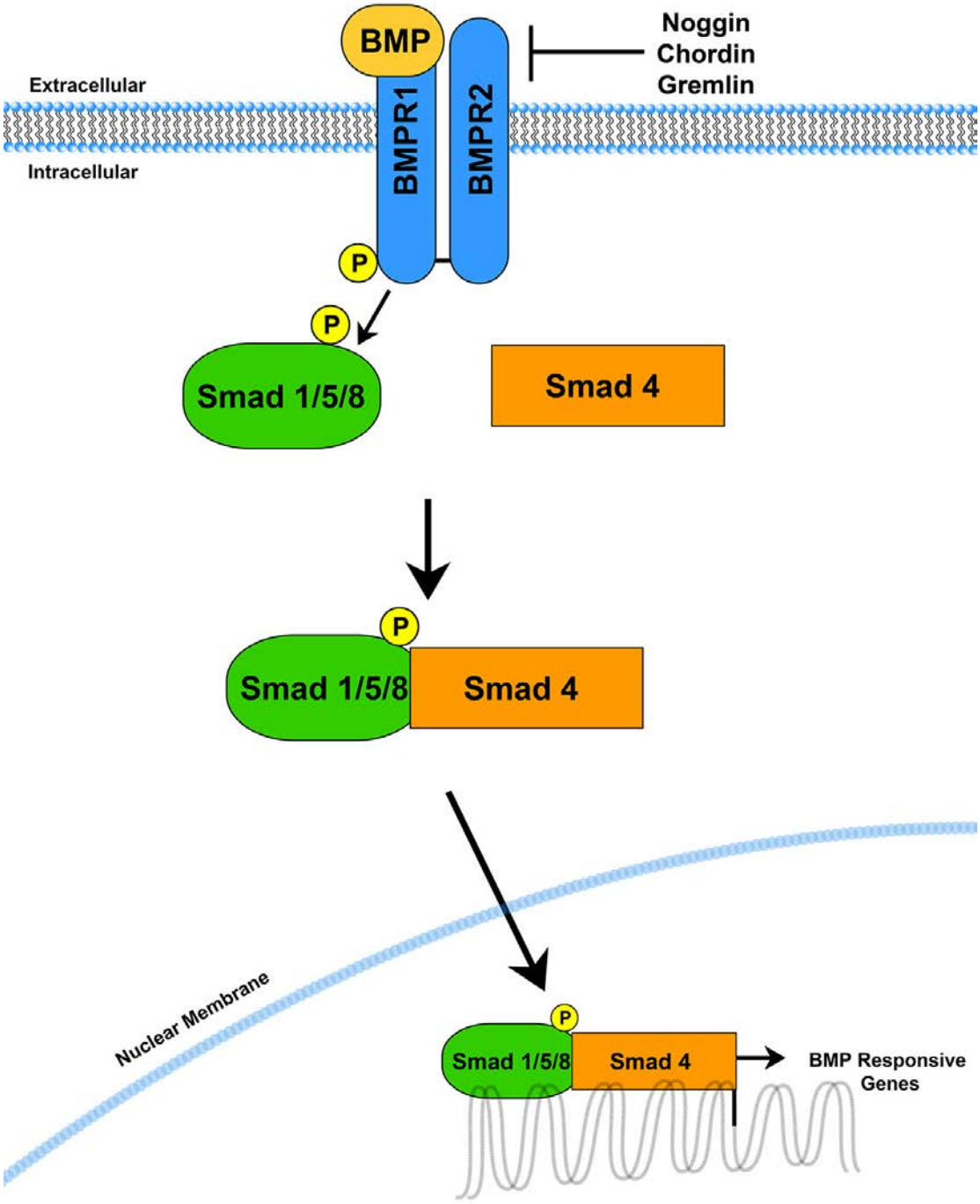

Figure 1.4 The BMP signalling pathway.
Extracellular BMP ligand binding to the transmembrane BMP receptors Type I and Type II. Phosphorylation of the Type I receptor by the Type II BMPR leads to the intracellular activation of Smad1, 5 or 8. This Smad protein will then phosphorylate Smad4, where they can enter the nucleus as a dimeric complex and activate BMP response elements.

1.4.3 Ectodysplasin A Signalling

The role of the Ectodysplasin A (EDA) pathway has been investigated in the development of a number of ectodermal derived organs. Signalling through this pathway involves the binding of EDA A1, a member of the tumor necrosis factor (TNF) family, to a death domain transmembrane receptor, EDAR (Srivastava et al., 1997; Headon and Overbeek, 1999). EDA ligand binding to EDAR leads to the recruitment of the intracellular adaptor protein EDAR Associated Death Domain (EDARADD). Recruitment of EDARADD to the receptor leads to the formation of a complex containing the cytoplasmic proteins TNF Receptor Associated Factor 6 (TRAF6), TGF-β Activated Kinase 1 (TAK1) and TAK Binding Protein 2 (TAB2) (Morlon et al., 2005). This leads to the activation of the IκB kinase complex (IKK), which is a compound of two kinase sub-units, IKK1 and IKK2, as well as the regulatory component NF-kappaB essential modulator (NEMO) (Döffinger et al., 2001; Morlon et al., 2005). Activation of the IKK complex triggers recruitment and the phosphorylation of inhibitor kappa-B (IκB), a nuclear factor-kappaB (NFκB) inhibitor. Phosphorylation of IkB leads to its degradation, and NFκB translocates into the nucleus where it acts as a transcription factor, regulating target genes involved in cell proliferation, differentiation and survival (Gilmore, 2006; Oeckinghaus and Ghosh, 2009).

Requirement for the EDA signalling pathway in both nasal gland and tracheal SMG development has been investigated (Grüneberg, 1971; Rawlins and Hogan, 2005). Interestingly, analysis of the *Tabby* mouse, the knockout model of the gene required for *Eda*, showed that specific groups of the anterior nasal glands were completely absent while others developed normally (Grüneberg, 1971). In another study, *Edar* expression was seen within the tracheal epithelium at early stages of tracheal SMG development at P4 (Rawlins and Hogan, 2005). Tracheal SMGs were also completely absent in the adult *Tabby* mouse, as well as in the early *Edaradd* knockout at P7, indicating that EDA signalling is required for early SMG initiation and budding (Rawlins and Hogan, 2005). Human patients with mutations in EDA, EDAR or EDARADD suffer from the disorder hypohidrotic ectodermal dysplasia (HED), which gives rise to developmental defects in teeth, hair, salivary glands and, in keeping with the mouse data above, develop problems associated with the respiratory glands of the upper and lower airways (Smythe et al., 2000).

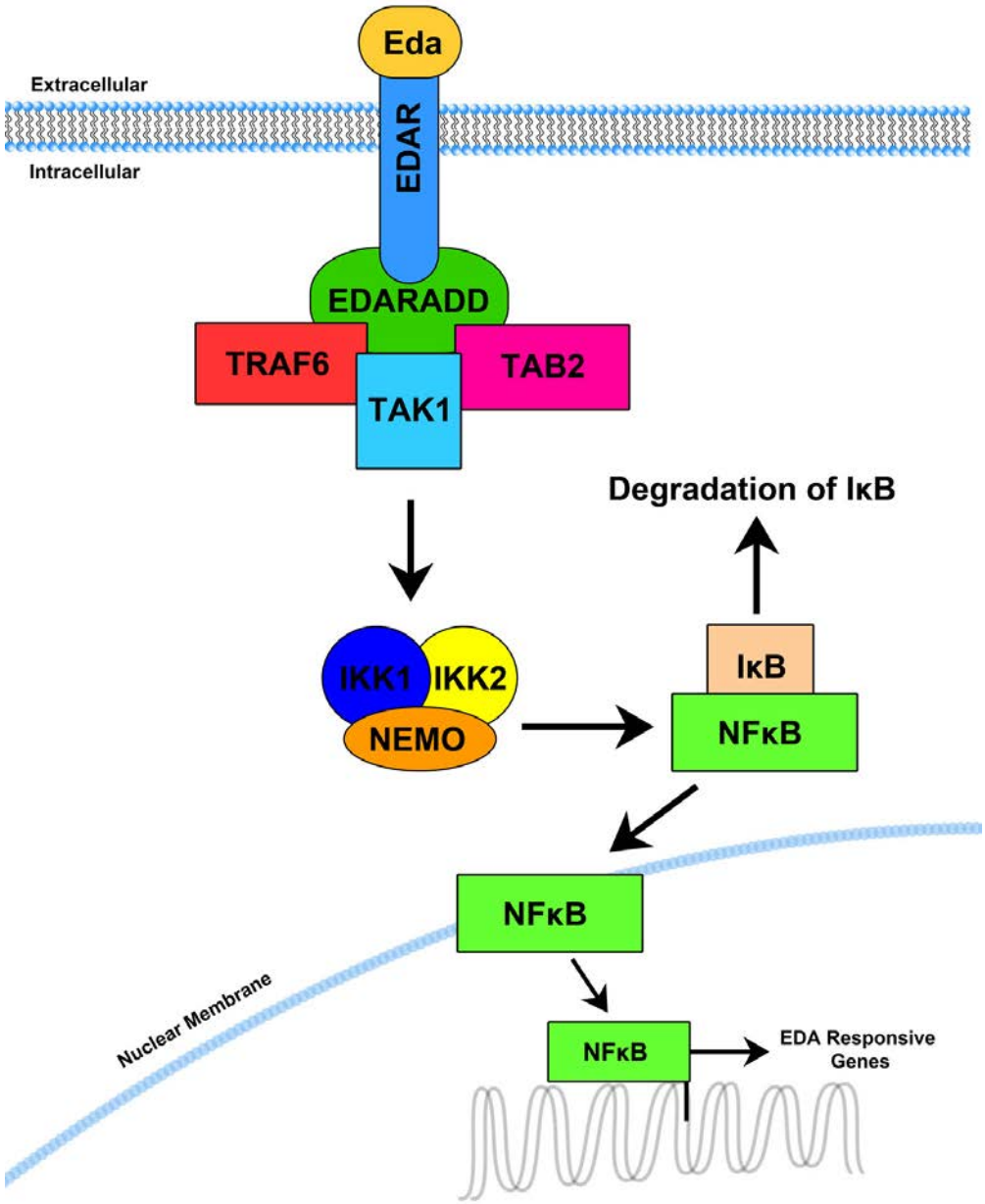

Figure 1.5 The Ectodysplasin A signalling pathway.
EDA ligand binding to its transmembrane receptor EDAR recruits EDARADD and a TRAF6-TAK1-TAB2 complex is formed. This complex activates the IKK complex containing kinases IKK1, IKK2 and NEMO. The IKK complex recruits and phosphorylates IκB, leading to its degradation. The inhibitory function of IκB is now diminished and NF-κB can translocate in to the nucleus where it functions as a transcription factor, targeting genes involved in a multitude of developmental processes.

1.4.4 Fibroblast Growth Factor (FGF) Signalling

Rawlins & Hogan (2005) established that in *Fgf10* heterozygous (+/-) mice at P20 fewer tracheal SMGs had developed. Of the glands that did develop, they were only located anteriorly by the CC and C1 and had not undergone full branching while no glands were seen between the more posterior cartilaginous rings (Rawlins and Hogan, 2005). The exact role of *Fgf10* however, or other *Fgfs,* during nasal and tracheal SMG development has not been elucidated. Considering this, the work of this thesis has focused on uncovering the role of FGF signalling in the early patterning of the respiratory SMGs.

1.5 FGF Family of Signalling Factors

1.5.1 FGF Ligands

FGFs make up one of the largest family of polypeptide proteins critical for tissue patterning and development. As the brain is a rich source of fibroblasts, the first FGFs (FGF1 and FGF2) were discovered as bovine pituitary cell mitogens (Gospodarowicz, 1975). Today, 22 members (FGF1-FGF22) of the FGF family are known within the human genome (Ornitz and Itoh, 2001). Despite their sequence similarities to other FGF ligands, FGF11-FGF14 however, do not bind to fibroblast growth factor receptors, so therefore are not considered as true FGF ligands (Olsen et al., 2003). The genomic locations of each *FGF* gene varies, with the exception of *FGF3, FGF4* and *FGF19* which are found linked on chromosome 11 in humans and chromosome 7 in mice (Ornitz and Itoh, 2001). The length of the coding sequences in all human *FGF* genes also varies from 5kb (in *FGF3* and *FGF4)* to 100 kb (*FGF12*) (Ornitz and Itoh, 2001). These diverse structures allow FGFs to play differential roles during both embryonic development and adult tissue homeostasis. During embryonic organogenesis, FGFs are critical for cell processes such as proliferation, differentiation and migration (Tsuboi et al., 1990; Sun et al., 1999; Lanner and Rossant, 2010), with FGF signalling being imperative for normal craniofacial development (Stanier and Pauws, 2012) as well as limb and lung morphogenesis (Min et al., 1998; Sekine et al., 1999). In adults, the roles of FGFs are highlighted in wound healing processes, nervous system maintenance and tissue repair (Werner, 1998; Barrientos et al., 2008).

1.5.2 FGF Receptors

Four cell membrane-bound FGF receptors (FGFRs) have been identified in vertebrates, each having different affinities for different FGF ligands. The four receptors, FGFR1-FGFR4, are composed of the common protein structure of most tyrosine kinase receptors (Johnson et al., 1990). This structure can be divided into three core areas referred to as (A) the extracellular domain, (B) the transmembrane domain and (C) the intracellular domain (Figure 1.6). The extracellular region of the receptor acts as the ligand-binding area and is comprised of three immunoglobulin-like domains (IgI-III) (Lee et al., 1989). The IG superfamily of proteins is one of the largest found in the human genome and one of the most important in protein interactions. These domains are so called as they share a common 70-100 amino-acid complex with immunoglobulins (Barclay, 2003). Furthermore, a region of acidic amino acids is located between IgI and IgII, which is known as the "acid box" (Figure 1.6). This acidic stretch is hypothesised to play a role in auto-inhibition of the FGF receptor (Kalinina et al., 2012). The single-span region of the receptor within the plasma membrane is known as the Transmembrane Domain (TM) and aids in receptor dimerization stability upon ligand binding (Li and Hristova, 2010). The intracellular domain of the receptor, found within the cell, is the signal transducing area of the receptor. It is composed of tyrosine kinase domains (TKs) with a carboxyl–terminal tail, and upon receptor dimerization, this tail is phosphorylated and intracellular signalling pathways are triggered.

Through mRNA alternative splicing processes, splice variants of the FGFRs are formed (Figure 1.7). The presence of an alternatively spliced exon within the IgIII domain of the receptor gives rise to one of three potential receptor isoforms; IIIa, IIIb or IIIc (Yayon et al., 1992; Miki et al., 1992) (Figure 1.7). This only occurs in FGFR1-FGFR3, as it has been demonstrated that only the IIIc isoform occurs in FGFR4 (Vainikka et al., 1992). This mechanism allows a single gene to give rise to alternative isoforms of a receptor, rendering the receptors promiscuous for ligand affinities (Ornitz et al., 1996). For example, in the case of FGFR2 (Figure 1.7), the splice variant IIIb binds to FGF3, FGF7 and FGF10 with high affinity, while the IIIc receptor binds to FGF2, FGF4, FGF6, FGF8 and FGF9 (Ornitz et al., 1996). Not only do these two receptor isoforms display different ligand affinities, they also differ in their tissue expression patterns with FGFR2IIIb (FGFR2b) found primarily in

epithelium and FGFR2IIIc (FGFR2c) in mesenchymal cells (Peters et al., 1992; Orr-Urtreger et al., 1993). Therefore alternative sequences of FGFRs and their isoforms, along with differential sequences of FGF ligands, create a repertoire of ligand-receptor binding specificities.

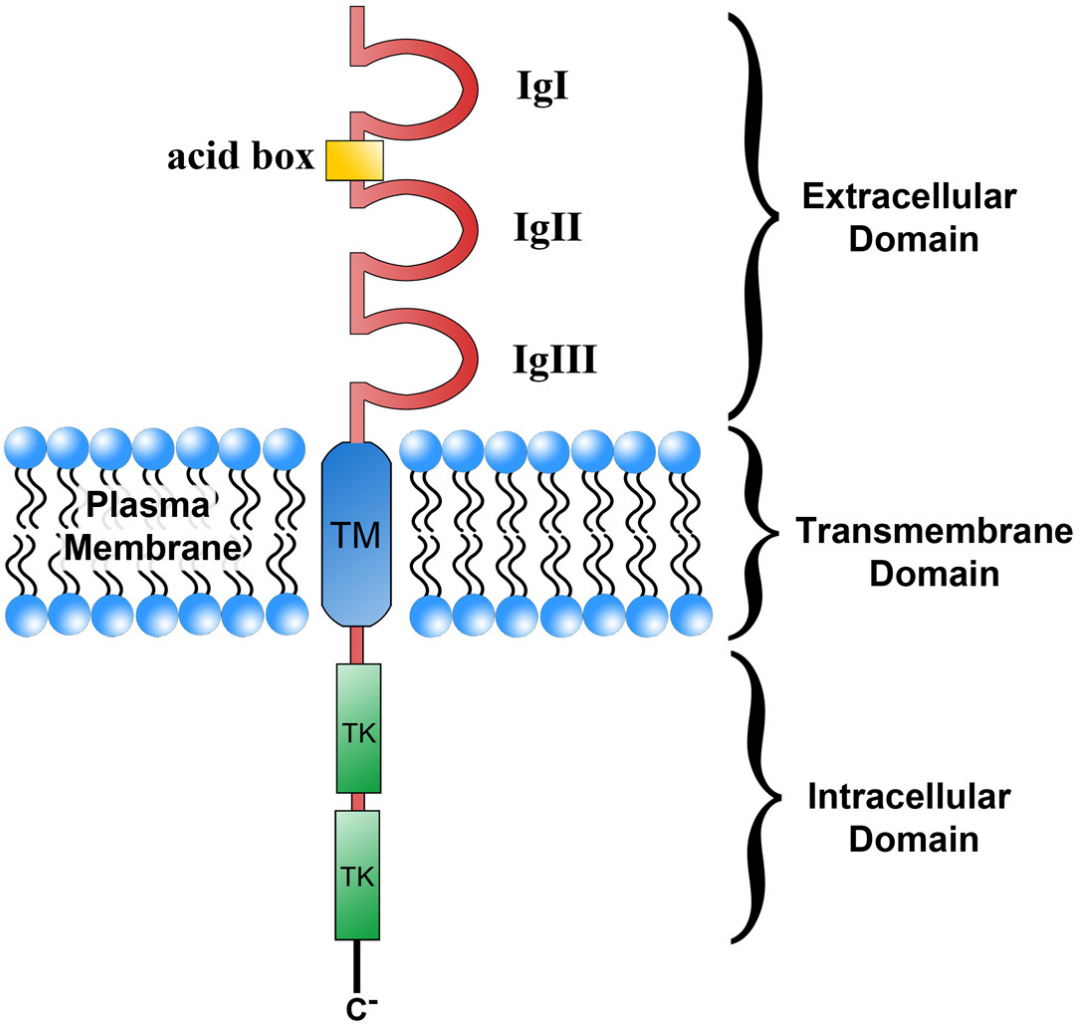

Figure 1.6 The general structure of FGFRs.
The membrane bound FGFRs have a conserved protein structure similar to that of all tyrosine kinase receptors. The extracellular domain consists of three immunoglobulin-like domains (IgI, IgII and IgIII). Between IgI and IgII lies a stretch of 8-amino acids known as the "acid box". The region of the receptor that is found within the plasma membrane is known as the Transmembrane Domain (TM). The intracellular domain found within the cytosol consists of two split tyrosine kinase domains (TK) and a carboxyl-terminal tail (C^-). It is this tail that undergoes phosphorylation upon ligand-receptor binding and an intracellular cascade is triggered.

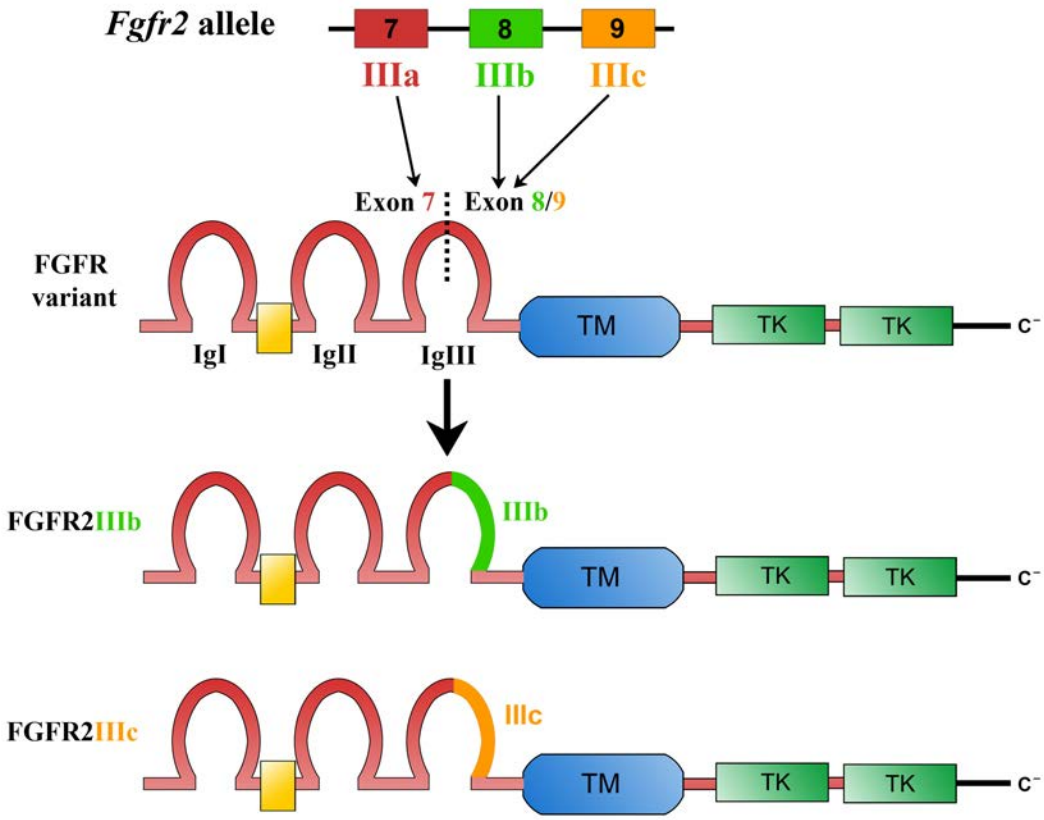

Figure 1.7 Generation of FGFR2 splice variants by alternative splicing.
Different FGFR isoforms are generated by alternative splicing mechanisms. Alternative usage and interpretation of exon 8 and exon 9 of the *Fgfr2* allele into the IgIII of FGFR2 generates either the IIIb or IIIc isoform respectively.

1.5.3 FGF Intracellular Signalling Pathway

The initiation of an intracellular signalling transduction pathway relies on extracellular binding of ligands to the receptor. FGFs are referred to as monomeric growth factors, meaning each ligand can only bind to one receptor (Spivak-Kroizman et al., 1994). FGF signalling, similar to all TK activated pathways, requires dimerization of two receptors, therefore two monomeric FGF ligands are recruited, with one ligand binding with high affinity to both the IgII and IgIII domains of the extracellular region of each FGFR (Schlessinger, 2000)(Figure 1.8). FGF proteins do however contain two binding sites, allowing for binding to their high affinity receptor as well as a cell surface Heparan Sulphate Proteoglycan (HSPG) molecule (Pye and Gallagher, 1999)(Figure 1.8). This additional binding to HSPG causes a conformational change within the FGF protein, allowing it to bind stably to its FGFR and facilitates receptor dimerization (Spivak-Kroizman et al., 1994; Faham et al., 1996; Loo et al., 2001).

Receptor dimerization then leads to the intracellular phosphorylation of the TK domains of each FGFR (Schlessinger, 1988; Jiang and Hunter, 1999). Following TK phosphorylation, a number of intracellular signalling cascades are triggered that are required for a multitude of developmental processes (Figure 1.8). These include the phospholipase C gamma (PLC-ϒ) pathway which initiates calcium release and activates protein kinase C to influence cell motility (Burgess et al., 1990; Mohammadi et al., 1991), and the phosphatidylinositol-3 kinase (PI3K) which activates Akt/protein kinase B needed for the mediation of cell survival (Ong et al., 2001)(Figure 1.8, B). The most common route of FGF signalling during developmental processes is through the activation of the rat sarcoma homologue (RAS)/mitogen-activated protein kinase (MAPK) cascade. This pathway functions in activating target genes involved in cellular differentiation and proliferation (Figure 1.8, B).

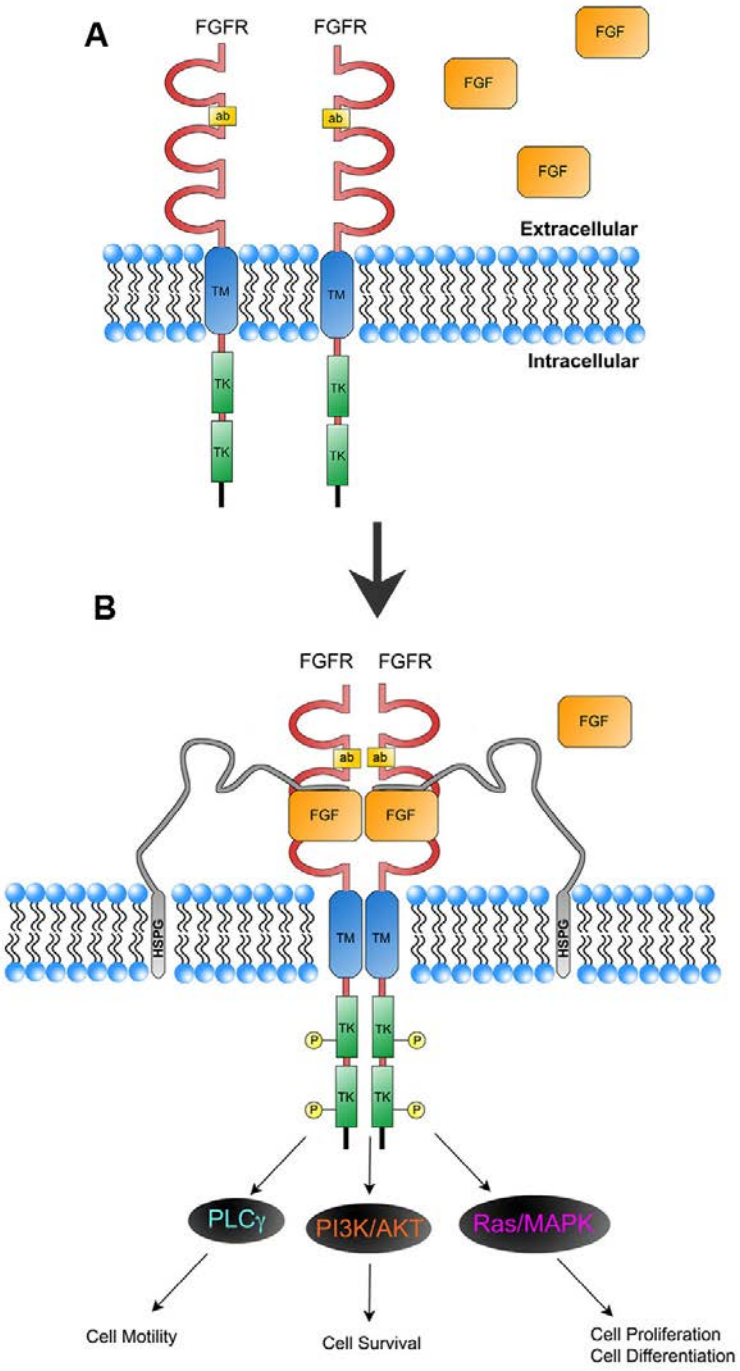

Figure 1.8 FGFR receptor dimerization and activation of intracellular pathways. (A) Receptors exist singly within the cell membrane in their inactive form before binding with extracellular FGF ligands (orange). (B) Two FGF ligand molecules are required to bind to two cell membrane bound FGF receptors for successful FGFR dimerization. Binding with cell surface HSPG is also critical for successful dimerization and signalling. Upon ligand binding tyrosine kinase domains (TK) are activated within the cytosol, which triggers the onset of intracellular pathways such as PLCγ, PI3K/AKT and Ras/MAPK.

1.5.4 The Ras/MAPK Pathway

Considering the various structures and form of FGF ligands, FGF receptors and the diverse pathways triggered by FGF signalling, the story of the FGFs is a complex one. For the sake of this study, investigation was focused primarily on the Ras/MAPK pathway and the role of this cascade during SMG development. Following FGFR dimerization and auto-phosphorylation of its TK domains, the lipid-anchored docking protein FGFR Substrate-2 (FRS2) is phosphorylated and its tyrosine phosphorylation sites bind to the adapter protein Growth Factor Receptor Bound Protein 2 (Grb2) (Kouhara et al., 1997) (Figure 1.9). The binding of Grb2 to the FRS2 and the RTK recruits Son of Sevenless (SOS), a guanine nucleotide exchange factor, to the cell membrane which then binds to Grb2 forming a complex (Pierre et al., 2011). The location of this complex allows it to activate the cell membrane bound G-protein Ras. In its inactive state Ras is bound to the nucleotide guanosine diphosphate (GDP). When bound to SOS, GDP is exchanged with guanosine triphosphate (GTP), which then activates Ras (Figure 1.9). The activated GTP bound Ras then recruits effector proteins to the cell membrane, in particular Raf, a protein kinase usually found in the cytosol (Leevers et al., 1994) (Figure 1.9). This recruitment phosphorylates and activates Raf, which in turn phosphorylates the MAPK kinase MEK (MEK1/MEK2) on its serine and threonine residues (Crews et al., 1992; Leevers et al., 1994; Gardner et al., 1994). MEK kinase then phosphorylates MAPKs such as extracellular signal-regulated protein kinases (ERKs)(Figure 1.9). Following activation, ERKs translocate into the nucleus and activate target transcription factors such as PEA3 and ERM, which belong to the E-twenty-six (ETS) family of transcription factors (Wasylyk et al., 1998; Yordy and Muise-Helmericks, 2000) (Figure 1.9). These are required to mediate cell differentiation, mitogenesis and proliferation.

1.5.5 Downstream Targets of the MAPK Pathway

Members of the ETS domain transcription factor family all contain a conserved sequence within their DNA-binding domain. This ETS domain is a winged helix-turn-helix structure that binds to target DNA motifs with a central 5'-GGA(A/T)-3' sequence (Watson et al., 1988; Sharrocks et al., 1997). Conserved sequences within the remaining amino acid domains of each ETS family member also arise and based on these similarities, ETS proteins are categorised into subfamilies. For example, the PEA3 (polyoma enhancer activator 3) subfamily contains three ETS-domain

transcription factors, ETV1, PEA3 (or ETV4) and ERM (or ETV5). The three PEA3 family transcription factors are almost 50% identical in their overall structure, with 95% identity in the ETS-domain (*reviewed in* de Launoit et al. 1997). Extensive studies have shown that the PEA3 group of ETS domain transcription factors are targets of MAPK signalling and are involved in Ras-induced cell transformation processes (Janknecht, 1996; Wasylyk et al., 1998; Yordy and Muise-Helmericks, 2000). Due to this function, the ETS domain transcription factors are critical for cell proliferation and differentiation mechanisms in a multitude of tissue types during embryonic development (Chotteau-Lelièvre et al., 1997; Remy and Baltzinger, 2000; Paratore et al., 2002; Chotteau-Lelievre et al., 2003).

1.5.6 Modulators of the MAPK Pathway

Being a complex pathway, there are also a number of modulators of FGF signalling that work through feedback loops to tightly regulate activity. Evolutionary conserved Sprouty (Spry) is both induced by and inhibits the Ras/MAPK pathway involved in FGF signalling. With four members in mammals (Dikic and Giordano, 2003), it has been identified that SPRY can antagonize the pathway in one of two ways. Firstly, SPRY1 and SPRY2 can bind to Grb2 preventing its phosphorylation of SOS and subsequent activation of Ras (Hanafusa et al., 2002)(Figure 1.9). Secondly, SPRY2 and SPRY4 can also inactivate the pathway further downstream by binding to Raf and preventing MAPK activation (Yusoff et al., 2002; Sasaki et al., 2003)(Figure 1.9). Other attenuators of the pathway have also been identified such as *Sef* in zebrafish (Fürthauer et al., 2002) and nuclear *map kinase phosphate* 1 (MKP1) and cytoplasmic MKP3 in zebrafish and chick (*reviewed in* Tsang & Dawid 2004).

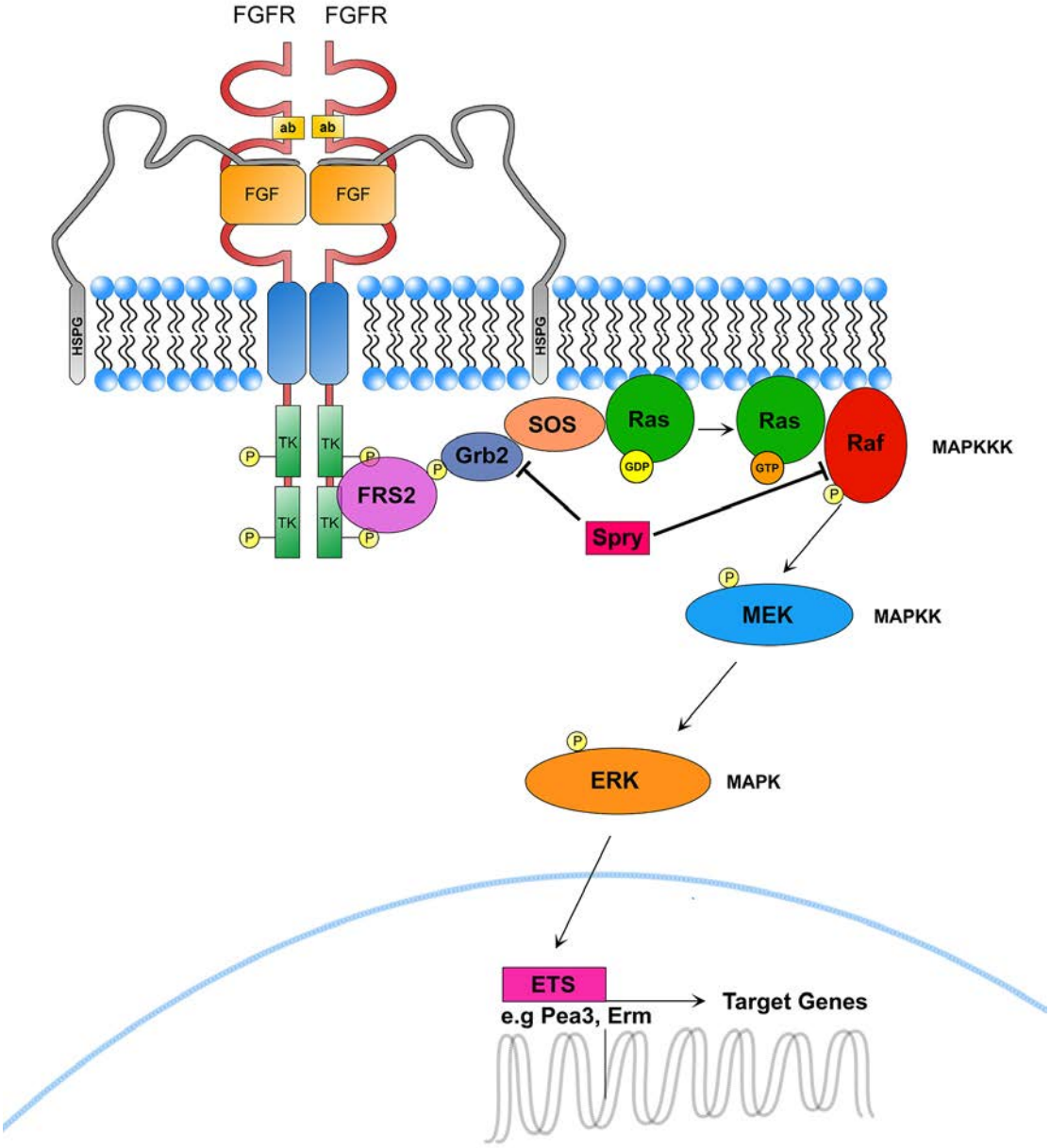

Figure 1.9 Schematic drawing of the Ras/MAPK signalling pathway activated by FGF-FGFR binding.
Extracellular ligand binding triggers intracellular phosphorylation of FGFR TK domains. This leads to the phosphorylation of FRS2, which allows the formation and activation of the Grb2 and SOS complex. The complex permits the guanosine nucleotide exchange of membrane bound Ras, from GDP to GTP. The activated GTP-bound Ras recruits Raf to the membrane and phosphorylates the Raf protein. Activated Raf phosphorylates the MAPK kinase (MAPKK) MEK, which in turn phosphorylates the MAPK ERK. Activated ERK translocates into the nucleus where it targets specific transcription factors essential for cell proliferation and differentiation. Sprouty (Spry) molecules act as negative feedback regulators by inhibiting SOS activation by binding to Grb2 or by preventing the phosphorylation of MEK by binding to and inhibiting the action of Raf.

1.6 Branching Morphogenesis

Branching morphogenesis is the elegant developmental process where a single tube arises from an endothelial or epithelial sheath and undergoes continual budding and clefting to create a complex network of branched tubes. The entire process involves a multitude of cell behaviours such as proliferation, migration and differentiation, as well as epithelial interactions with adjacent tissues and extracellular matrix. Many structures have evolved this branched architecture as it allows for a large surface area to be contained in a small volume of space, thus making it ideal for organs that function in transporting liquid or gas. The sprouting tubes are composed of endothelial cells in the branched vasculature and lymphatic systems, while they are composed of epithelial cells in most other branched structures of the body. For relevance to this study, the branching of epithelial structures will be discussed.

1.6.1 Branching of the Drosophila melanogaster Tracheal System

The tracheal system of the fruit fly (*Drosophila melanogaster*) is a complex branched structure that has provided immense insight into the cellular and genetic mechanisms involved in the process of branching morphogenesis *in vivo*. Although comprising of only approximately 80 cells, this respiratory structure supplies oxygen to every cell of the body and provides an ideal model system for investigating branching (Samakovlis et al., 1996; Kerman et al., 2006). The process begins with 10 clusters, or placodes, of ectodermal derived epithelial cells forming along the surface of the *Drosophila* larva (Figure 1.10 A). These placodes are formed by cell proliferation, which cause epithelial sacs to invaginate into the underlying mesoderm (Samakovlis et al., 1996). Once the epithelial sacs are formed cell proliferation arrests. From these sacs, the tracheal branches develop, with their development being divided into three main stages; (1) Primary (2) Secondary and (3) Terminal branching (Samakovlis et al., 1996). The primary branches are formed from six buds arising from each epithelial sac at stage 12 of fruit fly development (Figure 1.10 A and B). At stage 15 of development, two secondary branches arise in a uniform fashion from the primary branches (Figure 1.10 C and D) followed by the sprouting of numerous terminal tubes at stage 16 (Samakovlis et al., 1996).

Investigation into the signalling mechanisms patterning the fruit fly tracheal system elucidated a role for FGFs. *Drosophila* have one FGF ligand homologue, encoded by

the gene b*ranchless (bnl)* and two FGFRs, encoded by the genes *breathless (btl)* and *heartless (htl)*. Studies have shown that mutations in both *btl* and its ligand *bnl*, led to defective tracheal cell migration and abnormal tracheal branching (Lee et al., 1996; Sutherland et al., 1996). Although tracheal pit formation is FGF independent, and relies on another *Drosophila* ligand encoded by the gene *trachealess* (*trh*) (Isaac and Andrew, 1996), *bnl* expression surrounding the epithelium acts as a chemoattractant for the outgrowth of both the air sacs and the primary branch cells, and activates *btl* expression within the epithelial cells (Sutherland et al., 1996; Glazer and Shilo, 1991; Sato and Kornberg, 2002)(Figure 1.10 A-B). Once the primary branches elongate and reach the *bnl* expressing cells, elongation of the primary branch ceases (Figure 1.10 C). The high level of Bnl ligand signal induces the expression of the ETs domain transcription factor *pointed* (*pnt*) within the tubule epithelial cells which in turn activates *spry* expression (Hacohen et al., 1998). Spry then functions in inhibiting the expression of *bnl* in distal tubule cells, restricting the influence of Bnl to the tracheal tip cells, which then form secondary branches (Hacohen et al., 1998) (Figure 1.10 C-D). The terminal branches do not develop as stereotypically as the primary and secondary. Their sprouting and extension is triggered by oxygen level detection (Jarecki et al., 1999). Hypoxic conditions do however trigger *bnl* expression and through Btl, terminal branches develop similar to the primary and secondary branches (Jarecki et al., 1999).

1.6.2 Branching of the Mammalian Lung

A similar invagination mechanism is observed during the development of the endodermal mammalian trachea and lung. The trachea and oesophagus arise from the primitive anterior foregut through a series of morphological changes involving endodermal and mesodermal interactions at E9 in mice and about 4 weeks into gestation in humans (*reviewed in* Warburton et al. 2005). Initially, two folds emerge from the ventral side of the foregut tube. One of these, the proximal protruding fold is known as the ventral diverticulum, which later becomes the laryngotracheal tube (Clark, 1999; Ioannides et al., 2002) while the distal protrusion becomes the ventral pancreas, biliary system and liver (El-Gohary et al., 2010). The laryngotracheal tube undergoes bifurcation resulting in the outgrowth of two separate lung buds. In mice, one bronchiole branch extends from the left, while four branches extend from the right bud (Metzger et al., 2008). In humans, two bronchiole branches extend from the

left bud while three branches elongate from the right bud. A further two branches extend from each bronchiole branch; eventually ending in terminal tubes whose ends will form the alveoli of the lungs. The three-step patterning of murine lung branching is tightly regulated and stereotypical throughout development (Metzger et al., 2008).

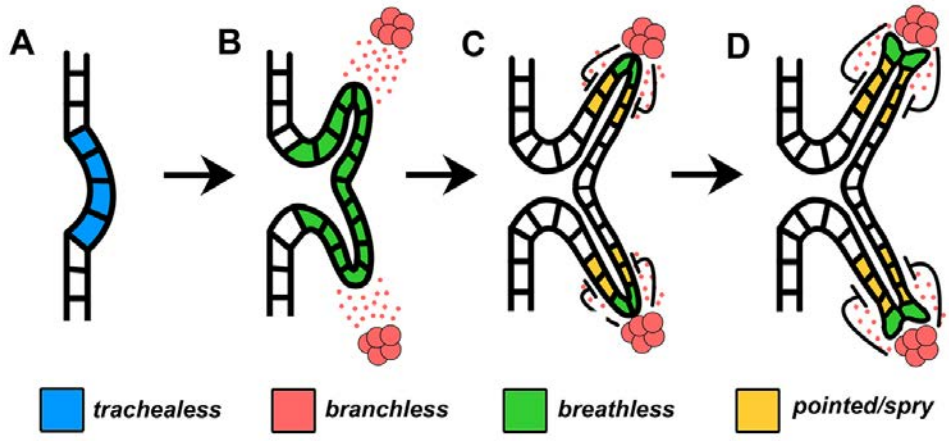

Figure 1.10 Branching morphogenesis of the *Drosophila melanogaster* tracheal system.
(A) The selection of placodal cells requires *trachealess* expression. (B) The outgrowth of the placode is caused by *branchless* expressing cells acting as a chemoattractant. Localisation of *branchless* in the mesenchyme attracts the primary branches from the original epithelial sac. Epithelial cells express the receptor *breathless.* (C) When the primary branches have elongated, they arrest growth when they reach cells of high *branchless* expression. This high concentration induces *pointed*, followed by *sprouty,* within the epithelial cells inhibiting branching in the more proximal tubes. (D) Through Breathless*, branchless* expressing cells induce secondary branch formation in the most distal epithelial cells.

FGFs are required at all stages throughout mammalian lung development (Bellusci, Grindley, et al., 1997; Min et al., 1998; Weinstein et al., 1998). In particular FGF10 and its receptor FGFR2b are critical for early lung branching morphogenesis (Peters et al., 1994; Bellusci, Grindley, et al., 1997). The *Fgf10* gene is located on chromosome 13 (13A3-A4) and chromosome 5 (5p12-p13) in mice and humans respectively (Crackower et al., 1998; Emoto et al., 1997). The role of *Fgf10* and its receptor *Fgfr2b,* is emphasised by the shared defects of both *Fgf10* homozygous (-/-) and *Fgfr2b* -/- mice, who die at birth due to agenesis of the lungs (Sekine et al., 1999; Min et al., 1998; De Moerlooze et al., 2000). FGF10 plays a similar role to

Branchless, as it acts as a chemoattractant for lung budding from the laryngotracheal tube and subsequent initial bronchiole elongation (Bellusci, Grindley, et al., 1997). *Fgf10* is expressed in the splanchnic mesenchyme surrounding the foregut endoderm as early as E9.5 in the mouse when the two lung buds are originating, with higher levels of *Fgf10* RNA detected adjacent to the larger right bud (Bellusci, Grindley, et al., 1997). As development continues from E10.5-E11.5, and as bronchiole buds stem from the left and right presumptive bronchi branches, *Fgf10* is expressed in the mesenchyme around emerging buds (Bellusci, Grindley, et al., 1997). *Fgf10* expression is maintained in the surrounding mesenchyme as branching morphogenesis continues, while its receptor *Fgfr2b* is expressed in the epithelial branches of the lung (Peters et al., 1992, 1994; Bellusci, Grindley, et al., 1997). Furthermore, *Fgf10* can induce ectopic bud formation from lung epithelium in culture (Bellusci, Grindley, et al., 1997). Similar to the *Drosophila* tracheal system, it has been shown that FGF signalling through FGFR2b induces *Spry2* expression, which inhibits the downstream activation of Ras pathway molecules (Tefft et al., 1999; Mailleux et al., 2001). Sonic hedgehog (Shh) signalling from the branching lung stalks has also been shown to negatively regulate *Fgf10,* as *Fgf10* expression increases in the surrounding mesenchyme in *Shh* knockout studies (Bellusci, Grindley, et al., 1997; Pepicelli et al., 1998; Miller et al., 2004). Additionally, upregulation of *Shh* expression in transgenic lungs leads to a decrease in *Fgf10* transcripts in the splanchnic mesenchyme (Bellusci, Grindley, et al., 1997).

1.6.3 Branching of the Mammalian Salivary Gland

Mice and humans have three pairs of major salivary glands that secrete saliva into the oral cavity: the parotid (PG), submandibular (SMDG) and sublingual glands (SLG), as well as numerous minor salivary glands which are located in the tongue, palate, cheeks and lips (Hand et al., 1999). The murine SMDG has been an exceptional model of branching morphogenesis both *in vivo* and *ex vivo* as it can be readily isolated and grown in *in vitro* organ culture (Borghese, 1950). Its stages of development can be divided into distinct steps (Melnick and Jaskoll, 2000). First evidence of the SMDG is seen when it is in its *Pre Bud stage* at about E11.5 where a thickening in the oral ectoderm forms a SMDG placode (Figure 1.11, A). By E12.5, continuous cell proliferation causes this placode to elongate and invaginate into the underlying mesenchyme as a solid stalk of cells (Figure 1.11, B). At this *Initial Bud*

stage, mesenchymal cells begin to condense around the SMDG bulb, forming the salivary gland capsule in which the SMDG and SLG are enclosed (Borghese, 1950; Miletich, 2010). At about E13.0, the initial epithelial bud begins to sprout branches. This stage is referred to as the *Pseudoglandular stage* and is brought about by initial bud clefting and outgrowth of new epithelial stalks (*reviewed in* Miletich 2010) (Figure 1.11, C). Continual clefting and elongation of solid stalks proceeds to the *Canalicular stage* at E15.5 where lumen formation through a process of cavitation begins throughout the main gland ducts and branches (Figure 1.11 D). Spaces form within the epithelial stalks, which eventually, at the *Terminal Differentiation* stage, beginning at E17.5, start to fuse to form one continuous lumen, elegantly hollowing out branches into epithelial tubes (Melnick and Jaskoll, 2000; Wells and Patel, 2010) (Figure 1.11, E). The first signs of cellular differentiation can be identified by the first detection of mucin transcripts at E14, however mucin proteins are not evident in the end buds until E17 (Figure 1.11 E) (Jaskoll et al., 1998).

It has been shown that murine SMDG development requires an interaction between mesenchymal FGF10 and its epithelial receptor FGFR2b for successful branching morphogenesis (Ohuchi et al., 2000). Previous reports indicate that *Fgf10* is not required for initial salivary gland bud formation, which is more dependent on *Fgf7,* however *Fgf10* is crucial for successional epithelial duct elongation and branching morphogenesis (Jaskoll et al., 2005; Steinberg et al., 2005). *Fgf10* is expressed in the mesenchyme underlying the presumptive salivary gland epithelium from E11.5 (Wells et al., 2013). *Ex vivo* manipulation of SMDGs in organ culture demonstrates that exogenous FGF10 peptide applied at both the *Prebud* and *Pseudglandular stage* gives rise to a significant increase in number of epithelial branches due to an increase in epithelial cell proliferation (Jaskoll et al., 2005). Furthermore application of FGF10 to isolated SMDG epithelial rudiments induces duct elongation in a dose dependent manner by stimulating proliferation at the tips of ducts (Steinberg et al., 2005). Jaskoll et al. (2005) showed in *Fgf10* null mice that the SMDG initiated to its *Initial Bud* stage at E12.5 however it was unable to develop further, and at E13.5 any epithelial evidence of the SMDG was absent. Unlike the *Fgf*10 knockouts, heterozygous *Fgf10* +/- mice are viable and in mouse pups at postnatal day (P) 0, SMDGs were present but had fewer ducts and terminal buds (Jaskoll et al., 2005). Another study by Entesarian et al. (2005) investigated *Fgf10* +/- adult salivary glands and concluded

they were hypoplastic compared to WTs yet the histology of the SMG and SLG were similar to WT counterparts.

Expression of *Spry 1* and *Spry 2* is apparent throughout the SMDG epithelium during both *Initial Bud* and *Pseudoglandular stages* while *Spry 4* is restricted to the distal epithelial cells only (Zhang et al., 2001). This suggests that negative feedback regulators are involved in controlling the influence of FGF signalling on more distal ductal cells. Furthermore, application of the MEK 1/2 inhibitor UO126 in *in vitro* cultured salivary glands inhibited the effects of FGF10 on epithelial stalk elongation, indicating that FGF10 induced cell proliferation is working through ERK 1/2 (Steinberg et al., 2005).

In humans, mutations in *FGF10* or its receptor *FGFR2b*, lead to Lacrimo Auriculo Dento Digital (LADD) syndrome (OMIM 149730), also known as Levy-Hollister syndrome. This rare autosomal dominant disorder was first characterized by Hollister et al. (1973) who reported anomalies in a Mexican man and five of his eight children. These defects included hypoplasia or aplasia of the lacrimal glands of the eyes, obstruction of the nasolacrimal duct, cup shaped ears, hearing loss, tooth abnormalities, and digit and limb malformations (Hollister et al., 1973). Although dry mouth was a symptom of the original patients identified, it wasn't until later that studies elucidated that in addition to the lacrimal gland defects, hypoplasia, atresia and aplasia of the salivary glands were also characteristic of the disease (Shiang and Holmes, 1977; Thompson, Pembrey, and J. M. Graham, 1985). A milder form of this disease, known as Aplasia of Lacrimal and Salivary Glands (ALSG) (OMIM 180920), also occurs and gives rise to the same symptoms as LADD, most often including xerothalmia (dryness of the eye) and xerostomia (dry mouth) (Wiedemann, 1997; Milunsky et al., 1990).

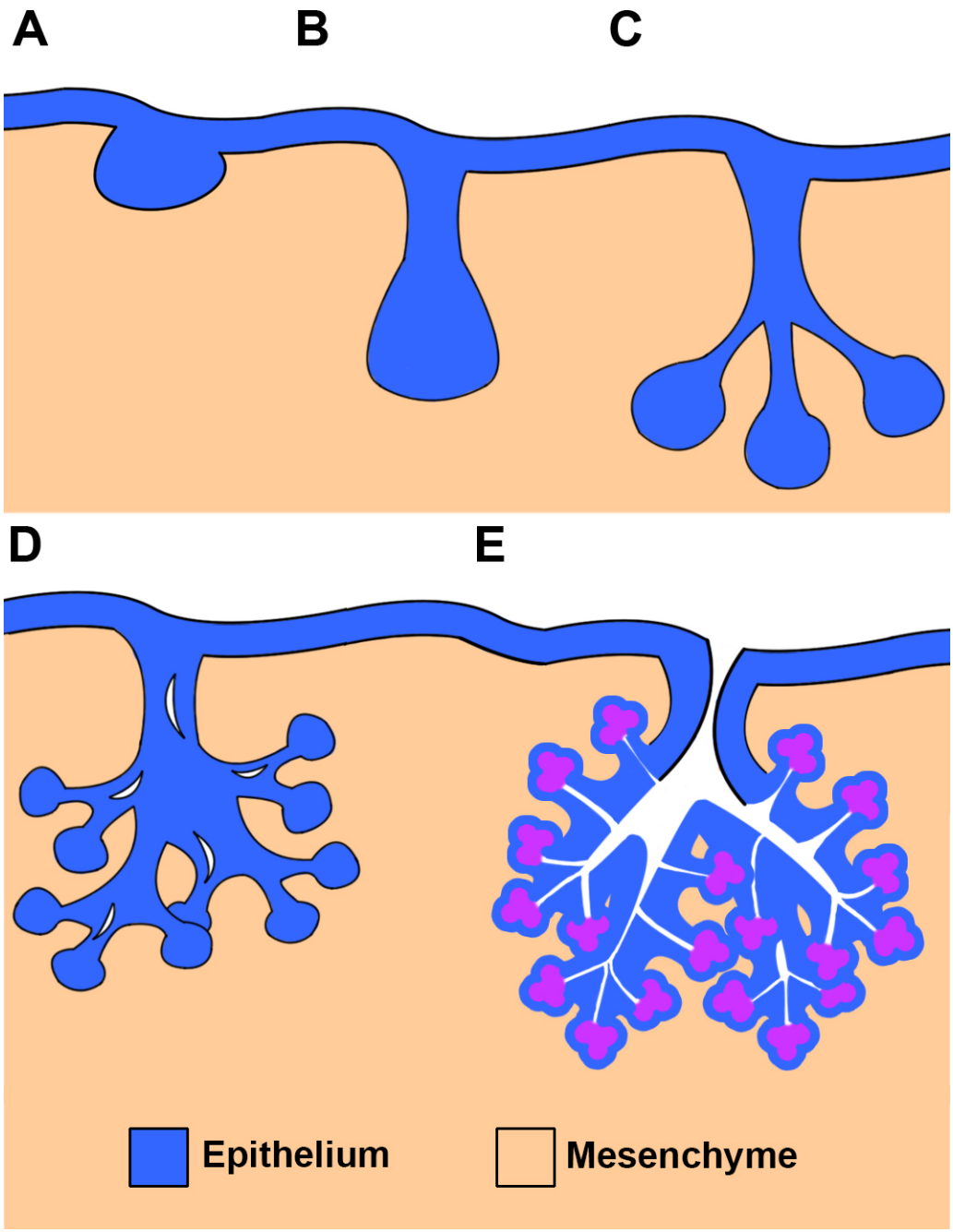

Figure 1.11 Branching morphogenesis of the mammalian salivary gland.
(A) ***Prebud stage*****:** Salivary gland morphogenesis is first evident at E11.5 as an epithelial placode invaginating from the oral epithelium into the underlying mesenchyme. **(B)** ***Initial Bud stage*****:** By E12.5, the epithelial cells proliferate and a solid bulb like structure forms. **(C)** ***Pseudoglandular stage*****:** Sprouting of epithelial branches is clear by E13.5. **(D)** ***Canalicular stage:*** By E15.5, continual branching has occurred and canalization has begun to create spaces within the solid epithelial stalks. **(E)** ***Terminal Differentiation stage*****:** By E17.5, branching continues and luminal spaces have connected to form a continuous lumen within the gland. Cellular differentiation is evident in the distal epithelial acini (purple).

1.7 Aims of this Thesis

It is evident that the respiratory SMGs play a critical role in maintaining airway homeostasis and host defence. Disruption in gland cellular composition and function can lead to severe diseases and the molecular mechanisms at the basis of these defects need to be elucidated. The aim of this thesis is to follow gland development, in both the nasal cavity and trachea, and uncover the role of FGF signalling during their morphogenesis.

The main goals of this work include:

1. To uncover the development and temporal localisation of the anterior nasal glands in the mouse and investigate the cellular processes involved in their morphogenesis.
2. To analyse the phenotype of anterior nasal and tracheal SMGs in *Fgf10 -/-* and *Fgf10 +/-* mice and delineate the expression patterns of other *Fgfs* and their downstream targets during SMG development.
3. Considering the phenotype in *Fgf10 +/-* adults previously described (Rawlins and Hogan, 2005), I aim to investigate whether a reduction in SMGs has a negative effect on the mucociliary clearance and overall respiratory health of these animals.
4. To investigate the salivary gland dysfunction in *Fgf10 +/-* mice and analyse the influence reduced saliva flow has on oral health.

2.1 Animals

2.1.1 Animals

Animals were housed in the Biological Services Unit (BSU), New Hunt's House, Guy's Campus, King's College London. For tracing normal gland development, mice of CD1 background were used. Staff of the BSU maintained all CD1 mice and carried out timed mating and plug checking procedures.

Fgf10-deficient mice were first generated by Min et al. (1998) (Mouse Genome Informatics ID 1099809). Homozygous (*Fgf10* -/-) and heterozygous (*Fgf10* +/-) mice were generated by targeted mutation of exon 1 of the *Fgf10* allele of 129X1/SvJ clones. Positive clones were injected into fertilized C57BL/6 females. Chimeric males that were produced were then crossed with 129 SVJ or Swiss black females (Min et al., 1998). Heterozygote males and females from each line were crossed to produce *Fgf10* +/- and *Fgf10* -/- mice. *Fgf10* +/- were crossed with CD1 mice upon arrival to the Craniofacial Development and Stem Cell Laboratory, King's College London by Dr. Albert Basson and kept on this background for this study.

Fgfr2b -/- specimens have been previously described (De Moerlooze et al., 2000) (Mouse Genome Informatics ID 2153811). *Fgfr2b* -/- mice were generated by Cre-mediated excision of the floxed IIIb exon (exon 8) of 129X1/SvJ positive clones. Chimeras were generated by injecting *Fgfr2IIIb*$^{-/-cond}$ eggs into fertilized C57Bl mice with pCAGGs Cre vector (De Moerlooze et al., 2000). Samples of E18.5 *Fgfr2b* -/- mice investigated in this study were taken from slide stocks in the Craniofacial Development laboratory that had kindly been provided previously by Dr. David Rice, University of Helsinki, Finland.

2.1.2 Embryo Collection

Mice were mated in the late evening and a midnight mating was assumed. Midday of the day at which a vaginal plug was discovered was recorded as embryonic day (E) 0.5. Pregnant female mice were culled by cervical dislocation and carried on ice to the Craniofacial Development laboratory, Guy's Hospital.

2.1.3 Postnatal Pup Collection

The day female mice littered down was recorded as P0. Pups were humanely culled using an interperitoneal injection of 20% sodium pentobarbital solution (JML, RM190) at a concentration of 100mg/kg body weight.

2.1.4 Adult Collection

For the collection of adult specimens, where tracheal tissue was not required, animals were culled by cervical dislocation. As this method damages the trachea, adult males and females were culled by exposure to rising levels of CO_2 gas for studies where the tracheal tissue was needed.

2.2 Dissection and Preparation of Tissue

2.2.1 Preparation of Embryonic Tissue

Uteri were dissected from pregnant dams and transferred to ice cold phosphate buffered saline (PBS) (Oxoid). Embryos were collected on the required ages based on the date of vaginal plug discovery. Embryos were carefully dissected by uterine wall and fetal membrane removal. After dissection, embryos were staged accurately by weight (Peterka et al., 2002) and by external features (Theiler, 1989). In the case of collection of *Fgf10* transgenic embryos, tail clips of embryos were carefully collected using a sharp scissors and were gently transferred to 1.5ml eppendorf tubes for genotyping. Specimens were decapitated and heads were fixed in 4% paraformaldehyde in PBS (PFA) overnight at 4°C. Tracheas were also collected for older staged embryos at E18.5 and fixed overnight. For tissue collected for *in situ* hybridisation procedures, all solutions used were made up with PBS treated with diethylpyrocarbonate (DEPC) (Sigma).

2.2.2 Preparation of Postnatal and Adult Tracheal Tissue

Following sacrifice by rising levels of CO_2, animals were transferred to the Craniofacial Development laboratory on ice. Under a dissection microscope, an incision was made through the sternum and the rib cage was opened. Tracheal tissue was identified and the trachea was dissected out using a sharp scissors by a clean anterior cut through the thyroid ligament above the thyroid cartilage, and a posterior cut between the tracheal cartilage rings by the bronchial bifurcation. Tracheas were fixed overnight in PFA at 4°C.

2.2.3 Tissue Dehydration, Embedding and Sectioning

Following overnight fixation, tissue underwent two 30-minute washes in PBS at RT followed by dehydration washes in increasing methanol concentrations (Table 2.1). After dehydration, tissue was put in Isopropanol (Sigma Alrdrich) overnight at 4°C. Following another brief isopropanol wash, tissue was transferred to glass vials, as plastic containers are not suitable for subsequent clearing steps. Samples were then cleared in 1,2,3,4 Tetrahydronapthalene (Sigma Aldrich) at RT, until tissue appeared transparent. Samples then underwent four 60 minute washes in liquid premium polyisobutylene histological wax (Ultraplast, Solmedia) at 65°C. If required, occasionally samples would be transferred to fresh wax and stored at 4°C overnight. The next morning, tissue would be placed at 65°C for an hour, or until wax had melted, and wax washes would resume. At a Leica EG1150H, samples were then transferred into metal moulds where they would be positioned accurately. Tissue was solidified at the base of the metal mould by placing the mould on a 4°C cold plate. A labelled plastic embedding cassette (VWR International) was then placed on the top of the wax block and more hot wax would be added to keep it in place, ensuring no air bubbles formed. The mould was then transferred to a larger cold stage and left to solidify for 30 minutes at 4°C. Wax blocks were then stored at RT until required.

Table 2.1 Solution composition and washing conditions of dehydrating methanol series.

Dehydration Step	Solution Composition	Washing Temperature	Overnight Storage Temperature
PBS	100% PBS	Room temperature	4°C
30%	30% methanol, 70% PBS	Room temperature	4°C
50%	50% methanol, 50% PBS	Room temperature	4°C
70%	70% methanol, 30% deionised H_2O	Room temperature	4°C
80%	80% methanol, 20% deionised H_2O	4°C	-20°C
90%	90% methanol, 10% deionised H_2O	4°C	-20°C

95%	95% methanol, 5% deionised H_2O	4°C	-20°C
100%	100% methanol	4°C	-20°C
100%	100% methanol	-20°C	-20°C

2.2.4 Tissue Sectioning and Mounting

Excess wax was trimmed from wax blocks using a razor blade, so embedded tissue was tightly framed. Using a Leica RM2245 microtome, serial 9µm sections were cut through tissue and collected. For anterior nasal gland analysis, sagittal sections were collected along the left/right axis through the entire embryonic head. For tracheal tissue analysis, frontal sections were collected from the ventral to dorsal plane. Tissue sections were collected as long ribbons where they were then cut into individual sections using a razor blade and placed on the surface of water in a paraffin section mounting bath (Electrothermal) set at approximately 42°C. This warm heat allowed wax sections to flatten out smoothly where they could then be mounted on Superfrost™ plus microscope slides (Thermoscientific). For those tissue sections designated for *in situ* hybridisation analysis, serial sections were mounted on alternative slides to allow the detection of different RNA probes on comparable sections. Additionally, DEPC treated H_2O was used in the water bath for mounting sections required for *in situ* hybridisation. Slides were then left on a slide drying bench (Thermoscientific) overnight at 42°C to allow tissue to adhere to the slide. Slides were then stored in a slide box at 4°C.

2.3 Histological Staining

2.3.1 Haematoxylin and Eosin with Alcian Blue Staining

Haematoxylin and Eosin (H&E) stain is one of the most common techniques used to stain acidic and basic structures of tissues. Haematoxylin, a basic dye, is used to stain acidic structures purple, such as heterochromatin in the nucleus and parts of the cytoplasm containing RNA. In contrast, Eosin an acidic dye, will stain basic structures a pinkish red, such as the cytoplasm and muscle fibres. In addition to these dyes, Alcian Blue can by applied to visualise mucopolysaccharides (Mowry, 1956). This characteristic makes Alcian Blue a suitable dye for visualising SMGs as mucous cells, and mucus secretion will be stained.

H&E with Alcian Blue staining was carried out by either Dr. Alasdair Edgar (Craniofacial Development Department, King's College London) or myself. Slides were dewaxed by immersion in Histoclear II™ (National Diagnostics), twice for 10 minutes. Tissue was then rehydrated by decreasing volumes of industrial methylated spirit (IMS) (Solmedia) in deionised H_2O (100%, 90%, 70%, 50%) for two minutes in

each step and rinsed in deionised H_2O. Samples were then stained in Ehrlich's Haematoxylin (Solmedia) for 10 minutes followed by a 10-minute rinse under running water and then a two-minute rinse in deionised H_2O. Sections were placed in acid alcohol (1% HCl in 95% IMS) for 15 seconds followed by another 10-minute rinse under running water and a two-minute rinse in deionised H_2O. Tissue was then stained in 0.5% aqueous Eosin (Lamb) for 5 minutes and washed for two minutes in deionised H_2O. Samples were dehydrated in increasing IMS in deionised H_2O concentration steps (70%, 90%, 100%, 100%) for two minutes each. Slides were immersed in Histoclear II™ twice for 5 minutes and then mounted using Neo-mount® mounting medium (Merck Millipore), coverslipped and left to dry overnight in a fume hood.

2.3.2 Trichrome Staining

Trichrome staining again consists of Haematoxylin and Alcian Blue dyes however the process has an additional staining step in Sirius Red. By exposing tissue to Sirius Red, collagen-containing structures, such as bone and connective tissue are darkly stained red. This staining method was used for nasal gland analysis as bone appears in the craniofacial regions during later embryonic stages.

Slides were dewaxed by immersion in Histoclear II™ twice for 10 minutes. Tissue was then rehydrated by decreasing volumes of IMS in deionised H_2O (100%, 90%, 70%, 50%) for two minutes in each step and rinsed in deionised H_2O. Samples were stained in 1% Alcian Blue dissolved in 3% acetic acid (Analytical Reagents) pH2.5 for 10minutes followed by a 10-minute rinse under running water and a two-minute rinse in deionised H_2O. Slides were then immersed in Ehrlich's Haematoxylin for 10 minutes followed by another 10-minute rinse under running water and a two-minute rinse in deionised H_2O. For staining differentiation, samples were then placed in 2.5% phosphomolybdic acid (Fluka Biochemica) for 10 minutes and washed in deionised H_2O. Slides were then left soaking in 0.5% Sirius Red in saturated Picric Acid (BDH) for one hour. Sections were rinsed twice in 0.5% acetic acid in deionised H_2O and blotted dry. Tissue was then put through two 5-minute steps in 100% IMS and two 5-minute steps in Histoclear II™. Slides were mounted using Neo-mount® mounting medium, coverslipped and left to dry in a fume hood overnight.

2.4 Genetic Determination of Animals

2.4.1 Postnatal and Adult Ear Clipping

Collection of ear tissue from postnatal or adult mice was carried out in the BSU, New Hunts House, Guy's Campus by either Alex Huhn (Craniofacial Development Department, King's College London) or myself. A forceps and ear punch (VetTech Solutions Ltd.) were sprayed with 70% ethanol and dried thoroughly. Equipment was then passed through a Bunsen burner flame to sterilise and left to cool to RT. Animals were gently, yet securely held by the scruff of the neck and a small piece of ear tissue was collected using an ear punch. This tissue was transferred into a sterile labelled 1.5ml eppendorf tube and brought to the Craniofacial Development laboratory.

2.4.2 Isolation of Genomic DNA

Genomic DNA was extracted from embryonic tail clips or postnatal and adult ear clips. Purification steps were carried out by either Andrew Donkin (Craniofacial Development Department, King's College London) or myself. Tissue clips were digested overnight in 0.5mg/ml Proteinase K in DirectPCR® tail or ear lysis buffer (Peqlab) at 55°C on a hotblock (Techne Dri-Block). The next day, samples were heated to 85°C for 45 minutes to inactivate the Proteinase K. Samples were allowed to cool to RT.

2.4.3 Polymerase Chain Reaction

Prior to the preparation of samples for the polymerase chain reaction (PCR), all equipment was sterilised by U.V light exposure using a PCR Workstation (Alpha Laboratories). To labelled PCR tubes DNA template samples, Fgf10 oligonucleotide primers (Sigma), Kapa 2G robust hot start ready mix (Kapa Biosystems) and PCR grade nuclease-free H_2O (Promega) were added in the following volumes per 1.5ml eppendorf:

DNA template	0.5µl
Fgf203 primer	0.625µl
Fgf204 primer	0.625µl
Fgf233 primer	0.625µl
Fgf234 primer	0.625µl
Kapa ready mix	6.25µl
Nuclease-free H_2O	3.25µl

The Kapa 2G robust hot start ready mix contains all the vital ingredients for successful DNA amplification including DNA polymerase, $MgCl_2$ and dNTP (dATP, dTTP, dGTPand dCTP) nucleotides. Primers used to detect wildtype *Fgf10* locus were 5'-GAGGAAATGCTGCGCACAATGTATACTCGG-3' (Fgf203 forward primer) and 5'-GGATACTGACACATTGTGCCTCAGCCTTTC-3' (Fgf204 reverse primer) while the mutant *Fgf10* locus was detected by primers 5'-GCTTGGGTGGAGAGGCTATTC-3' (Fgf233 forward primer) and 5'-CAAGGTGAGATGACAGGAGATC-3' (Fgf234 reverse primer) of the neo-cassette insert (Sekine et al., 1999). In addition to the collected DNA template sample tubes, a negative control tube containing a DNA template from a CD1 strain mouse, and a positive control tube containing a DNA template from an *Fgf10* +/- mouse was processed using the same techniques as sample tubes. PCR was then carried out in a G-storm Thermal Cycler under the "Kapa 2g Robust" program for suitable conditions for DNA samples.

Following PCR, 2.5µl of 5x Green GoTaq® Reaction Buffer (Promega) was added to each tube and 8.5µl of amplified DNA was run in a 2% agarose gel to confirm PCR products.

2.4.4 Agarose Gel Electrophoresis

To test the presence of nucleic acid fragments in a sample, agarose gel electrophoresis was routinely carried out using either a 1 % or 2% agarose gel. Firstly, 0.5g or 1.0g of agarose (Eurogentec) was weighed out and diluted in 50ml of Tris-acetate-EDTA (TEA) buffer for a 1% or 2% gel respectively. Agarose powder was dissolved in TAE by heating the solution for two minutes on high power in a microwave with intermittent swirling. Once the powder had dissolved, the gel was cooled by running cold water over its glass container while swirling. Once cool, but not solid, 1µl of ethidium bromide (Fischer Scientific) was added and the gel was mixed. Ethidium bromide fluorescently labels nucleic acids so they can be visualised under U.V light. The gel was poured into a mould and a comb inserted to form individual wells. Gel was left to completely solidify at RT for 30 minutes.

Once solid, the gel was removed from its mould and placed gently in an electrophoresis tank (Scie-Plas HU6 Mini) and TAE was poured into the tank until the

gel was covered. To the first well of the gel, 7µl of DNA ladder (NEB Biolabs Quickload 1kb ladder for DNA and Promega 100bp ladder for RNA) was added. To the other wells 7µl of nucleic acid-containing samples were loaded. In the case of amplified DNA from tissue clips, these were loaded after Green Buffer addition (see section *2.4.3*). For DNA and RNA samples isolated from plasmid DNA, 2µl of nucleic acid sample was added to 3µl of H_2O and 2µl of Blue Loading Dye (Promega) and loaded into each well. The lid was placed on the electrophoresis tank and an electric current was triggered by turning the tank on. This current passes from the cathode to the anode of the tank, causing the nucleic acid samples to migrate south toward the anode. The electric current was usually run at 110V for 30 minutes however time was reduced significantly to approximately 5-10 minutes for more fragile RNA samples. When complete, the gel was carefully removed from the tank and placed in a U.V transilluminator (UVP). The door was closed securely and the U.V light turned on to visualise bands. Images were captured and printed on a Mitsubishi P91 printer.

2.5 Molecular Biology

2.5.1 Bacterial Plasmid DNA Transformation and Amplification

Before bacterial cell transformation with plasmid DNA was carried out, a Lysogeny Broth (LB) medium and a LB agar were prepared and autoclaved (Table 2.2). For growth of bacterial colonies, LB agar plates were prepared containing the antibiotic Ampicillin (Sigma). Solid LB agar was heated in the microwave until all agar had turned to liquid. This liquid LB was placed in a 50°C waterbath for 30-60 minutes to ensure agar dropped to that temperature. At 50°C Ampicillin will not be denatured, yet the agar can remain as a liquid. Ampicillin was added at a concentration of 200µl/1ml of agar and the solution was mixed by swirling. On a clean bench next to a lighted Bunsen burner, approximately 30mls of agar was poured into 9cm petri dishes (Sterilin, Fisher Scientific). Lids were partially placed on petri dishes and they were left to solidify for 30 minutes next to the lighted Bunsen burner. Once solidified, lids were placed fully on the dishes, plates were turned upside down, wrapped in Parafilm® M (Fluka Biochemica) and stored at 4°C. By storing upside down, any condensation that forms in the dishes will be restricted to the underside of the lid and will not collect on the LB agar.

Table 2.2 Composition of LB medium and LB agar used for bacterial amplification and growth.

LB medium	
NaCl	1%
Bacho-Tryptone (Oxoid)	1%
Bacto-Yeast Extract (Oxoid)	0.5%
LB agar	
NaCl	1%
Bacho-Tryptone	1%
Bacto-Yeast Extract	0.5%
Bacteriological Agar (Sigma)	2%

Competent bacteria cells (DH5®α, Invitrogen) were removed from -80°C storage and left to thaw on ice for 30 minutes. To introduce plasmid DNA into bacterial cells (i.e transform) 1µl of plasmid DNA was added to 30µl of competent cells in a DNase and RNase free 1.5ml eppendorf tube. To ensure no bacterial antibiotic resistance, a control tube containing 1µl of autoclaved H_2O in 30µl of competent cells was prepared and processed in the exact same conditions as the plasmid DNA. To enhance competency and create pores in the bacterial cell walls, eppendorfs were subjected to heat shock by placing in a 42°C waterbath (Grant) for 45 seconds. Tubes were then put back on ice and left for a further two minutes.

To each tube, 900µl of LB medium was added and tubes closed tightly. Tubes were then shaken vigorously in an ISF-1-W Kuhner shaker for one hour at 37°C. In these conditions, bacterial growth is stimulated. To each agar plate, 100µl of transformed bacterial cells was added and spread all around the agar using a sterile bacteria spreader. Lids were placed on dishes and were left to dry at room temperature for 15 minutes. Once dry, plates were turned upside down and incubated overnight at 37°C. By incubating upside down, bacterial colonies are encouraged to grow individually.

Following overnight incubation, bacterial plates were checked for colonies. As control plates were not incubated with antibiotic resistant containing plasmids, no colonies could grow due to Ampicillin in the LB agar. To a 15ml Falcon tube, 5ml of

LB medium with 5µl of Ampicillin was added. Close to a lighted Bunsen burner, a single colony of bacteria was collected from each agar plate using a pipette tip and the tip was placed in the tube with the LB medium. The tube was closed loosely and left to shake vigorously over night at 37°C. The following morning, tubes containing a milky broth verified positive bacterial growth. To keep stock of plasmid containing bacteria, 300µl of the bacteria-LB medium solution was collected and added to 700µl of glycerol (Sigma) and stored at -20°C. The remaining bacterial cells were spun down at 4,000rpm for 10 minutes to form a bacterial cell pellet and the supernatant was discarded.

2.5.2 Bacterial Plasmid DNA Extraction and Purification

Using a QIAprep® Miniprep kit (Qiagen), DNA was extracted from bacteria and purified. The process first involves re-suspension of the bacterial cells in TE buffer with added RNase A (P1 buffer). EDTA in the TE buffer chelates cations such as Mg^{2+} and Ca^{2+} which are needed for proper DNase activity, while the RNase destroys any RNA contamination within the bacterial cell sample. Cells are then lysed in alkaline conditions in P2 buffer, a solution containing 200mM NaOH and 1% SDS. Following the break up of the bacterial cell wall, the alkali denatures both chromosomal and plasmid DNA. The third step involves the washing of cells in a solution containing Guanidine-HCl and potassium acetate (KOAc). This acidic KOA re-natures plasmid DNA but allows the precipitation of chromosomal DNA from the solution. Tubes were then spun for 10 minutes at 13,000rpm to collect debris as a pellet and leave plasmid DNA suspended in the supernatant. This supernatant was then poured through a QIAprep spin column, and spun for 1 minute at 13,000rpm. This step binds the plasmid DNA to the silica gel membrane within the column allowing any other contaminants to pass through the column as flow through, which is then discarded. Column walls were then washed with PB buffer, a solution containing 5M Guanidine-HCl and 30% isopropanol, which eliminates any possible nuclease activity and spun down at 13,000 rpm for one minute, discarding the flow through. Another wash in PE buffer, a solution containing 10mM Tris-HCl (pH 7.5) and 80% ethanol, which solubilizes smaller pieces of DNA other than the target plasmid, removing them from the wall of the column. Columns were again spun for 1 minute at 13,000rpm and flow through discarded. Deionised H_2O was then added to the column and let sit for one minute, followed by a spin at 13,000rpm for one minute. Flow

through containing pure plasmid DNA was collected and plasmid samples were stored at -20°C.

2.5.3 Linearization of Plasmid DNA

As plasmid DNA is circular, it must be linearized using a restriction enzyme downstream of the target sequence in order for a RNA probe to be transcribed. To carry out this digestion, 2µl of plasmid DNA was incubated on a hotblock at 37°C for two hours along with 2µl of restriction enzyme buffer, 0.2µl of 10mg/ml Bovine Serum Albumin (BSA), 13.8µl of deionised H_2O and 2µl of appropriate restriction enzyme (Table 2.3). To confirm the linearization of DNA, 2µl of cut DNA was run on a 1% agarose gel, next to 1µl of uncut plasmid in the same gel.

2.5.4 Preparation of Digoxygenin(dig)-labelled Riboprobes

To generate a dig-labelled RNA probe from the linearized DNA template, cut plasmid DNA was incubated with the following reagents:

DEPC treated H_2O	7.5µl
5 x transcription buffer	4µl
0.1M DTT	2µl
Dig-U NTPs	2µl
RNase inhibitor	0.5µl
Linearized plasmid DNA	3µl
Appropriate polymerase (Table 2.3)	1µl

DNA templates being transcribed with the polymerases T3 and T7 were incubated for one hour at 37°C, while those requiring SP6 polymerase were incubated at 42°C. After one hour, another 1µl of appropriate polymerase was added and the reaction was incubated for another one-two hours. After incubation 2µl of DNAse1 was added and all tubes were left on the hotblock for 15 minutes. The presence of RNA was then tested by running 2µl of the sample in a 1% agarose gel. RNA was then precipitated by adding 100µl of DEPC treated H_2O, 10µl of 4M lithium chloride (LiCl) and 300µl of ice cold ethanol to the mixture and the sample was left overnight at -20°C.

Following precipitation, probes were spun down for 10 minutes at 13,000rpm. RNA pellets were identified in the bottom of the tube and supernatant was removed

carefully using a pipette fitted with a filter tip. The probe pellet was then washed with 70% ethanol in DEPC treated H_2O for five minutes. Probes were spun down again for another 10 minutes and supernatant discarded carefully. Tubes were allowed to air dry for 5 minutes. The pellet was then diluted in 30µl of DEPC treated H_2O and stored at -20°C.

Table 2.3 cDNA plasmid vectors and gene inserts used for riboprobe generation.

Gene (all mouse)	Plasmid vector	Restriction enzyme required for linearization	RNA polymerase required for riboprobe generation	Source
Fgf7	pGEM3	EcoR1	SP6	Dr. I. Mason (Mason et al. 1994)
Fgf10	pBluescript SK (+)	BamH1	T3	Dr. I. Mason (Bellusci et al., 1997)
Fgfr2 (marker of both IIIb and IIIc isoforms)	pBluescript KS	HindIII	T3	Dr. K. Peters (Peters et al., 1992)
Spry1	pBluescript II	EcoR1	T7	Dr. G. Martin (Minowada et al., 1999)
Pea3	pGEM3	XbaI	SP6	Dr. J. Hassell (Xin et al., 1992)

2.5.5 In Situ Hybridisation of Embryonic Tissue with Dig-labelled Riboprobes

For *in situ* hybridisation with dig-labelled riboprobes, embryonic nasal and tracheal tissue was prepared as outlined in section **2.2**. Using a forceps cleaned with RNase Away (Molecular Bioproducts) and rinsed with DEPC treated H_2O, slides were transferred to glass coplin jars that had been baked at 200°C. All steps of this protocol were carried out rocking gently at RT, unless otherwise stated.

Sections were dewaxed in two washes of Histoclear II™ for 10 minutes and tissue rehydrated in decreasing concentrations of ethanol in DEPC treated PBS (100%, 95%, 90%, 80%, 70%, 50%, 30%) for 5 minutes each. Sections underwent two 5-minute DEPC PBS washes and were fixed for 30 minutes in PFA. Tissue was washed in Proteinase K buffer (20mM Tris/HCl and 1mM EDTA pH7.2) containing 10µg/ml of Proteinase K. Proteinase K is a broad-spectrum serine protease that can digest any contaminating nucleases that may attack nucleic acids. Slides were put in a 5 minute DEPC PBS wash followed by a 30 minute fixation step in PFA and another two 5 minute washes in DEPC PBS. Samples were then washed in 2x saline-sodium citrate (SSC) buffer, to control stringency of washing steps. Tissue was washed in Tris/Glycine Buffer (100mM Trizma-base, 100mM glycine), while the hybridisation solution was prepared in the fume hood (Table 2.4).

Table 2.4 Composition and volumes of reagents required to make 10ml of hybridisation solution.

DEPC treated H_2O	1.7ml
5M NaCL	1.5ml
10x PE	1ml
10% BSA	100µl
5% Heparin	100µl
10mg/ml tRNA	100µl
Formamide	5ml
10% SDS	500µl

To prepare samples for hybridisation with dig-labelled riboprobes, slides were incubated in hybridisation buffer for 3 hours at 55°C. Before the end of this step, riboprobes were prepared at a concentration of 2µl probe/300µl hybridisation solution. Probes were denatured by heating at 85°C for 5 minutes. In a fume hood, slides were carefully removed from the coplin jars using RNase free forceps and placed in a humid chamber. To each slide 300µl of probe solution was added to each slide and a sterile coverslip placed on top. Remaining hybridisation solution was poured on the tissue paper in the humid chamber to prevent drying out of slides. The

lid was placed over the humid chamber and wrapped tightly with Parafilm® M to airlock the container. Samples were then incubated at 55°C overnight.

The next day, slides were removed from the humid chamber in the fumehood and placed in a coplin jar. Samples underwent a series of washes in SSC at different concentrations and temperatures (Table 2.5). After this series, tissue was washed in NTE (0.5M NaCl, 10mM TrisHCl pH7.0, 5mM EDTA pH8.0) at 37°C for 10 minutes followed by a 10 minute wash in NTE with 10µg/ml RNase A at 37°C. Another wash in NTE was carried out at 37°C for 15 minutes followed by a rinse in 2xSSC at RT. Slides underwent hourly washes in 2xSSC at 50°C, 1xSSC at 55°C and 1xSSC at 60°C, followed by a 30 minute wash in 1xSSC at RT. Tissue was then blocked for one hour in 10% Boehringer Blocking Reagent (BBR) (Roche) in Maleic Acid Buffer (100mM maleic acid (Analytical Reagents), 150mM NaCl, 0.1% Tween-20) (MABT). Slides were then removed from the coplin jars and placed in a fresh humid chamber with tissue paper soaked in deionised H_2O. To each slide, 300µl of 1:5000 anti-digoxygenenin alkaline phosphatase conjugated antibody (Roche) in 1% BBR in MABT was added and a coverslip placed on top. Slides were then incubated overnight at 4°C.

Table 2.5 Times and temperatures of SSC washes carried out on the second day of *in situ* hybridisation.

Reagent	Time	Temperature
2xSSC	20 minutes	Room temperature
2xSSC	20 minutes	Room temperature
2xSSC	20 minutes	50°C
1xSSC	20 minutes	55°C
1xSSC	20mintues	60°C
1xSSC	10 minutes	Room temperature

Slides were removed from the humid chamber and placed in coplin jars where they underwent three 10 minute washes and one 20 minute wash in Tris-buffered saline (50mM Tris-HCl pH7.4, 150mM NaCl) with 0.1% Tween® 20 (Sigma) rocking at RT. Tissue was then put through three 10 minute washes in freshly made NTM

(100mM NaCl, 100mM Tris-HCl pH9.5, 50mM $MgCl_2$). Slides were then tapped dry on tissue paper and placed in a humid chamber with tissue paper soaked in deionised H_2O. To each slide 300µl of BM-purple staining solution was added and slides were coverslipped. The lid of the humid chamber was placed on tightly to block out any light and slides were left at RT. Slides were checked twice a day for development of BM-purple. If BM-purple was coming up slightly purple in colour, solution was refreshed. Once tissue sections had developed showing mRNA localisation and staining, slides were washed in two 10 minute washes in PBS, fixed for 20 minutes with PFA and put through a further three 10 minute washes in PBS. Slides were mounted with Aquatex® mounting medium (Millipore), coverslipped and left to dry at RT. Once dry, slides were stored at RT in slide boxes.

Sections were observed under a light microscope (Nikon Eclipse 80i) and images taken with a Nikon Digital Sight DS-Fi1 camera. Image collages were created using Adobe Photoshop CS5.1.

3.1 Introduction

3.1.1 The Nasal Glands and Their Secretions

The nose is one of the initial entry points of inhaled air into the respiratory system. Therefore the epithelial lining cells of the upper respiratory tract are exposed to the highest concentrations of inhaled toxins and debris. It is the anterior nasal glands, along with the goblet cells of the respiratory epithelium (RE) that provide the first line of defence within the airway. The function of these respiratory glands is to secrete mucus into the nasal cavity where it traps airborne pathogens within inspired air, preventing them from progressing to the lower airway tubes and lungs. These mucous secretions also play an important role in warming and humidifying air, preventing the drying out of delicate respiratory tissue. The nose is the principal organ for sense of smell, and it is also believed that the mucus produced by the respiratory glands dissolves odorant molecules to help them be picked up by olfactory stimulation (Getchell and Getchell, 1992). Unlike humans, mice are obligate nasal breathers, therefore the nose and nasal environment of these animals are critical in maintaining respiratory health and homeostasis. For that reason, they provide an ideal model to study respiratory nasal gland development and function.

3.1.2 The Nose

In order to understand the developmental locations and progressions of the anterior nasal glands, the structure of the nose must be understood. In humans and rodents, the nose can be divided into three main areas known as the vestibule, the respiratory region and the olfactory region (Figure 3.1, A). The nasal vestibule is the opening site of the nose and is lined with a stratified squamous epithelium. Moving into the nasal cavity a transition into a RE occurs (Figure 3.1, A). Gross et al. (1982) showed that in mice the RE accounts for 47.5% and 45% of the total surface area of the nasal cavity in 7 week and 16 week old mice respectively. The periphery of the RE stops suddenly and the epithelium becomes olfactory in nature. In the same study the olfactory epithelium (OE) accounted for 45% and 47% of the nasal surface area in 7 week and 16 week old mice respectively (Gross et al., 1982). The primary functions of the RE is to moisten and protect the cavity while the OE houses an enrichment of olfactory receptor neurons, required for the sense of smell (Popp and Martin, 1984; Purves et al., 2004). The RE and OE are supplied with mucosal secretions by goblet cells and

the respiratory submucosal glands, and the Bowman's glands respectively (Bojsen-Moller, 1964; Frisch, 1967).

To appreciate the morphology of the nasal cavity, the capsule can be divided into the medial and lateral walls (Figure 3.1, B and C). The medial wall of the cavity is a simple plane of tissue that covers either side of the cartilaginous nasal septum (Figure 3.1, C). Shelves of bone known as conchae or turbinates curve the lateral wall of the cavity (Figure 3.1, B and C). The most anterior shelf is referred to as the superior concha, the middle shelf as the medial concha while the lower shelf is called the inferior concha (Figure 3.1, B and C). By protruding from the lateral wall, these conchae create channels within the nasal chamber over which air can flow. These channels are known as meatuses and adopt the same name as their overlying concha (Figure 3.1, B and C). Additionally, there are four pairs of connected air filled cavities found in the nose, known as the paranasal sinuses (Figure 3.1, C). The lining of these spaces is continuous with the nasal RE and OE and secretions are drained directly or indirectly into the nose (Figure 3.1, C, black dotted line). The maxillary sinus is the largest of the sinuses and is located lateral to the main nasal chamber (Figure 3.1, C). The frontal sinuses are the second largest of the group and are found above the eyes and between the eyes lie the ethmoidal sinuses (Figure 3.1, C). A fourth pair of sphenoid sinuses is found behind the eyes and nasal cavity. The function of the paranasal sinuses is disputable however it is believed they decrease the weight of the skull as well as warming and humidifying inspired air with their mucosal secretions.

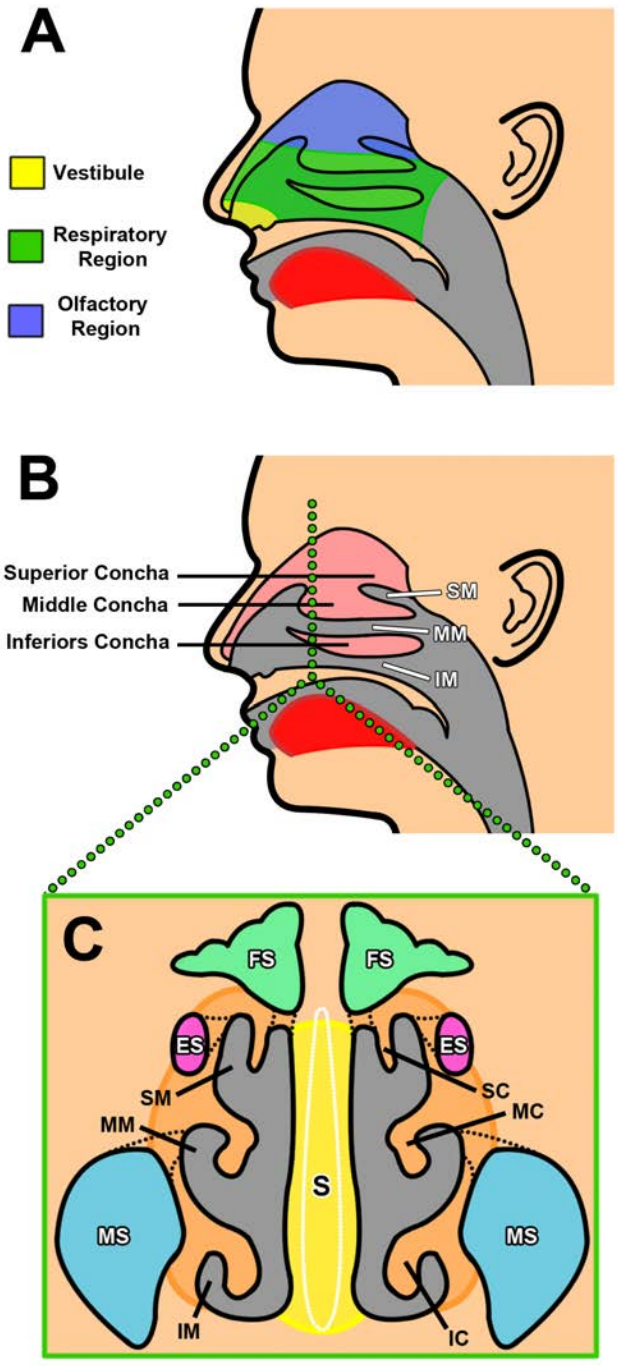

Figure 3.1 Anatomy of the nose and paranasal sinuses.
A) Sagittal view of the three distinct areas of the nose; vestibule, respiratory and olfactory regions. **(B)** Sagittal view of the lateral wall showing the curved concha and the inter-conchal meatuses. **(C)** Frontal section through the nasal chamber showing the position of the medial walls (yellow) on either side of the septum (S). Image shows the location of the superior concha (SC), the medial concha (MC) and the inferior concha (IC) of the lateral wall (orange) and their underlying meatuses. The frontal image also delineates the location the paranasal sinuses. SM=superior meatus; MM=middle meatus; IM=inferior meatus; FS=frontal sinus; ES=ethmoidal sinus; MS=maxillary sinus. Dotted black lines indicated opening of sinuses into nasal cavity found at a more caudal plane.

3.1.3 Morphology of the Anterior Nasal Glands

It has been referenced in the literature that Broman (1921) first described the topography of the anterior nasal glands and created plastic reconstructions of the glands and ducts of rodents (Bojsen-Moller, 1964; Grüneberg, 1971). According to the manuscripts published in the mid-twentieth century, it was Broman (1921) who categorised and named the nasal glands into different groups based on their location and timing of when they first arose (Bojsen-Moller, 1964; Grüneberg, 1971). Although mentioned and reviewed in these early anatomical studies, the work of Broman has been described as "lost in recent literature" (Bojsen-Moller, 1964). Considering this, his primary names and descriptions of the glands have continued throughout the years and his work undoubtedly provided the backbone of future research on anterior respiratory gland development.

3.1.3.1 Lateral Nasal Gland 1 or the Steno's Gland

The lateral nasal gland 1, more commonly called the Steno's Gland, is the largest of the nasal glands (Grüneberg, 1971). The gland is located beneath the wall of the maxillary sinus and releases its product into an extremely long excretory duct, which opens into the nasal cavity near the nasal vestibule. The Steno's gland, analogous to the anterior nasal gland in humans, is classified in some animals as solely serous in nature however in others it is seromucous (Moe and Bojsen-Moller, 1971; Bojsen-Moller, 1967). In dogs the Steno's gland is considered to play a principal role in thermoregulation while in marine birds it is primarily a salt gland (Wells and Widdicombe, 1986; Butler, 2002). Studies in rodents have elucidated that its secretion contains bactericidal proteins indicating an essential role in airway protection (Moe and Bojsen-Moller, 1971).

3.1.3.2 The Lateral Nasal Glands

The lateral nasal glands (LNGs) are found throughout the lateral wall of the nasal chamber. Similar to the Steno's gland they have long ducts that open into the airway lumen close to the nasal vestibule, however, these glands are found within the submucosa of the lateral wall at more caudal locations. Up to 40 lateral nasal glands have been described in rabbits while approximately 20 have been reported in adult mice (Bojsen-Moller, 1964). Further research and descriptive analysis of this subset of glands is extremely lacking.

3.1.3.3 The Medial Nasal Glands

The medial nasal glands (MNGs) are found within the submucosa of the medial wall on either side of the septum. Their long ducts open at rostral locations while their glands progress caudally and are seen anterior to the vomeronasal organ in rodents. These glands have been previously described in the rat, which can have four to five MNGs project into the septal mesenchyme (Bojsen-Moller, 1964). The MNGs have been described as having serous acini by light microscopy (Kerjaschki, 1974).

3.1.3.4 The Maxillary Sinus Glands

The maxillary sinus glands are located anterior and posterior to the maxillary sinus and drain their secretions directly into the sinus cavity through short wide tubules. Investigation of these glands in the rat showed that they are solely serous in nature (Vidić, 1971).

From the literature currently cited, it is evident that interest and investigation into the anterior nasal glands is significantly lacking in recent times. Due to the roles played by the respiratory glands in a number of diseases and nasal conditions, it is crucial we understand their exact involvement and behaviours. Current studies avoid the SMGs of the upper airway however and concentrate more so on those of the tracheobronchial tree. As the anterior SMGs are different in nature, separate exploration of their development and function is imperative.

3.1.4 Mechanisms of Lumen Formation

The morphogenesis of epithelial tubes is a huge field of current research. Strategies used to create hollow epithelial tubes can be species specific and even tissue specific. Epithelial tissue has distinct characteristics such as (A) tight cell-to-cell adhesion, (B) unique inter-cellular junctions, (C) distinct apical-basal polarity and (D) a basement membrane on which the epithelial cells lie (*reviewed in* Andrew & Ewald 2010). When an epithelium undergoes branching morphogenesis, modulations of all these features must be made in order to allow cells to carry out successful organogenesis. One of these modulations is ductal formation, where a hollow tube through which liquid or gas can be transported successfully must be created. There are two main developmental strategies that have been reported to complete tubulogenesis in branched structures.

3.1.4.1 Formation of Tubes with Preformed Lumens

The first method of tubulogenesis is the process by which epithelial tubes elongate with preformed lumens. This combination of epithelial placode invagination and lumen expansion is known as "budding" and occurs during development of the mammalian lung, as described in *Chapter 1.* The same mechanisms can be seen in the developing salivary gland of the fruit fly, *Drosophila melanogaster* (Kerman et al., 2006). During *Drosophila* gland invagination, cells of the gland placode undergo apical constriction. With this process, also referred to as the "purse string model", nuclei of placodal cells relocate to a basal position within the cell, allowing the apical regions of the cell to contract and form wedge-shaped cells (Baker & Schroeder 1967; Ettensohn 1985; Myat & Andrew 2000). This change in cell shape leads to the infolding of the epithelial sheet and a pit is formed. It has also been suggested that this strategy requires increased cell adhesion and changes to the underlying extracellular matrix (Hogan and Kolodziej, 2002). A continual wave of cell-shape change spreads to the more anterior placodal cells, leading to further internalization of these cells. This causes orthogonal elongation of the gland duct, without the occurrence of apoptosis (Myat and Andrew, 2000; Hogan and Kolodziej, 2002).

3.1.4.2 Formation of Tubes from Solid Epithelial Cords

Another method by which lumens form is referred to as 'canalization' and can be seen during mammalian salivary gland development, as outlined in *Chapter 1*, as well as the developing mammary gland (Humphreys et al., 1996; Melnick and Jaskoll, 2000). Following the condensation of unpolarised epithelial cells into a placode, a solid cord of cells extends into the underlying mesenchyme. Usually around the onset of branching morphogenesis, small spaces, or microlumena will begin to form within the epithelial stalk. These spaces then merge later in development to form one continuous lumen. The processes by which these original microlumena, as well as successional lumen formation occurs, are unclear, however contrasting hypotheses suggest the mechanism involves either programmed cell death (PCD) or PCD independent mechanisms.

3.1.4.3 Apoptosis and Lumen Formation

To maintain homeostasis in a multi-cellular organism, a constant balance between cell division and cell death is maintained. To carry out this function, PCD or apoptosis is a fundamental signalling process that occurs in all tissues throughout adult life. It is

also employed during development to help shape newly formed tissues. An example of apoptosis can be seen during limb morphogenesis where large areas of undifferentiated mesodermal cells undergo apoptosis to sculpt out digits in the developing limb (Hurle et al., 1996).

Once PCD is triggered by either external or internal stimuli, a cascade of factors within the cell itself drives the eradication of the cell. These factors are part of either the "intrinsic" pathway triggered by internal stimuli, or the "extrinsic" pathway initiated by external intercellular information (Figure 3.2). The most frequent internal stimulus is irreparable DNA damage, which activates the tumour repressor molecule p53 in the nucleus. P53 translocates into the cytosol and activates the pro-apoptotic Bcl-2 protein Bax (Chipuk et al., 2004). Bax permeabilises the membrane of mitochondria leading to the leaking of apoptotic molecules, principally cytochrome *c,* from the organelle into the cytoplasm (Reed, 1997; Green and Reed, 1998; Schuler et al., 2000) (Figure 3.2). In the cytosol, cytochrome *c* binds to Apoptosis Protease Activating Factor 1 (APAF-1) and inactive Caspase-9 (Zou et al., 1999). The formation of this protein complex causes hydrolysis and the inhibitor domain of Caspase-9 dissociates and Caspase-9 is cleaved (Figure 3.2). This activation of Caspase-9 triggers a cascade of the "effector" Caspases (Caspase-3, 6 and 7), the proteins that are responsible for the cleavage of DNA, destruction of cytoskeletal proteins and consequently the demise of the entire cell (Li et al., 1997; Porter and Jänicke, 1999) (Figure 3.2).

The "extrinsic" apoptotic pathway is triggered by external stimuli such as infection, environmental stresses (e.g. O_2 depletion, cell-to-cell junction detachment), growth factors and hormones. Almost every cell in the body houses Tumor Necrosis Factor Receptors (TNFR) in their cell membrane. A subset of six receptors from this family are known as the "death receptors" and are responsible for triggering apoptosis within the cell following binding with their respective ligands. Fas and TNFR1 are the principal death receptors that bind to their extracellular ligands Fas-L and TNF respectively. Ligand-receptor binding leads to the activation of the common intracellular motif of both Fas and TNFR known as a "death domain" (Itoh and Nagata, 1993). Upon activation of Fas, the cytosolic adaptor protein Fas-associated protein with Death Domain (FADD) is recruited along with the inactive form of

Caspase-8, forming what is known as the "death inducing signal complex" (DISC) (Figure 3.2). When TNFR is activated DISC is formed with the addition of Tumor Necrosis Factor Receptor Type 1-associated Death Domain protein (TRADD). Hydrolysis of the inhibiting region of Caspase-8 occurs, cleaving and activating Caspase-8, which then triggers the Caspase cascade and thus the final stages of PCD (Figure 3.2).

During murine mammary gland development, microlumen within the duct begin to fuse at approximately E18 (Hogg et al., 1983). At this stage peripheral luminal cells remain intact and will become the epithelial lining. Additionally, PCD is seen to begin in excess cells at a distance from the lumen (Hogg et al., 1983). Over the next 24 hours, apoptosis spreads and is seen within the basal cells of the epithelial cord (Hogg et al., 1983). It is suggested that this method occurs to eliminate unnecessary cells within the mammary gland duct, as an epithelial lining of only one-three cells thick is required (Hogg et al., 1983). Apoptosis has also been reported to cavitate the terminal end buds of the mammary gland (Humphreys-Beher, 1996).

It has been suggested that apoptosis plays a similar role during submandibular salivary gland (SMDG) lumen formation, with canalization of microlumen first seen within the main ducts during the *Early Canalicular stage* at E15.5, and identified in the terminal end buds approximately a day later at the *Late Canalicular stage* (Jaskoll and Melnick, 1999). By the *Terminal Bud stage* at approximately E18.5, these microlumen begin to coalesce to from one contiguous lumen (Jaskoll and Melnick, 1999). PCD detection within the epithelium was seen to mirror lumen formation. At E15.5 many apoptotic cells were identified in the main ducts and some within the terminal end buds (Jaskoll and Melnick, 1999). By E17.5, at the *Early Terminal Bud stage*, PCD was more prevalent within the end buds, and apoptotic cells were less prevalent in the main ducts (Jaskoll and Melnick, 1999). In SMDG *in vitro* organ culture, PCD has been detected in the mesenchyme adjacent to the developing gland, while some apoptotic cells were seen within the branching epithelium, in newly forming lumens (Hoffman et al., 2002; Walker et al., 2008; Nedvetsky et al., 2014).

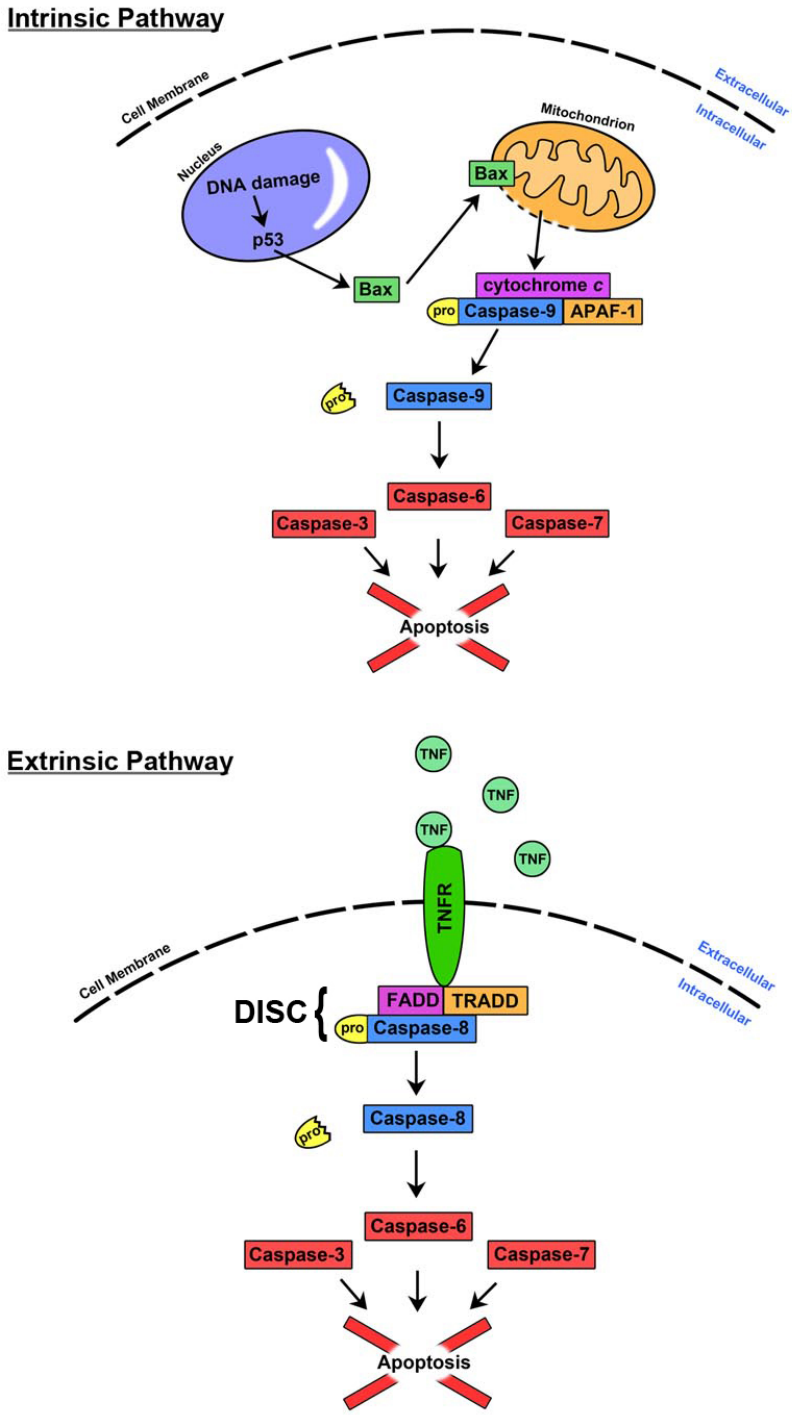

Figure 3.2 The intrinsic and extrinsic apoptotic pathways.
The **intrinsic pathway** is triggered by an intracellular stimulus. This activates pro-apoptotic molecules in the cytosol, such as Bax, which permeabilise the outer membrane of mitochondria. Cytochrome *c* is released into the cell where it binds to APAF-1 and inactive proCaspase-9. Caspase-9 autoactivates by hydrolysis of its inhibiting region. The cleaved Caspase-9 functions in activating the Caspase cascade that recruits Caspase-3, 6 and 7, which are responsible for DNA fragmentation and the destruction of the cell. The **extrinsic pathway** involves activation by an extracellular ligand that binds to a transmembrane death receptor. The DISC within the cell, containing FADD, TRADD and inactive proCapsase-8, is activated. Caspase-8 then cleaves and initiates the Caspase cascade.

3.1.4.4 Non-apoptotic Lumen Formation

The involvement of the nervous system on salivary gland function has long been known (Pavlov, 1906). While it is well established that development and differentiation of epithelial structures is influenced by a number of environmental cues from surrounding mesenchyme and endothelial tissue, more recent research has elucidated a role for the parasympathetic nervous system during salivary gland regeneration (Proctor and Carpenter, 2007) and morphogenesis (Knox et al., 2010; Ferreira and Hoffman, 2013). A recent study demonstrated that the parasympathetic submandibular ganglion (PSG) nerve supply is imperative for both lumen formation and lumen expansion of the SMDG (Nedvetsky et al., 2014). It was described that this method of nerve-induced canalization is independent of PCD mechanisms. Although some apoptotic cells were identified in SMDG lumens, as previously described (Walker et al., 2008), successful lumen cavitation occurred in SMDGs cultured with the pan-caspase inhibitor Z-VAD-FMK (Nedvetsky et al., 2014). Furthermore, E17 salivary glands in *Bax* null mutant mice were phenotypically normal, having undergone successful lumen formation (Nedvetsky et al., 2014). As opposed to PCD hollowing out SMDG ducts and end buds, the findings of this study demonstrated that this process was mediated, at least in part, by the PSG nerve supply. When nerve outgrowth and innervation were inhibited in *in vitro* culture lumen formation was disrupted (Nedvetsky et al., 2014). Inhibition of the neurotransmitter Vasoactive Intestinal Peptide (VIP), and its receptor VIPR1, gave rise to defective luminal cell aggregations, and exogenous VIP protein application caused narrow ducts in SMDG *in vitro* culture (Nedvetsky et al., 2014). Therefore it appears that VIP released by the PSG regulates SMDG cord hollowing.

It has been reported that nerves ensheath the acini of the Steno's gland in both dogs and rats (Bast, 1924; Moe and Bojsen-Moller, 1971), however innervation patterning or lumen formation mechanisms have not been investigated in the developing respiratory glands.

3.1.5 Progenitor Cell Populations

In recent times, research has focused on the role of progenitor cells during development, homeostasis and repair of complex 3D epithelial structures. Considering the constant exposure of the respiratory airways and lungs to airborne pathogens, it is

critical to characterize different stem and progenitor cell niches within respiratory epithelium, to elucidate their roles in airway disease, and to unveil solutions for gene therapy. Compared to other structures such as the skin and intestine (Clayton et al., 2007; Doupe et al., 2012), the lungs have a slow rate of cell turnover. Following injury however, the pulmonary system undergoes rapid repair. To date, research has shown that different populations of progenitor cells may found in distinct regions of the pulmonary system, suggesting that differential niches of progenitors are recruited in the trachea, bronchioles and alveoli (Kim, 2007; Rawlins and Hogan, 2006; Rawlins et al., 2009). This is complimented by the fact that the airway lining changes in a proximal-distal fashion. As outlined in *Chapter 1*, the upper airways have a ciliated pseudostratified epithelium. Within this epithelium lie secretory goblet and Clara cells. Additionally, mitotically active basal cells are found closest to the basement membrane, however unlike epithelial cells, they have no luminal contact. Moving further down the pulmonary system to the bronchi in mice, or the bronchioles in humans, a transition to a simple columnar epithelium with a mixture of ciliated cells, non-ciliated secretory Clara cells, and neuroendocrine cells are found. No basal cells are identified in these distal airways. Finally, the epithelia of the lungs are composed of Type I and Type II pneumocytes.

Advances in lineage tracing techniques have allowed the establishment of possible heterogeneous progenitor cell populations within the airway (Rawlins and Hogan, 2006; Rawlins et al., 2009). For example, using a *Scgb1a1-CreER*™ knock in mouse to trace the lineage of Scgb1a1 positive Clara cells within the mouse lung, it was shown that Clara cells act as long-term progenitors in the distal bronchioles, giving rise to ciliated cells during development and adult homeostasis (Rawlins et al., 2009). In the trachea however, the Clara cells act more so as transit amplifying cells in response to injury, while their long-term progenitor population is composed of Scgb1a1 negative basal cells (Rawlins et al., 2009).

It has been shown in a number of epithelial structures such as the tongue, stomach and skin, that keratin 5 (K5) expression, usually paired with K14 expression, is seen within the most basal undifferentiated cells of complex epithelia, closest to the basement membrane (Rentrop et al., 1986; Schweizer et al., 1988; Lersch and Fuchs, 1988). The keratins are a family of 20 intermediate filament proteins essential for the

construct of the cells cytoskeleton (Fuchs, 1983). In the anterior trachea of mice, K5 is expressed in the basal cells while K14 is detected in specific groups of these cells (Rock et al., 2009, 2010). More recent studies have elucidated that these basal cells are multipotent progenitor cells within the human and mouse airways (Hong et al., 2004; Cole et al., 2010; Rock et al., 2010). Considering this however, little is known of the differentiation of these basal cells, as well as their role in airway disease pathogenesis. Borthwick et al. (2001) showed high K5 promoter activity within the ductal cells of the tracheal SMGs using a K5βgal6000 transgenic mouse. Using lineage tracing analysis, it was elucidated that K5+ basal cells of the tracheal respiratory epithelium gave rise to both secretory and ciliated cells during development (Rock et al., 2009). Additionally the same K5 positive cells gave rise to these cells types during tissue repair after injury (Rock et al., 2009).

3.1.6 Aims of Study

- To delineate anterior nasal gland development and distinguish the temporal localisation of each gland type during both duct elongation and gland branching stages using histological and optical projection tomography methods.

- To culture the nasal glands *in vitro*, to follow their dynamic development.

- To analyse the relationship between lumen formation, programmed cell death and innervation in the anterior nasal glands.

- To investigate possible basal cell progenitor populations within the nasal epithelium and the SMGs during critical developmental stages.

3.2 Materials and Methods

3.2.1 Immunofluorescence Analysis

3.2.1.1 Primary and Secondary Antibody Addition

Paraffin wax sections were dewaxed in three 10 minute washes of Histoclear and rehydrated in decreasing ethanol concentrations at RT (Table 3.1). Tissue underwent one wash in PBS and was put through an antigen retrieval wash of 30 minutes in Tris-EDTA buffer (pH 9.0) at 95°C. Samples were left for 90 minutes to cool down to room temperature (RT). Sections then underwent one 10 minute wash in PBS followed by 20 minutes in PBS with 0.5% Triton® X-100 (Sigma-Aldrich, T9284). Slides were transferred to a lidded moist container known as a humid chamber. To each slide, 150µl of blocking solution (10% goat serum and 1% BSA in PBS with 0.1% Triton® X-100) was added and tissue was blocked for one hour at RT. Sections were incubated overnight at 4°C with appropriate primary antibodies in blocking solution in the humid chamber (Table 3.2). Three one-hour washes in PBS were carried out, followed by a one-hour incubation in the humid chamber with suitable secondary antibody in blocking solution at RT (Table 3.2). Sections then underwent six five-minute washes in PBS in a coplin jar wrapped in tinfoil to omit light. Slides were mounted with Fluoroshield™ with DAPI (Sigma-Aldrich) mounting medium and cover slipped. Slides were put in a dry chamber that omitted all light, and kept at 4°C.

3.2.1.2 Confocal Microscopy

Once the slides were dry, sections were scanned using a Leica TCS SP5 confocal microscope and Leica Application Suite Advanced Fluorescence (LAS-AF) software. Selected sections were scanned using the 10x, 20x or 40x lenses to capture specific stages of gland development. Images were saved in both .lif and .tif formats, and scale bar measurements were set by LAS-AF software. Images were collected as collages and labelled using Adobe Photoshop CS5.1 software and saved in .jpeg format.

Table 3.1 Ethanol concentrations for paraffin wax rehydration for immunofluorescence analysis.

Ethanol Concentration	Time of Wash
100%	10 minutes
100%	10 minutes
100%	10 minutes
90%	10 minutes
70%	10 minutes
50%	10 minutes

Table 3.2 Primary and secondary antibodies used in immunofluorescence studies.

Target Tissue Type	1° Antibody	Primary Antibody concentration	Product Code, Company	Secondary Antibody	Secondary Antibody concentration
Nerves	mouse anti-neurofilament	1:50	2H3-S, DSHB	Alexa-fluor 488 goat anti-mouse	1:500
Epithelial basal /progenitor cells	rabbit anti-cytokeratin 5	1:200	AF138, Covance	Alexa-fluor 568 goat anti-rabbit	1:500
Apoptotic Cells	Rabbit anti-Caspase-3	1:200	9661S, Cell Signaling	Alexa-fluor 568 goat anti-rabbit	1:500

3.2.2 In Vitro Organ Culture

3.2.2.1 Collection of Fresh Tissue

It is very important to imitate a tissue's natural environment *in vitro* to ensure successful growth and development during organ culture. To provide growth factors and hormones, a supportive culture medium is crucial. For *in vitro* organ culture of the anterior nasal glands, a complete culture medium was made up using Advance Dulbecco's Modified Eagle Medium F12 (DMEM F12) (Invitrogen) with added 1% Glutamax™ (Invitrogen) and 1% Penicillin-Streptomycin (Invitrogen) antibiotics.

E14.5 CD-1 embryos were collected (described in *Chapter 2*) and transferred to ice cold culture medium. These ages were chosen as the Steno's gland has elongated and the LNGs are budding at E14.5. Stages after initial bud formation were chosen to

ensure correct location of the nasal glands as buds could be identified under the microscope.

3.2.2.2 Organ Culture Equipment Preparation

Before beginning the culturing technique all instruments (scissors, forceps, tungsten wire) were cleaned thoroughly with 70% ethanol in dH_2O and allowed to dry at RT. Instruments were then sterilised in a Germinator 500™ for approximately 30 seconds and allowed to cool at RT before using. Throughout the culturing process, these steps were repeated to ensure instrument sterility.

Organ culture dishes were then prepared. These consisted of a Falcon™ central well organ culture dish (BD-*Falcon 35-3037*) containing 2mls of autoclaved H_2O in its most outer well and 1ml of DMEM-F12 in its central well. An autoclaved metal grid, with a central hole removed, was then placed on top of the central well. Lids were placed on the culture dishes while tissue was being prepared.

3.2.2.3 Tissue Dissection and Culturing

A rostral-caudal incision, using a tungsten needle, was made through the mouth between the maxilla and the mandible (Figure 3.3, A). This isolated the nasal region, eyes and anterior brain from the rest of the embryo. Following this, brain tissue was removed and the remaining tissue was placed, palatal shelf down, on a clean mounting disk (Figure 3.3, B). Excess medium was removed from the disk using filter paper. The mounting disk was then placed on the table of a McIlwain tissue chopper (MTC/2, Mickle Laboratory Engineering). With the blade force set to maximum, tissue was then cut into sagittal 300μm thick sections using the chopper (Figure 3.3, C) (Alfaqeeh and Tucker, 2013). Tissue slices were then immediately transferred to a petri dish containing pre-chilled medium and observed carefully under a Leica MZFiii dissection microscope. For the Steno's gland, complete slices containing the Steno's duct were chosen for culture (Figure 3.4, A). This was decided upon as the Steno's gland duct migrates through a large mesenchymal area of the middle concha and the whole duct was attempted to be isolated (Figure 3.4, A). With the culture of LNG buds, the middle conchal lip of tissue, of which the LNG buds arise, was dissected and kept for culture (Figure 3.4, B). This conchal lip was chosen, as it contains the exact epithelium of which the LNGs bud from, therefore other irrelevant tissue could be discarded (Figure 3.4, B).

Tissue sections were carefully transferred to small pieces of nucleopore filters (VWR) (Figure 3.4, C). Approximately three sections of tissue were placed on each filter and adequate space between each section was ensured. Filters were then placed on top of metal grids within organ culture dishes, allowing underlying medium to gently touch the filter (Figure 3.4, C). This ensures tissue is nourished by the underlying medium but not immersed in the liquid itself. Lids were put back on and dishes were placed in a 5% CO_2/95% O_2 Nuaire™ DH Autoflow-CO_2 Air-Jacketed incubator. The dishes were then incubated for four days at 37°C. Dishes were removed from the incubator every 24 hours to take pictures at RT. Tissue sections were photographed with a Leica DFC300 Fx camera, and placed immediately back in the incubator after each photo was taken.

3.2.3 Optical Projection Tomography (OPT)

Tissue mounting and OPT optics were carried out by Dr. Alistair Edgar (Craniofacial Development and Stem Cell Biology, King's College London). Whole head samples from E17.5 CD1 mice were fixed overnight in 4% PFA at 4^{o}C. Samples underwent two 30 minutes washes in PBS followed by permeabilisation in 0.1% Triton in PBS for 3 hours, rocking at RT. Heads were equilibrated in PBS, embedded in 1% low-melting point agarose (Invitrogen) and glued on magnetic aluminium mounts with ethyl 2-cyanoacrylate. Solidified agarose surrounding samples was cut at sharp angles to remove any excess gel. Samples were then dehydrated in 100% methanol and cleared in a mix of one-part benzyl alcohol to two-parts benzyl benzoate (BABB).

Specimens were imaged in a Bioptonics 3001 OPT scanner (Bioptonics, Edinburgh, UK) at a pixel size of 3.2 μm. Single images were acquired at 0.9^{o} intervals. White light shadow and fluorescence emission images were collected by a CCD camera. Three-dimensional (3D) reconstructions were generated using N-Recon Software (Skyscan) and channel overlays were rendered using Bioptonics Viewer. Rendered frames were concatenated into movie clips using QuickTime Pro (Apple). Epithelial autofluorescence was used as a means to identify ducts and glands in 3D videos.

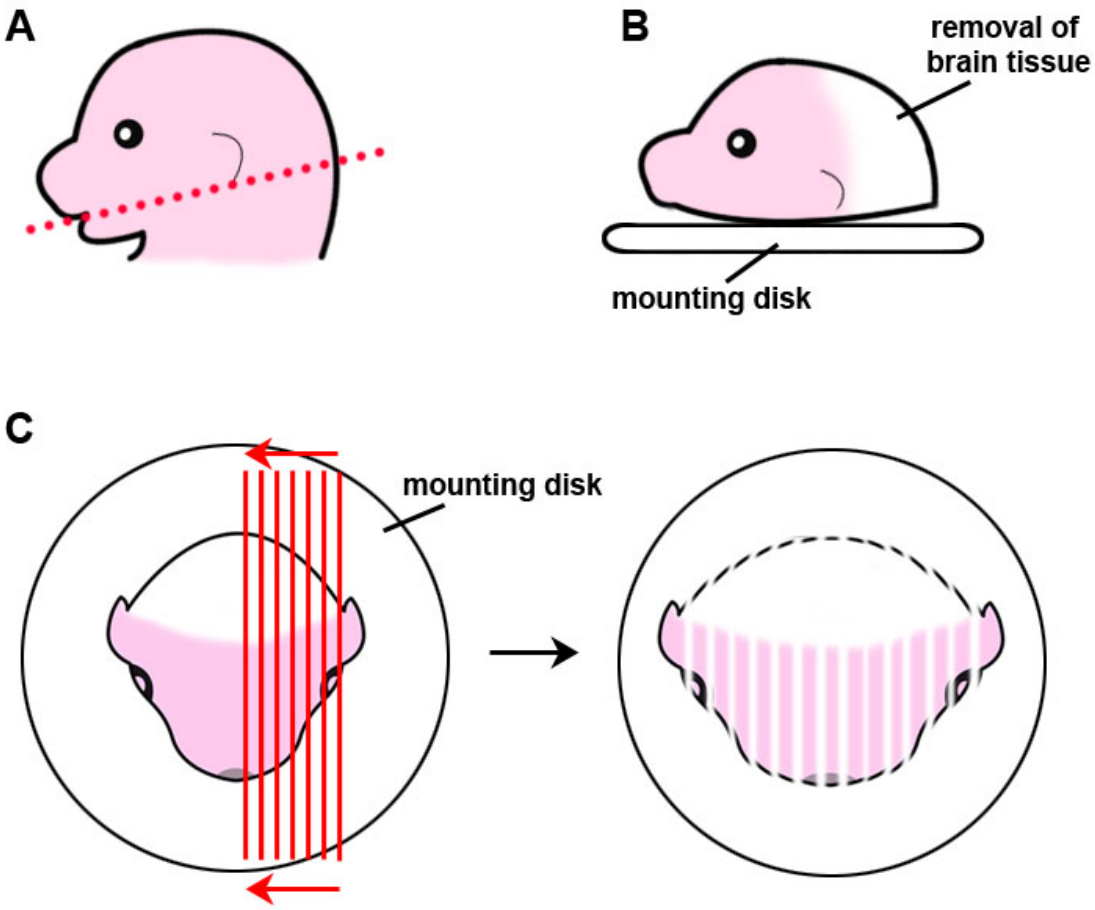

Figure 3.3 Dissection and tissue sectioning of E14.5 mouse heads for *in vitro* organ culture of anterior nasal glands.
(A) The head of freshly collected embryos is dissected (along red dotted line), isolating the maxilla and nasal region. **(B)** Brain tissue is removed and the remaining anterior head is placed on a chopping mounting disk, with the palatal shelf facing down. **(C)** Using a tissue chopper, tissue is sectioned into 300μm sections. These sections are then inspected and gland buds identified. Appropriate sections are then chosen and trimmed for culture.

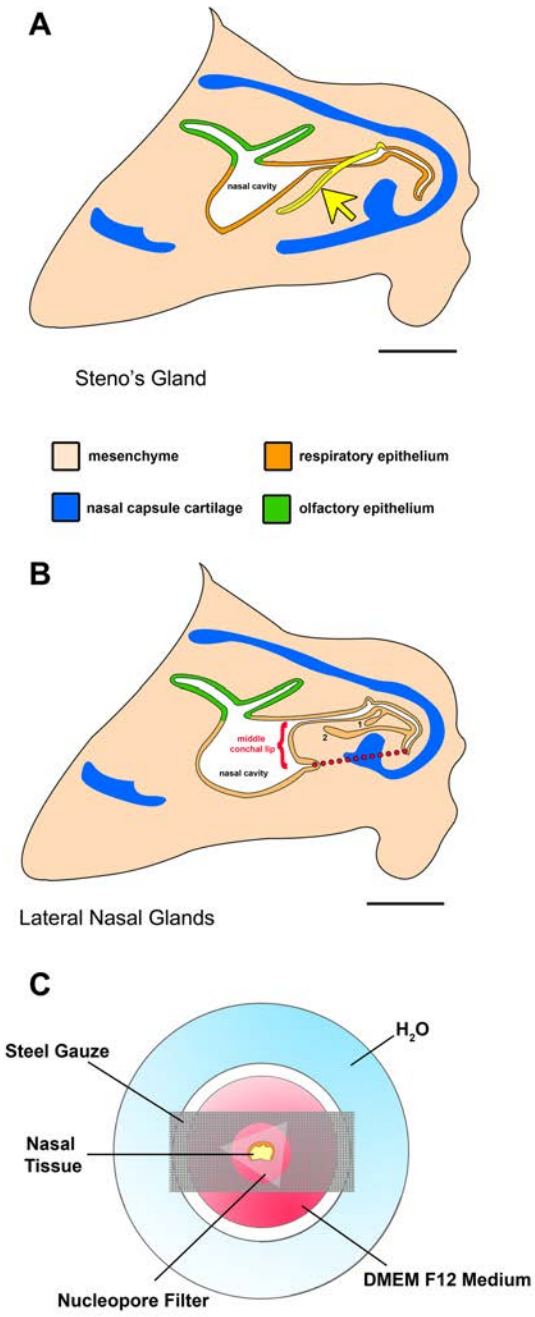

Figure 3.4 Isolated nasal tissue sections and culturing method for E14.5 anterior nasal glands.

(A) Illustration of chosen nasal section for Steno's gland duct (yellow) organ culture. As the Steno's duct moves through a large plane of the nasal region, whole 300µm sections were cultured to follow its development. **(B)** Appearance of nasal sections containing the elongating gland buds of LNG2 (2) and LNG3 (3). From this, the protruding lip of tissue jutting from the middle concha, of which the LNG buds are located, was dissected (red dotted line) and cultured. (**C)** Central well slice organ culture method used to culture nasal glands *in vitro*. Isolated tissue is placed on a nucleopore filter, which is suspended above a bath of DMEM-F12 medium by a piece of sterile steel gauze. The outer well of the culture dish contains autoclaved H_2O, to ensure tissue does not dry out during incubation period. Scale bar = 500µm.

3.3 Results

3.3.1 Anterior Nasal Gland Development

3.3.1.1 Positioning of the SMGs Within the Nasal Region

The anterior nasal glands have long ducts that open close to the nares but their distal branched glands are located in more caudal heterogeneous locations at the back of the nasal cavity. Considering this, we investigated the anterior nasal glands in 3D using an OPT approach of late stage E17.5 CD1 embryonic heads (n=3), to understand the layout and morphology of these glands. It was difficult to visual glands in the whole head due to their location deep within the nasal capsule (Figure 3.5, A), although the MNGs could be observed when viewed down the cranial midline (Figure 3.5, B and C). We therefore turned to analysis of sagittal frames collected through the entire head by OPT (Figure 3.6). Using this method, glands could be followed from their opening locations, along their ducts and eventually to their distal branched gland (Figure 3.6). Having established the general layout of the glands by OPT we could then turn to histological methods to further understand the pattern of nasal gland development.

3.3.1.2 Steno's Gland Development

Between E12.0 and E12.5 the Steno's duct buds from the respiratory epithelium anterior (REA) on the septal side at the nasal vestibule (n=5) (Figure 3.7, A-D). The budding of the duct occurs as the pseudostratified REA dips inwards and invaginates into the underlying mesenchyme (Figure 3.7, A-D). As the bud arises, an indentation in the REA is formed (Figure 3.7, C-D). At E13.5 duct elongation proceeds over the superior nasal meatus and distally extends through the mesenchyme of the middle concha (n=4) (Figure 3.7, E-H). The REA indentation continues as the Steno's duct lumen, simultaneously with the growing duct. A day later at E14.5, the distal tip of the duct has reached the mesenchyme below the respiratory epithelium of the maxillary sinus cavity (n=4) (Figure 3.7, I-L). At this location, duct elongation ceases and the Steno's gland begins to branch distally over the next 24 hours (Figure 3.7, J - red brackets).

At E15.5 the extending gland branches and end buds were apparent (n=4) (Figure 3.8, A-C). Branching of the Steno's gland continued over the next 3 days. The first sign of acinar cell differentiation was observed at E16.5 (n=3) (Figure 3.8, D-F). Alcian blue

stained mucus was evident in some acinar cells of the developing gland as well as within the lumen of the more proximal Steno's duct (Figure 3.8, inset image F). Continual branching proceeded through to E17.5, when the Steno's gland is observed to be much larger and acini more numerous (n=6) (Figure 3.8, G-I). At this stage the majority of acinar cells were now producing mucus as indicated by Alcian Blue staining in the gland (Figure 3.8, G-I).

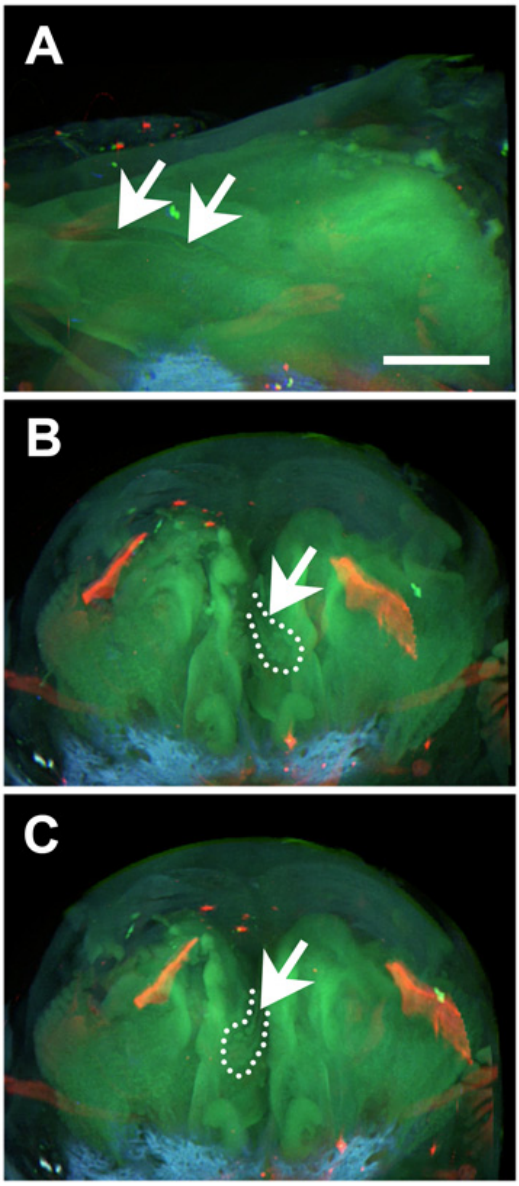

Figure 3.5 Morphological analysis of the anterior nasal glands using 3D OPT.
(A) Some nasal gland ducts are observed in the sagittal view of the 3D E17.5 mouse, however they are difficult to identify to which subset of glands they belong. The medial nasal glands can be identified when viewing down the midline of the embryonic head on both the right (B) and left (C) side of the nasal septum. Scale bar = 200μm.

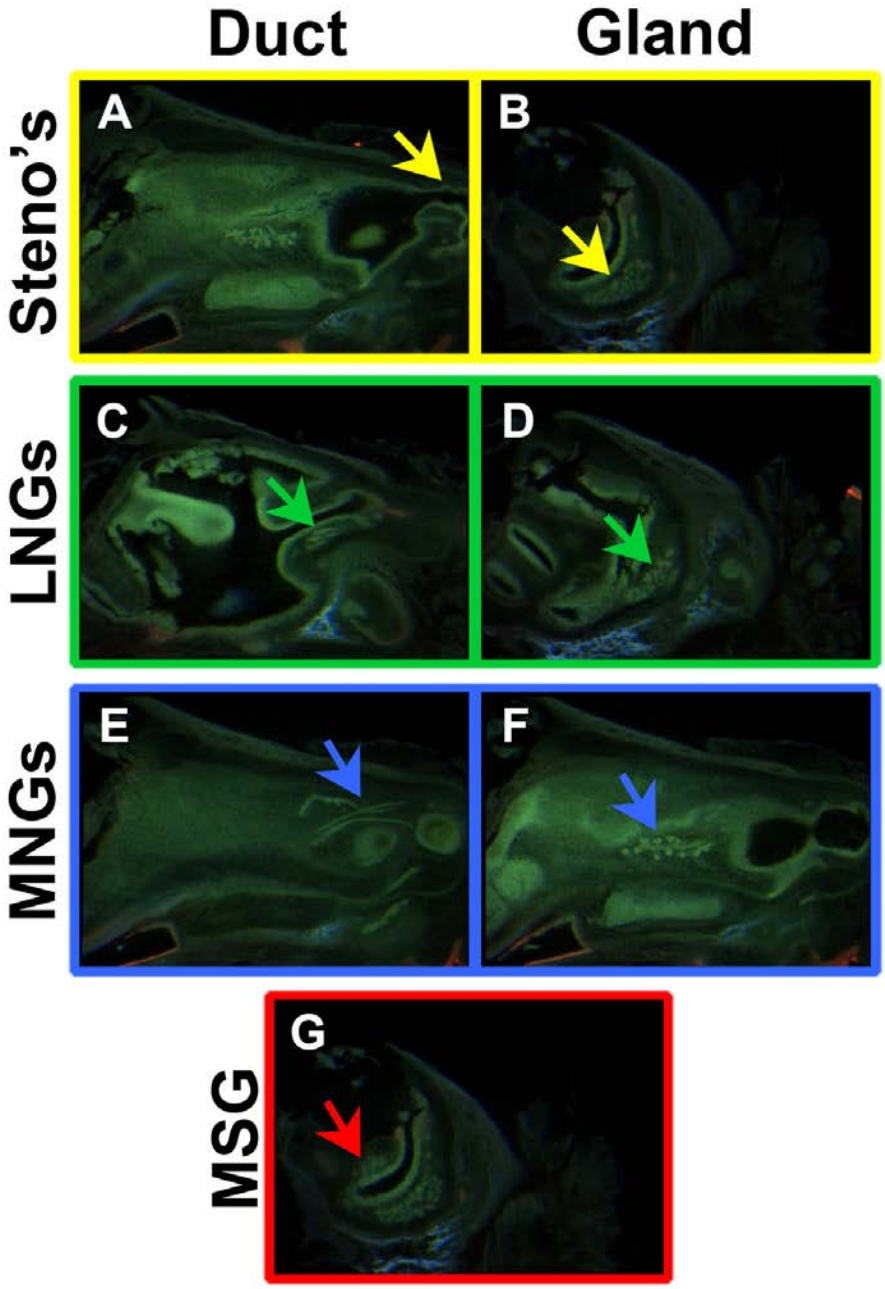

Figure 3.6 Morphological analysis of the anterior nasal glands using single sagittal frames of E17.5 heads by OPT.
(A) The Steno's duct opening located in the rostral nasal regions close to the nares, and (B) the Steno's gland, found more caudally beneath the maxillary sinus. (C) The ducts of LNG2, LNG3 and LNG5 extend in parallel to the nasal cavity with their glands branching (D) above the Steno's gland. The MNG ducts (E) and glands (F) are observed within the mesenchyme of the nasal septum. (G) The MSG branches close to the maxillary sinus.

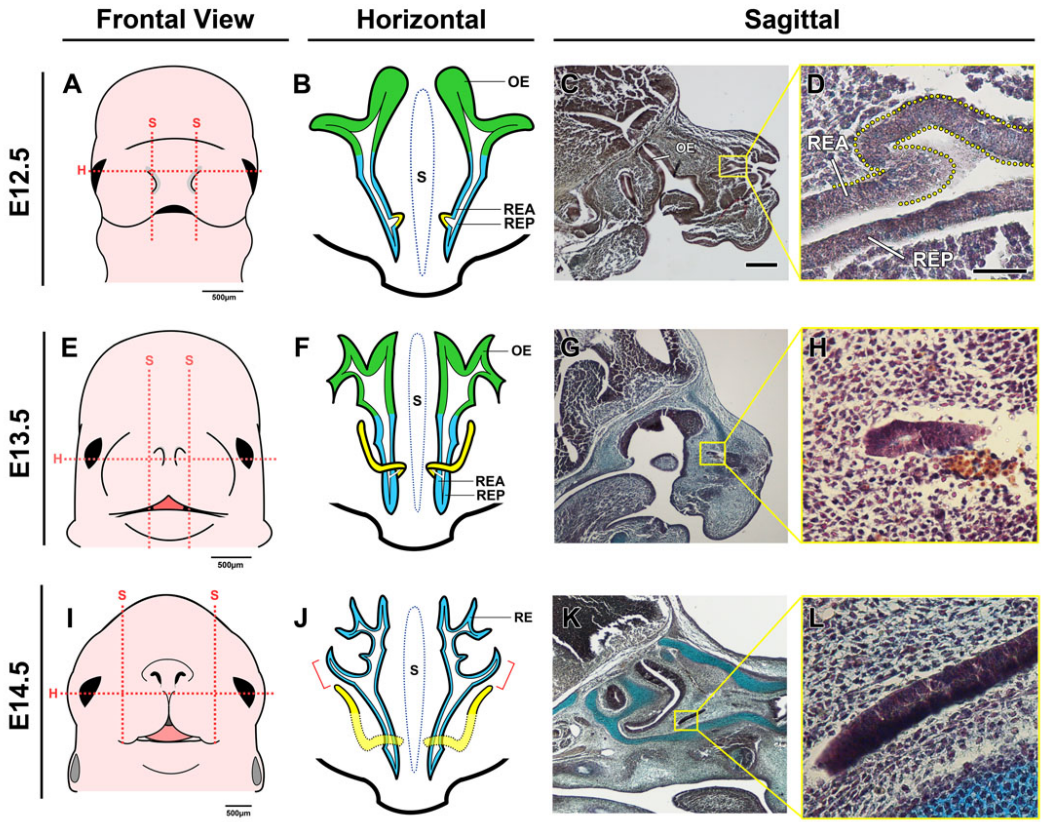

Figure 3.7 Steno's duct elongation.
(A-D) The epithelial budding of the Steno's duct is seen between E12.0 and E12.5 from the respiratory epithelium anterior (REA). (E-H) By E13.5, the Steno's duct elongates over the nasal cavity and caudally extends through the mesenchyme of the medial concha. (I-L) By E14.5 the distal tip of the Steno's duct has reached the mesenchyme beneath the maxillary sinus to the location of where the Steno's gland will branch (red bracket). C,G,K scale bar = 300μm; D,H,L scale bar = 500μm.

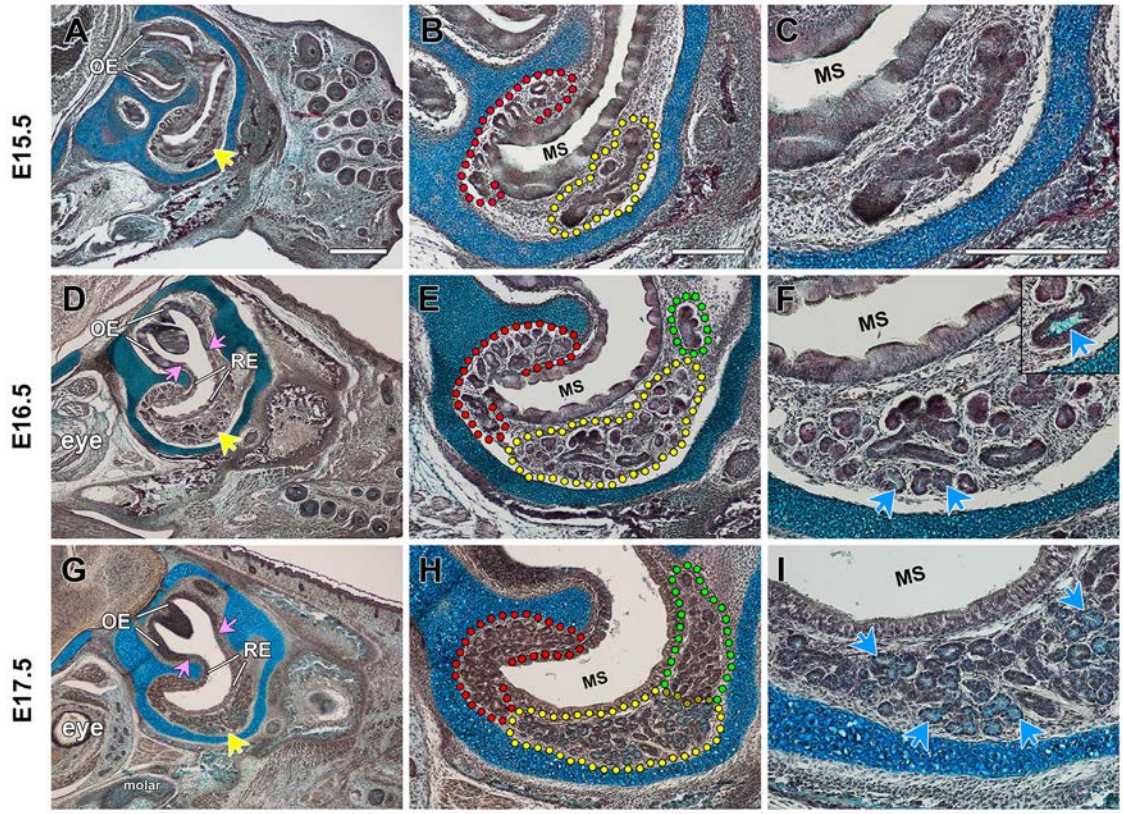

Figure 3.8 Branching of the Steno's gland.
(A-C) The Steno's gland begins to branch from the Steno's duct between E15.0 and E15.5. The first signs of end buds are seen at E15.5. (D-F) Further branching continues and end buds have begun to differentiate into acini by E16.5. Mucus production is visible in some acinar cells (blue arrows) and inside the Steno's Duct (inset image F). (G-I) By E17.5 the Steno's gland is continually branching and acinus differentiation is well established with most acinar cells producing mucus (blue arrows). Respiratory epithelium (RE); olfactory epithelium (OE); maxillary sinus cavity (MS); Steno's gland (yellow arrows and dotted line); MSG (red dotted line); LNG2 (green dotted line). Division of RE to OE shown by pink arrows. A,D,G scale bar = 500μm; B,E,H scale bar = 250μm; C,F,I scale bar = 250μm.

3.3.1.3 Lateral Nasal Gland Development

In this study four LNGs, LNG2-LNG5, were identified to bud, elongate and branch during embryonic stages. All the LNGs budded from the respiratory epithelium posterior (REP) that covers a lip of tissue that protrudes from the rostral end of the middle concha (Figure 3.9). LNG2 was the first to undergo bud initiation between E13.5 and E14.0 from the REP at the nasal vestibule closest to the nares (Figure 3.9 and Figure 3.10 B-D). Unlike the Steno's gland duct, which dips into the underlying mesenchyme forming a dent in the REA, the budding of LNG2, and all the LNGs, involved the invagination of a solid swelling of cells from the REP into the mesenchyme. At E14.5, LNG2 had caudally extended as a solid cord of cells through the mesenchyme of the middle concha (Figure 3.10, F-H). At this stage LNG3 was observed to be at the late bud stage, having extended slightly from the REP at a location anterior to the distal tip of the extending LNG2 duct, and just beneath the opening of the Steno's duct into the airway lumen through the REA (Figure 3.9 and Figure 3.10, F-H). Additionally at E14.5, LNG4 and LNG5 were observed to be budding from the REP covering the most rostral side of the middle concha, and caudal to the distal end of the LNG2 duct respectively (Figure 3.10, F-J).

By E15.5, the duct of LNG2 had reached its final destination beneath the maxillary sinus, above the branching Steno's gland (Figure 3.11, A-C). The duct of LNG3 had elongated parallel to that of LNG2, with its distal tip found rostral to the end of the arrested LNG2 duct (Figure 3.11, A-C). LNG4 had elongated posteriorly through the middle concha and its distal tip had emerged in the mesenchyme below the enclosing cartilage of the nasal capsule (Figure 3.11, D-E). The LNG5 duct had elongated caudally through the middle concha and arrests rostral to the ends of LNG2 and LNG3 (Figure 3.11, F-G). LNG5 sat adjacent to a curve in the nasal cartilage, which shall be referred to as the nasal cartilage grove.

By E16.5, LNG2 had branched distally above the Steno's gland, showing the formation of end buds (A-C). The beginning of lumen formation within the acini of LNG2 was apparent at this stage (Figure 3.12, C – white arrows). No mucus production was evident in acinar cells of LNG2 at this stage. The distal tip of LNG3 duct had reached the caudal end of the middle concha, where it was found lying rostral to the branching LNG2 (Figure 3.12, A-C). LNG3 had begun branching

morphogenesis as the first signs of end buds were observed (Figure 3.12, C – green arrows). LNG4 was at a similar stage of development with the formation of end buds noted at its distal end below the nasal cartilage capsule (Figure 3.12, D-F). The duct of LNG5 had elongated through the middle concha beneath the respiratory epithelium, parallel to the ducts of LNG2 and LNG3, and had arrested close to the location of the nasal cartilage groove, where it began branching over the next 24 hours (Figure 3.12, G-I).

By E17.5, LNG2 had undergone extensive branching and cells had arranged into distinct acini (Figure 3.13, A-C). The distal gland of LNG3 had also undergone similar branching and clear lumens were identified within acini (Figure 3.13, A-C). No cellular differentiation was evident at E17.5 in both the LNG2 and LNG3 as no mucus staining was detected by Alcian Blue staining. LNG4 had formed numerous branches and terminal end buds and cavitation had begun within acini (Figure 3.13, D-F). LNG5 had begun to form distal epithelial gland buds close to the nasal cartilage grove and lumen formation had progressed from the duct to acini (Figure 3.13, G-I).

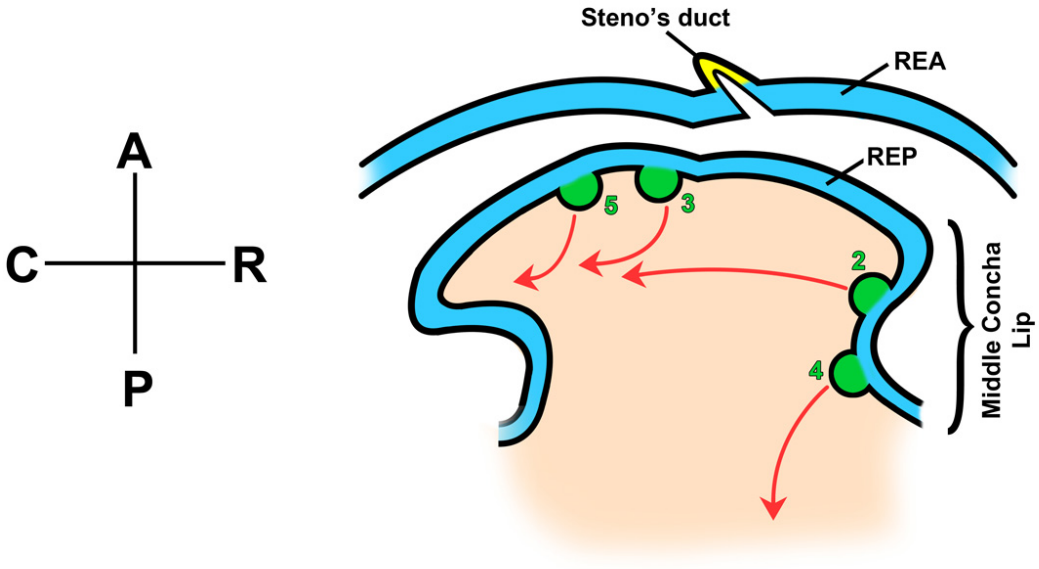

Figure 3.9 Budding locations of the lateral nasal gland ducts from the protruding lip of the middle concha.
The LNG2 bud is first seen at E13.5 arising from the REP at the most rostral area of the conchal lip. It will extend caudally though the middle concha as development continues. At E14.5, LNG3 arises from the anterior area of the lip, underneath the opening of the Steno's duct through the REA, and will extend caudally adjacent to the duct of LNG2. At E15.5, LNG4 initiates below the origin of the LNG2 and extends posteriorly through the mesenchyme of the concha where it will eventually branch beneath the nasal cartilage capsule, anterior to the palatal shelf. LNG5 also initiates at E15.5, where it will elongate adjacent to the ducts of LNG2 and LNG3. Gland buds (2-5) shown in green, direction of future extending duct shown by red arrows. Schematic is taken at a sagittal view. Axis describes anterior (A), posterior (P), rostral (R) and caudal (C).

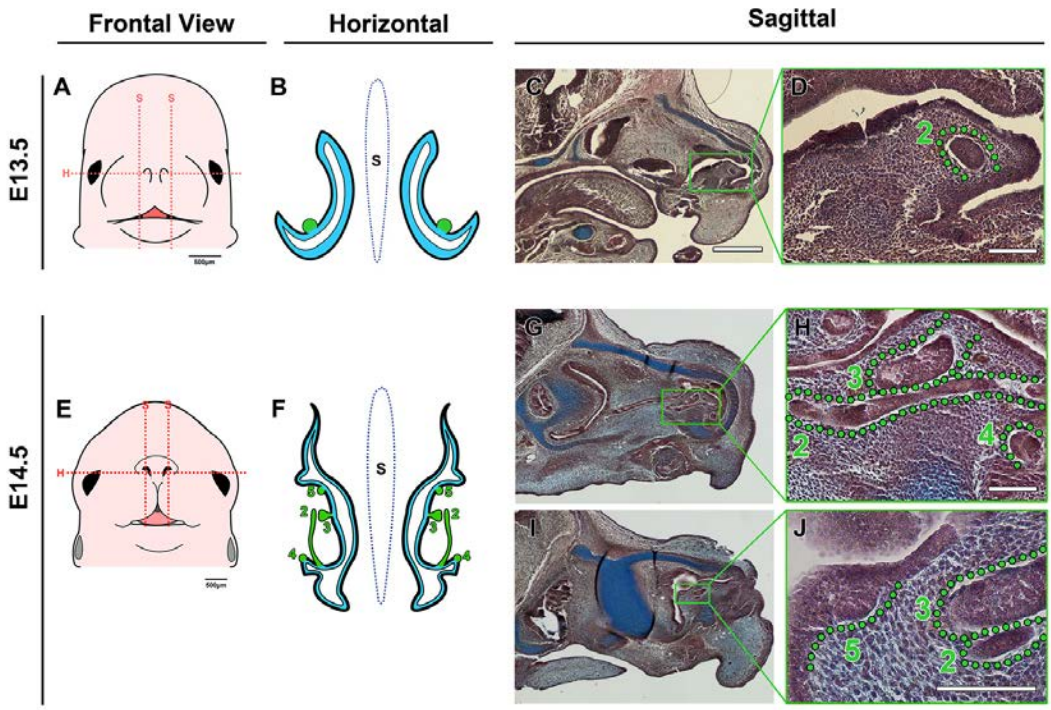

Figure 3.10 Lateral nasal duct elongation during E13.5 and E14.5 of development.
(A) Sagittal (S) and horizontal (H) planes through an E13.5 mouse head showing the location of the LNG2 bud. **(B)** Horizontal schematic representation of LNG2 budding from the middle conchal lip. **(C)** Sagittal histological section showing the location of the middle conchal lip and the LNG2 bud in the nasal region. (**D)** The epithelial bud of LNG2 at E13.5. **(E-F)** Schematics showing location and appearance of the elongated LNG2 and the budding LNG3-5 at E14.5. **(G-H)** At E14.5 the LNG2 has elongated caudally as a solid stem. LNG3 has budded and begun to elongate and LNG4 is seen at a slightly earlier budding stage. **(I-J)** LNG5 is at its initial bud formation stage a E14.5. C,G,I scale bar = 500μm; D,H,J scale bar = 100μm.

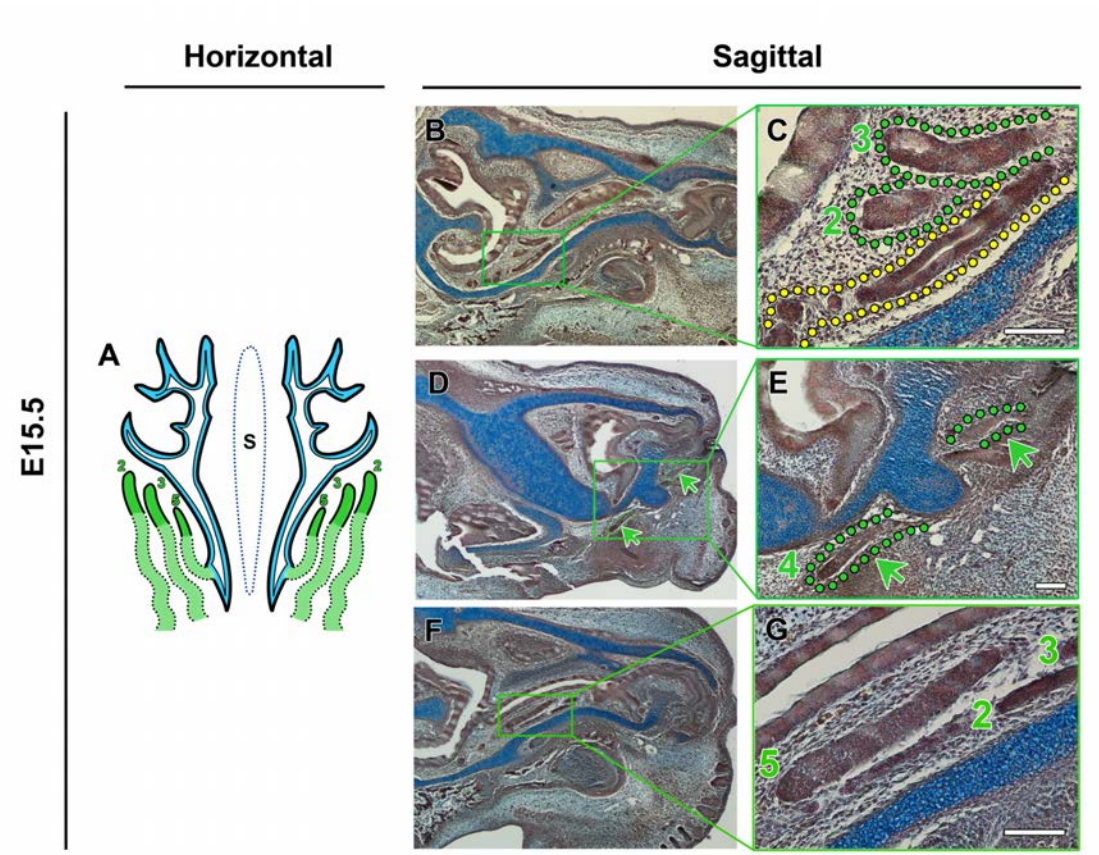

Figure 3.11 Lateral Nasal Gland duct elongation at E15.5.
(A) Schematic showing the progression of the LNGs by E15.5. **(B-C)** A sagittal section shows the distal tips of LNG2 and LNG3 ending within the mesenchyme above the branching Steno's gland (yellow). **(D-E)** LNG4 has elongated posteriorly with its distal tip emerging below the nasal cartilage capsule. **(F-G)** LNG5 has elongated parallel to the ducts of LNG2 and LNG3 however the end of this duct is found at a more rostral location near the cartilage groove.

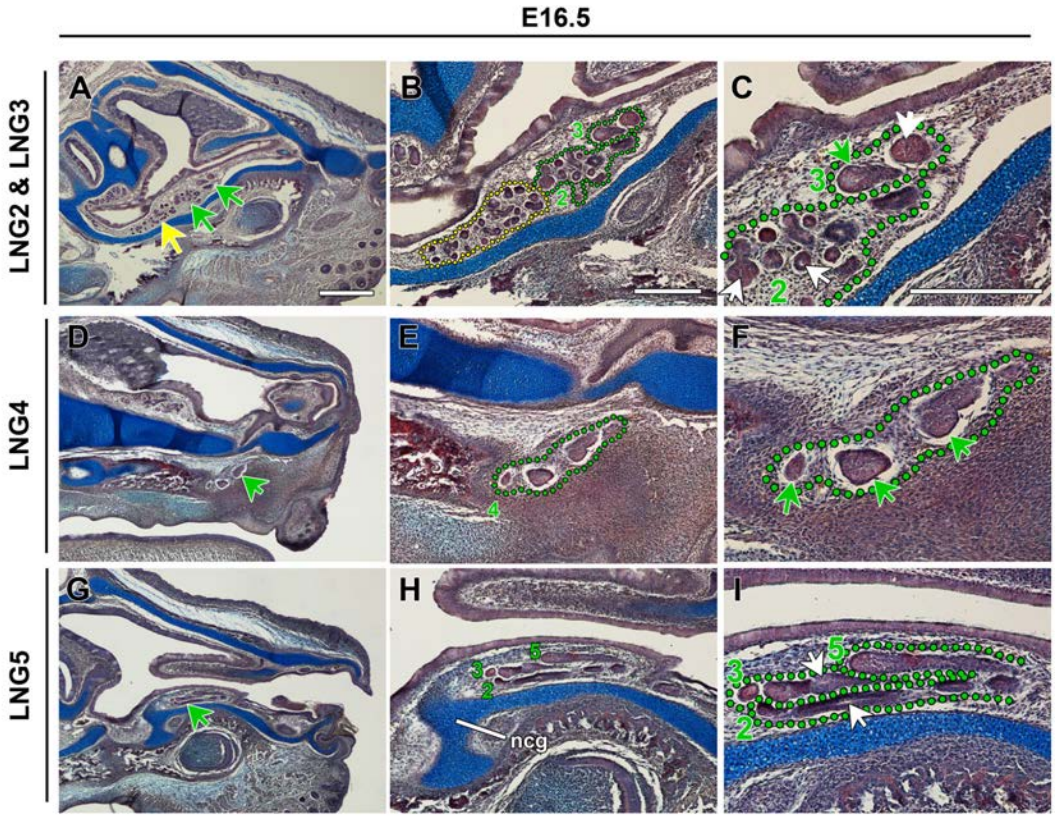

Figure 3.12 Onset of Branching of the LNGs at E16.5.
At E16.5 the LNGs begin branching of their distal glands. **(A-C)** LNG2 is the first to undergo branching between E15.5 and E16.5. At E16.5 many terminal end buds are apparent and cavitation has begun within the gland acini (**C** - white arrows). LNG3 has also begun to branch at E16.5 as seen by the appearance of end buds (**C** – green arrows). **(D-F)** At E16.5 the onset of branching of the LNG4 beneath the nasal capsule is evident (**F** – green arrows). (**G-I**) The distal tip of LNG5 has not begun to branch at E16.5. A clear lumen is seen in the ducts of LNG2 and LNG3 at this stage (**I** – white arrows). **A,D,G** scale bar = 500µm; **B,E,H** scale bar = 250µm; **C,F,I** scale bar = 250µm.

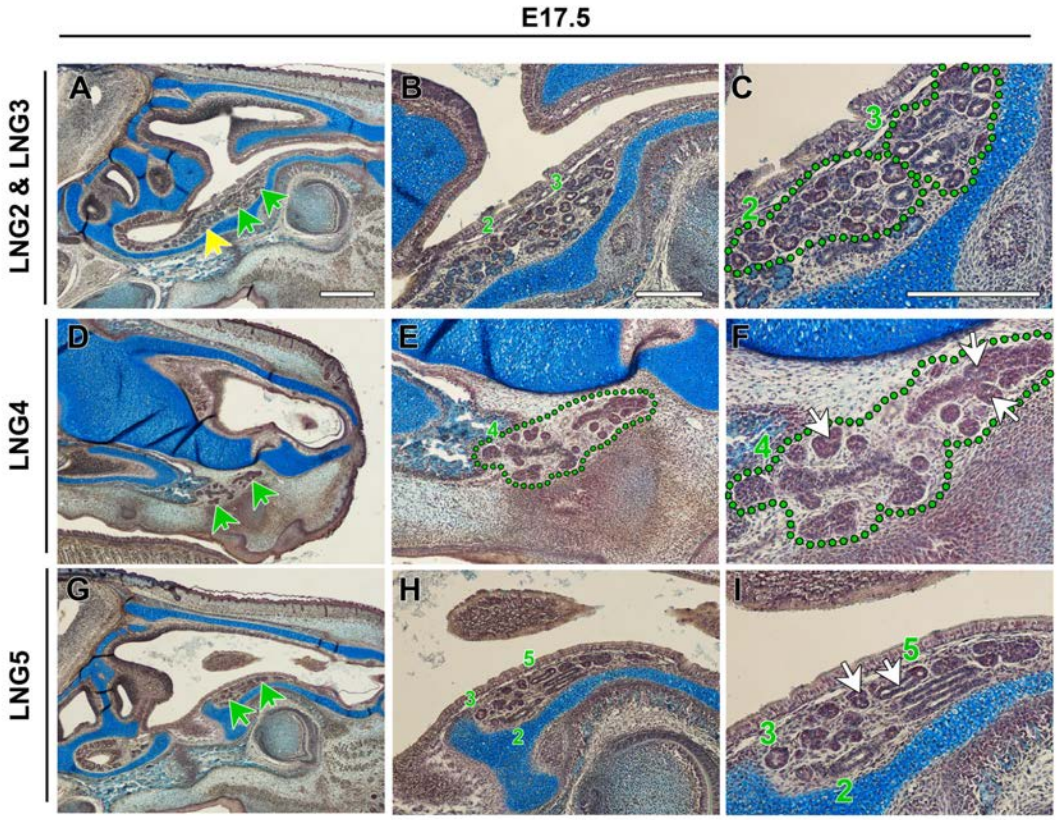

Figure 3.13 Branching of the LNGs at E17.5.
At E17.5 all the LNGs are seen to have undergone branching of their distal glands. (**A-C**) LNG2 and LNG3 have branched and formed distinctive acini with lumens. (**D-F**) LNG4 has formed branches and terminal end buds and lumen formation has just begun within acini. (**G-I**) LNG5 has also begun to branch with a clear lumen seen within its duct and lumen formation at its initial stages within acini. **A,D,G** scale bar = 500µm; **B,E,H** scale bar = 250µm; **C,F,I** scale bar = 250µm.

3.3.1.4 Medial Nasal Gland Development

Medial nasal gland (MNG) development was easier to follow compared to that of the LNGs. All MNGs budded from the respiratory epithelium covering either side of the nasal septum of the medial wall and elongated and branched within the mesenchyme of the septum (Figure 3.14, A-R). MNG1 and MNG2 were the first to bud between E14.0 and E14.5. At E14.5 ducts of these two medial glands had elongated (Figure 3.14, A-F). By E15.5 these ducts had elongated into the central area of the septum while MNG3 had budded and elongated to the midline of MNG1 and MNG2 (Figure 3.14, G-L). Through another plane of mesenchyme it is clear that branching of MNG1 had begun by E15.5 (Figure 3.14, inset image L). Branching had progressed by E16.5 in MNG1 and end bud formation was also underway in MNG2 (Figure 3.14, M-O). MNG3 had elongated adjacent to the ducts of MNG1 and MNG2 at E16.5 (Figure 3.14, M-O) and began its branching over the next 24 hours. At E17.5, MNG1, 2 and 3 had all branched, with branches and terminal end buds all crossing over one another (Figure 3.14, P-R). MNG4 had also elongated and begun its branching at E17.5, indicated by the presence of end buds (Figure 3.14, P-R).

3.3.1.5 Maxillary Sinus Gland Development

The maxillary sinus glands budded and branched from the respiratory epithelium at both the anterior and posterior walls of the maxillary sinus. They did not have a long gland duct like the other anterior nasal glands, they rather branched within the mesenchyme close to the epithelium. The anterior and posterior sinus glands underwent the same developmental patterning so for expediency the development of only the posterior MSG will be explained. At E14.5, no evidence of a MSG was seen (Figure 3.15, A-C) however by E15.5 branching of the MSG was apparent close to the respiratory epithelium (Figure 3.15, D-F). At this stage the MSG was observed to invaginate into the mesenchyme with preformed lumens within the branching epithelium. Branching of the MSG epithelium continued over the next two days of embryonic development with lumens constantly present within the end buds (Figure 3.15, G-L).

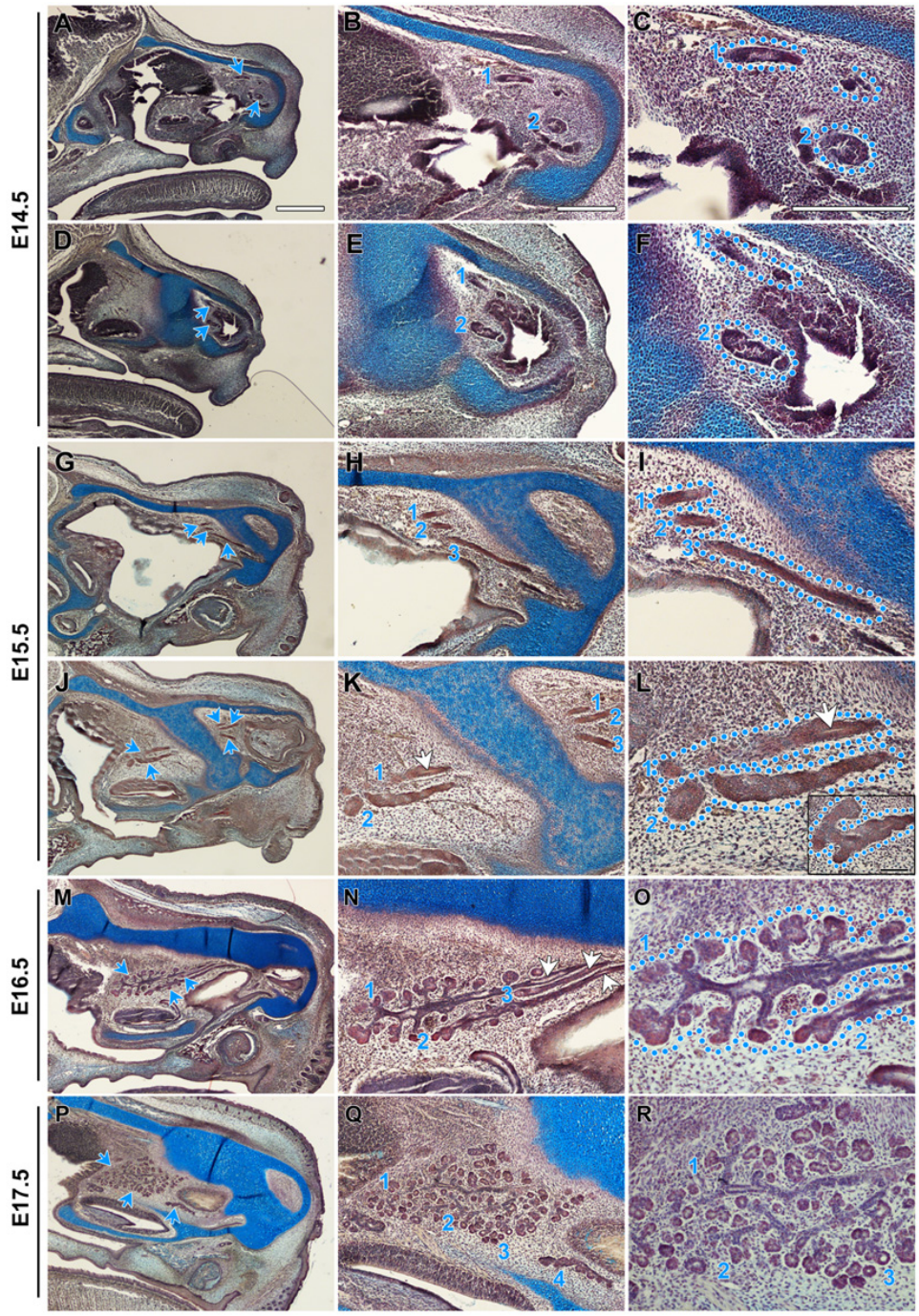

Figure 3.14 Medial nasal gland development.
(**A-F)** The development of the medial nasal glands begins between E14.0-E14.5 with the budding and elongation of the ducts of MNG1 and MNG2. (**G-L**) The MNG1 and MNG2 ducts elongate to the central septal area by E15.5 and branching has initiated at the distal tip of MNG1 (inset image L). MNG3 has also budded and elongated, with its distal end adjacent to the midline of the MNG1 and MNG2 ducts (G-I). (**M-O**) Branching of MNG1 has progressed by E16.5 with an array of branches and terminal end buds apparent at this stage. MNG2 has also begun branching. The distal tip of MNG3 has extended close the branching ends of the other MNGs. (**P-R**) Branching continues in all the MNGs in the central region of the septum. MNG4 has emerged by E17.5 has an elongated duct and the onset of branching has begun. **Column 1** scale bar = 500μm; **Column 2 and 3** scale bar = 250μm.

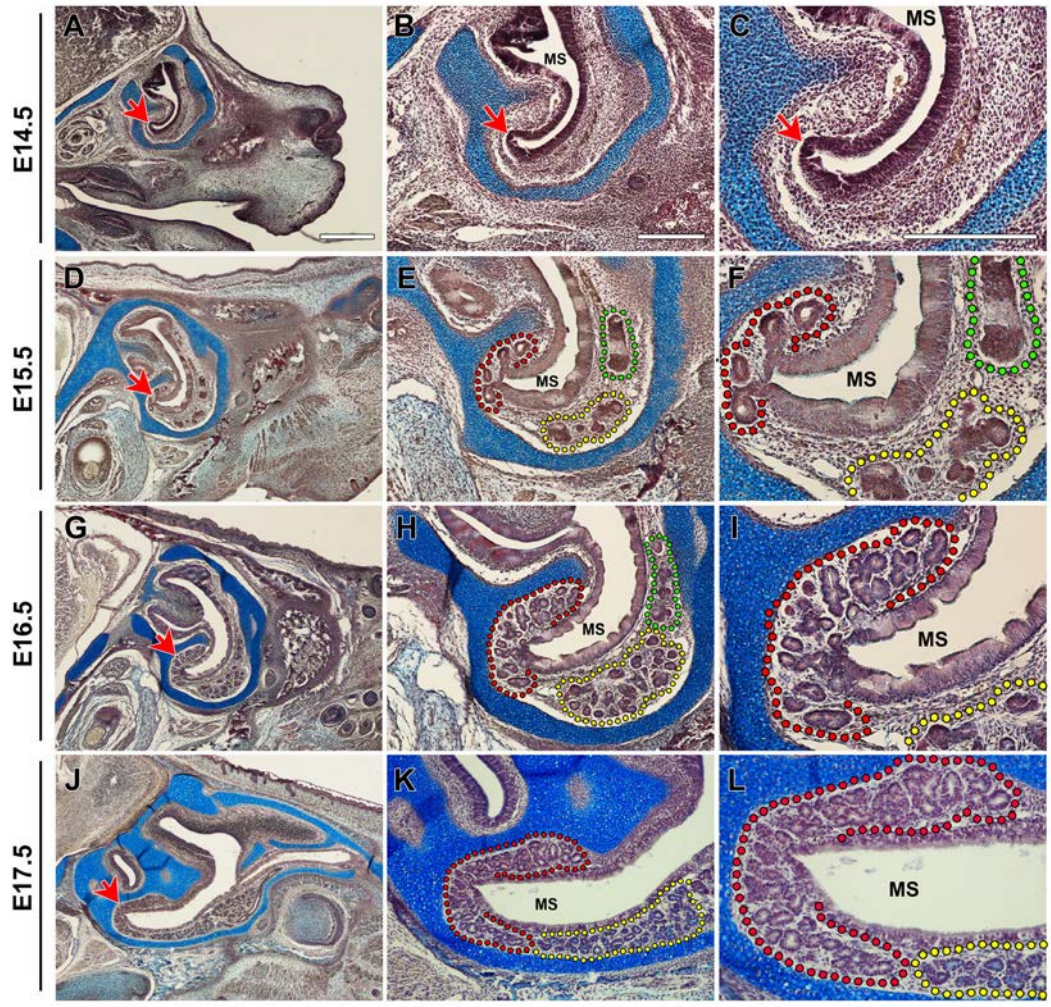

Figure 3.15 Maxillary sinus gland development.
Maxillary sinus gland initiates between E14.5 and E15.5. (**A-C**) No MSG primordium is evident at E14.5. (**D-F**) At E15.5 the MSG is seen to have invaginated and branched into the mesenchyme close to its opening in the respiratory epithelium. The MSG continues to branch and grow at E16.5 (**G-I**) and E17.5 (**J-L**). MSG = red, Steno's gland = yellow, LNG2 = green. MS = maxillary sinus cavity. **Column 1** scale bar = 500μm; **Column 2 and Column 3** scale bar = 250μm.

3.3.2 In Vitro Organ Culture of the Anterior Nasal Glands

In vitro organ culture is an invaluable technique that allows ex vivo manipulation of organ development. We attempted to culture the Steno's gland and the Lateral nasal glands using the slice organ culture method to follow gland development *in vitro* and to allow future experimentation and manipulation of anterior nasal gland development.

Following dissection of nasal tissue at E14.5, development of both the Steno's gland (Figure 3.16, A-D) and LNG2 and LNG3 (Figure 3.16, E-H) could be followed in culture. The Steno's gland began its first stages of gland branching after 24 hours (Figure 3.16, C) of organ culture and continued to branch after 48 hours (Figure 3.16, D). At the time of collection at E14.5, LNG2 had begun elongation, and the LNG3 bud had initiated its extension into the underlying mesenchyme (Figure 3.16, E and F). Following 48 hours of culture, both LNG ducts had elongated and branching of distal LNG glands has begun (Figure 3.16, G). Branching of the LNG glands continued successfully over the next 48 hours (Figure 3.16, H).

3.3.3 Lumen Formation and Apoptosis During Gland Development

As described above (see ***3.3.1***), different sets of anterior nasal glands undergo different mechanisms to ensure successful lumen formation within gland ducts. While the Steno's gland and MSG develop with preformed lumens, the LNG and MNG ducts form lumens approximately two days after they bud and begin elongation. To elucidate if apoptosis plays a role in lumen formation, investigation into the activation of cleaved Caspase-3 protein during gland development was carried out by immunofluorescence analysis.

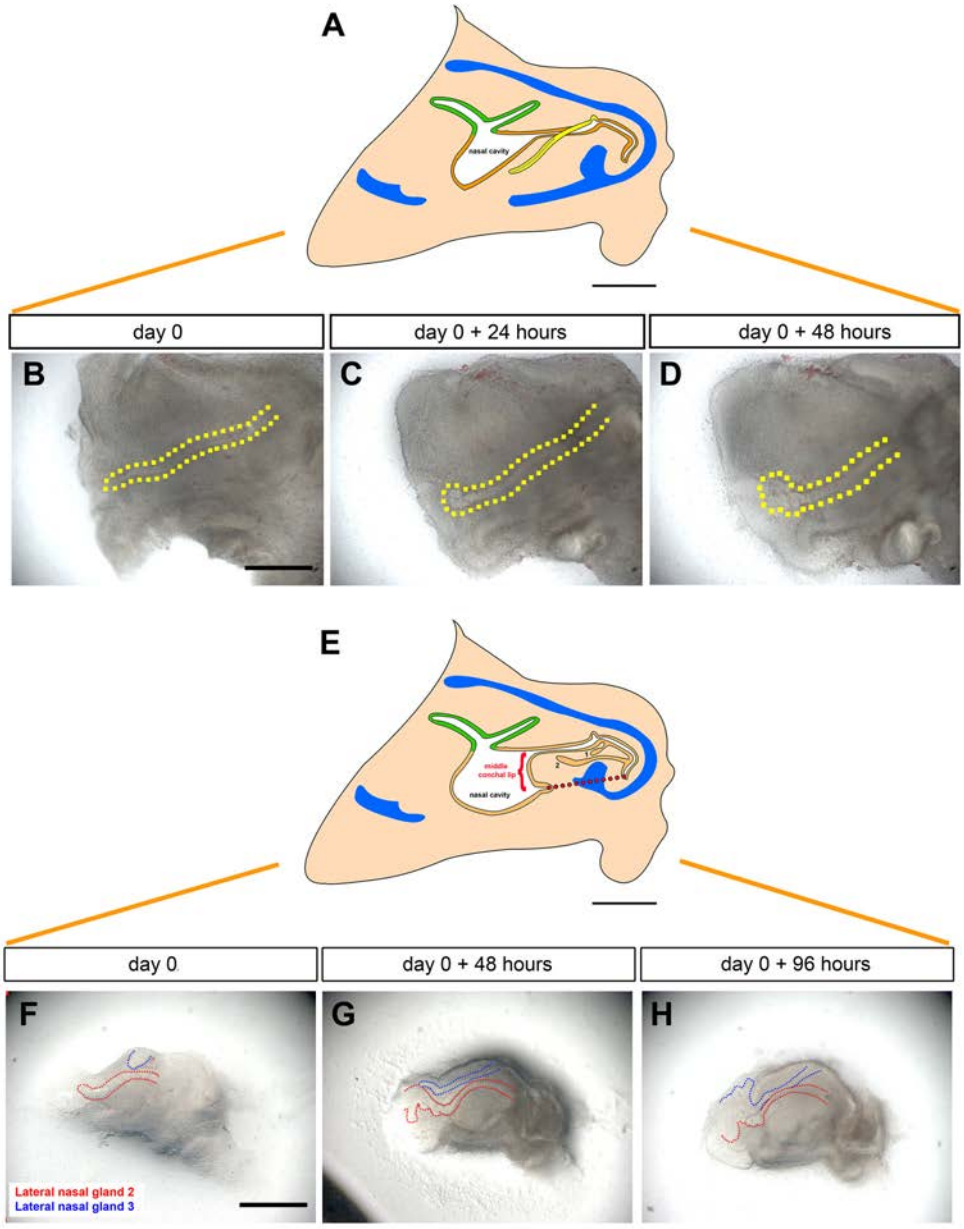

Figure 3.16 *In vitro* organ slice culture of the E14.5 anterior nasal glands.
(A-D) Culture of the Steno's gland duct collected at E14.5. (A) Illustration of the nasal tissue section that has the Steno's duct incorporated. (B) Appearance of Steno's duct on day of dissection. Duct has elongated caudally and contains a lumen. (C) After 24 hours the tip of the Steno's duct appears to have undergone initial gland budding. (D) Gland branching has continued on day 2 of culture. (**E-H)** Culture of LNG2 and LNG3 at E14.5. (E) Illustration of the nasal tissue section containing the LNG buds. From these sections the middle conchal lip was removed and cultured. (F) Extent of LNG duct elongation on day of collection. LNG2 has elongated caudally while LNG3 has undergone initial budding. (G) After 48 hours both LNGs have elongated and undergone branching of their distal glands. (H) Branching can be followed clearly and has continued to form distal LNG gland after 96 hours of culture. Scale bars = 500μm.

3.3.3.1 Apoptosis During Steno's Gland Development

At E12.5, the Steno's bud had invaginated into the underlying mesenchyme from the REA. Caspase-3 positive apoptotic cells were detected in the epithelium of the duct close to the duct opening at the REA into the airway lumen (n=2) (Figure 3.17, A). At E14.5 (n=2), when the duct had elongated caudally, no apoptotic cells were found in the proximal Steno's duct opening but activated Caspase-3 was observed in cells between the REA and REP (Figure 3.17, B). At the distal Steno's duct, some apoptosis was detected (Figure 3.17, C). At E15.5, an odd apoptotic cell was found within the REA near the Steno's duct opening (n=2)(Figure 3.17, D). At this same stage the distal Steno's gland had begun branching morphogenesis. Apoptosis was seen was observed in some cells dispersed throughout the proximal (Figure 3.17, G) and middle (Figure 3.17, H) Steno's duct, and within acini of the branching Steno's gland (Figure 3.17, I). By E18.5 no apoptosis was detected within the Steno's duct (n=2).

3.3.3.2 Apoptosis During Lateral Nasal Gland Development

Between E14.5-E15.0, when LNG2 and LNG3 had budded and elongated, the ducts were seen as a solid cord of cells (Figure 3.18, A-B, LNG3). No apoptosis was detected in these ducts at this stage. An odd Caspase-3 positive cell was detected within the REP and the distal tip of LNG3 however (Figure 3.18, A-B, white arrows). At E14.5 when LNG4 is initiating, no apoptosis was seen within this epithelial bud. At E15.5, lumen formation was noted within the proximal ducts of LNG2, 3 and 5 (Figure 3.18, C-D). No Caspase-3 was expressed in any cells of the ducts. Some apoptosis was found at the distal tip of LNG5 at this stage (Figure 3.18, D, white arrows). By E16.5, when LNG2 and LNG4 have begun distal gland branching, lumens had formed in all of the LNG ducts (Figure 3.18, E). An odd Caspase-3 positive cell was noted in the forming end bud of LNG2 (Figure 3.18, F), however none were found within the branching gland of LNG4 (Figure 3.18, G).

3.3.3.3 Apoptosis During Medial Nasal and Maxillary Sinus Gland Development

By E14.5-E15.0, lumen formation is underway in MNG1. No apoptosis was detected in the MNG1 ducts however at this stage (Figure 3.19, A-B). By E15.5, some Caspase-3 positive cells were seen in the duct and the budding distal end of MNG1 only (Figure 3.19, C-D). No apoptosis was occurring in the other MNG ducts at E15.5

(Figure 3.19, C-D). At E16.5, an odd apoptotic cell was detected in the proximal opening of MNG2 (Figure 3.19, E), however no Caspase-3 positivity occurred in the rest of the ducts of all the MNGs at this stage (Figure 3.19, F). An odd Caspase-3 positive cell was identified within the branching gland of MNG1 at E16.5 (Figure 3.19, G).

As the MSGs are undergoing initial budding and branching between E14.5-E15.0 no apoptotic cells were apparent (Figure 3.19, H). By E15.5, the branched MSGs were evident (Figure 3.19, I). No apoptosis was detected within gland acini, however Caspase-3 positive cells were observed within the respiratory epithelium of which the gland is branching from (Figure 3.19, I, white arrows). Similarly at E16.5 as the MSG continues branching, no apoptosis was detected within the gland itself but an odd Caspase-3 positive cell was seen within the respiratory epithelium (Figure 3.19, J).

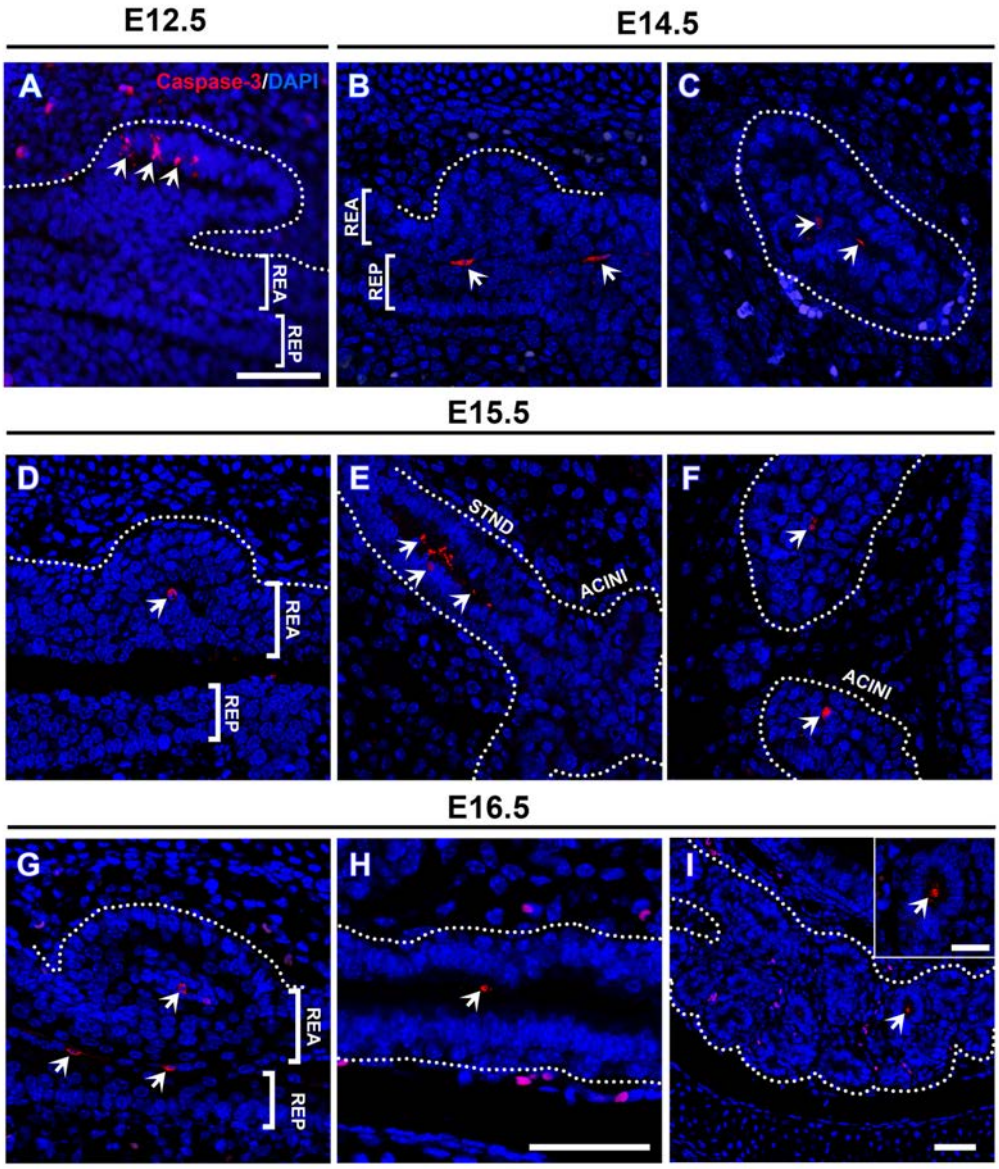

Figure 3.17 Activated Caspase-3 during Steno's Gland development.
(A) Apoptosis is seen in proximal epithelial cells of the invaginated Steno's duct at E12.5. **(B-C)** As the Steno's duct elongates apoptotic cells are seen at the base of the REA close to the opening of the duct into the airway lumen (B). At the distal tip of the duct some apoptotic cells are identified (C). **(D-F)** At E15.5 an odd apoptotic cell is seen in the epithelium near the opening of the Steno's duct (D). At the distal end of the Steno's duct apoptosis is evident in the duct at the location of the branching gland (E). Some Caspase-3 expression was seen sparingly in cells within the new epithelial buds (F). By E16.5, the overall amount of apoptotic cells seemed reduced with an odd Caspase-3 positive cell seen throughout the gland from the duct opening (G), mid-duct (H) and the distal acini (I). **A-I** scale bars = 50μm, inset image I scale bar = 25μm.

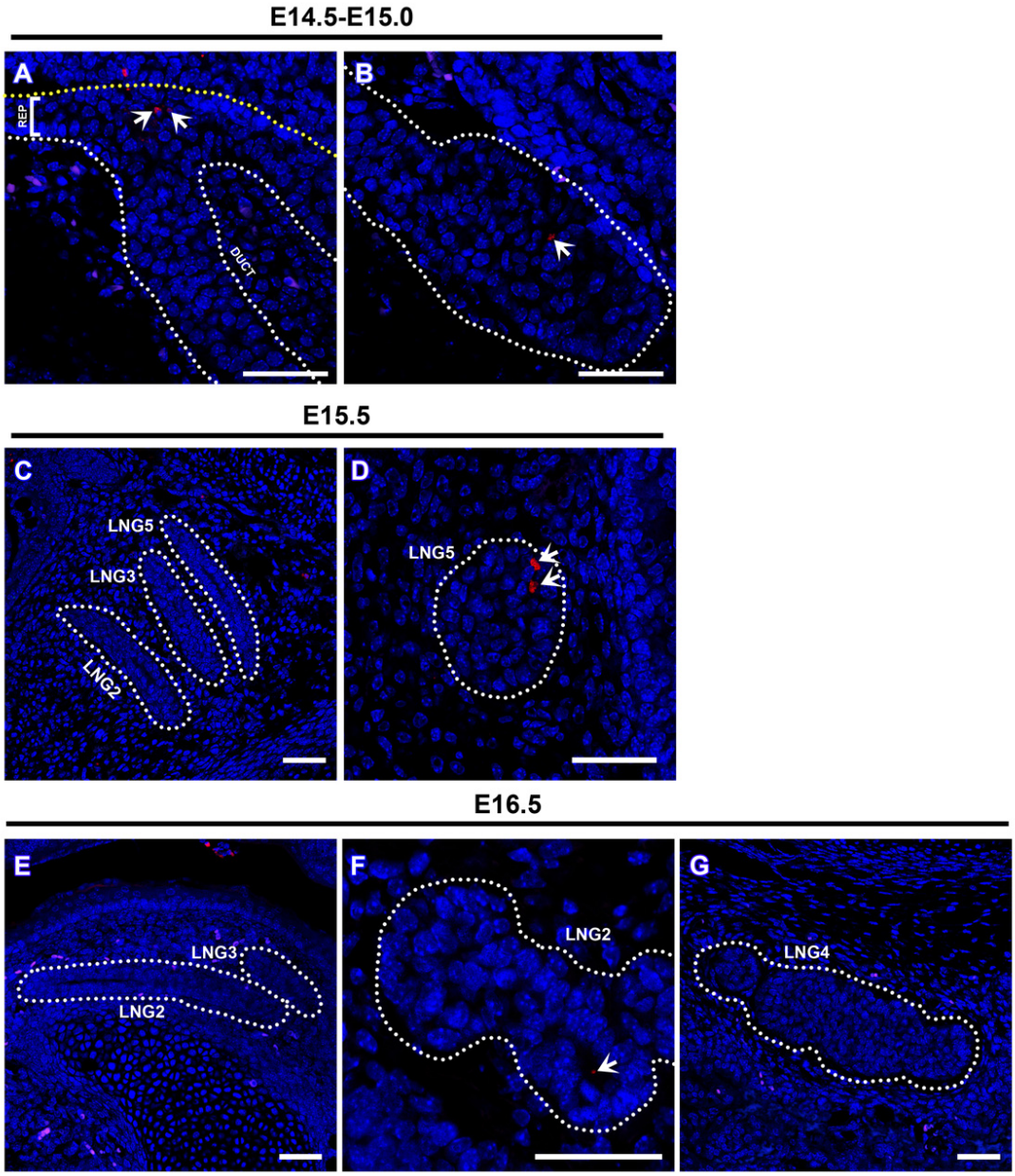

Figure 3.18 Activated Caspase-3 during Lateral Nasal Gland development.
(A-B) Between E14.5 and E15.5, as LNG2 and LNG3 bud and elongate as solid cords of cells, no apoptosis is seen within the future duct structures. An odd Caspase-3 positive cell was noted within the distal tip of LNG3 (B, white arrow). **(C-D)** Lumen formation is underway in the LNGs by E15.5. Sporadic expression of Caspase-3 was seen however only in the distal end of LNG5 (D, white arrows). **(E-G)** Lumens are clear within the ducts of the LNGs by E16.5, yet no Casapse-3 was seen in ductal cells. In the budding gland of LNG2, an odd apoptotic cell was noted (F, white arrow). No apoptosis was seen as LNG4 distally branched (G). Scale bars = 50μm.

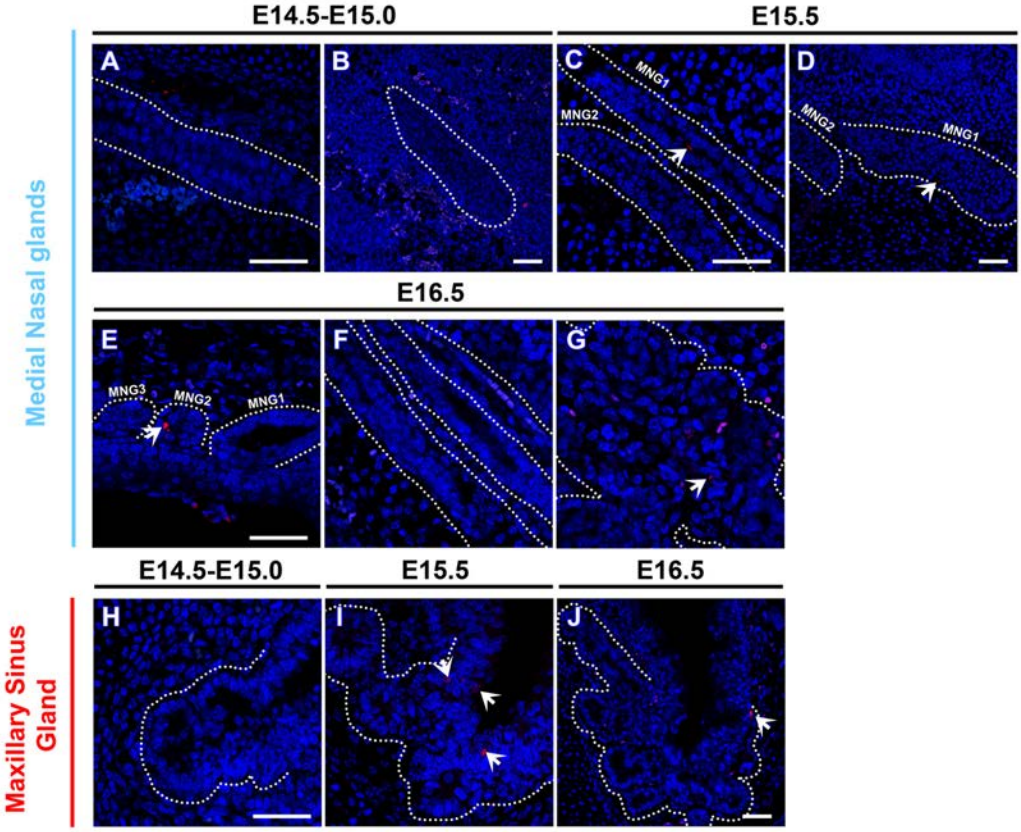

Figure 3.19 Activated Caspase-3 during Medial Nasal and Maxillary Sinus gland development.

(A-C) No apoptosis is seen within MNG1 between E14.5-E15.0. **(C-D)** An odd Caspase-3 positive cell was seen within the duct and end bud of MNG1 at E15.5. No apoptosis was seen in the other MNGs. **(E-G)** One apoptotic cell was seen in the proximal opening of MNG2 at E16.5. All other MNG ducts were apoptosis free. An odd Caspase-3 positive cell was seen in the branched MNG1 gland. **(H-J)** During MSG gland development no apoptosis was seen in gland cells, but rather within the respiratory epithelium of which the MSG branches (white arrows). Scale bars = 50μm.

3.3.4 Progenitor Cell Populations and Nerve Innervation During Anterior Nasal Gland Development

To gain more knowledge of the characteristics of the nasal glands during development we decided to investigate progenitor cell populations within the glands using the basal epithelial cell progenitor marker K5. As previous research has indicated a role of epithelial-nerve interactions during gland development, particularly during lumen formation, we also looked at the nerve innervation of the glands, by Neurofilament protein detection.

3.3.4.1 Keratin-5 and Neurofilament Detection During Steno's Gland Development

As the nasal pit forms and the middle conchal lip arises at E12.5, K5 expression was detected within cells of the respiratory epithelium at the most rostral location of the nasal vestibule (n=2)(Figure 3.20, A). As the respiratory epithelium runs more caudally and forms the Steno's duct, K5 expression was absent in basal epithelial cells of both the epithelium of the conchal lip and the Steno's duct (Figure 3.20, B). As development proceeded to E13.5, K5 expression was seen all throughout the REP of the conchal lip (n=2)(Figure 3.20, C and D). No K5 expression was found in the REA however, or in any of the basal cells of the Steno's duct (Figure 3.20, D and E). At a more caudal position, some K5 expression began to become apparent within the respiratory epithelium of the maxillary sinus at E13.5 (Figure 3.20, F). No innervation was detected associated with the Steno's duct during E12.5 and E13.5 of duct elongation. This suggests that a K5+ progenitor cell population, as well as nerve innervation, is not required for the outgrowth and elongation of the Steno's duct.

By E14.5, K5 expression had spread throughout the REA and all throughout the Steno's duct (n=2)(Figure 3.21, A-D). Expression was more intense within the basal cells of the respiratory epithelium of the maxillary sinus above where the Steno's gland duct had arrested elongation (Figure 3.21, B and C, pink arrows). At E14.5, innervation seemed to have developed close to the Steno's duct with rich neurofilament expression seen in close proximity to the medial and proximal end of the duct (Figure 3.21, C and D, green arrows). No innervation was detected more rostral near the duct opening into the nasal cavity. This indicates that there is an arrival of nerve innervation just prior to the branching of the distal Steno's gland, suggesting that nerves may play a role in branching morphogenesis.

At E15.5, the Steno's duct had begun to branch distally into the Steno's gland. K5 expression was clearly identified within ductal cells and some expression was apparent within the branching acini (n=2)(Figure 3.22, A-C, pink arrows). Innervation surrounded the proximal Steno's duct and gland while branching occurred (Figure 3.22, A-C, green arrows). By E18.5, K5 expression was strong in the basal cells of the respiratory epithelial cells of the maxillary sinus (n=2)(Figure 3.22, D-E). K5 expression was not detected in a consecutive line of cells close to the basement membrane of the olfactory epithelium however was expressed sporadically in some cells of the olfactory epithelium (Figure 3.22, D, blue dotted line). Ductal cells and distal gland acinar cells of the Steno's gland had clear K5 expression at E18.5 (Figure 3.22, E-F). By this stage, innervation was evident throughout the distal Steno's gland (Figure 3.22, E-F).

3.3.4.2 Keratin-5 and Neurofilament Detection During Lateral Nasal Gland Development

By E14.5, as the LNG have budded and begun elongation, K5 was expressed throughout the RE of the nasal cavity. By E14.5-E15.0, LNG2-5 had budded and most had elongated as ducts. As they did so, K5 was seen within the basal cells of all the LNGs (Figure 3.23, A-D). Innervation is also detected in close proximity to each LNG at this early stage of duct elongation (Figure 3.23, A-D). At E15.5, the LNGs proceeded more caudally with K5 expression still strong in the basal cells of each duct (Figure 3.24, A-C). LNG2 had begun to branch at E15.5 and K5 was expressed within some cells of the branching gland buds (Figure 3.24, C). As all glands have branched by E18.5, K5 is seen more widespread throughout the terminal end buds of each gland (Figure 3.24, D-G). Innervation was also detected throughout each gland (Figure 3.24, D-F) as well as running parallel to the LNG ducts (Figure 3.24, G).

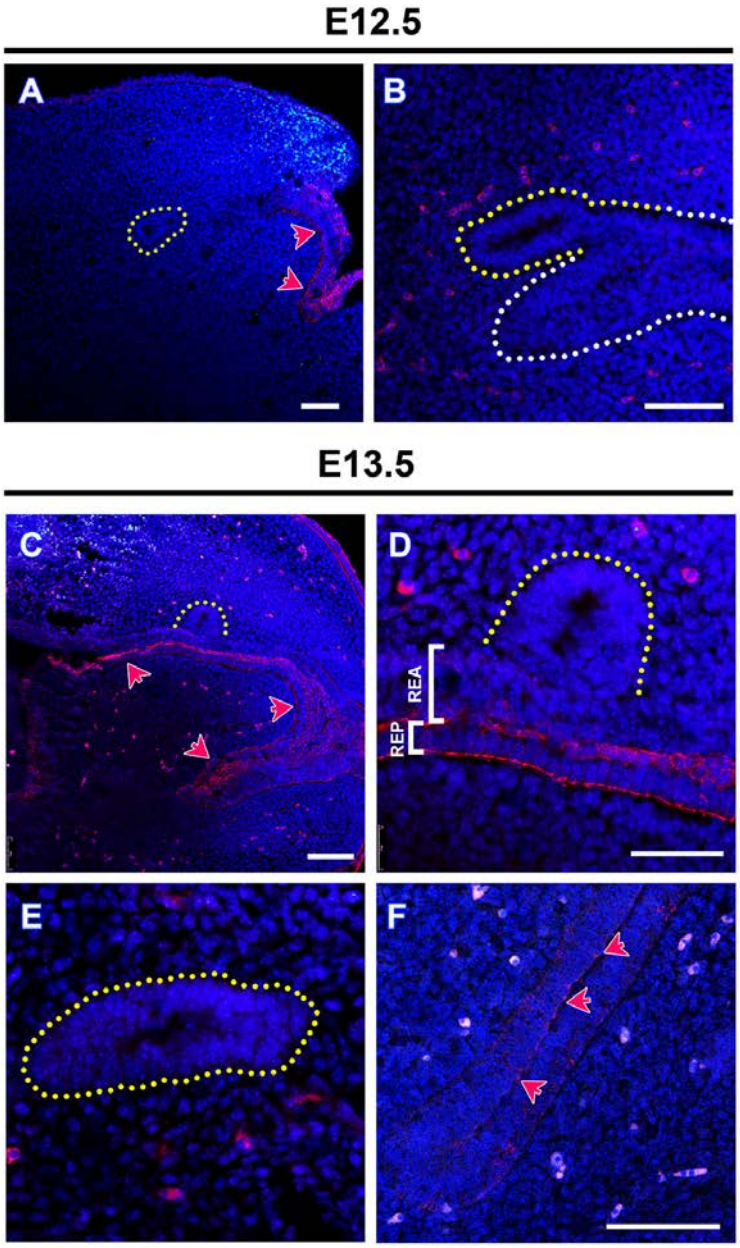

Figure 3.20 Keratin-5 (red) and neurofilament (green) expression during early Steno's gland duct development.
(A-B) K5 expression is seen in the most rostral respiratory epithelium of the middle concha at E12.5. No K5 is seen within the cells of the Steno's duct. (C-F) K5 has spread throughout the REP by E13.5 but is absent in the REA (C-D). No K5 is seen within the cells of the Steno's duct (E). Some K5 expression is seen within the epithelium of the maxillary sinus (F). No innervation was detected associated with the Steno's duct during E12.5 and E13.5 of duct elongation. REA – respiratory epithelium anterior; REP - respiratory epithelium posterior, Steno's duct = yellow dotted line. Scale bar = 50μm.

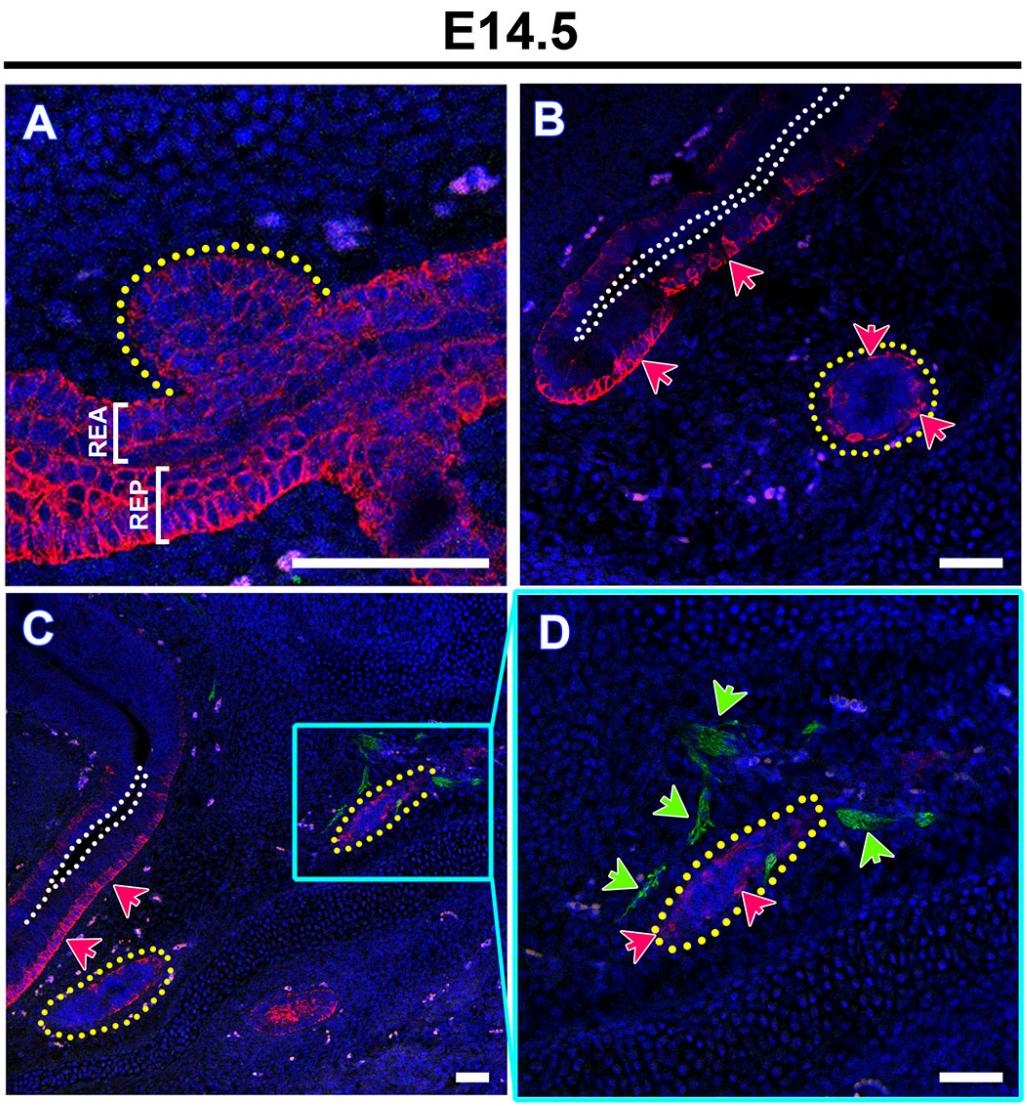

Figure 3.21 Keratin-5 (red) and neurofilament (green) expression during Steno's gland development at E14.5.
(A-D) By E14.5, K5 expression has spread all throughout the RE of the nasal cavity. K5 expression has also spread throughout the basal cells of the Steno's duct (B-D). Innervation is now seen in close proximity to the distal end of the Steno's duct (C-D). REA – respiratory epithelium anterior; REP – respiratory epithelium posterior; maxillary sinus epithelium (white dotted line); Steno's gland – yellow dotted line; pink arrows – K5 expression; green arrows – neurofilament expression. Scale bars = 50μm.

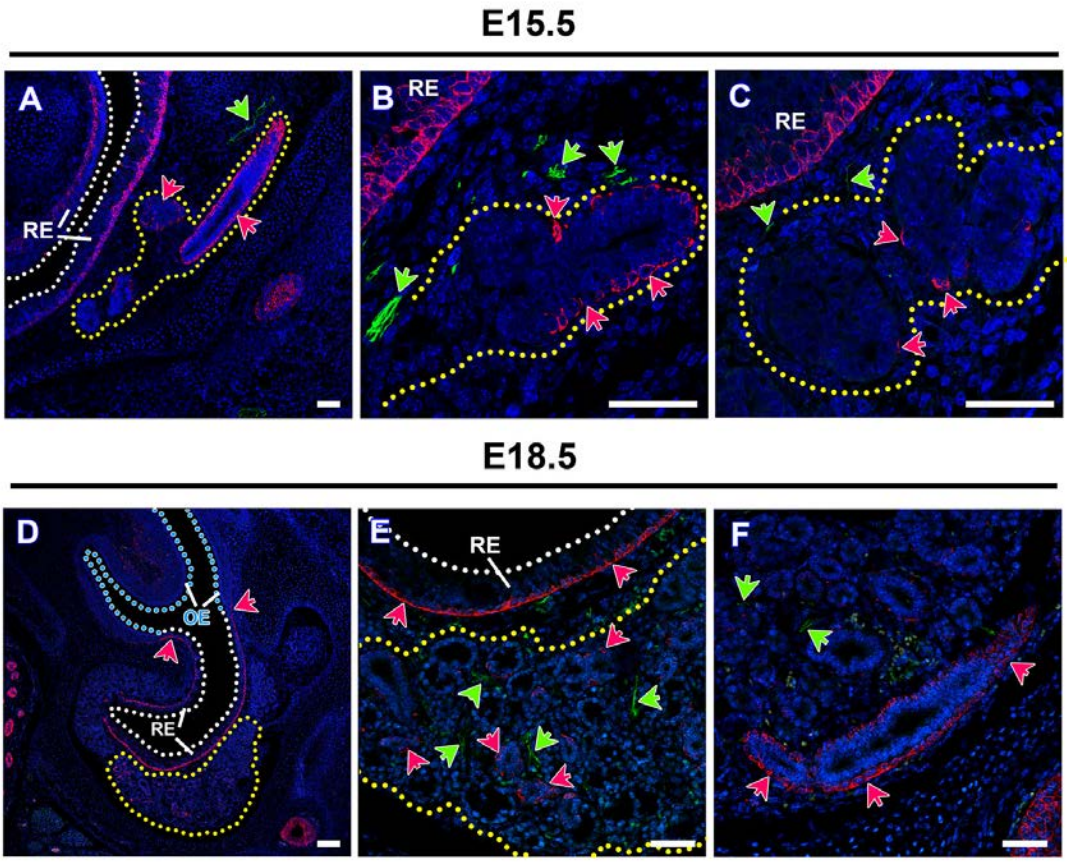

Figure 3.22 Keratin-5 (red) and neurofilament (green) expression during Steno's gland branching morphogenesis.
(A-C) As the Steno's gland branches at E15.5, K5 expression is seen in distal branching end bud cells. Innervation has also spread to envelop the branching buds (B and C, green arrows). (D) At E18.5, K5 is expressed in basal cells of the respiratory epithelium of the maxillary sinus however sporadic detection is seen in cells of the olfactory epithelium. (E-F) K5 expression is found within acinar cells of the Steno's gland and basal cells of the duct while nerves are seen wrapped through the distal gland at E18.5. RE - respiratory epithelium (white dotted line); OE – olfactory epithelium (blue dotted line); Steno's gland – yellow dotted line; pink arrows – K5 expression; green arrows – neurofilament expression. Image D scale bar = 100μm; all other scale bars = 50μm.

3.3.4.3 Keratin-5 and Neurofilament Detection During Medial Nasal Gland Development

Similarly to the LNGs, the MNGs begin budding and elongating at about E14.0. At E14.5, as the MNG ducts extend, K5 was detected within ductal basal cells (Figure 3.25, A-C). Nerves were also seen to be in close proximity to the MNG ductal cells as each duct was elongating (Figure 3.25, A-C). At E15.5, rich K5 expression was observed within the ducts of MNG1-3, as well as clear innervation between the elongating ducts (Figure 3.25, D-F). Some K5 expression was found within the distal branching epithelial tip of MNG1, with nerves seen close by (Figure 3.25, F). By E18.5, when all the MNGs have branched as glands, K5 expression was clear in ductal cells and distal acinar cells (Figure 3.25, G-I). Innervation was prominently associated with the MNG ducts (Figure 3.25, G) and within the distal glands (Figure 3.25, I).

3.3.4.4 Keratin-5 and Neurofilament Detection During Maxillary Sinus Gland Development

K5 expression was prominent within basal cells of the RE as the MSG branched immediately from the epithelium. At E14.5-E15.0 budding of the MSGs had begun. K5 expression arrested within the basal cells of the RE in the location of the branching gland but was observed in some distal epithelial cells of the gland itself (Figure 3.26, A). A day later at E15.5, branching of the gland continued, again with some K5 expression within gland cells (Figure 3.26. B-C). The first sign of nerve innervation of the MSG was observed at E15.5 (Figure 3.26, C, green arrows). By E18.5, the MSG was undergoing continual branching, yet no K5 expression was observed within gland acini cells (Figure 3.26, D-E). Some nerves were detected close to acini cells (Figure 3.26, D-E), however not as much as was detected in the other anterior nasal glands.

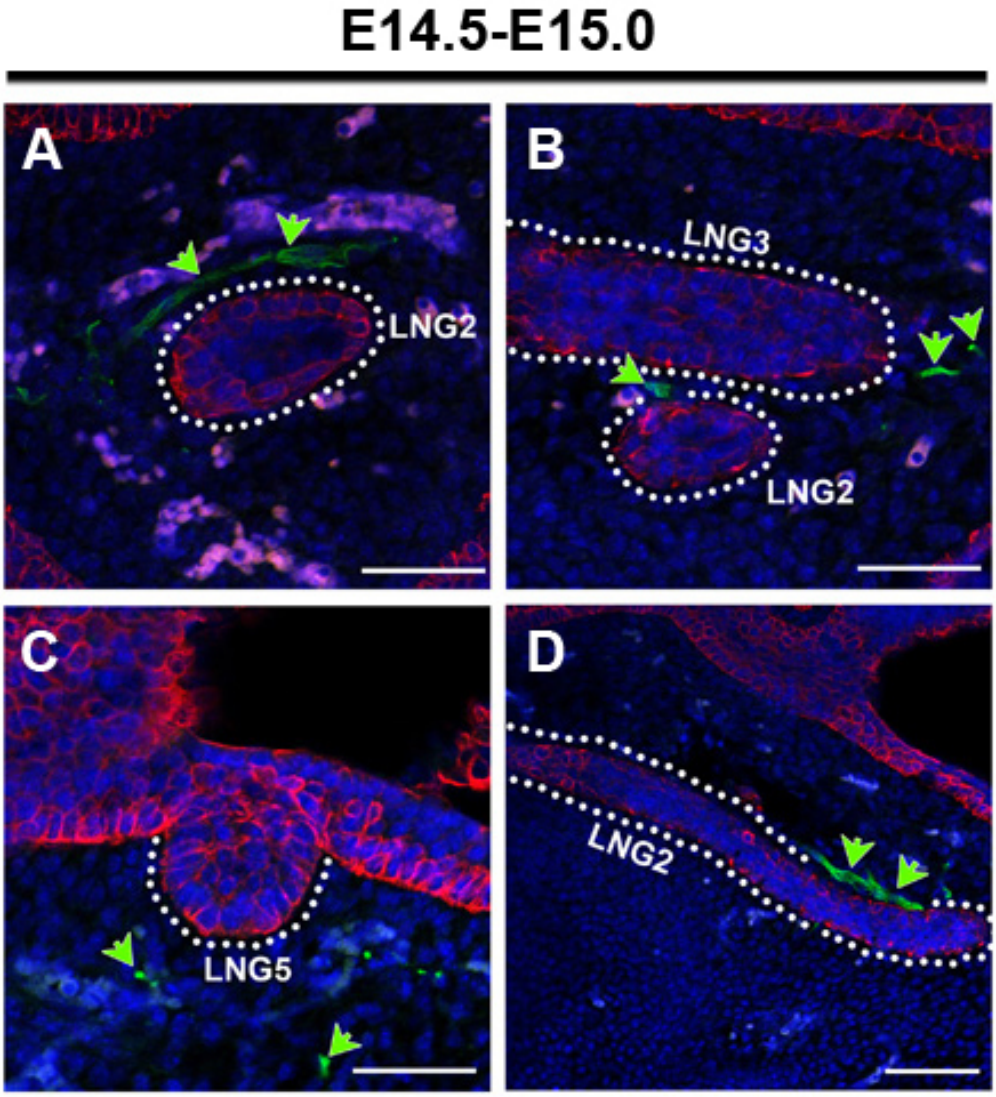

Figure 3.23 Keratin-5 (red) and neurofilament (green) expression during lateral nasal gland development at E14.5.
(A-D) K5 expression is seen in the basal cells of all budding and elongating LNGs between E14.5 and E15.0. Innervation indicated by neurofilament expression is also seen close to all elongating LNGs. Innervation = green arrows. Scale bars = 50μm.

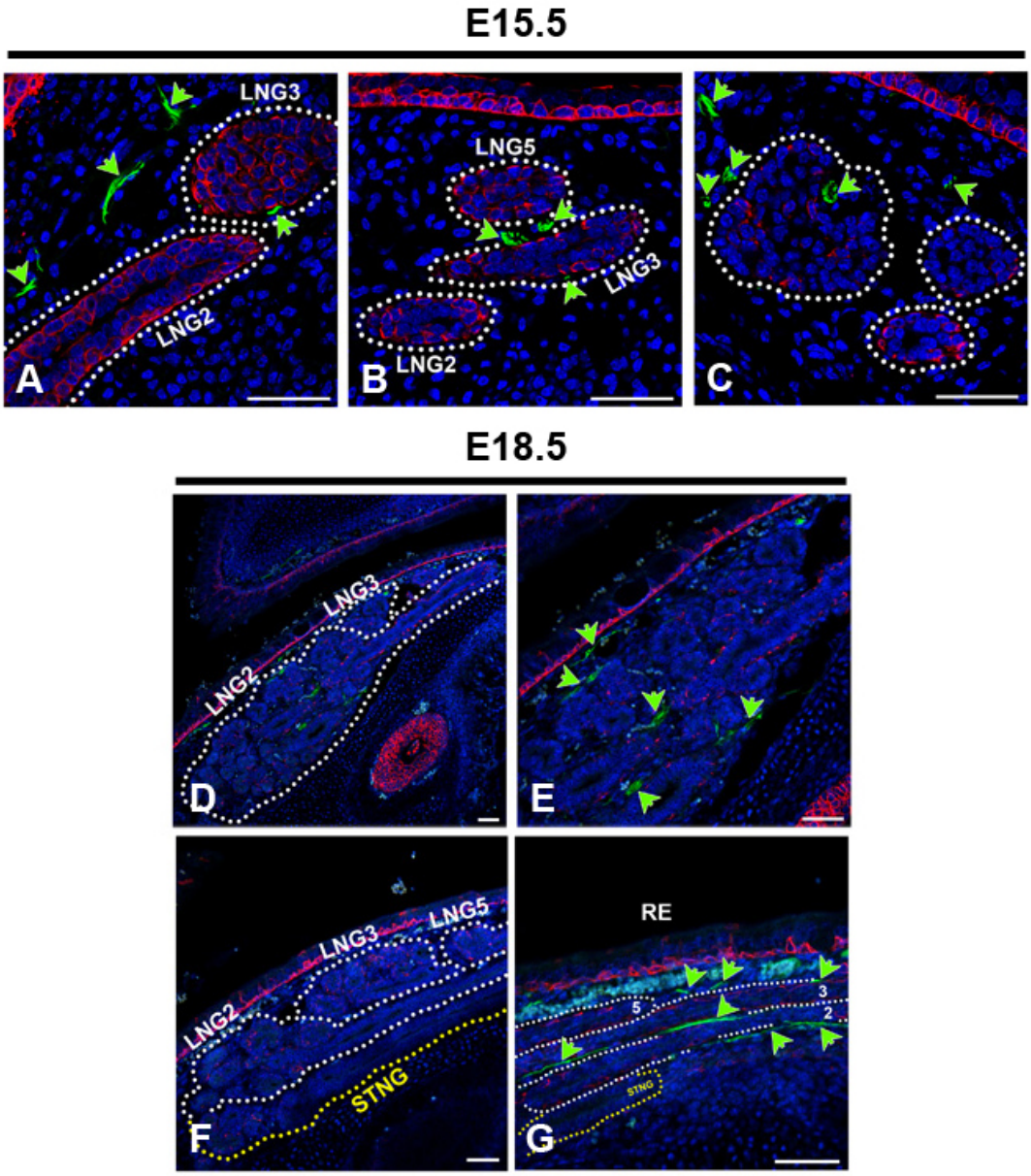

Figure 3.24 Keratin-5 (red) and neurofilament (green) expression during lateral nasal gland development at E15.5 and E18.5.
(A-C) K5 is maintained within ductal cells during LNG elongation and seen within the branching gland buds of LNG2 at E15.5 (C). **(D-G)** At the later stage of E18.5, K5 has spread into terminal end bud epithelial cells of all the branched LNGs and innervation is rich around each distal gland. Nerves are also seen to run parallel to the ducts of LNG2, LNG3 and LNG5 (G). Innervation = green arrows. Scale bars = 50µm.

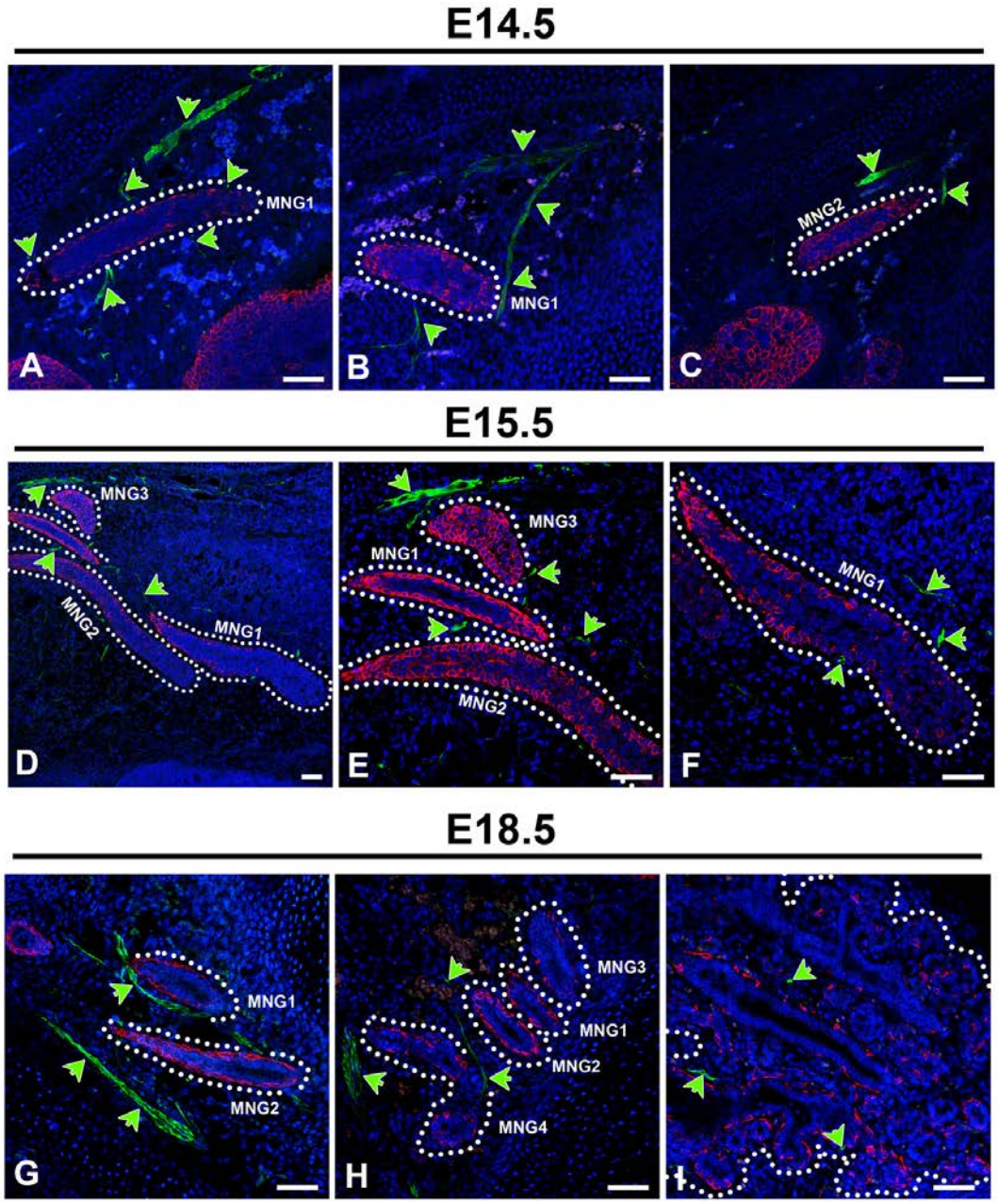

Figure 3.25 Keratin-5 (red) and neurofilament (green) expression during Medial nasal gland development.
(A-C) K5 expression is seen within all MNG ducts at E14.5. Innervation is also seen in close proximity to the elongating ducts. **(D-F)** As development continues to E15.5, K5 expression continues within the MNG ducts and also spread to the distal branching tip of MNG1 (F). Nerves are seen associated with all ducts. **(G-I)** At E18.5, K5 positivity is seen within distal gland acini of each MNG (I). Nerves are also evident close to MNG ducts and within the distal glands. Innervation = green arrows. Scale bars = 50μm.

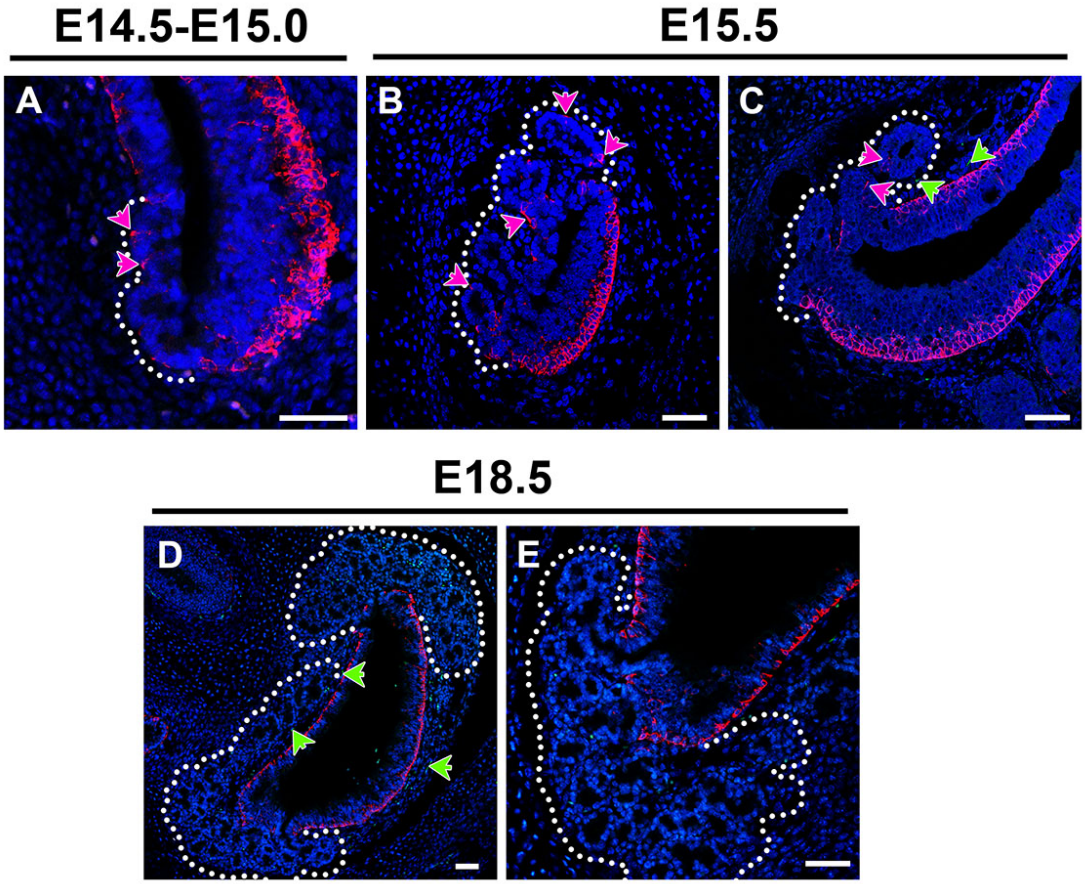

Figure 3.26 Keratin-5 (red) and neurofilament (green) expression during Maxillary Sinus Gland development.
(A) K5 is strong within basal cells of the RE. Some K5 expression is seen in distal MSG gland cells (pink arrows). **(B-C)** Branching has continued and some K5 is still seen within gland cells (pink arrows). Innervation is also evident close to MSG acini (green arrows). **(D-E)** No K5 is seen within MSG gland cells by E18.5. Innervation is seen however not very many nerves were noted close to the MSGs (green arrows). Scale bars = 50μm.

3.4 Discussion

3.4.1 Anterior Nasal Gland Development

In the mid-twentieth century, researchers analysed and delineated anterior nasal gland topography and physiology (Brunner, 1942; Bojsen-Moller, 1964), however modern investigation of these respiratory glands is severely lacking. Although their scattered arrangement can be complex, with their long ducts and branched glands distributed throughout different regions of the nasal mucosa, the importance of these glands cannot be ignored. With an estimated 150 glands per cubic millimetre of nasal mucosa reported in adult humans (Brunner 1942), the nasal glands play a critical role in maintaining airway homeostasis as they provide the first line of defence within the respiratory system. Previous studies have named and described the temporal location of the glands in mice, and other mammals (Brunner 1942; Bojsen-Moller 1967; Moe & Bojsen-Moller 1971; Bojsen-Moller 1964), however these manuscripts fail to give descriptive explanations and illustrative aids to help the researcher locate and differentiate all groups of glands. The aim of this study was to thoroughly investigate and describe the patterning of the anterior nasal glands in a mouse model, in the hopes to clarify the development and arrangement of the glands and encourage future research into their cellular and molecular behaviours.

3.4.1.1 The Steno's Gland

The orifice of the budding Steno's duct can be clearly identified in the mouse at E12.5 as the REA invaginates into the underlying mesenchyme forming an indentation in the epithelium. Steno's duct elongation can then be followed over the next 48 hours, as the duct proceeds with a distinctive lumen. This has already been stated by Grüneberg (1971) however no histological or illustrative description was provided. We have shown in these results the temporal location of the budding and elongating Steno's duct as well histological evidence of its appearance. Through schematic diagrams we have also explained the craniofacial planes of which the Steno's duct elongates, in the hopes to clarify its journey for future studies.

The distinct morphological stages of Steno's gland development have also been categorised into different stages, where general time frames are provided for investigation into bud formation, duct elongation, distal gland branching and acinar differentiation (Table 3.3). This categorization will hopefully aid research into the

delineation of different cellular mechanisms occurring during these different stages of gland morphogenesis.

Table 3.3 Approximate stages of the distinct morphological events of anterior nasal gland development.

Gland Name	Approx. age of budding	Approx. age of initial lumen formation	Approx. age of onset of branching
Steno's Gland	E12.0	-	E15.5
LNG2	E13.5	E14.5-E15.0	E16.5
LNG3	E14.0-14.5	E15.0	E16.5
LNG4	E14.5	E15.5	E16.5
LNG5	E14.5	E15.5	E17.0
MNG1	E14.0	E14.5	E15.5
MNG2	E14.5	E15.5	E16.5
MNG3	E15.5	E16.5	E17.0
MNG4	E16.0	E17.5	E17.5
MSG	E14.5-E15.0	-	E15.0

3.4.1.2 The Lateral Nasal Glands

Bojsen-Moller (1964) reviewed anterior nasal gland development and reported that up to 20 LNGs had previously been described in mice. From this current study, we report the first five LNGs (Steno's gland and LNG2-5) are found to bud and elongate during embryonic murine development. This suggests that continual LNG budding and branching occurs during postnatal development. Unlike the Steno's gland, LNG2-5 appeared to follow a similar developmental mechanism by elongating as a solid cord of cells, which hollow out approximately 24 hours after initial bud formation, to form a lumen. Distal LNG glands also began to branch 48 hours subsequent to gland budding. Although developing similarly, LNG2, 3 and 5 elongated caudally and branched close to the Steno's gland, while LNG4 elongated posteriorly and branched below the nasal cartilage capsule. This suggests that LNG4, although structurally similar to the other LNGs, could be following a different molecular signal that attracts its elongating gland duct in a posterior direction, compared to a caudal attractant guiding its other LNG counterparts. By delineating this directional differentiation

between the LNGs, a model system is proposed to understand different mechanisms of cellular proliferation and chemo-attractant interactions. Regardless of this difference in spatial-temporal development, all the LNGs appeared to follow the same pattern of cavitation and branching morphogenesis.

3.4.1.3 The Medial Nasal Glands

Development of the medial nasal glands was relatively simple to follow as their ducts elongated and branched through the clear plane of mesenchymal tissue on either side of the nasal septum. The orifices of their ducts were found on the vestibular side of the nasal septum. The MNGs have been previously described in the rat, which can have four to five MNGs project into the septal mesenchyme (Bojsen-Moller, 1964). The rat MNGs do not stain with Periodic-Acid Schiff (PAS) or Alcian Blue staining (Bojsen-Moller, 1964). Analysis of the four MNGs of the mouse have also been carried out (Broman, 1921; Kerjaschki, 1974). These glands have previously been reported to be exclusively made up of serous cells (Bojsen-Moller, 1964; Kerjaschki, 1974) and in this study, no Alcian Blue staining was seen within their acini, suggesting these glands are exclusively serous in nature. While all the MNGs look similar and undergo comparable developmental strategies, investigation into their ultrastructure has delineated distinguishable differences between these glands (Kerjaschki, 1974). It has been shown that MNG4, shows homologous characteristics to serous salivary glands, with its gland cells having common characteristics as serous cells, however MNG1-3 stand alone as their own distinct gland type (Kerjaschki, 1974). What differentiates MNG1-3 from the fourth is that they possess “light” and “dark” endpiece cells within their glandular acini when analysed by electron microscopy (Kerjaschki, 1974). These “light” and “dark” cells have been described in the Bowman’s glands of the olfactory epithelium, where “light” cells contain electron-dense serous secreting vesicles while the “dark” cells contain electron-lucent mucous secreting vesicles (Getchell and Getchell, 1992). These compositional differences of these glands may also explain why in this study we see MNG1-3 elongate and branch in the same plane and at similar time points, when MNG4 arises in the more rostral septum and develops slightly later. While all are considered ‘Medial Nasal Glands’, for future studies it is advised to be aware of their differences.

3.4.1.4 The Maxillary Sinus Gland

The maxillary sinus glands differed from their other nasal gland counterparts, as they began branching morphogenesis immediately after bud formation, giving rise to a tubulo-alveolar gland close to the respiratory epithelium. This structure allows the MSG to drain its secretion directly into the sinus cavity through its short and wide excretory ducts. Research on the MSG in rat found it to be an exclusively serous gland (Vidić and Greditzer, 1971) and begins its development at embryonic day 16 (Vidić, 1971). In the mouse, we have shown that the MSG undergoes a similar method of development as in the rat however is first seen to bud from the epithelium of the maxillary sinus at approximately E15.0. This gland then rapidly branches over the next three days of embryological development, moving through the submucosa of the maxillary sinus in both an anterior-posterior and a left-right direction. By E17.5, the peripheral edge of the MSG can be first seen in the first sagittal section entering the nasal cavity, while its anterior and posterior edges can be seen to extend around the maxillary sinus. No Alcian Blue staining was present in the MSG, suggesting that this gland is exclusively serous in nature.

3.4.2 Lumen Formation in the Anterior Nasal Glands

3.4.2.1 The Steno's Gland and Maxillary Sinus Gland Develop with Preformed Lumens

From our analysis, it is clear that both the Steno's gland and the MSG, although different in nature, develop with preformed lumens in their ducts, a method similarly seen in the developing lung (see *Chapter 1*). Lung bud outgrowth follows the budding pattern driven by apical constriction similar to that described in the *Drosophila* salivary system (Burri and Moschopulos, 1992; Meyer et al., 2004). PCD has been shown to play an important role in the modelling of developing lung tissue in fetal and postnatal rodents, however apoptosis is absent within the lung epithelium during initial stages of budding and branching (Kresch et al., 1998). This indicates that apoptosis does not play a part in lumen formation and that lumen expansion is a sufficient method to create a distinct hollow space within the lung.

In this study, some apoptotic cells were seen within the epithelium of the Steno's duct and gland. Many Caspase-3 positive cells were seen in the ductal epithelium close to its orifice at E12.5 when the duct is undergoing initial elongation. This PCD could

possibly be triggered to help carve out a clear opening into the nasal cavity, as it is seen in the most proximal cells, to aid in mucous expulsion out of the gland duct. A similar mechanism is seen in early mammary gland development as at E18 apoptosis is seen in excess epithelial cells at a distance from the newly formed lumen (Hogg et al., 1983). This PCD then continues to spread to the basal cells of the forming tube (Hogg et al., 1983). It is suggested that this method occurs to eliminate unnecessary cells within the mammary gland duct, as an epithelial lining of only one-three cells thick is required (Hogg et al., 1983).

Another noticeable area of apoptosis was seen in the distal Steno's duct at E15.5. These Caspase-3 positive cells were located close to the distal formation of end buds as the Steno's gland begins morphogenesis, and it is suggested that this helps cavitate regions of the duct where future branches will form, allowing the flow of mucous into the main collecting duct. A few apoptotic cells were seen throughout the Steno's duct and gland through all stages of development but due to their sporadic nature it is thought that these are undergoing normal tissue homeostasis mechanisms.

No Caspase-3 positive cells were seen within the MSG during any stages of branching morphogenesis suggesting that apoptosis does not play a role in MSG development and that this gland may adopt a method of tubulogenesis similar to that seen in the Steno's duct and mammalian lung.

3.4.2.2 Apoptotic Canalization does not Occur in LNGs and MNGs

As the LNGs and MNGs begin their first stages of branching morphogenesis as solid cords of epithelium, it was hypothesised that these tubes undergo canalization to form ductal structures. While this has been reported in mammalian tissues such as the mammary gland end buds and salivary gland ducts (Humphreys et al., 1996; Melnick and Jaskoll, 2000), it does not seem to occur in the anterior nasal glands. By analysis of Caspase-3 within the gland cells during their branching morphogenesis, no significant amount of apoptosis was detected in the LNGs and MNGs during any stages of development. As these glands form lumens within the first 24 hours following budding, it is suggested that they undergo alternative methods of tubulogenesis. For example, the method of *cord hollowing* is observed in the gut of zebrafish (Wallace and Pack, 2003; Ng et al., 2005). Through this process, cells of the

cord undergo weak polarization and form cell-to-cell junction complexes with neighbouring cells. Polarization leads to the formation of a small lumen in the apex of each cell. These lumena then merge to form one large lumen in the centre of the duct. During this process no apoptosis is recruited to help lumen formation (Wallace and Pack, 2003; Ng et al., 2005).

In the LNGs and MNGs, detection of Caspase-3 seemed to occur randomly in a few cells through different planes of the glands indicating sporadic apoptosis was occurring. This suggests that PCD is not required to create a luminal space but may be adopted to maintain a clear duct. This strategy is seen in three-dimensional cell models using kidney epithelial cell lines (Martín-Belmonte and Yu, 2008). When MDCK cells were grown in Matrigel, an environment that promotes rapid cell polarization, cells rearrange to form a luminal space, like in cord hollowing. When cultured in collagen, which slows down the rate of polarization, apoptosis was recruited for lumen formation, similar to the cavitation process (Martín-Belmonte and Yu, 2008). To test this hypothesis *in vivo,* polarization of LNG and MNG glands cells could be analysed by immunofluorescent labelling using polarization markers such as Claudins and Integrins, to delineate if cell polarization is occurring within gland cells. Additionally, using the culture method described in this chapter, glands could be grown *in vitro* and exposed to polarization inhibitors, such as the Rho-associated kinase (ROCK) inhibitor Y27632, to delineate if a switch from cord hollowing to cavitation occurs.

Furthermore, the observation that innervation is present during all stages of LNG and MNG stalk elongation, however absent during duct extension of the Steno's gland, compliments the recent finding that a nerve supply is essential for successful lumen formation within the SMDG ducts (Nedvetsky et al., 2014). A model process of four distinct stages was proposed to ensure cavitation within SMDG ducts (Nedvetsky et al., 2014). Firstly, proliferation and aggregation of luminal cells along the midline of the epithelial stalk is observed. Polarisation of these cells then lead to the formation of microlumena within the epithelial stalk, due to the reorganization of cells (Nedvetsky et al., 2014). As development continues, these microlumena coalesce to form one continuous lumen, which then undergoes expansion to form a distinct hollow duct (Nedvetsky et al., 2014). It was shown that this method of lumen formation was

independent of PCD and relied on the neurotransmitter vasoactive intestinal peptide (VIP) for successful cavitation (Nedvetsky et al., 2014). Due to the rich nerve supply associated with the LNGs and MNGs during their stalk elongation and ductal formation stages, we hypothesise that a similar mechanism of lumen formation may be adopted in these glands, as to that of the SMDG.

Thus, as different groups of nasal glands undergo different processes of tubulogenesis, they provide a valuable model system for the study of molecular and cellular mechanisms required for cell rearrangement and lumen formation.

3.4.3 Progenitor Cell Populations in the Anterior Nasal Glands

As the Steno's gland budded and elongated during the first two days of development (E12.5-E14.5), K5 expression was absent in the REA, of which it protrudes, and the cells of the Steno's duct itself. By E14.5, K5 had spread in a wave along the rostral/caudal axis, and was seen all throughout the RE of the nasal cavity. This wave now ensured K5 was expressed in the basal cells of both the REA and the entire elongated Steno's duct. The onset of this wave of expression delineates that K5 was not required for initial Steno's duct budding and elongation, however as the distal Steno's gland began to branch at E15.5, a reservoir of K5 positive cells were present at the distal duct. K5 positive cells have been identified as progenitor cells in tracheal epithelium, postnatal mammary gland and prostate development (Rock et al., 2009; Sun et al., 2010; Shen et al., 2008). Knox et al. (2010) showed through lineage tracing experiments that K5+ cells are also progenitor cells of developing embryonic SMDGs and that depletion of K5 proliferation, by innervation removal, leads to a reduction in salivary gland terminal end buds. As development progressed, innervation was apparent surrounding the buds of the branching Steno's gland. K5 expression is seen within ductal and endbud epithelial cells of the salivary gland by the *Pseudoglandular stage* at E13.0 (Lombaert et al., 2011). No studies have investigated earlier K5 expression during prebud or initial bud stage however, so a direct comparison with the Steno's gland duct stage cannot be made. It has been shown that the EGFR antagonist PD168393 (PD), and the epithelial muscarinic receptor inhibitor 4-DAMP (DAMP, *N*-2-chlorethyl-4-piperidinyl diphenylacetate) both completely inhibit proliferation, and thus differentiation, of K5+ basal progenitor cells in the salivary gland (Knox et al., 2010). Application of these inhibitors to Steno's gland cultures at

E14.0, when distal gland budding is about to begin, would delineate if K5 is critical for distal Steno's gland branching,

By E13.5, when the first signs of LNG gland budding occurred, K5 expression was seen within the basal cells of the REP. By E14.5, when the MNGs began budding, again basal cells of the REA were K5+. As a result of this rostral/caudal wave of K5 expression, epithelial buds of both LNGs and MNGs expressed K5 at this initial stage of development. Whether these progenitor cells are critical for bud formation can be tested using the PD and DAMP culture methods described above. It may be plausible that K5 progenitor cell populations are not required for structures that bud and elongate by the 'budding' mechanism, however may be critical to maintain epithelial cell condensations of those branching structures that develop by the elongation of solid cords. As the distal Steno's gland may cleft and bud with solid branches, this would also explain why K5+ cells were present close to the distal end buds.

Additionally, we report that no nerves were detected in close proximity to the elongating Steno's duct between E12.5 and E14.5. After E14.5, neurofilament expression detected innervation close to the midline and distal end of the Steno's duct as it began gland branching, a similar time as to when K5 expression was detected in the distal Steno's gland. In comparison, nerves were detected in close proximity to the developing LNGs and MNGs during all stages of budding, stalk elongation and branching morphogenesis. Due to the timing of K5 expression within ductal cells, and the development of proximal nerves, it is suggested that signalling from the nerve supply may play a role in the expression of K5 in the basal epithelial progenitor cells. This nerve-epithelial interaction is well established in the mouse SMDG (Knox et al., 2010; Lombaert et al., 2011). In *ex vivo* SMDG culture experiments where the parasympathetic submandibular ganglion (PSG) was removed, K5 expression in gland end buds and ducts reduced to less than 25% compared to those cultured with an intact PSG (Knox et al., 2010). Furthermore, culture of PSG-free SMDGs with carbachol, an acetylcholine analogue, increased the K5 progenitor cell population and rescued, to some extent, salivary gland morphogenesis (Knox et al., 2010). Considering this, we suggest that due to the development of nerves mirroring the wave of K5 positivity running through the nasal epithelium, innervation may be

required to induce and maintain K5 progenitor cell expression in the branching stages of Steno's gland development and all stages of LNG and MNG morphogenesis.

K5 expression was never seen in the epithelial cells of the maxillary sinus gland. Strong K5 expression was present all throughout the basal cells of the RE of the maxillary sinus, and the entire nasal cavity. Due to the MSG having short ducts and branching close to the RE, it is expected that the K5+ basal cells of the RE provide the MSG with its progenitor cell population.

4.1 Introduction

Considering the importance of the submucosal glands (SMGs) in maintaining airway homeostasis and the significant role they play in a number of respiratory diseases, very little is known about the signalling molecules and intercellular cues that shape these branched organs. Looking at other structures that develop in a similar fashion, such as the mammalian lung, submandibular salivary gland (SMDG), hair follicles and teeth, dynamic expression of conserved signalling pathways such as Bone Morphogenetic Proteins (BMPs), canonical Wnt/βcatenin, and Eda/Edar, are all recruited to tightly control cellular and morphological changes that occur during budding, extension and in some cases, branching of epithelial tissue (Thesleff, 2003; Cardoso and Lü, 2006; Jaskoll and Melnick, 2006; Rishikaysh et al., 2014). As outlined in *Chapter 1*, previous studies have delineated the requirement for these pathways during SMG development. In the case of the development of the tracheal glands, *Bmp4* expression is widespread throughout the mesenchyme beneath the airway epithelium during stages of bud induction and extension, while later, as glands are branching, *Bmp4* expression is restricted to mesenchymal cells surrounding the newly forming gland end buds (Rawlins and Hogan, 2005). Signalling through the Eda/Edar pathway is also essential as tracheal SMGs are absent in *Tabby* male adult mice as well as *crinkled* mice, which are knockouts of Eda and Edaradd respectively (Rawlins and Hogan, 2005). Research on the anterior nasal glands also show that some, but not all of these glands are absent in the *Tabby* mouse (Grüneberg, 1971). Furthermore *Lef-1* and Wnt signalling are required for early nasal gland bud initiation (Duan et al., 1999; Driskell et al., 2004, 2007). The involvement of Wnts during later stages of duct elongation and gland branching of the nasal glands however has not been investigated.

As covered in *Chapter 1,* it is evident that the role of *Fgf10*, and its receptor *Fgfr2b*, is pivotal for cell proliferation, epithelial growth and extension of stalks during development of many branched organs (Sekine et al. 1999; Bellusci, Grindley, et al. 1997; Jaskoll et al. 2005 and *Chapter 6*). *Fgfs* are also required for successful tracheal gland morphogenesis as hypoplastic glands are observed in *Fgf10 +/-* adult mice (Rawlins & Hogan, 2005 and *Chapter 5*). Expression of downstream readout genes and target transcription factor expression within branching epithelial structures has

also emphasised the role FGF signalling during branching morphogenesis (Zhang et al., 2001; Liu et al., 2003). Considering this, we wanted to investigate the role FGF signalling plays during embryonic nasal gland development.

4.1.1 Aims of Study

- To delineate expression patterns of mesenchymal *Fgf10* and *Fgf7* mRNA and epithelial *Fgfr2* mRNA during stages of duct elongation and gland branching in each of the embryonically developing nasal glands.
- To investigate the expression patterns of the downstream readout *Spry1* and the target ETS domain transcription factor *Pea3*, to understand where FGF signalling is active.
- To highlight the role of *Fgf10* in nasal gland development by investigating gland phenotypes in WT, *Fgf10* +/- and *Fgf10* -/- embryos.
- To uncover the role played by *Fgfr2b* signalling during gland development by investigating phenotypes in the *Fgfr2b* -/- mouse.

4.2 Results

4.2.1 FGF Signalling and Anterior Nasal Gland Development

To follow temporal localisation of *Fgfs* during normal gland development, *in situ* hybridisation was adopted to locate expression of *Fgf10* and its receptor at duct elongation and gland branching developmental stages. Additionally, detection of other *Fgfs* signalling through the FGFR2b receptor, along with downstream target and FGF signalling readout genes *Spry1* and *Pea3*.

4.2.1.1 Fgf10 and Fgfr2 Expression During Anterior Nasal Gland Development

At E13.5, as the Steno's duct is elongating through the mesenchyme of the middle concha, *Fgf10* expression was detected distal to the end of the extending duct (n=1) (Figure 4.1, D). At the same stage *Fgfr2* mRNA was found in the distal epithelial cells of the extending duct (n=1) (Figure 4.1, G). A day later, when the Steno's duct has reached the area below the maxillary sinus, *Fgf10* expression was observed throughout the mesenchyme (n=2) (Figure 4.1, E – yellow arrow). This is where the Steno's gland begins to branch over the next 24 hours. *Fgfr2* expression was found within the distal cells of the elongated Steno's duct at E14.5 (n=2) (Figure 4.1, H). When the Steno's gland was branching at E16.5, *Fgf10* expression was apparent throughout the mesenchyme surround the end buds of the gland (n=2) (Figure 4.1, F). *Fgfr2* mRNA was evident within the epithelial cells of the gland buds during this stage of branching morphogenesis (n=2) (Figure 4.1, I).

At E14.5 the duct of LNG2 had begun its elongation through the middle conchal mesenchyme and the bud of LNG3 was emerging from the epithelium of the middle conchal lip (Figure 4.2, A-B). At this stage *Fgf10* was expressed in the conchal mesenchyme surrounding both the extending LNG2 (Figure 4.2, C) and the budding LNG3 (Figure 4.2, D). At this same stage, *Fgfr2* is expressed in the ductal epithelial cells of the elongating LNG2 (Figure 4.2, E) and the within the cells of the LNG3 bud (Figure 4.2, F). As LNG2 and LNG3 were branching at E16.5, *Fgf10* was expressed throughout the mesenchyme surrounding the developing end buds (Figure 4.3, C), as well as adjacent to the end of the LNG5 duct (Figure 4.3, D). *Fgfr2* was expressed within the end bud epithelial cells of LNG2 and LNG3 (Figure 4.3, E) and within the distal duct of LNG5 (Figure 4.3, F). At E16.5, when the LNG4 duct is elongating

beneath the nasal septum, *Fgf10* was expressed in the mesenchyme surrounding the extending duct (Figure 4.4, B) and *Fgfr2* within the ductal cells (Figure 4.4, C).

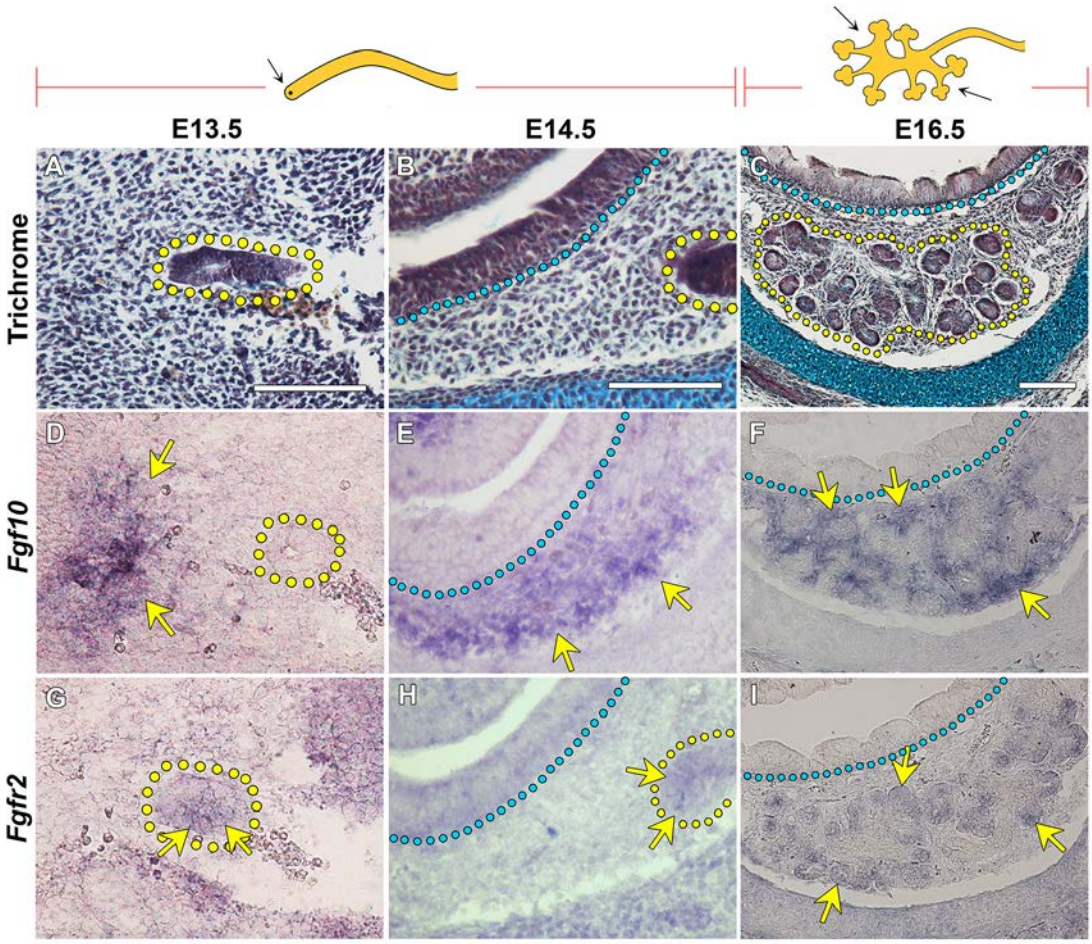

Figure 4.1 *Fgf10* and *Fgfr2* expression during Steno's gland development.
Trichrome stained sagittal sections of the distal Steno's duct (A-B) and gland (C) at respective stages of development. (D) *Fgf10* mRNA is detected in the mesenchyme adjacent to the elongating Steno's duct at E13.5. (E) At E14.5, *Fgf10* expression is seen all throughout the mesenchyme beneath the maxillary sinus epithelium in the location of where the Steno's gland will branch. (F) At E16.5 when the Steno's gland is undergoing continual branching, *Fgf10* is seen in the mesenchyme surrounding the distal gland buds. (G) *Fgfr2* expression is seen within the distal epithelial cells of the Steno's duct at E13.5. (H) At E14.5, *Fgfr2* mRNA is detected in the maxillary sinus epithelium and the distal epithelial cells of the Steno's duct. (I) During gland branching stages at E16.5, *Fgfr2* expression is evident in the distal epithelial cells of the gland end buds. Steno's gland outlined in yellow; blue dotted line outlines the basement membrane of the maxillary sinus epithelium. Scale bar = 100μm.

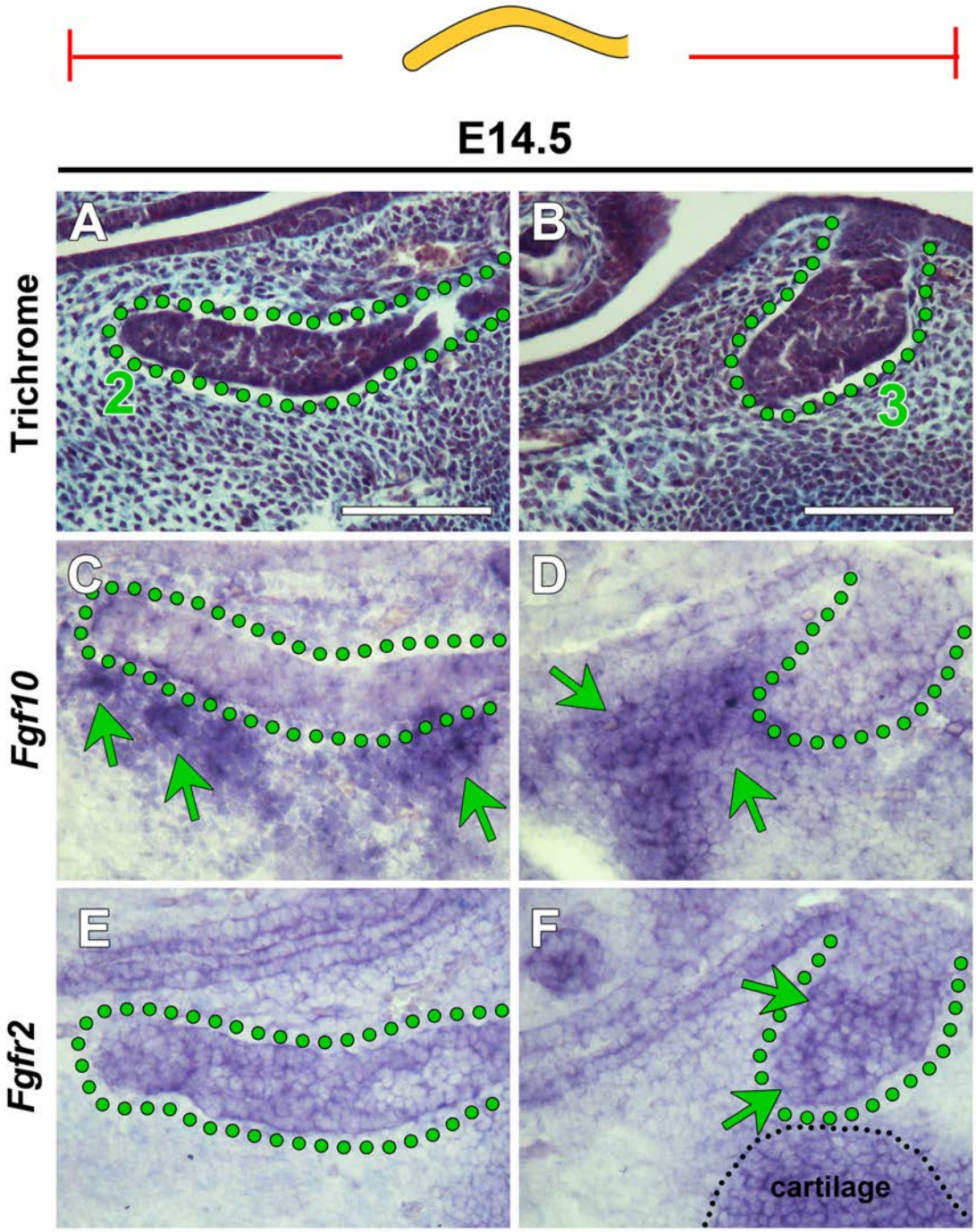

Figure 4.2 *Fgf10* and *Fgfr2* expression during LNG duct elongation.
(A-B) Trichrome staining of the LNG2 duct (A) and LNG3 bud (B) at E14.5. (C-D) *Fgf10* expression is found throughout the mesenchyme adjacent to the elongating LNG2 and surround the invaginating LNG3 bud. (E-F) *Fgfr2* is expressed within the epithelial cells of both the LNG2 and LNG3. LNGs outlined in green. Scale bar = 100μm.

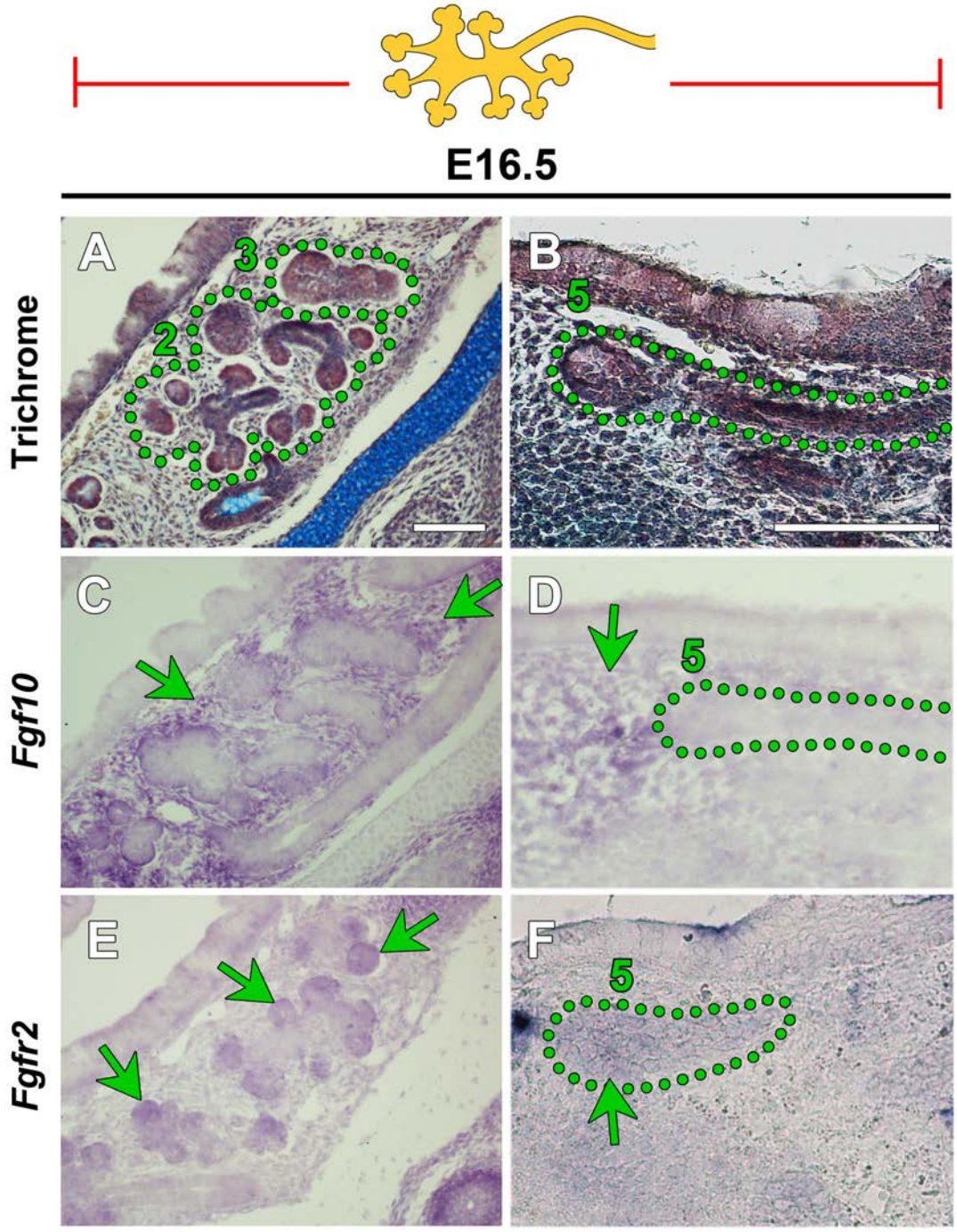

Figure 4.3 *Fgf10* and *Fgfr2* expression during LNG gland branching.
(A) Trichrome staining of LNG2 and LNG3 branching glands. (B) Trichrome staining of the LNG2 and LNG3 ducts as well as the LNG5 elongating duct, at a more rostral plane. (C) *Fgf10* expression is seen throughout the mesenchyme surrounding the branching LNG2 and LNG3 buds. (D) Some *Fgf10* expression is maintained in the mesenchyme close to the extended LNG2 and LNG3 ducts, as well as in the mesenchyme close to the extending LNG5 duct. (E) *Fgfr2* expression is clearly seen in the branching epithelial buds of LNG2 and LNG3. (F) Some *Fgfr2* expression is seen within some epithelial cells od LNG2 and LNG3 and in the distal epithelial cells of the extending LNG5. LNGs outlined in green. Scale bar = 100μm.

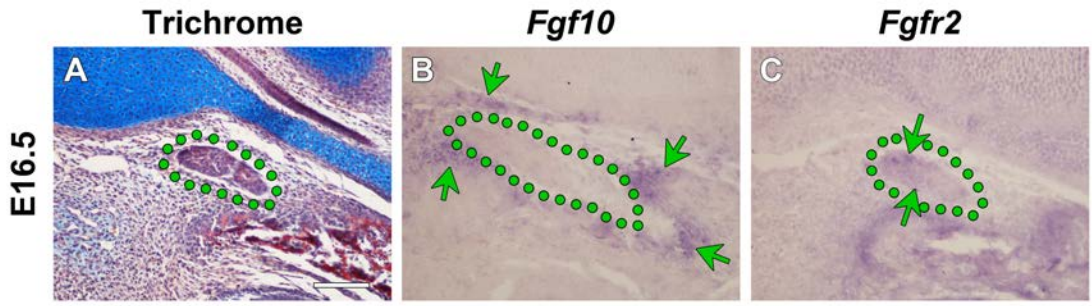

Figure 4.4 *Fgf10* and *Fgfr2* expression during LNG4 development.
(A) Trichrome staining of the elongating LNG4 (green outline) duct found beneath the nasal capsule. (B) *Fgf10* is expressed in the mesenchyme below the nasal capsule surrounding the LNG4. (C) *Fgfr2* is expressed within the epithelial cells of the LNG4 duct.

Fgf10 is expressed throughout the mesenchyme of the nasal septum at E14.5 when the MNG gland ducts are elongating (Figure 4.5, C). At this stage *Fgfr2* expression is noted in the epithelial cells of the extending MNG1 duct (Figure 4.5, E). At the branching stages of the MNGs at E16.5, *Fgf10* still surrounds the extending glandular branches and *Fgfr2* is expressed within the gland buds (Figure 4.5, D & F)

Similar to all the other nasal glands, *Fgf10* is seen throughout the mesenchyme adjacent to the MSG primordium at E14.5 (Figure 4.6, C), with *Fgfr2* expression seen within the maxillary sinus epithelium from which the MSG buds (Figure 4.6, E). When the MSG is branching at E16.5, *Fgf10* expression is maintained throughout the epithelium adjacent to branching MSG end buds (Figure 4.6, D). At this same stage, *Fgfr2* expression is lost within the maxillary sinus epithelium however it is apparent in the distal tips of the branching MSG end buds (Figure 4.6, F).

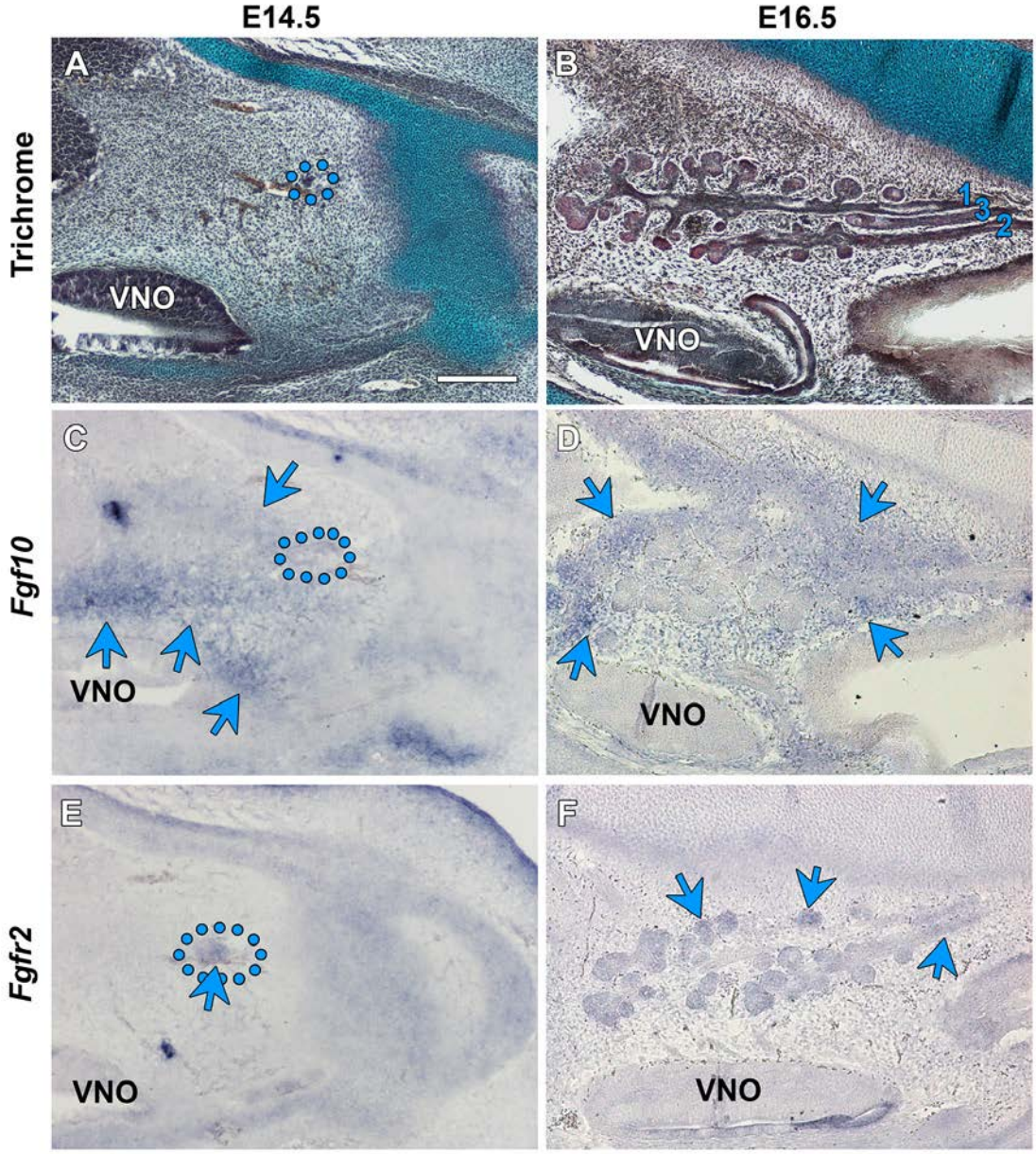

Figure 4.5 *Fgf10* and *Fgfr2* expression during MNG Development.
(A) Trichrome stained tissue section through the nasal septal mesenchyme at E14.5 and (B) through the branched MNGs at E16.5. (C) A section through the septum showing *Fgf10* expression all throughout the mesenchyme adjacent to the elongating MNGs. (D) *Fgf10* is expressed in the mesenchyme surrounding the branching MNGs at E16.5. (E) *Fgfr2* is expressed in the distal tip of the elongating MNG1. (F) *Fgfr2* mRNA is detected in the distal tips of the branching glandular buds. MNG1 duct outline in blue. Scale bar =200μm.

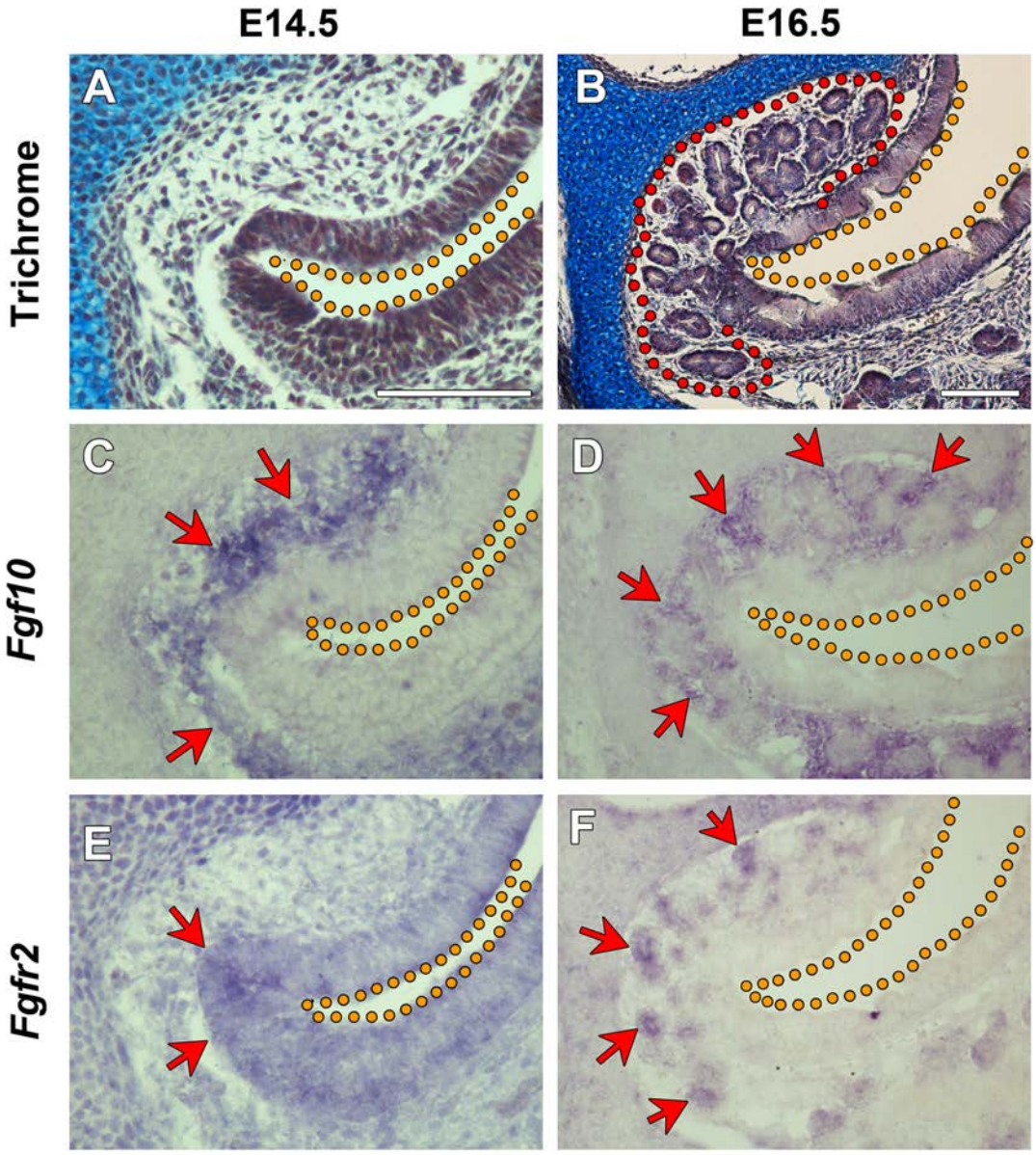

Figure 4.6 *Fgf10* and *Fgfr2* expression during maxillary sinus gland development.
(A) Trichrome staining of the position at which the MSG is about to begin its initial budding at E14.5. (B) Trichrome staining of the branching MSG at E16.5. (C) *Fgf10* is expressed throughout the mesenchyme surrounding the MSG primordium. (D) By E16.5 when the MSG is branching *Fgf10* is seen in the mesenchyme surrounding the branching MSG end buds. (E) *Fgfr2* is expressed in the maxillary sinus epithelium of which the MSG buds at E14.5. (F) By E16.5, *Fgfr2* expression is lost from the maxillary sinus epithelium but seen within the distal end buds of the MSG. Red dotted line outlines the MSG; orange dotted line outlines the maxillary sinus lumen. Scale bar = 100μm.

4.2.1.2 Spry1 and Pea3 Expression During Anterior Nasal Gland Development

Spry1, a negative-feedback regulator of tyrosine kinase signalling, and an immediate target of FGF signalling, was expressed in the distal epithelial cells of the elongating Steno's duct at E14.5 (n=2) (Figure 4.7, A). At E15.5 (n=1), when the Steno's gland was branching, *Spry1* was seen again within the epithelial cells of the extending gland buds and maintained within buds during continual branching at E16.5 (n=2) (Figure 4.7, C and E). At these same stages, *Pea3,* a downstream target of the MAPK signalling pathway, was also expressed in the epithelial cells of the extending Steno's duct at E14.5 (n=1) (Figure 4.7, B) and within the budding glands at both E15.5 (n=1) and E16.5 (n=2) (Figure 4.7, D and F).

Similar expression patterns of *Spry1* and *Pea3* were seen during LNG development. Both genes were expressed within the peripheral epithelial cells of LNG4 as it buds at E14.5 (Figure 4.8, A and B). At late E15.5, *Spry1* and *Pea3* expression was observed in cells of the newly forming gland buds of the branching LNGs (Figure 4.8, C and D). This expression was maintained within the end buds at E16.5 (Figure 4.8, E and F).

Again, expression of *Spry1* and *Pea3* during MNG1 duct elongation was restricted to the distal cells of the extending duct (Figure 4.9, A and B). As the MNGs continue formation and elongation at E15.5, some *Spry1* and *Pea3* was expressed within the newly budding glands (Figure 4.9, C and D). As the MNGs successional branching occurs at E16.5, *Spry1* and *Pea3* are expressed in the distal epithelial bud cells (Figure 4.9, E and F).

At E14.5, just before the MSG begins its budding and immediate branching, *Spry1* expression was seen throughout the basal epithelial cells of the maxillary sinus epithelium and some of the underlying mesenchyme (Figure 4.10, A). At the same stage of E14.5, *Pea3* was expressed by some cells of the maxillary sinus epithelium from which the MSG will bud (Figure 4.10, B). By E15.5 when MSG branching was evident, *Spry1* was seen in the distal epithelial bud cells (Figure 4.10, C). Some *Pea3* expression was also seen within these distal cells (Figure 4.10, D). *Spry1* expression was maintained in the gland buds during continual branching at E16.5 (Figure 4.10, E) and also *Pea3* expression was also apparent in the gland buds (Figure 4.10, F).

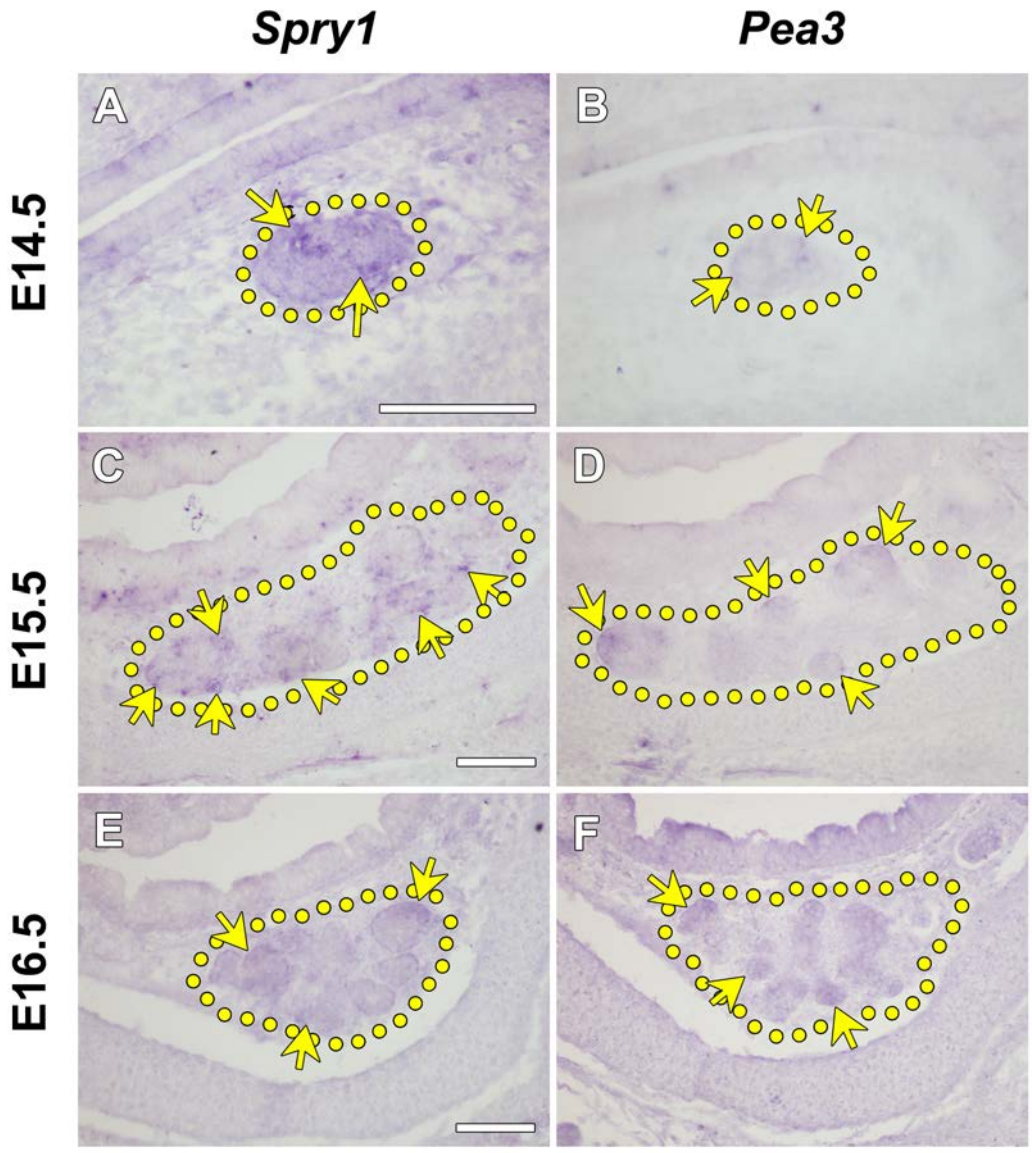

Figure 4.7 *Spry1* and *Pea3* expression during Steno's gland development.
(A-B) *Spry1* and *Pea3* expression is evident in the distal type of the elongating Steno's duct at E14.5. (C) At E15.5 *Spry1* expression is seen within the epithelial gland buds of the branching Steno's gland. (D) *Pea3* is expressed in the most peripheral epithelial cells of the branching Steno's gland. (E-F) Expression of both *Spry1* and *Pea3* is maintained in the gland buds as branching continues at E16.5. Scale bar = 100μm.

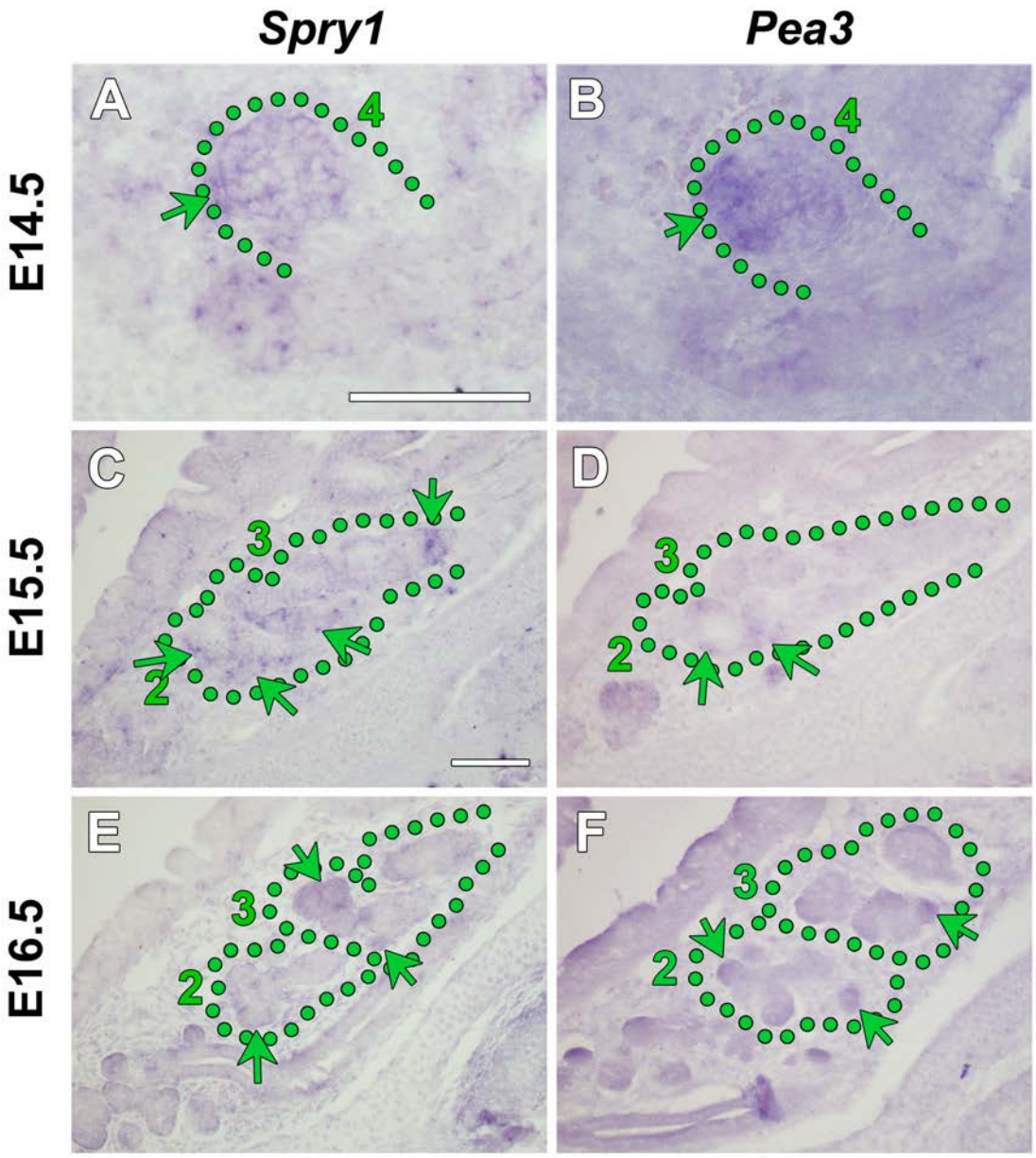

Figure 4.8 *Spry1* and *Pea3* expression during LNG development.
(A-B) As LNG4 is budding *Spry1* and *Pea3* expression is detected in the distal epithelial cells of the bud. (C-D) At E15.5, *Spry1* and *Pea3* expression is localised to the branching epithelial buds of the distal glands. (E-F) This was again seen at E16.5 where *Spry1* and *Pea3* are seen in the distal epithelial gland buds. Scale bar = 100μm.

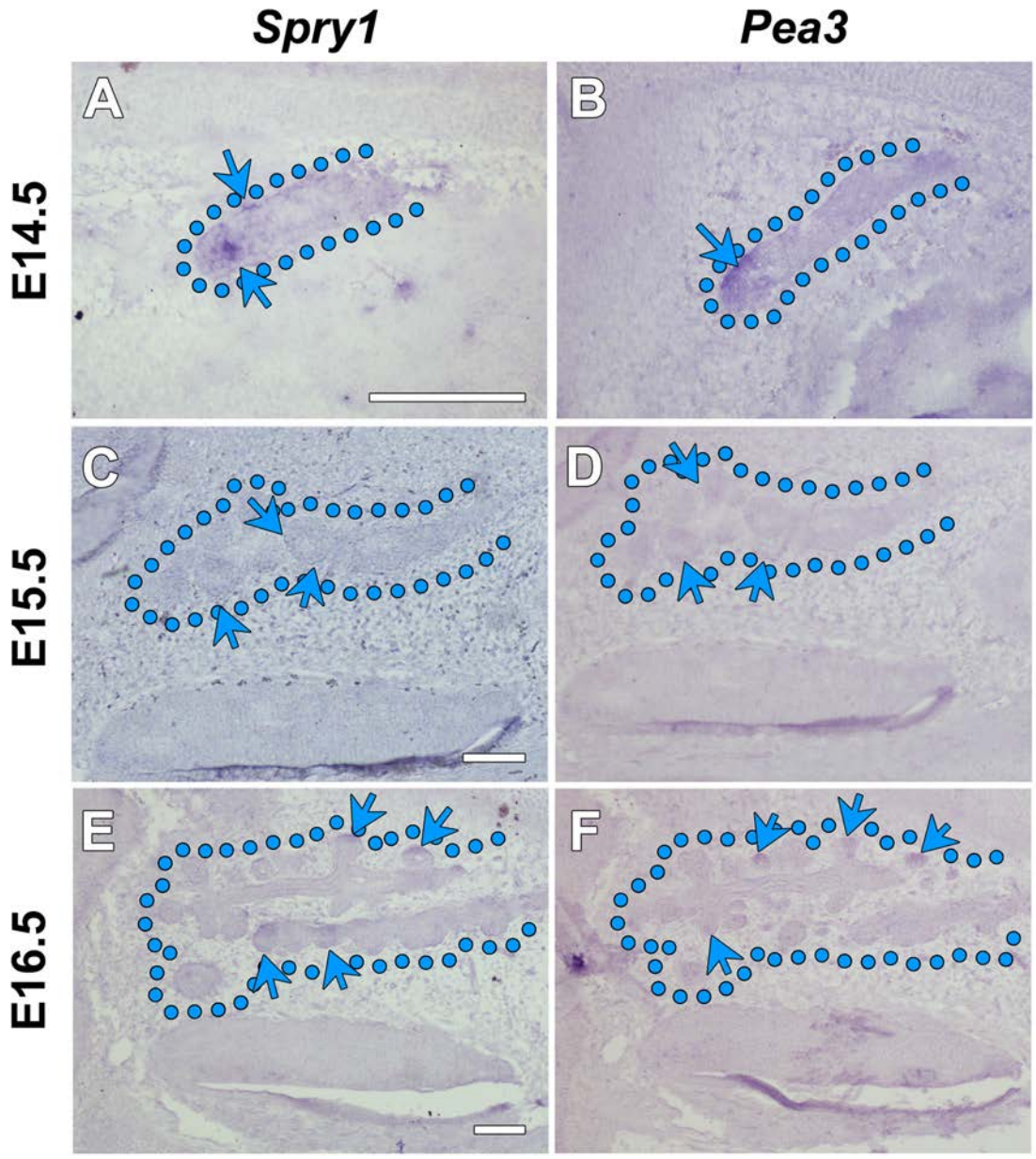

Figure 4.9 *Spry1* and *Pea3* expression during MNG development.
(A-B) At E14.5 when the MNG1 duct is elongated *Spry1* and *Pea3* expression is seen in the distal tip of the ducts. (C-D) A day at E15.5 the distal cells of the newly forming gland buds express *Spry1* and *Pea3*. (E-F) As continual gland branching occurs, *Spry1* and *Pea3* expression is seen in the distal gland buds. Scale bar = 100μm.

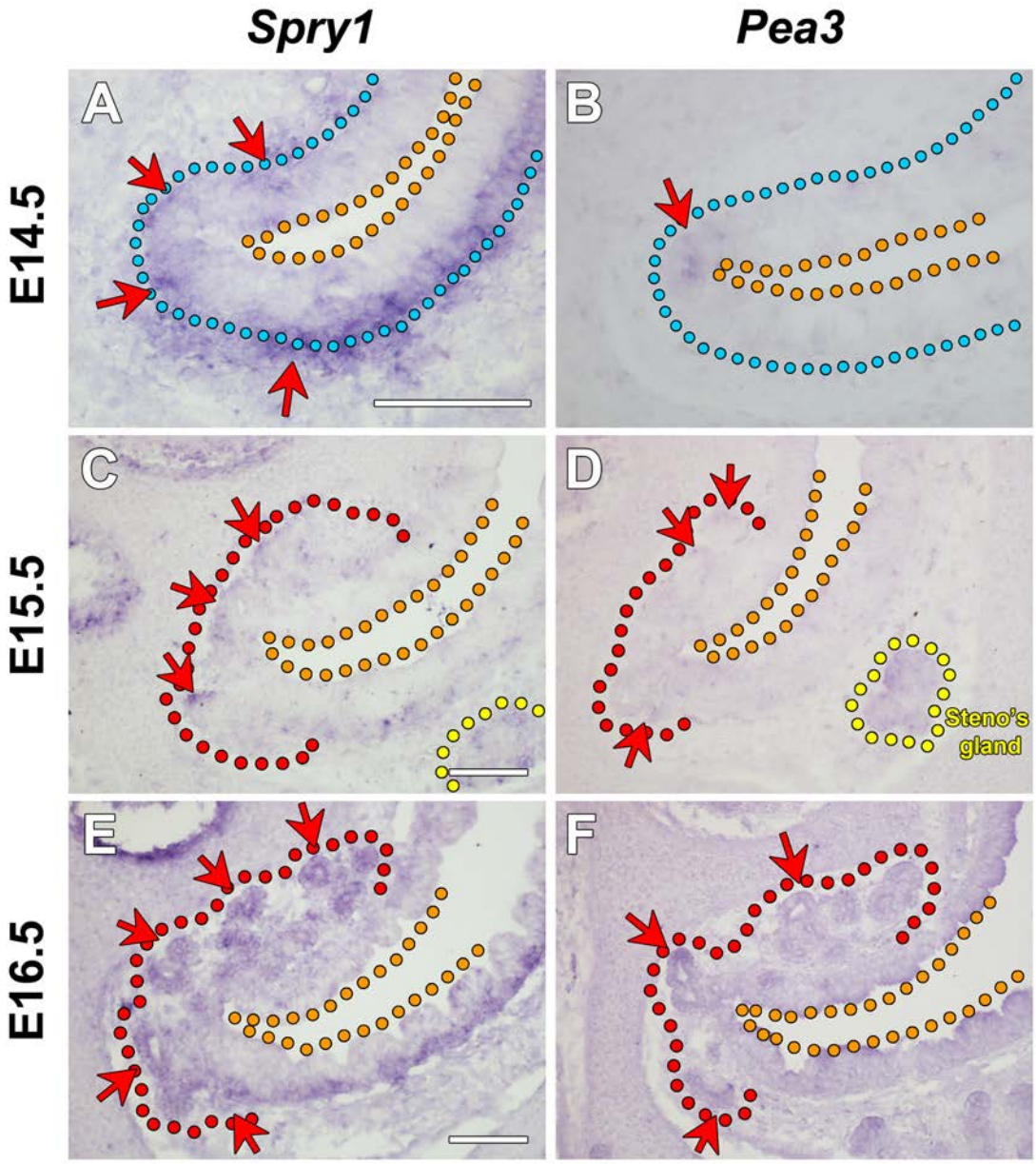

Figure 4.10 *Spry1* and *Pea3* expression during MSG development.
(A) At E14.5 priors to MSG budding *Spry1* is seen within the maxillary sinus epithelium (blue outline) as well as some of the underlying mesenchyme. (B) Some *Pea3* expression was seen within some cells of the maxillary sinus epithelium of which the MSG will bud. (C) As the MSG (red outline) is branching at E15.5, *Spry1* expression is seen in the distal end bud epithelial cells. (D) Slight *Pea3* expression was also seen in these distal bud cells. (E) At E16.5 when continual branching of the MSG occurs *Spry1* expression is evident in the gland buds. (F) *Pea3* expression is also seen in the end buds of the MSG glands and in the surface of the maxillary sinus epithelium. Orange dotted line outlines the maxillary sinus epithelium. Steno's gland is outlined in yellow. Scale bar = 100μm.

4.2.2 Fgf10 is Critical for Early Steno's and Maxillary Sinus Gland Development

To define the role of *Fgf10* in anterior nasal gland development, we analysed the gland phenotype in WT (n=3), *Fgf10* +/- (n=5) and *Fgf10* -/- (n=5) mice at E17.5 when the majority of the anterior nasal glands have elongated and branched. Investigation of the Steno's gland showed that this gland was completely absent in *Fgf10* -/- mice (Figure 4.11, G-I). The gland did develop however in *Fgf10* +/- animals, as its duct elongated to the correct location underneath the maxillary sinus and branching of the gland occurred (Figure 4.11, D-F). The amount of branches of the Steno's gland was reduced however in the *Fgf10* +/- (Figure 4.11, E and F) compared to WT littermates (Figure 4.11, B and C). Additionally, the MSG was absent with complete loss of *Fgf10* (Figure 4.11, I). Similarly to the Steno's gland, the MSG did develop in *Fgf10* +/- mice however branching was noticeably reduced (Figure 4.11, F) compared to that observed in WTs (Figure 4.11, C).

4.2.3 Fgf10 is Critical for Steno's Gland Duct Invagination

At E12.5 when the Steno's gland duct arises from the respiratory epithelium anterior (REA) and invaginates into the mesenchyme of the middle concha, an epithelial pit was observed in both WT (n=3) and *Fgf10* +/- (n=3) mice (Figure 4.12, A & B). At the same stage in *Fgf10* -/- mice however, no pit was apparent arising from the REA yet a slight swelling indicating formation of an epithelial placode was observed (n=3) (Figure 4.12, C). This phenotype indicated that FGF10 signalling is critical for the initial invagination of the duct of the Steno's gland.

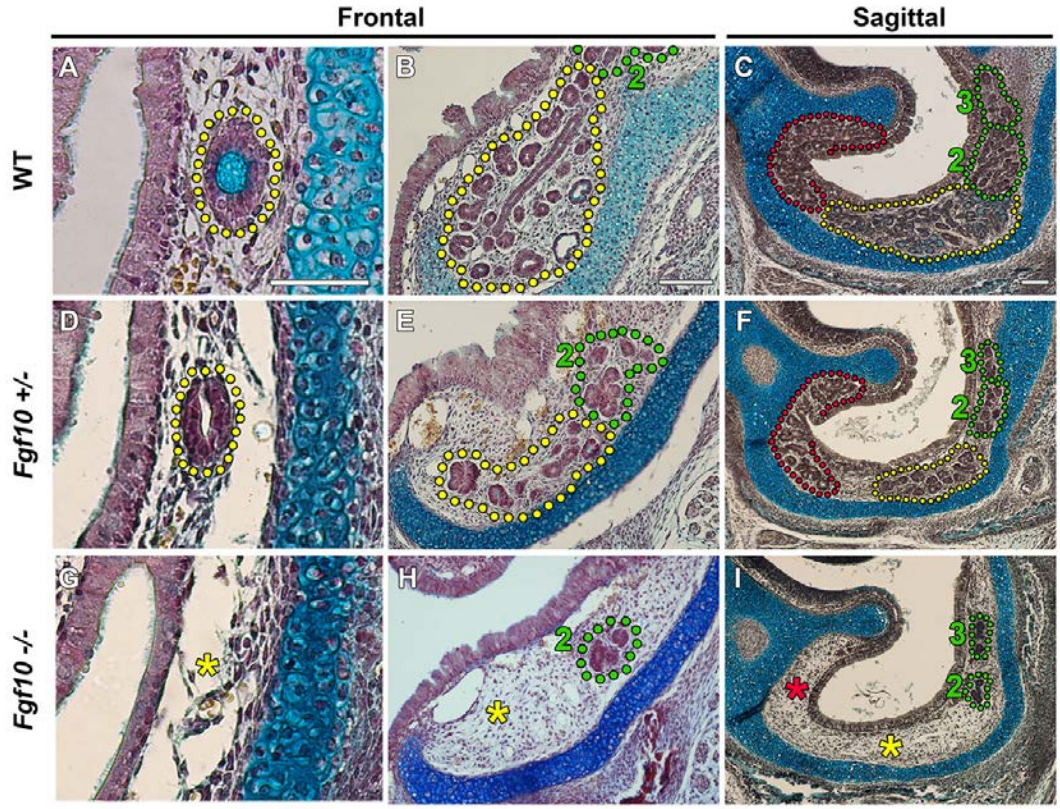

Figure 4.11 The Steno's gland and MSG are absent in *Fgf10 -/-* mice.
Frontal and sagittal sections through the nasal cavity at E17.5. The Steno's duct (A) and gland (B-C) are well established in WT animals at E17.5, as well as the MSG (C – red line). (D-F) The glands have developed in *Fgf10* +/- littermates however reduced branching is evident. (G-I) The Steno's duct (G) and gland (H-I), and the MSG (I) are completely absent in the *Fgf10* -/- animal. The LNG ducts extend to their correct location in the *Fgf10* -/- however branching of the distal glands is severely defective (H-I). Steno's gland = yellow; MSG= red; LNG2&3=green; asterisks represent absent gland. C**olumn1** scale bar=50μm, **Column2** and **3** scale bar=100μm.

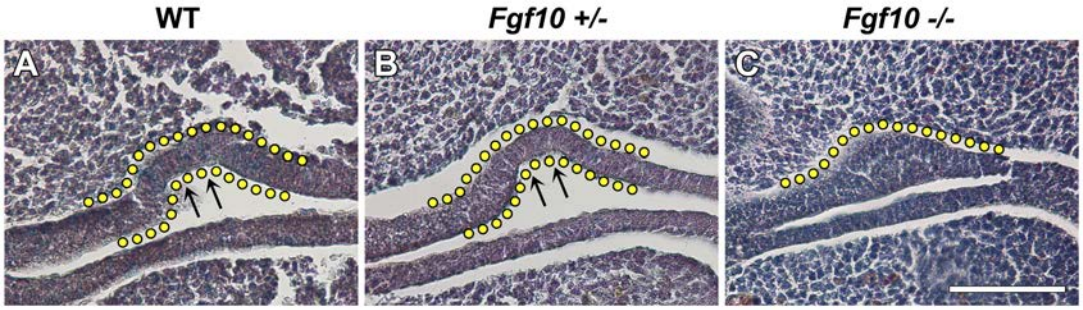

Figure 4.12 *Fgf10* expression is required for initial Steno's bud invagination
(A) Indentation of the Steno's gland duct is observed in WT animals at E12.5 (B) Similar development is seen in *Fgf10* +/- littermates as the Steno's duct dips into the underlying mesenchyme**.** (C) No ductal pit is found in the *Fgf10* -/- mouse. An epithelial placode swelling occurs however, and development appears to arrest at this stage. Scale bar = 100μm.

4.2.4 Fgf10 is required for Successful Branching of the Lateral and Medial Nasal Glands

The LNGs are found in both *Fgf10 +/-* and *-/-* mice at E17.5. Their ducts have budded and elongated to the correct locations when compared to WT specimens (Figure 4.13, A-F). Branching of the distal glands was affected however with a slight reduction observed in the heterozygotes (Figure 4.13, D-E) and a more significant reduction in branches in the homozygotes (Figure 4.13, G-H). When the MNGs have elongated and branched throughout the septal mesenchyme in WTs at E17.5 (Figure 4.13, C), in *Fgf10 +/-* mice they developed to the same stage, however fewer gland branches were observed (Figure 4.13, F). In *Fgf10 -/-* littermates, the MNGs were severely defective with ducts elongating, yet were truncated with considerably reduced branches (Figure 4.13, I).

4.2.5 Fgfr2b is Critical for Steno's Gland, MSG, LNG4 and MNG Development

To elucidate if other FGF ligands working through the same receptor as FGF10 were critical for nasal gland development, the gland phenotype was investigated in *Fgfr2b* knockout mice at E18.5 (n=2). Similarly to *Fgf10* homozygous mutants, the Steno's duct (Figure 4.14, A-B) and gland (Figure 4.14, C-D) were completely absent in *Fgfr2b -/-*. Furthermore, similar to the *Fgf10 -/-* phenotype, the MSG was also absent in the *Fgfr2b* knockout (Figure 4.15, C-D). Additionally, unlike the *Fgf10 -/-* phenotype, the MNGs were also absent with complete loss of *Fgfr2b (*Figure 4.15, A-B). This indicates that other FGFs that bind to FGFR2b with high affinity are required for MNG duct elongation and branching.

Investigation of LNG development showed that the LNG2 duct budded and elongated in *Fgfr2b* deficient mice however branching of the distal LNG2 gland was severely truncated (Figure 4.14, C-D). A similar phenotype is seen with LNG3 as its duct (Figure 4.14, C-D) and a reduced distal gland (Figure 4.16, A-B) were found in *Fgfr2b* deficient animals at E18.5. Interestingly, loss of *Fgfr2b* leads to the complete absence of LNG4, as observed underneath the nasal cartilage capsule at E18.5 (Figure 4.16, C-D), suggesting that other FGFs that bind to FGFR2b are required for LNG4 development. LNG5 developed similarly to that of LNG2 and LNG3, as its duct extended to the correct location however branching of the distal gland was defective (Figure 4.16, E-F).

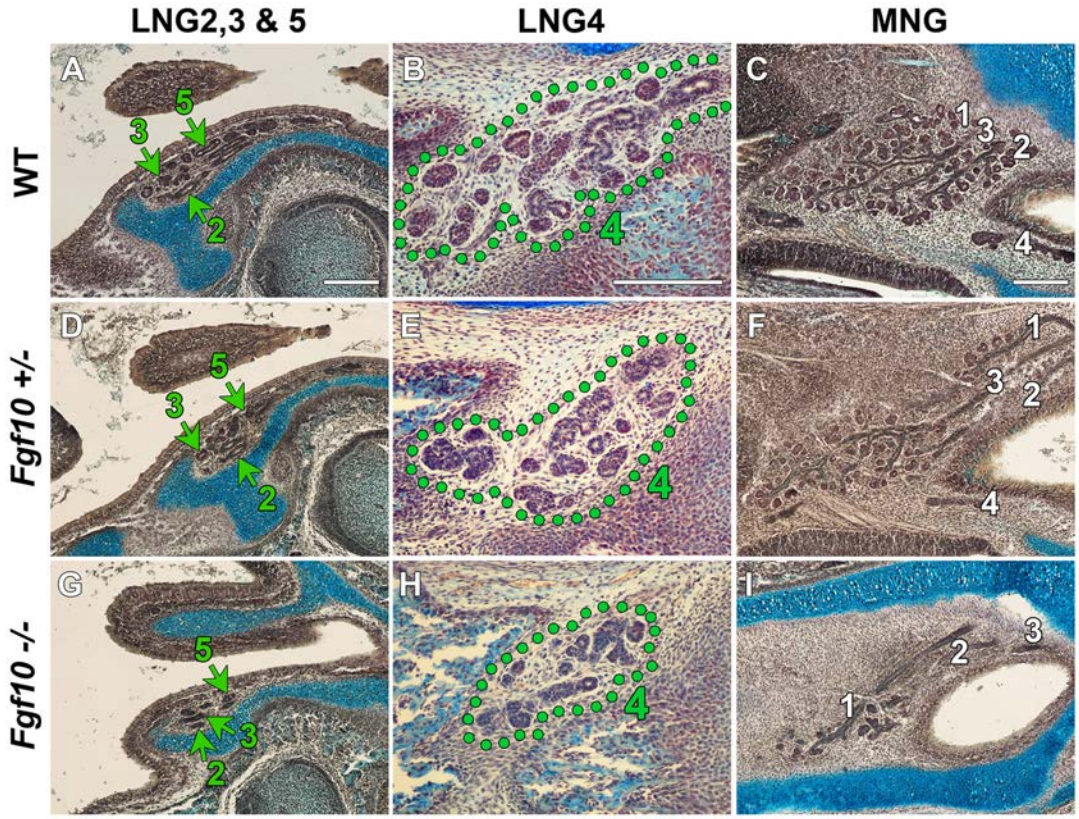

Figure 4.13 *Fgf10* expression is required for the branching of the distal LNG and MNGs.

(A) Gland branches of LNG3 and 5, and the duct of LNG2, are found beside the nasal cartilage groove in WT animals. (B) LNG4 has extended beneath the nasal septum and has branched extensively. (C) MNG1-3 are well established in the WT at E17.5, and MNG4 has elongated and begun branching. (D-F) A similar phenotype is seen in *Fgf10* +/- littermates, however branching of all of the distal glands is slightly reduced. (G) Branching is severely defective in LNG3 and 5 in the *Fgf10* -/- animal. (H) LNG4 has extended and undergone some branching but again the number of branches is significantly reduced. (I) Ducts of MNG1-3 have elongated in the *Fgf10* -/- mouse at E17.5 however branches extending from the distal duct are severely truncated. Scale bar = 200μm.

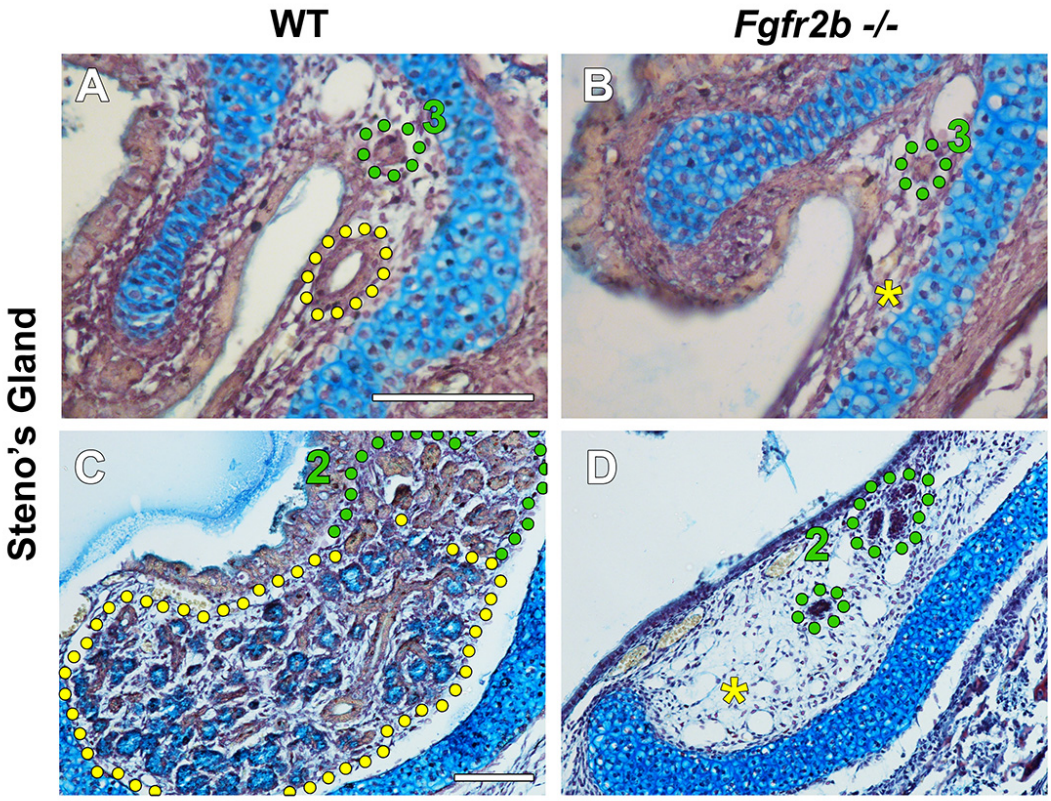

Figure 4.14 *Fgfr2b* expression is critical for Steno's gland development.
(A-B) Frontal sections of E18.5 nasal tissue shows the Steno's duct present in WT (A) and absent in *Fgfr2b -/-* animals (B). The duct of LNG3 is found in both WT and *Fgfr2b* deficient mice. (C) The distal LNG2 and Steno's gland are seen clearly in WT. (D) The Steno's gland is completely absent in *Fgfr2b -/-* mice. LNG2 is found in *Fgfr2b -/-* animals however branching of the gland is extremely defective, with only truncated end buds found (D). Asterisks indicate absence of the Steno's gland. Scale bar = 100μm.

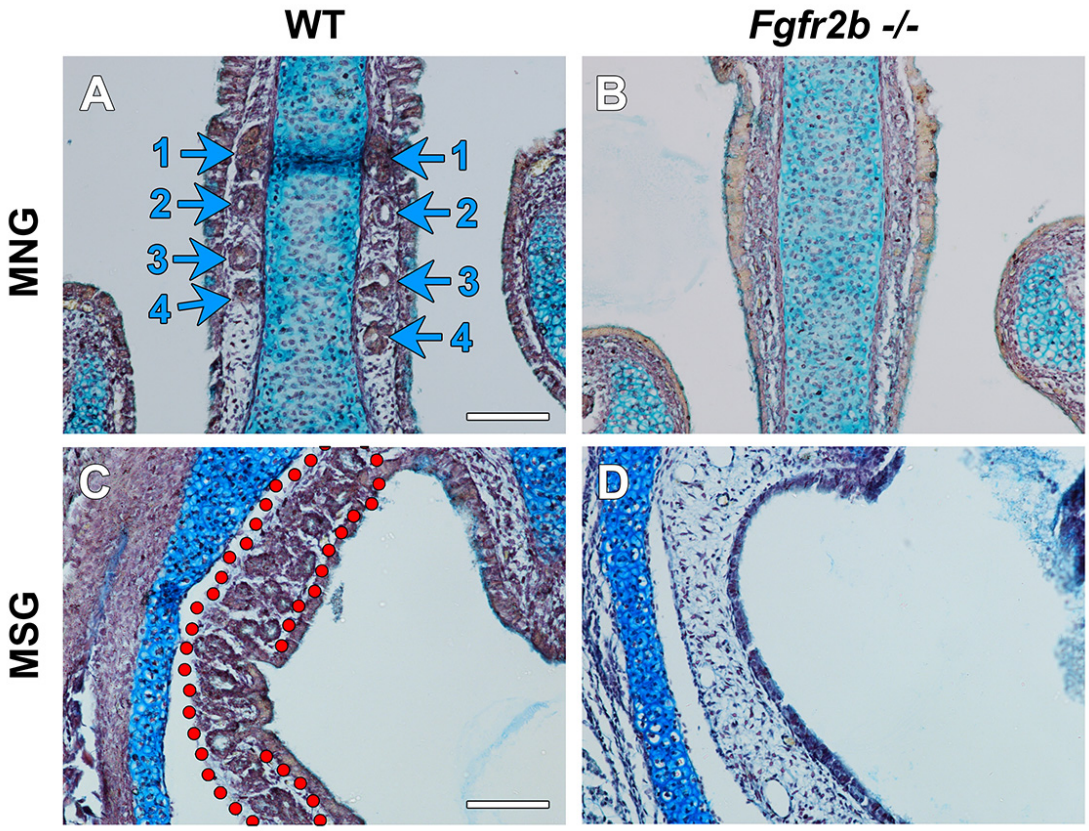

Figure 4.15 *Fgfr2b* expression is critical for Medial and Maxillary Sinus Gland development.

(A-B) The MNGs are completely absent in *Fgfr2b* -/- mice compared to their WT littermates. (C-D) The MSG develops from the maxillary sinus epithelium in WTs however does not develop in *Fgfr2b* deficient mice, seen at E18.5. Scale bar = 100μm.

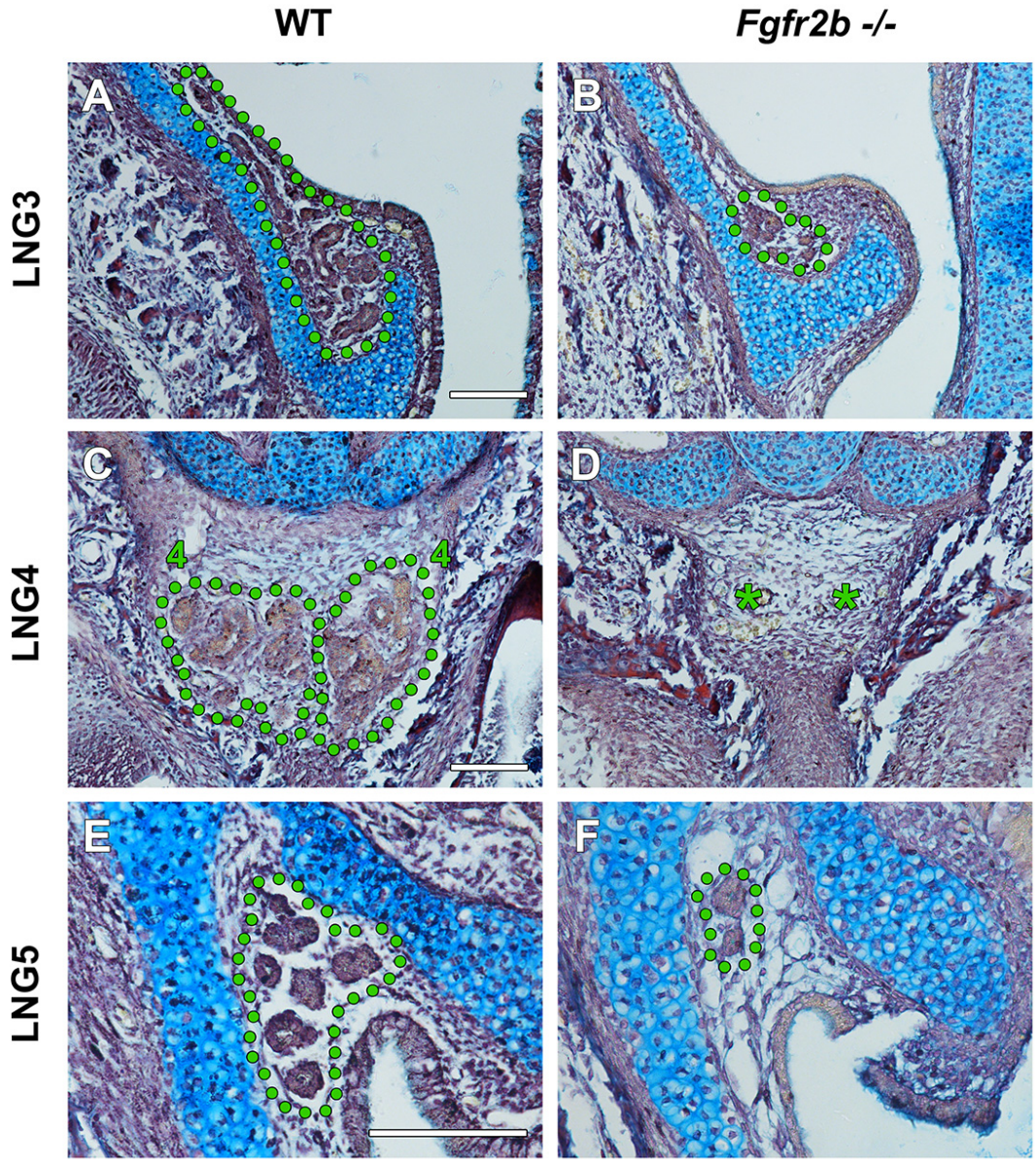

Figure 4.16 *Fgfr2b* expression is critical for LNG4 formation and LNG3 and LNG5 distal gland branching.

Frontal histological sections of E18.5 embryos. (A-B) The LNG3 duct extends to the same location in *Fgfr2b* -/- mice however branching of the distal gland is severely reduced. (C-D) Both LNG4 glands are found below the nasal cartilage capsule in WT animals, however are completely absent with the loss of *Fgfr2b*. (E-F) The LNG5 duct develops in *Fgfr2b* -/- mice yet branching of a distal gland is truncated. Asterisks indicate absence of the LNG4. Scale bar = 100µm.

4.2.6 Fgf7 Expression During Anterior Nasal Gland Development

Considering the absence of the MNGs in the *Fgfr2b* -/- mouse, yet the presence of MNG ducts and primary branches in the *Fgf10* homozygous embryo, we decided to investigate the expression pattern of *Fgf7* during normal gland development, as this ligand is closely related to FGF10 and also binds to FGFR2b with high affinity.

Fgf7 was not found in the mesenchyme surrounding the Steno's gland during any of the duct elongation stages (Figure 4.17 A-C) or gland branching (Figure 4.17, D). *Fgf7* expression was observed surrounding the nasolacrimal duct (NLD) and this was used as a positive control of gene expression (Figure 4.17, A and D inset image). No *Fgf7* expression was associated with LNG or MSG development (Figure 4.18 A-D). Unlike the other anterior nasal glands however, *Fgf7* expression was observed throughout the septal mesenchyme at E14.5 (n=2)(Figure 4.18, E). As the MNG ducts were elongating *Fgf7* expression was maintained in the anterior septal mesenchyme close to the elongating ducts (n=2)(Figure 4.18, F). These results suggest that MNG duct elongation and primary branching may be reliant on *Fgf7*, more so than that of *Fgf10.*

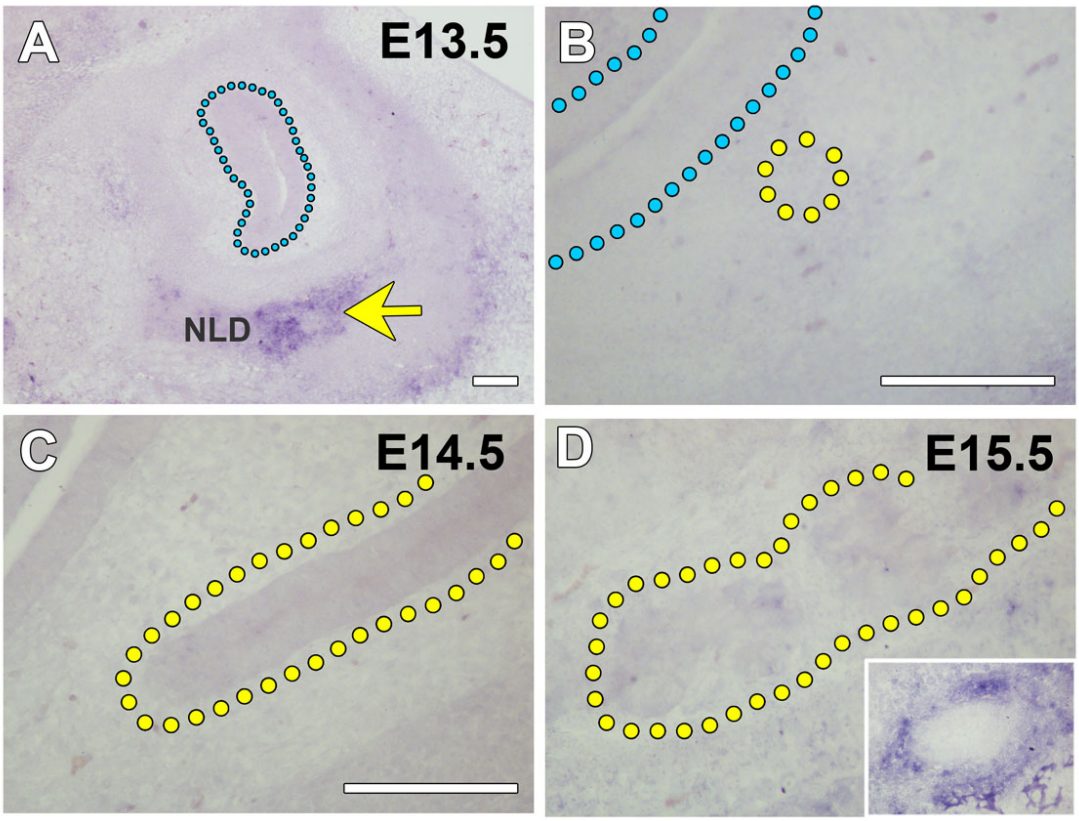

Figure 4.17 *Fgf7* expression during Steno's gland development.
(A) At E13.5, the mesenchyme surrounding the maxillary sinus is absent of *Fgf7*, however *Fgf7* expression was found surrounding the NLD at this stage (arrow). (B) No *Fgf7* expression is detected adjacent to the distal tip of the Steno's duct at E13.5. (C) At E14.5 no *Fgf7* expression is associated with the elongating Steno's duct. (D) When the Steno's gland is branching at E15.5 no *Fgf7* is observed near the branching gland. *Fgf7* expression is still maintained in the mesenchyme surrounding the NLD (D - inset image). Scale bar = 100μm.

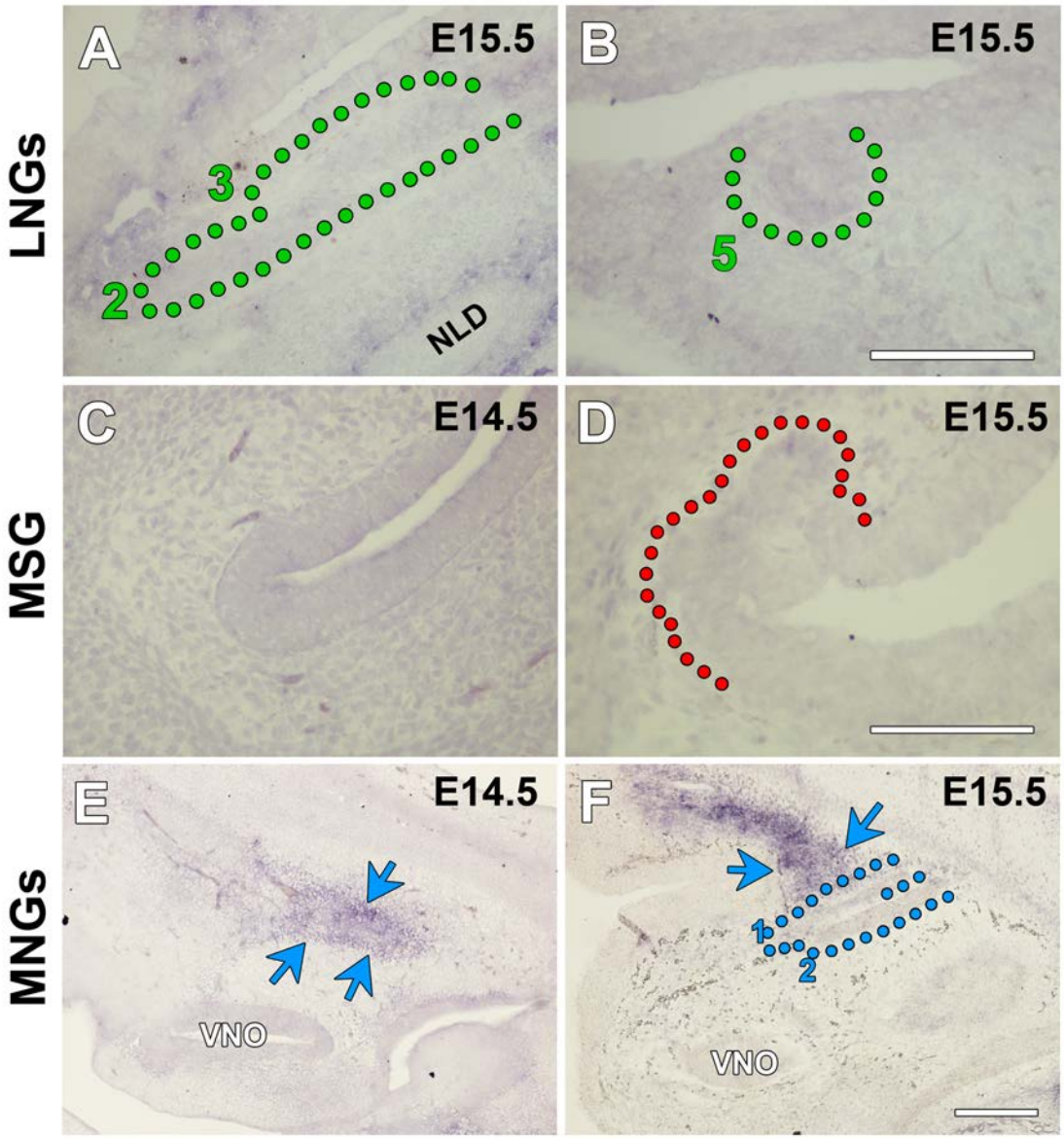

Figure 4.18 *Fgf7* expression during anterior nasal gland development.
(A) *Fgf7* expression is not found associated with the elongate LNG2 and 3 ducts or (B) the budding LNG5 at E15.5. (C) *Fgf7* expression is not associated with the epithelium where the MSG will bud at E14.5 or (D) surrounding the branching MSG at E15.5. (E) At E14.5, a section through the nasal septum shows *Fgf7* expression throughout the mesenchyme. (F) At E15.5, *Fgf7* expression is seen in the anterior mesenchyme of the nasal septum close to the elongating MNG ducts. A-D scale bar = 100μm, E-F scale bar = 200μm.

4.3 Discussion

4.3.1 Fgf10 is Essential for Anterior Nasal Gland Branching Morphogenesis

The anterior nasal glands provide a wonderful model for studying branching morphogenesis due to their long duct elongation stage and subsequent gland branching. This allows the investigation of different pathways and signalling molecules involved in these distinct stages of organogenesis. In this study, it was elucidated that *Fgf10* is essential for gland branching of all of the anterior nasal glands. Although branching of the glands occurs in an array of temporal locations, expression of *Fgf10* mRNA was seen throughout the mesenchyme surrounding the gland end buds of all glands during their branching stages. This expression pattern of *Fgf10* is similar to that seen during mammalian lung development as *Fgf10* mRNA is localised to the mesenchyme surrounding newly developing lung buds (Bellusci, Grindley, et al., 1997). In the lung, *Fgf10* has been shown to trigger cell proliferation and act as a chemoattractant (Bellusci, Grindley, et al., 1997; Park et al., 1998), and the expression pattern described in our study suggests a similar role in nasal SMG development. Examination of the *Fgf10* mutant mouse also emphasised that with one copy of *Fgf10* present in the heterozygotes, branching of the nasal glands occurs however is slightly reduced and in the complete absence of *Fgf10* in the homozygotes, gland branching is seriously defective with only the presence of severely truncated end buds at the distal ductal tips. The heterozygous phenotype observed is consistent with the lacrimal gland and salivary gland aplasia present in the mouse model and human LADD syndrome (Entesarian et al. 2007 and *Chapter 6*). As the number of branches is reduced in the *Fgf10* +/- animals, this suggests that *Fgf10* is involved in cleft formation and branch extension. This hypothesis is supported by similar research using other branching models. When the submandibular salivary gland (SMDG) is cultured *ex vivo* with antisense oligonucleotides for FGFR2b, glands develop with a decreased amount of gland branches, however this phenotype can be rescued by the addition of FGF10 (Steinberg et al., 2005). Furthermore, *ex vivo* culture of lung, lacrimal and the SMDG with WNT3A has been shown to inhibit clefting and reduce the number of epithelial branches (Dean et al., 2005; Patel et al., 2011). It is understood that this stimulation of the canonical Wnt pathway regulates *Fgf10* levels, as knockdown of β-catenin leads to upregulation of *Fgf10* in both the lacrimal gland and the lung (Dean et al., 2005). Using *in vitro* culturing methods of the SMDG, Koyama et al. (2008) showed that epidermal growth factor (EGF) was the

main cause of cleft formation as it increased the number of branches when cultured with normal salivary glands, and stimulated clefting in those glands that had been cultured without mesenchyme. Culture of mesenchyme-free glands with FGF10 did not stimulate cleft formation, however it did result in the elongation of stalks and the expansion of endpieces (Koyama et al., 2008). Furthermore, branch elongation in the presence of FGF10 has been shown to be independent of the MAPK pathway, and potentially works through the PLCγ pathway (Koyama et al., 2008). It is therefore suggested that *Fgf10* plays a similar role in the growth and proliferation of anterior nasal glands during branching morphogenesis. This hypothesis is supported by the phenotype shown by both the LNGs and the MNGs in the *Fgf10* knockout mouse. While branching morphogenesis is significantly defective, truncated branches do form in these glands suggesting that *Fgf10* is essential for elongation and expansion of gland branches as opposed to the formation of clefts from the ducts or primary branches. To delineate this further, *in vitro* slice culture of the nasal glands could be employed and exposed to the MEK inhibitor U0126 and PLCγ inhibitor U73122 to investigate the influence this has on branching morphogenesis of the distal nasal glands.

Expression patterns of *Spry1* and *Pea3* were restricted to the most distal epithelial buds of the branching end buds in all of the anterior nasal glands. This coincides with reports for other branching organs. *Spry1* expression has been reported in the branching lung buds between E11.5 and E14.5 (Zhang et al., 2001), and similarly seen in the distal epithelial buds and ducts of the SMDG during morphogenesis (Patel et al., 2011). *Pea3* expression was observed from E10.5-E18.5 in the most peripheral endodermal cells of the extending lung buds, as well as some expression found in the mesoderm (Liu et al., 2003). A similar expression pattern of this ETS domain transcription was also seen in SMDG branching morphogenesis, where *Pea3* expression was restricted to the distal epithelial buds and not found in the ductal structures (Patel et al., 2011). While *Spry* expression is a downstream read out of FGF signalling, it also plays a critical role in negatively regulating growth factor signalling from both the FGF and EGF families (Kramer et al., 1999; Reich et al., 1999). *Spry1* expression, as well as *Fgfr2* expression, appeared more widespread than *Pea3* expression, in nasal gland epithelial buds of consecutive tissue sections. This suggests

that while many cells within the buds are receiving an FGF signal, only the peripheral *Pea3* positive cells are triggering nuclear transcription factor activation leading to changes in cell behaviour.

4.3.2 Fgf10 Plays a Heterogeneous Role in Early Anterior Nasal Gland Development

The complete absence of the Steno's gland in the *Fgf10 -/-* mouse indicates this growth factor's pivotal role in the development of this structure. As explained in *Chapter 3,* this gland differs from the others as it buds approximately 24 hours earlier than the onset of the rest of the nasal glands and it also invaginates into the mesenchyme at its bud stage as an epithelial indentation, as opposed to a solid swelling of cells. If other branching structures that employ the same invaginating mechanism are considered, it is clear that *Fgf10* plays a similar role. As described before, the lung develops through a similar mechanism and agenesis of the lung occurs in *Fgf10 -/-* mice (Min et al., 1998; Sekine et al., 1999). The lacrimal gland of the eye also undergoes this tubular invagination from the conjunctival epithelium (Kammandel et al., 1999; Makarenkova et al., 2000). At approximately E13.5 when the lacrimal bud arises on the temporal side of the eye, *Fgf10* expression is seen in the periocular mesenchyme adjacent to the budding gland and distal to the tip of the gland as it is elongating at E14.5 (Makarenkova et al., 2000). Investigation of *Fgf10 -/-* mice at E18.5 showed the complete absence of the lacrimal gland (Makarenkova et al., 2000), a phenotype similar to that seen of the Steno's gland. A similar function for *Fgf10* however is employed in budding structures that arise as solid cords of cells. As mentioned before the SMDG arises at the *Initial Bud* stage at E12.5 in the *Fgf10*-null, however any epithelium structure is absent by E13.5 (Jaskoll et al. 2005). This shows similarity to the Steno's bud phenotype shown in the E12.5 *Fgf10 -/-*, as a swelling of the epithelium is seen however no duct primordia successfully invaginates into the underlying mesenchyme. Furthermore, *Fgf10* expression in the lateral plate mesoderm is essential for the outgrowth of the limb bud from the apical ectoderm (Ohuchi et al., 1997; Min et al., 1998; Sekine et al., 1999).

The absence of the MSGs in *Fgf10 -/-* is conclusive with the establishment that *Fgf10* is essential for branching morphogenesis, as these glands refrain from ductal formation and rather branch immediately from the maxillary sinus epithelium.

Apparent *Fgf10* expression surrounding the maxillary sinus, along with *Fgfr2b* and downstream targets *Spry1* and *Pea3* within the maxillary sinus epithelium and branching MSG end buds respectively, also confirm its significant role. It must be highlighted that MSG bud branching is solely tubular in nature, therefore adopting a branching mechanism similar to the ductal formation of the Steno's gland, however different to the gland formation of the salivary glands and all the other anterior nasal glands.

Expression of *Fgf10* mRNA in the mesenchyme adjacent to, as well as *Fgfr2* within the epithelium of both the LNGs and MNGs as their ducts are budding and elongating, was shown in this study by *in situ* hybridisation. While this suggests *Fgf10* is involved in early LNG and MNG bud outgrowth and duct elongation, its function is not critical however as these same ducts bud and elongate in the *Fgf10* -/- mouse. Due to the complexity of biological regulatory networks, removal of one or some of its elements does not necessarily contribute to its overall collapse (Jeong et al., 2000; Albert et al., 2000). Furthermore, expression of *Spry1* and *Pea3* during budding, duct elongation and branching of these glands highlights involvement of FGF signalling. Therefore, although the development of LNG and MNGs proceed without *Fgf10,* it cannot be ruled out that *Fgf10* does not play a role in early stages of their normal organogenesis. Their early ductal morphogenesis is unaffected however, with loss of *Fgf10* alone. This establishes that the function of *Fgf10* is conserved among some branching structures, however this role is not applicable to all biological cases.

4.3.3 Other Signalling Molecules are Essential for Anterior Nasal Gland Development

While the absence of *Fgf10* inhibited the complete development of the Steno's gland and the MSG, the LNGs and MNGs successfully budded, elongated as ducts and underwent some primary branch formation. This suggests that these glands either predominantly rely on other signalling factors for their early development, or compensation is made by other factors in the *Fgf10* knockout. A likely candidate for recruitment is *Fgf7*. The amino acid core of *Fgf7* shows over 60% sequence identity with that of *Fgf10*, making it the most structurally similar growth factor to *Fgf10* (Yamasaki et al., 1996). Biological functions are also conserved between these two

mesenchymally expressed *Fgfs,* emphasised by both their ligands having high affinity to FGFR2b and their interplay seen during branching morphogenesis of other structures. During mouse lung development, *Fgf7* is not expressed in the lung mesenchyme during early endoderm branching at E11.5 however *Fgf7* transcripts are detected when the lung is undergoing extensive branching between E13.5-E14.5 (Bellusci, Grindley, et al., 1997). Early studies using culture of mesenchyme-free endoderm with FGF7 protein showed that it stimulates endoderm stalk extension by inducing cell proliferation (Cardoso et al., 1997). Bellusci, Grindley, et al. (1997) elucidated that prolonged exposure to FGF7 only gave rise to stalk expansion in the mesenchyme-free lung cultures, while when cultured with FGF10, expansion was first induced followed by additional budding. While *Fgf7* expression was not as evident as that of *Fgf10* in the periocular mesenchyme during normal *in vivo* lacrimal gland development, application of an FGF7 bead to lacrimal gland explant cultures induced ectopic gland bud formation, similarly to FGF10 protein application, however not at as high a rate (Makarenkova et al., 2000). In comparison, culture of SMDGs with FGF7 only gave rise to moderate stalk extension and instead induced epithelial bud enlargement (Koyama et al., 2008). Inhibition of salivary gland branching by FGFR2b antisense oligonucleotides was also rescued by the addition of exogenous FGF7 which stimulated cell proliferation and end bud formation (Steinberg et al., 2005). A role of *Fgf7* during MNG ducts may be employed for successful expansion of the primary MNG buds or for duct elongation. The localisation of *Fgf7* mRNA in the nasal septum mesenchyme from E14.5-E15.5 when the MNG ducts are budding, elongating and beginning to branch as well as the absence of these glands in the *Fgfr2b* -/- mouse at E18.5, suggest that *Fgf7* function may be utilised by these developing glands. To elucidate the precise role of FGF7 during anterior nasal gland development, their phenotype should be investigated in the *Fgf7* knockout mouse (Guo et al., 1996). If *Fgf7* plays a compensatory role when functional *Fgf10* is lost, qPCR for *Fgf7* levels in nasal septal tissue in WT, *Fgf10* +/- and *Fgf10* -/- animals at different stages of MNG development could be carried out to explore if there is an upregulation of *Fgf7* expression. Furthermore, to uncover an *Fgf7*-*Fgf10* interaction, a double knockout mouse model of these two genes could be used and all anterior nasal glands investigated. Considering that LNG4 is also absent in the receptor knockout, the development of this gland using these suggested methods is also encouraged.

LNG2, LNG3 and LNG5 all bud and elongate as ducts to the presumptive branching location independent of FGFR2b signalling. It is possible that these glands rely more so on Ectodysplasin A signalling as Grüneberg (1971) described a severe phenotype of the lateral nasal glands in the *Tabby* mouse. While the glands are numbered in this study according to the times at which they arise, it is difficult to interpret whether Grüneberg's labels correspond to the labels we have used in our current work as there are no detailed schematic or histological images provided (Grüneberg, 1971). The paper does however state that the LNG3 bud arises in the *Tabby,* yet it does not progress after this stage. In contrast, LNG2 and LNG4 are said to not develop at all in the absence of Eda signalling (Grüneberg, 1971). With the help of the detailed developmental and morphological descriptions of the anterior nasal glands outlined in *Chapter 3*, it would be interesting to return to the *Tabby*, as well as the *downless* and *crinkled* mouse models, to uncover the precise role of the Ectodysplasin A pathway during development of each gland.

As described in *Chapter 1*, more recent studies have shown that activation of the canonical Wnt pathway occurs in early anterior gland development with *Lef-1* mRNA and protein expression observed at gland bud initiation stage (Driskell et al., 2004, 2007). Inconsistencies arise in these studies however. Firstly, it is not explained which nasal gland is investigated in these studies. From the images and time points stated it appears that the bud studied could be that of LNG3 or LNG5. Secondly, it is stated that *Lef-1* mRNA is expressed in this nasal gland bud at E16.5 (Driskell et al., 2004) while the LEF1 protein is expressed in the bud at E15.5 (Driskell et al. 2007). This order of RNA and protein expression could be explained if a different gland bud was investigated in each study. While this work has given valuable insight into *Lef-1* involvement in gland bud initiation, it cannot be said for certain if these results apply for all of the anterior nasal glands. Also, the role of Wnt signalling during the later stages of nasal gland development has not been investigated. Using the $Axin2^{lacz}$, it has been shown that Wnt/β-catenin signalling is restricted to the ductal structures of the developing SMDG, with its localisation seen at E14.5, during the *Pseudoglandular stage,* in the main gland duct and by E15.5 spreading into the smaller ducts (Patel et al., 2011). Wnt activity may be maintained in the ductal epithelial cells to ensure their long-range elongation before branching of a distal gland

occurs. Again, as it has been shown that Wnt signalling negatively regulates branching morphogenesis in other structures (Dean et al., 2005; Patel et al., 2011), this same strategy could be tested in the anterior nasal glands by *in vitro* culture of the gland ducts in the presence of the Wnt signalling inhibitor Dickkopf-related protein 1 (DKK1). DKK1 interacts with the LRP6 coreceptor, inhibiting its recruitment in the binding of extracellular Wnt to the Frizzled receptor (Bafico et al., 2001; Semënov et al., 2001). Addition of DKK1 may stimulate gland ducts to branch prematurely due to the absence of Wnt signalling. This inhibition may also cause the upregulation of *Fgfs* in the nasal mesenchyme and downstream targets of FGF signalling within the nasal gland epithelium.

From this study we want to emphasise that nasal SMGS not only adopt contrasting temporal locations and methods of development, they each employ different signalling factors and intracellular cues for their tightly controlled duct elongation and glandular branching stages.

5.1 Introduction

5.1.1 The Tracheal SMGs

Most of the tracheal SMGs are found in the anterior trachea above the first cartilage ring, adjacent to the cricoid cartilage, and spread posteriorly between the cartilage rings to the sixth ring in mice, but continue to the bronchi in humans (Sturgess and Imrie, 1982; Borthwick et al., 1999). The localisation of the SMGs allows the lubrication of the airway mucosa running from the upper and lower airways and provides a mucin-rich barrier against the environment. As outlined in *Chapter 1*, investigation into the tracheal SMGs has elucidated their role in a number of severe and life threatening respiratory diseases with SMG hyperplasia and mucus hyper-secretion common to most (Reid, 1960; Oppenheimer and Esterly, 1975; Aikawa et al., 1992). CFTR, the defected gene in patients suffering from cystic fibrosis (CF), is primarily expressed in the serous cells and some of the ductal cells of the SMGs (Engelhardt et al., 1992). While this suggests a functional defect in the glands of CF patients, defects in the developmental patterning of the SMGs in a CF mouse model has also been reported, suggesting an additional role during gland initiation (Borthwick et al., 1999). Despite the significance of SMG involvement in disease however, little research has focused on their normal patterning and the signalling cues required for their successful budding and branching.

One paper in particular has examined the timed developmental patterning of the tracheal glands in postnatal mice (Rawlins and Hogan, 2005). Here it was reported that the first sign of tracheal SMG initiation was described at P2, with SMG buds invaginating from the airway epithelium into the mesenchyme in the anterior trachea (Rawlins and Hogan, 2005). These buds had undergone extension and branching by P4, while new buds were still forming. The branching glands already showed signs of mucus production at this stage (Rawlins and Hogan, 2005). By P7, early-formed glands were evidently secreting mucus. Gland buds continually formed until P14, however new gland initiation was reported to have ceased by P21 (Rawlins and Hogan, 2005). In this same study, gland phenotypes were compared in WT and *Fgf10* +/- postnatal pups. At this stage anterior glands above the first cartilage ring (C1) in the WT animals were highly branched structures while the smaller glands between the cartilage rings were seen to extend passed C6 (Rawlins and Hogan, 2005). In contrast

to this the anterior SMGS in the *Fgf10 +/-* animals were significantly smaller with fewer branches, and the posterior localisation of the glands between the cartilage rings was also reduced (Rawlins and Hogan, 2005).

5.1.2 Tracheal SMG Mucus Secretion

Mucus hyper-secretion from the SMGs is a characteristic of many respiratory diseases such as asthma and cystic fibrosis (Rogers, 2004; Rowe et al., 2005). Animal models have been indispensible tools in gaining insight into these disease abnormalities and aetiologies. A number of CF mouse models have been generated to understand the biological processes that lead to the severe mucus hyper-secretion of this disease. Ianowski et al. (2007) tested the physiological function of normal and CF glands using an optical method originally described in sheep (Joo et al., 2001). Using the mouse model, tracheas were dissected, covered in a mineral oil layer on their mucosal side and exposed to different gland stimulants, to test which would be the most effective to induce a secretory response (Ianowski et al., 2007). Results of these experiments showed that the cholinergic agonist carbachol was the most effective in stimulating gland secretion in both WT and CF tracheal SMGs (Ianowski et al., 2007). As glands were triggered to secrete fluid, mucus bubbles formed within the oil layer, allowing secretion volumes and rates to be visualised.

5.1.3 Aims of Study

- To delineate the timed postnatal development of the tracheal SMGs with primary focus on the anterior glands adjacent to the cricoid cartilage.
- To carry out more extensive analysis of the tracheal SMGs in adult *Fgf10 +/-* mice.
- To investigate the early SMG phenotype in WT*, Fgf10 +/-* and *Fgf10 -/-* mice at gland initiation stages.
- To analyse if a defective gland phenotype in *Fgf10 +/-* adult mice leads to a reduction in mucus secretion into the airway lumen, using previously reported optical methods (Ianowski et al., 2007).
- If mutant glands produce less mucus, investigate if this compromises the pulmonary health of *Fgf10 +/-* animals by exposing these mice, and their WT littermates to airway sensitizers and allergens.

If a reduction in mucus negatively influences the mucocilliary barrier in *Fgf10 +/-* animals, these mice may be more likely to have a severe inflammatory response when exposed to airway irritants, than their WT counterparts. It is therefore important to understand the airway's response to inhaled particles and allergens.

5.1.4 The Airway and Allergy

While the airway mucous, beating cilia and protective respiratory epithelium provide one of the first lines of defence against harmful airborne inhalants, the body's immune system additionally aims to prevent invasion of harmful pathogens. Phagocytic cells and bactericidal enzymes within the airway mucous, as well as epithelial cell tight junctions, aim to protect underlying tissue from pathogen invasion. While this line of defence limits the passage of irritants, it has been shown that allergens can evade this epithelial-derived barrier, even in healthy animals (Holt et al., 1981; Sedgwick and Holt, 1983). In this situation, when an allergen, bacteria or virus is inhaled and bypasses the mucus barrier, specific antigens on their surface are detected by antigen presenting cells (APC) such as macrophages, dendritic cells and B cells (Unanue, 1984; Steinman, 1991; Rodriguez-Pinto, 2005)(Figure 5.1). While some of these antigens are digested by the APCs by phagocytosis, others are broken down and fragments of the antigens are presented on the cell surface along with other proteins known as the Major Histocompatibility Complex II (MHCII)(Germain, 1994) (Figure 5.1). Presentation of the antigen fragments along with the MHCII is critical for antigen detection by T helper 2 (T_H2) lymphocytes. Upon antigen recognition, T_H2 cells secrete cytokines (e.g Interleukin-4, -5 and -13), which leads to the recruitment of inflammatory cells, mainly mast cells and eosinophils, to the airways (Romagnani, 1991) (Figure 5.1). T_H2 cell activation additionally triggers B-cells to produce allergen-specific IgE antibodies (Romagnani, 1991). These IgE antibodies bind to specific receptors on the surface of mast cells, which are now sensitized to that particular antigen (Figure 5.1). Upon secondary exposure to the allergen, these IgE bound mast cells detect inhaled allergens, which cross-link the receptor bound IgE. Upon linking, mast cells release inflammatory mediators such as histamine and prostaglandins, which can cause local tissue responses such as vasodilation, venous permeability, fever and pain (Serafin and Austen, 1987; Metcalfe et al., 1997; Stone et al., 2010). These localised tissue responses also translate into allergic reactions such as sneezing, wheezing and itchy eyes. Repeated exposure to allergens can cause more

severe pulmonary reactions as the recruitment of mast cells and their inflammatory mediator release can lead to allergic rhinitis in the anterior airways as well as airway bronchoconstriction in the lower airways (Milián and Díaz, 2004). Additional research has also showed that T_H2 cells induce mucus hyper-secretion (Cohn et al., 1997). These repetitive inflammatory responses then lead to significant breathing difficulties due to airway remodelling and increased mucus production.

5.1.5 Murine Allergic Sensitization

As laboratory rodents do not instinctively develop asthma, researchers generally expose animals to inhalant allergens to provoke an asthmatic-like response. A traditional allergen used is ovalbumin (OVA) (Kumar et al., 2008). OVA is a glycoprotein found in large quantities in eggs of the chicken, *Gallus gallus,* that has been shown to trigger airway eosinophilia and pulmonary inflammation (Tomkinson et al., 2001). Inoculation of OVA alone, however, requires a great number of administrations to achieve sensitization so usually the antigen is administered in conjunction with an adjuvant. Inoculation of both these factors enhances airway hyper-responsiveness at a quicker and more effective rate (Nials and Uddin, 2008).

One adjuvant that is used is tumor necrosis factor alpha (TNF-α). TNF-α is a cytokine that plays a critical role in the mediation of inflammatory response (*reviewed in* Brightling et al. 2008). Upon inhalation of airborne allergens, it is released primarily by macrophages and mast cells (Thomas, 2001). TNF-α triggers an influx of inflammatory cells such as T-cells, eosinophils and neutrophils, to the site of inflammation and also induces respiratory structural cell changes such as the upregulation of adhesion molecules within the respiratory epithelium (Brightling et al., 2008). The involvement of TNF-α in the asthmatic inflammatory response was highlighted by the detection of both TNF-α mRNA and protein in the airways of sufferers of asthma (Ying et al., 1991; Bradding et al., 1994). Research has since elucidated that TNF-α is a key player required for the recruitment of T_H2 cells to the site of allergic response and have concluded that inhalation of recombinant TNF-α by healthy individuals leads to symptoms of airway hyper-responsiveness (Thomas et al., 1995; Thomas and Heywood, 2002). Considering these revelations, studies have adopted intranasal TNF-α inoculation mechanisms, along with OVA, to establish animal models of airway sensitization (Zhao et al., 2013).

5.1.6 House Dust Mites and Pulmonary Response

A common cause of allergic airway disease (AAD), as well as eczema, rhinitis and allergic conjunctivitis, is the exposure and sensitization to house dust mites (HDM)(Janson et al., 2001). HDM are minute eight-legged arthropods measuring approximately 300μm in length (Milián and Díaz, 2004). They prevail in all homes and fabrics as they feed on shed skin scales and organic detritus. Two common species of HDM, *Dermatophagoides pteronyssinus* and *Dermatophagoides farina* trigger pulmonary allergic response, with *D. pteronyssinus* predominating in the United Kingdom (Arlian et al., 2002).

HDM secrete a plethora of allergens that arise from whole dust mites, mite eggs and faecal pellets (Thomas et al., 2002). The most common of these proteins belong to the group 1 allergens, also referred to as *Der p I*, which are cysteine proteases excreted in HDM faeces (Tovey et al., 1981; Chua et al., 1988). Inhalation of these allergens and detection of *Der p I* antigen triggers IgE mediated immunological hypersensitivity, described above (Greene and Thomas, 1992).

Research has shown that children born with normal lung function are susceptible to developing asthmatic symptoms and reduced lung function within the first three to six years of life (Martinez et al., 1995; Lowe et al., 2005). Therefore an animal model investigating asthmatic progression is extremely valuable in understanding the pathogenesis of this allergic disease. Continuous intranasal exposure of adult mice to purified HDM extract for seven weeks gave rise to severe eosinophilic inflammation and an increase in T-cell activation and accumulation in the lung (Johnson et al., 2004). Additionally, analysis of lung tissue showed airway remodelling and goblet cell hyperplasia (Johnson et al., 2004). Saglani et al. (2009) used the same experimental strategy to establish a suitable neonatal model of allergen sensitization and early asthma development. Again, intermittent exposure to HDM extract gave rise to increased eosinophilic inflammation in both the airway lumen and lung digest (Saglani et al., 2009). Lung tissue exposed to HDM extract also demonstrated a significant increase in inflammatory infiltrate in the peribronchial and perivascular areas however not within the lung parenchyma itself (Saglani et al., 2009). Other asthmatic phenotypes observed in HDM inoculated neonates included increased T-cell count, higher IgE antibodies and airway remodelling characteristics such as

goblet cell hyperplasia and increased peribronchial collagen deposition (Saglani et al., 2009). In conclusion, murine intranasal inoculation with HDM gives rise to similar pathophysiogical features as seen in humans with asthma and elucidated that inhalation of this environmentally relevant allergen provided an ideal model to study airway protection mechanisms and pulmonary immune response.

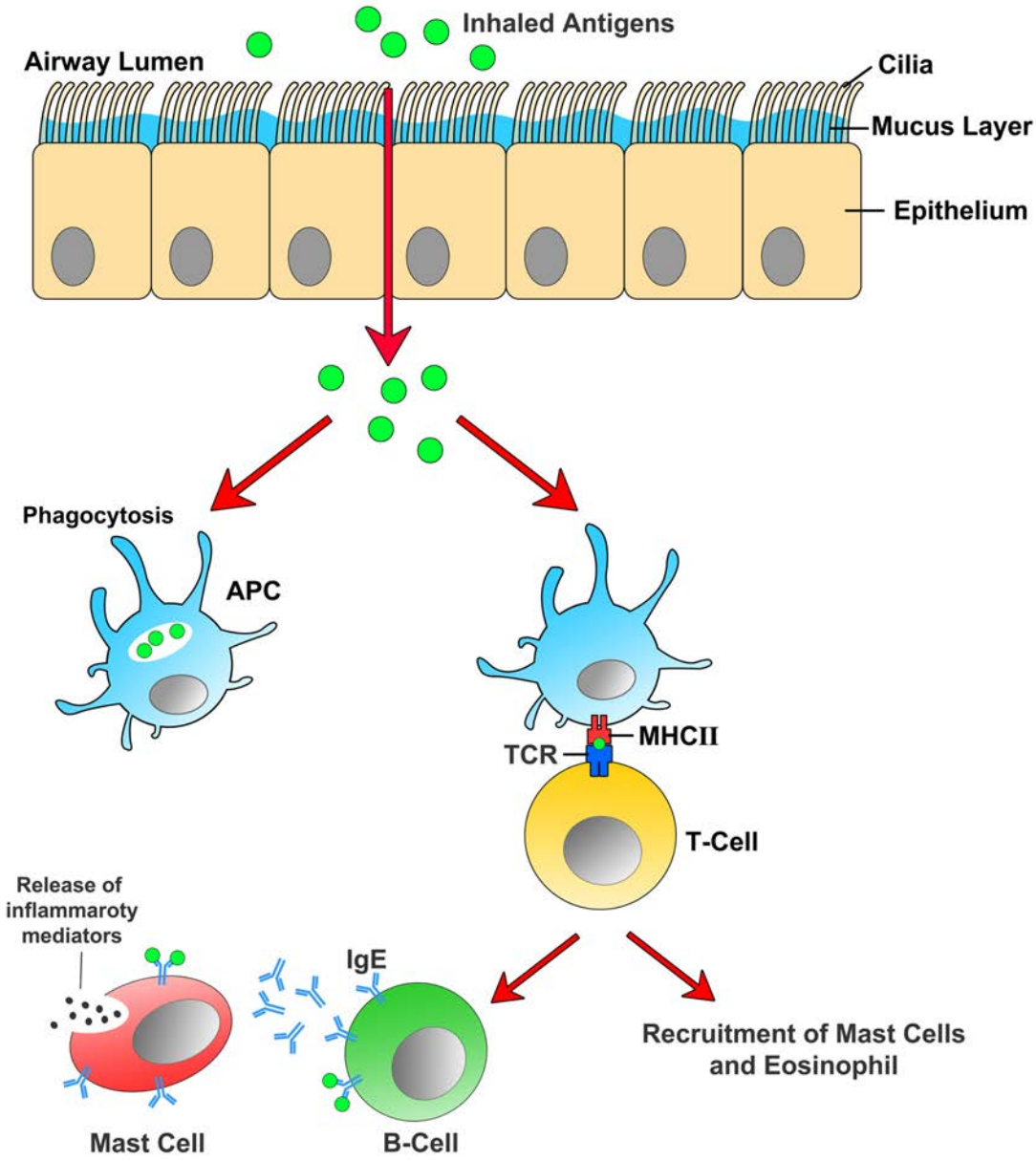

Figure 5.1 APC recognition and presentation of inhaled antigens.
Antigens of inhaled allergens may pass through the mucosal-epithelial barrier where they are recognized by Antigen Presenting Cells (APC), such as macrophages or dendritic cells. Antigens are either digested by APCs or broken down and fragments presented to T-cells via the MHCII complex. Binding of T-cells to antigen fragments occurs via a T-cell receptor (TCR). Upon antigen recognition, T-cells release cytokines to stimulate inflammatory cell recruitment. One response is that of B-cells which produce IgE antibodies specific to the inhaled allergen. These antibodies are released and bind to mast cell surface receptors. Repeated exposure to antigens is detected by these antibodies, causing mast cells to release inflammatory mediators that stimulate tissue responses.

5.2 Materials and Methods

5.2.1 Cartilaginous Staining of Embryonic Tracheal Tissue

Tracheas were dissected from E18.5 *Fgf10* WT and *Fgf10* +/- littermates and fixed overnight in 95% ethanol in deionised H_2O at 4°C. After 24 hours of fixation, fat from tissue was removed by storing tracheas in 100% acetone overnight at RT. Followed by two rinses in 95% ethanol, tracheas were then placed in Alcian Blue solution (15mg Alcian Blue 8GX in 80ml 95% ethanol and 20ml glacial acetic acid) for 24 hours rocking at RT. Tissue was rinsed with 95% ethanol twice for 30 minutes and stored in 95% ethanol overnight at RT. The ethanol was poured off and tracheas were cleared in 1% Potassium Hydroxide (KOH) for 3-4 hours. Tissue then went through a series of 1% KOH and glycerol solutions, all at RT, until specimens were finally stored in 100% glycerol (Table 5.1). Tracheas were then observed and photographed using a Leica MZFLiii dissection microscope fixed with a Leica DFC300 Fx camera.

Table 5.1 Concentration of 1% potassium hydroxide in glycerol solutions used in cartilaginous preparation of embryonic tracheal tissue.

1% KOH:Glycerol Solutions	Time
80:20	4 hours
60:40	4 hours
20:80	overnight
0:100	stored

5.2.2 Tracheal Mucus Secretion Analysis

5.2.2.1 Tracheal Tissue Preparation

Wildtype mice (n=4) and their *Fgf10* heterozygous littermates (n=6) aged 7-8 weeks were culled by exposure to rising levels of CO_2 and tracheas were immediately dissected. The thyroid gland and oesophagus were removed and the trachea was cut along the dorsal trachealis muscle (Figure 5.2, A). The following procedure was modified from the method used in (Ianowski et al., 2007). Using insect pins, the trachea was opened and pinned to a Sylgard® plate and the luminal mucosal surface was exposed (Figure 5.2, B). The mucosal side of each trachea was dried with an air spray and 5µl of mineral oil (Sigma) was added to the surface. Beneath the trachea,

2.5µl of D-MEM/F12 plus penicillin/streptomycin and 1% Glutamax (Invitrogen) medium was added to nourish the tissue during incubation (Figure 5.2, B). A damp piece of filter paper was also placed on the Sylgard® plate to provide a humid environment ensuring the oil layer would not dry out during incubation. Tracheal tissue was then placed in a 95% O_2: 5% CO_2 incubator at 37°C for 10 minutes. The exposed trachea was then placed, at RT, under a Leica MZFLiii dissection microscope fitted with a Leica DFC300 Fx digital camera. A further 2.5µl of DMEM medium containing 60µM of the cholinergic carbachol (Sigma) was added to the medium bath, giving a final concentration of 30µM carbachol stimulating the tracheal glands (Figure 5.2, B). Photographs of the anterior region of the trachea were taken every 30 seconds for 10 minutes to trace mucus bubble production.

After 10 minutes of exposure to carbachol, the amount of mucus bubbles produced were counted to show the amount of gland openings within the tracheal mesenchyme. As glands were found to only be present between the cricoid cartilage and first two tracheal rings in *Fgf10* +/- adults, bubbles only secreted in this area were chosen for the study. Viable bubbles for area measurement were those of which followed the criteria described in Ianowski et al. (2007): (a) a complete circular outline surrounding each mucus bubble as accurate measurements could be collected and (b) no fusion with adjacent droplets. For gland opening analysis, these criteria were not followed, as they were not required to count the amount of bubbles produced. Area (μm^3) and circumference (µm) of each bubble was calculated using ImageJ software. Additionally, the feret diameter, also known as the maximum caliper diameter, was measured for each bubble. This measurement is taken as the longest distance between two points of non-spherical shape. In this study, ferret diameter was calculated using ImageJ software. Overall trachea mucus secretion was calculated by the sum of all areas of each bubble per animal. Statistics and graphs were calculated using Microsoft Excel and Graphpad Prism software.

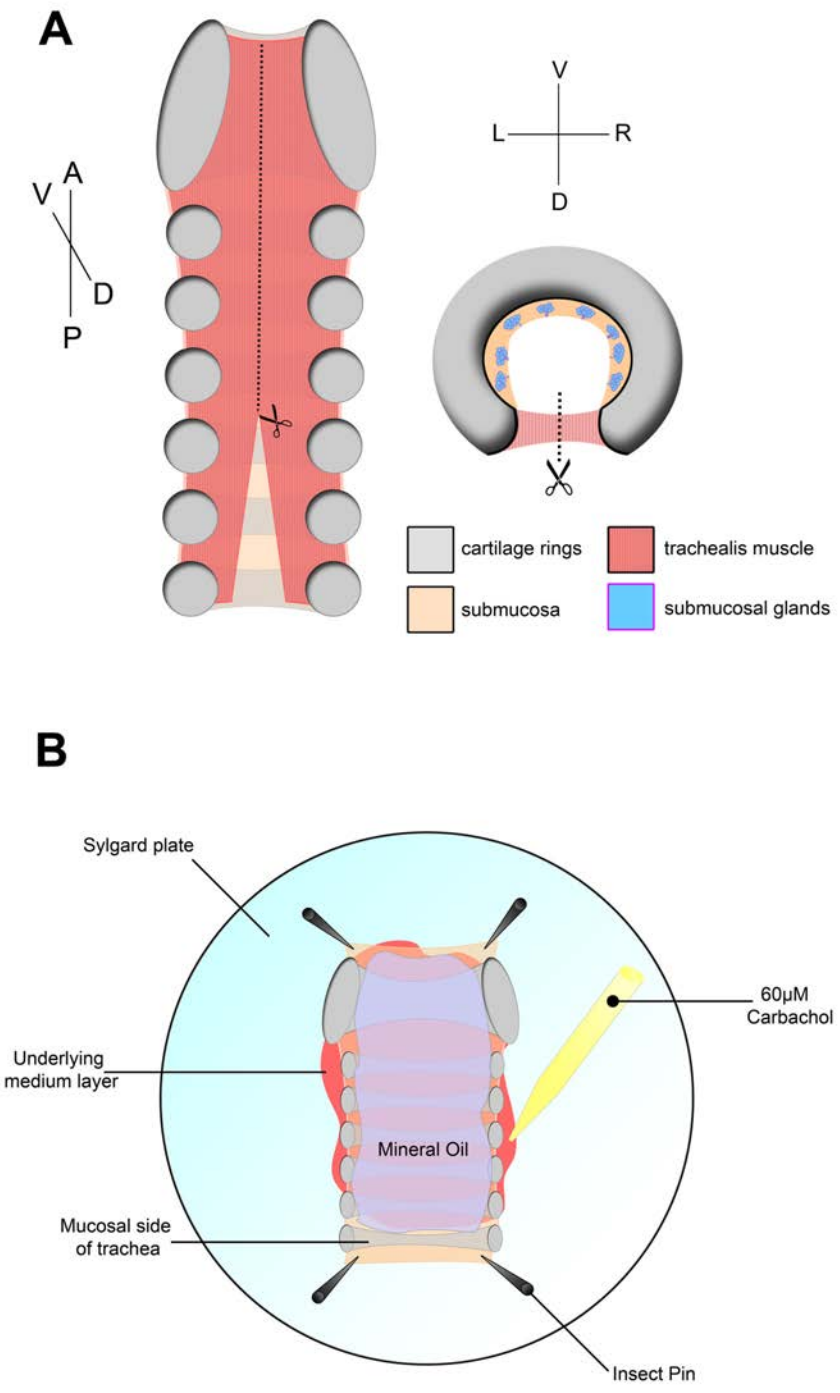

Figure 5.2 Dissection and preparation of tracheal for mucus production analysis. **(A)** Adult tracheas were dissected and cut along the dorsal trachealis muscle. **(B)** Tracheal tissue was flattened out and pinned down onto a sylgard plate, exposing the mucosal side. Medium was added underneath the tissue, while mineral oil was added on top of the mucosal side and gland openings. After 10 minutes of incubation, medium containing carbachol was added to the current medium bath. Mucus bubble production was observed and recorded for 10 minutes. Axis labels: anterior (A); posterior (P); ventral (V); dorsal (D); left (L) and right (R).

5.2.3 Respiratory Challenge of Adult Mice with Ovalbumin and TNF-α

5.2.3.1 Initiation of Respiratory Challenge and Tissue Treatment

Six-nine week old *Fgf10* WT and +/- littermates were briefly anaesthetized with 100% IsoFlo® isoflurane (Abbott) using a Fluovac unit. This was carried out in the BSU, New Hunts House, Guy's Campus, King's College London. Animals were placed in the chamber and exposed to vaporized isoflurane for approximately 4 minutes, or until mice were anaesthetized and a steady pace of breathing was maintained. Animals were held by scruffing the back of the shoulders. This positioning allows steady inhalation of nasal inoculant. Using a 200µl Eppendorf pipette, 50µl of either PBS control (WT n=2; *Fgf10* +/- n=2) or 20µg/ml of TNF-α and 1000µg/ml Alexa Fluor® 488 ovalbumin conjugate (Life Technologies) in PBS (WT n=6; +/- n=9) was slowly released on the nose of each animal. Mice were held steadily until all liquid was inhaled and were then placed upright in their cages allowing inoculant to be sufficiently inhaled while animals recovered. Cages were returned to their normal storage rooms. After 6 hours, mice were culled by exposure to CO_2 gas. In order for quick treatment following sacrifice, two mice were culled in the CO_2 chamber at a time. Animals were removed from the chamber and placed on their back. The chest area was sprayed with 70% ethanol in deionised H_2O to ensure there was no hair contamination during dissection. An incision was made through the chest to below the chin and skin was opened. Salivary glands were gently moved to the side to expose the anterior trachea. Extra care was taken during this step as not to cut any large blood vessels located throughout the neck area. The connective tissue membrane surrounding the trachea was removed and a small incision was made through the submucosa of the trachea between the anterior cartilage rings. A syringe fitted with a 20µl pipette tip was inserted down into the tracheal tube. The trachea and lungs were rinsed by flushing 1ml of PBS into the organs and then removing it again with the same syringe. This process is known as bronchoalveolar lavage (BAL) and in this case BAL fluid removed any residual OVA-Alexa-488 present in the airway cavity. The left lung was dissected and kept overnight in PBS at 4°C.

The next day individual lungs were transferred into 24-well plates containing 0.5ml of DMEM culture medium containing 10% fetal calf serum (FCS) in each well. Lungs were cut up into small pieces using sharp scissors and 25µl of 10mg/ml collagenase type IV (Sigma) was added to each well. Lung tissue was incubated in a 95% air: 5% CO_2 incubator at 37°C for 45 minutes. Cells were mixed thoroughly in medium by up and down pipette movements and transferred to 30ml sample tubes. Cells were washed with 20mls of Dulbecco's PBS (Sigma) and spun down at 200g for 10minutes in a Hettich Rotanta 46R bench top centrifuge. PBS supernatant was poured off and discarded leaving cells and approximately 100µl of PBS in the sample tube. Another 200µl of PBS was added to each tube and cells were shaken and left to sit for 5 minutes. From this, 100µl of cloudy cell solution was carefully transferred to a Falcon™ round bottom FACS tube, making sure not to transfer any pieces of residual lung tissue. Cells were then fixed in 100µl 2% PFA overnight at 4°C.

5.2.3.2 Fluorescence-Activated Cell Sorting (FACS)

FACS or Flow Cytometry is a technology used to count, sort and measure physical properties of single biological particles. The method is usually used to characterise the size, internal complexity and relative fluorescence intensity of cells suspended in a liquid sample. The method relies on disaggregating cells from a tissue sample and staining them with fluorescently labelled antibodies specific for antigens present on the membranes of target cell types. Stained cells are then passed through a channel where they are exposed to laser illumination. As cells pass through the laser intercept, the fluorescently labelled antigens on their cell surface scatter light. This split light is collected by specific detectors, which translate the optical signal into that of an electronic one where it is analysed by a computer.

Before each tube was loaded into the BD FACSCalibur™ (BD Biosciences), each sample was vortexed to re-suspend cells in solution. Analysis of samples began with a PBS control to set the gate for cell populations and to exclude autofluorescence and background staining. The samples of lung cells were then run through the FACS and using CellQuest™ software, cells positive for AlexaFluor®488 were detected and counted.

5.2.4 Respiratory Challenge of Adult Mice with House Dust Mites (HDM)

Every three days for three weeks CD1, *Fgf10* WT and *Fgf10* +/- animals were anaesthetized with isoflurane and given intranasal inoculations of PBS control, whole HDM (Allergon) or sonicated HDM in PBS (method outlined in section ***5.2.3***). Three concentrations of 25µg, 125µg or 625µg of HDM were administered in doses of 30µl in PBS. The last inoculation was given on Day 20 of challenge and animals were sacrificed 24 hours later on Day 21. Animals were culled by exposure to rising levels of CO_2 and BAL was carried out (method outlined in section ***5.2.3***). With all HDM experiments BAL fluid was collected and analysed as the effect of HDM inoculation on lung inflammation was to be determined by the presence of immune cells within the respiratory airway. BAL fluid was collected in FACS tubes and stored at 4°C until analysis. Following BAL collection, the left lung lobe and trachea were dissected and transferred to ice cold PBS. Lung tissue was dried using an air stream and weighed. Both lung and tracheal tissue were fixed in 4% PFA and were processed for histological staining with H&E and Alcian Blue.

To analyse airway inflammatory response, BAL fluid was spun down in a centrifuge for 5 minutes at 200g and 800µl of supernatant was discarded. Cells were re-suspended in the remaining 200µl and washed with 2.5ml of 1% FCS in PBS. Fluid was again spun down in a centrifuge for 5 minutes at 200g and supernatant removed. Tubes were flicked to re-suspend cells and 10µl of antibody mix containing 0.1µg of each antibody (Table 5.2) in FCS-PBS was added to each tube.

All anti-mouse antibodies used for FACS cell labelling were supplied by BioLegend®. To identify APC (macrophages and dendritic cells) FITC/AlexaFluor488-conjugated I-Ab and Granulocyte Receptor 1 (Gr-1) antibody was used. I-Ab is an alloantigen of the MHCII of APCs and Gr-1 is a cell surface receptor predominantly found in neutrophils. As this antibody will label macrophages, dendritic cells and neutrophils the application of an additional antibody CD11c conjugated to the dye PerCP-eF710® will label the APCs only, distinguishing them from the neutrophils. An antibody, conjugated to the fluorochrome phycoerythrin (PE), against the chemokine receptor CCR3 abundant on eosinophils was used to

identify these cells. Finally, to stain lymphocytes anti CD3 + B220-APC antibody was used. CD3 is expressed by all mature T-cells while B220 is expressed by B-cells.

Cells were left at RT for 10 minutes and were washed with 2.5mls of 1% FCS in PBS. Cells were spun down for 5 minutes in the centrifuge at 200g, supernatant discarded and fixed with 200µl of 1% formaldehyde.

FACS analysis was primarily carried out by Dr. Alistair Noble (Department of Asthma, Allergy and Respiratory Science, King's College London). Using CellQuest™ software, two regions were set based on CD3 + B220-APC antibody detection. Cells negative for CD3 + B220-APC (eosinophils, neutrophils and macrophages/dendritic cells) were grouped into "Region 1" while positive for CD3 + B220-APC (T-Cells and B-Cells) were grouped into "Region 2". Cells were then identified within these regions by antibody detection specific for each cell type (Table 5.2).

Table 5.2 Monoclonal antibodies and their conjugated fluorochromes used in FACS cell identification.

	IAb + Gr-1-FITC	CCR3-PE	CD11c-PerCPeF710	CD3 + B220-APC
Eosinophils	-	+	-	-
Macrophages/Dendritic Cells	+	-	+	-
Neutrophils	+	-	-	-
T-Cells	-	-	-	+
B-Cells	+	-	-	+

5.2.5 Statistical Analysis

Statistical significance between experimental groups was calculated in the mucus bubble analysis, OVA-TNF administration and HDM inoculation experiments using a Student's *t-test*. Graphs were generated using GraphPad Prism software.

5.3 Results

5.3.1 Anterior Tracheal SMG Development

As a first step in our aim to understand tracheal SMG development, early gland bud formation and extension stages were analysed in CD1 animals. All tissue sections were stained with Haematoxylin and Eosin with Alcian Blue and developmental stages were directed by previous studies (Thurlbeck et al., 1961; Keswani et al., 2011). Stage 1 of development is the initial bud stage where an epithelium swelling is seen to immerge from the respiratory epithelium (RE) (Figure 5.3, A). Stage 2 is characterised by the epithelial bud elongating into the underlying mesenchyme and cavitation occurs within this stalk to form a lumen (Figure 5.3, B). This is followed by Stage 3 where canalized stalks begin to branch within the underlying mesenchyme (Figure 5.3, C), while Stage 4 is classified as the cellular differentiation stage, indicated by mucus production within the gland (Figure 5.3, D). Investigation began at P2 as it had been previously reported that at this age early tracheal SMG buds initiate (Rawlins and Hogan, 2005). At this stage while SMG buds were found in the anterior tracheal mesenchyme in dorsolateral positions (Figure 5.4, F), glands that had progressed to the branching and mucus producing stages were found in the ventral mesenchyme (Figure 5.4, E). This result suggested that ventral SMGs were forming at an earlier age. Considering this, we traced back to E18.5 tracheas, where the invagination of some of these ventral gland buds was apparent, indicating that SMG development begins embryonically in the ventral trachea. At P0 ventral glands were observed at Stage 1 of budding, while others have extended and branched and had already begun Stage 3 of lumen formation (Figure 5.4, C). Furthermore, some gland buds were also found in more dorsolateral planes at P0 (Figure 5.4, D). By P1, branching continues in both the ventral and dorsal glands, as well as continued induction of new buds throughout the dorsolateral walls. By P4, the ventral and dorsolateral glands continued to undergo extensive branching and cellular differentiation (Figure 5.4, G and H).

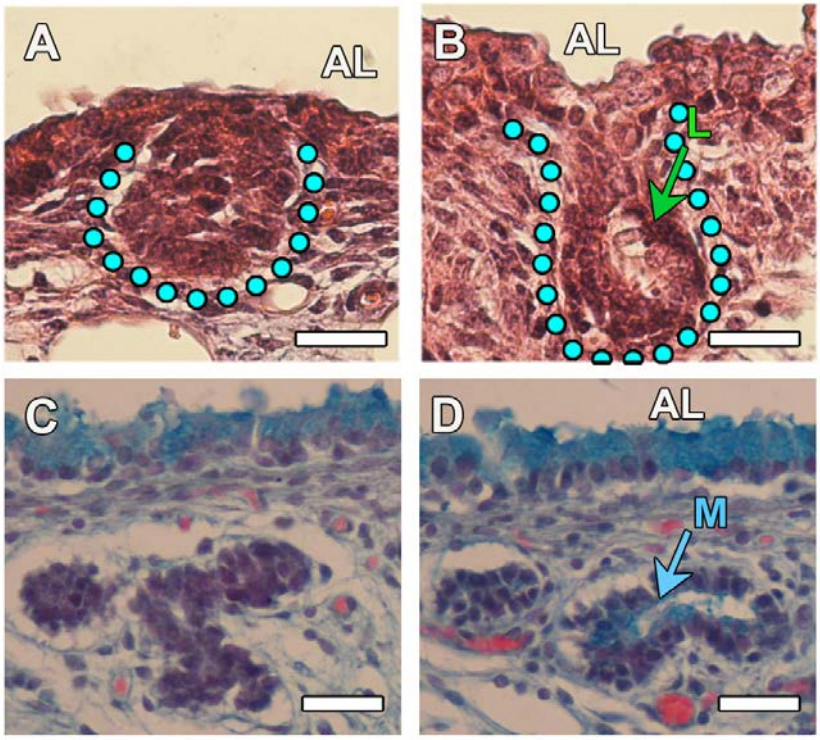

Figure 5.3 Stages of tracheal SMG development
(A) Stage 1: Tracheal SMG buds are first seen to invaginate from the RE into the underlying mesenchyme. (B) Stage 2: Elongation of the bud and cavitation of the epithelial stalk occurs. (C) Stage 3: Epithelial stalk undergoes clefting and branching (D) Stage 4: Cellular differentiation is observed indicated by mucus staining within the glands by Alcian Blue. AL= airway lumen, L= lumen, M= mucus. Scale bar = 25μm.

5.3.2 Anterior-Posterior Development of Tracheal SMGs

The first signs of SMG formation in a posterior direction between the first and second cartilage rings was observed in the ventral trachea at P4 (Figure 5.4, G). At P8, established anterior glands were continuing their branching as well as new glands appearing between C2 and C3 and progressively at P12 glands were found between C3 and C4 in ventral cross-sections. At P15 glands had developed between C4 and C5 and were producing mucus. Over these 10 days, it was noted that glands seemed to be developing in a gradient from the ventral to dorsal areas of the trachea, in conjunction with their posterior development. By P22, glands were well established and observed as posterior as C6, as previously reported in the mouse (Borthwick et al., 1999).

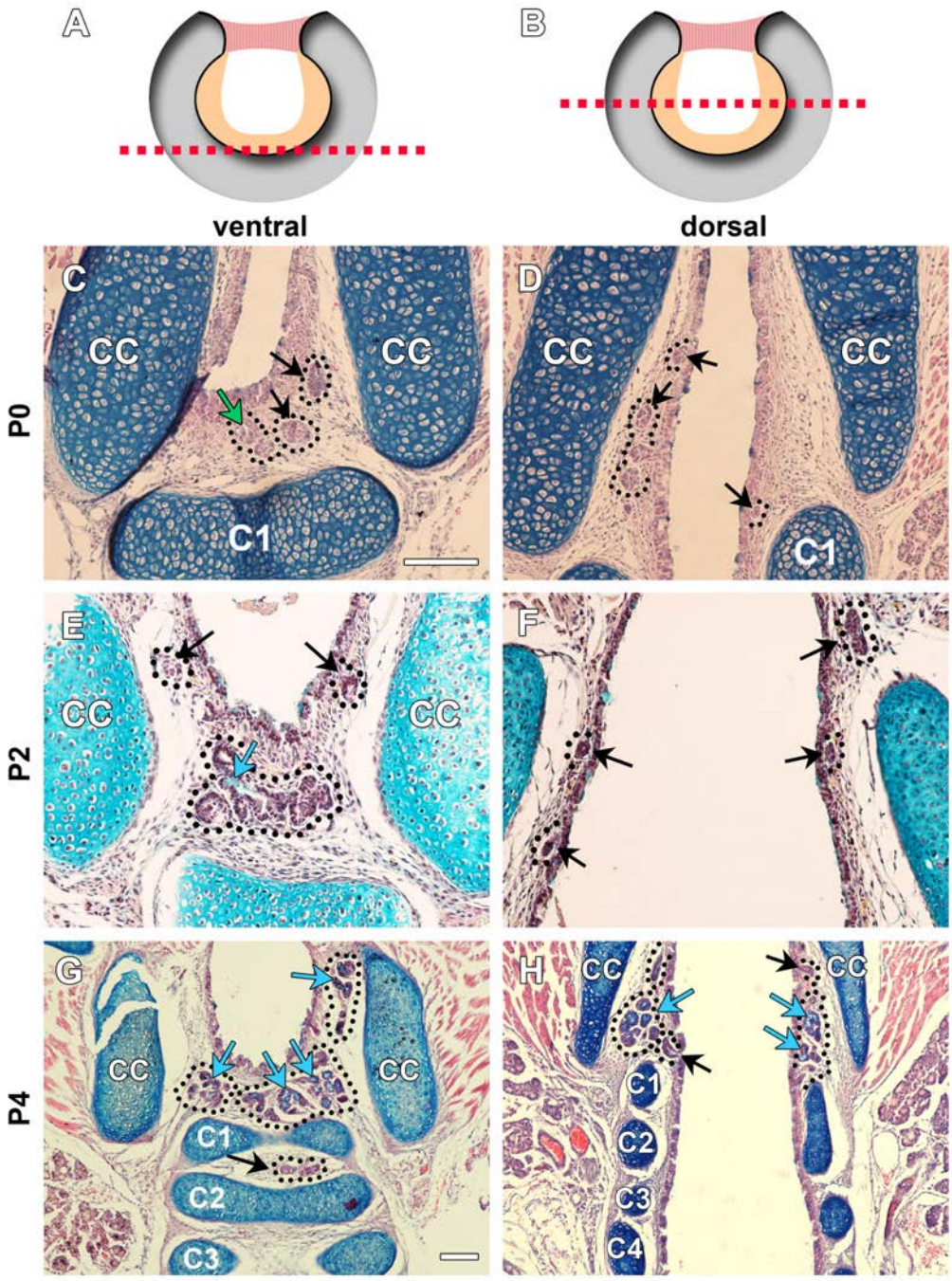

Figure 5.4 Normal postnatal tracheal SMG development.
(A-B) Schematic representations of the ventral (A) and more dorsal (B) tissue sections cut through postnatal tracheal tissue. (C) Glands are seen to have reached the lumen formation stage in the ventral trachea by P0, while more dorsally they are seen at the branching stage (D). (E) At P2 ventral glands have continued to branch and cellular differentiation is indicated by mucus staining within gland lumens. Continued budding of new glands is seen in more anterior dorsal positions (F). (G-H) By P4 glands have branched extensively in the ventral mesenchyme as well as in the dorsal trachea. Glands are also seen at the branching stage between C1 and C2 in the ventral trachea (G). CC=cricoid cartilage, C1=first cartilage ring, C2=second cartilage ring etc. Black arrow = developing gland, green arrow = lumen formation, blue arrow = mucus production. Scale bar=100μm.

5.3.3 Anterior and Posterior Tracheal SMGs are Reduced in Fgf10 +/- Adults

It has previously been reported that there is an altered SMG phenotype in adult *Fgf10* +/- mice (Rawlins and Hogan, 2005). In this study it was elucidated that there was a reduction in branching of the anterior SMGs adjacent to the cricoid cartilage and a severe reduction in the posterior expansion of the glands between each tracheal cartilage ring (Rawlins and Hogan, 2005). We investigated adult WT (n=7) and *Fgf10* +/- littermates (n=6) to ensure a similar phenotype in our mouse line. Analysis concluded a reduction in anterior tracheal SMGs in heterozygous animals compared to their WT littermates (Figure 5.5 A-B). Using histological methods it was difficult to conclude whether this was a reduction in branching of each gland, a reduction in the amount of glands within the anterior mesenchyme, or collectively both of these phenotypes. Variation in severity of this reduction was seen in *Fgf10* +/- mice however it was concluded that glands were always reduced in the heterozygous adults compared to WT littermates.

Analysis of SMGs between tracheal cartilage rings also showed a notable reduction in the anterior-posterior presence of the glands (Figure 5.5 C). WT littermates showed continuous SMG development between each cartilage ring, reaching the mesenchyme between C6 and C7 in 3/7 animals and even between C7 and C8 in one specimen (Figure 5.5 C). Two more WTs showed glands extending between C5 and C6, however in one of these animals, glands were missing between C4 and C5. The final WT specimen showed continual gland extension from the anterior trachea to above the fifth cartilage ring, no SMGs between C5 and C6, however glands were observed between C6 and C7 (Figure 5.5 C). In the six *Fgf10* +/- mice investigated, one adult had no glands past the first cartilage ring. Of the other five animals, two only showed small glands between C1 and C2 (Figure 5.5, C). Two more animals had glands past C1 and C2, with one of these showing another small gland past C5. Finally, the last *Fgf10* +/- had glands between each of the first four rings (Figure 5.5 C). In a previous study investigating tracheal SMG formation in the *Tabby* mouse of deficient Eda signalling, the pseudostratified columnar epithelium of the trachea showed a disorganized appearance and columnar epithelial cells were higher than observed in WT animals (Rawlins et al., 2007). In our study, no epithelial abnormalities were observed in the *Fgf10* +/- animals compared to their WT littermates (Figure 5.5, D and E).

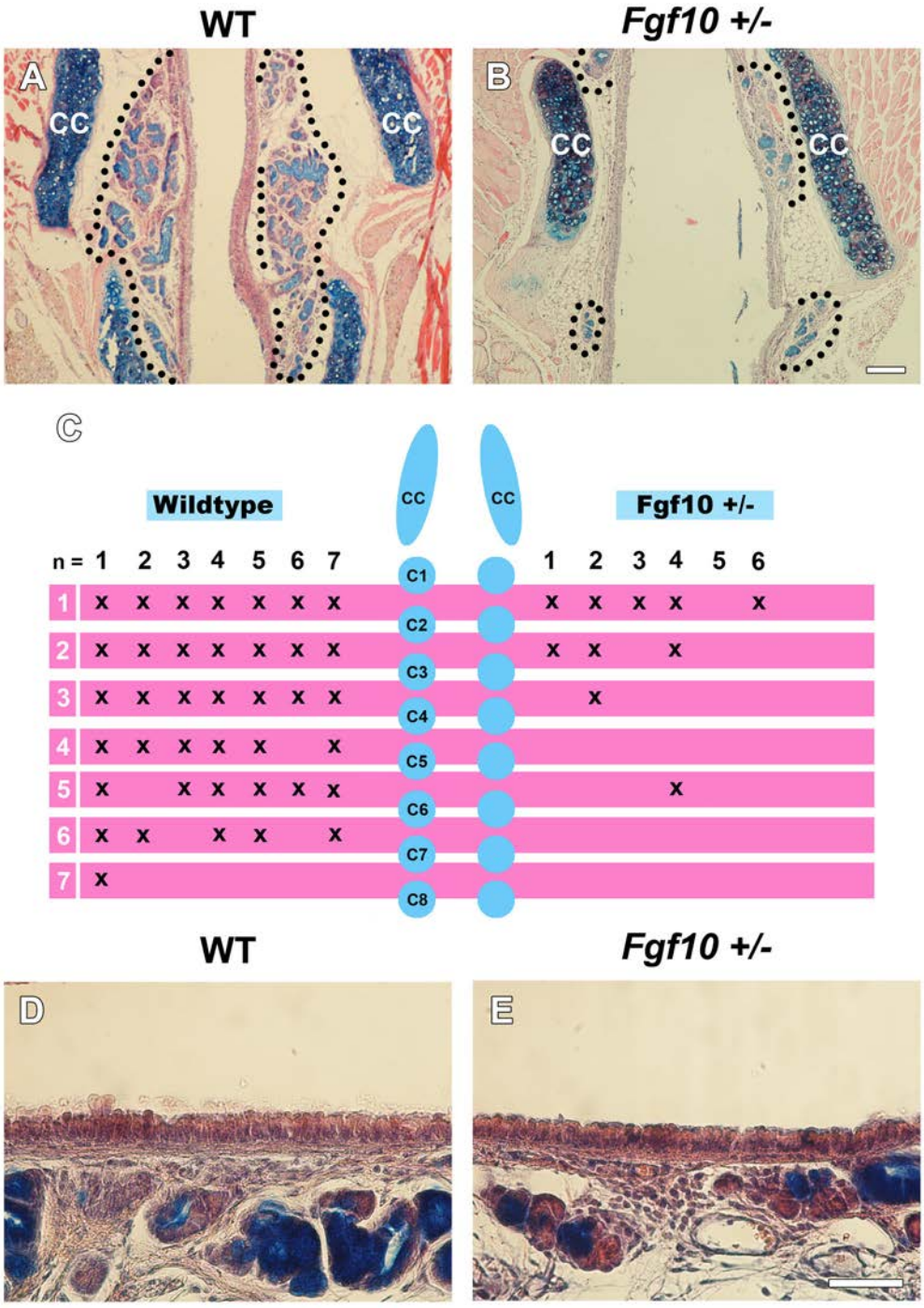

Figure 5.5 Anterior and posterior tracheal SMG phenotype of WT and *Fgf10* +/- adults.
(A-B) WT adults show extensively branched anterior SMGs adjacent to the cricoid cartilage (CC) while *Fgf10* +/- littermates show a significant reduction in glands in a similar plane. (C) Posterior extension of the SMGs is noticeably reduced in *Fgf10* +/- animals compared to their WT littermates. N numbers represent each specimen analysed while pink bars represent mesenchymal space where SMGs are found between each cartilage ring (C1-C8). (D-E) No differences were observed in the tracheal epithelium of adult WT and *Fgf10* +/- littermates. A and B; scale bar=100μm, D and E; scale bar=50μm.

5.3.4 Fgf10 +/- Embryos Show no Tracheal Cartilaginous Defect

Fgf10 has been shown to be expressed in the ventral tracheal mesenchyme from E12.5-E16.5 when tracheal patterning is underway (Sala et al., 2011). The significant role of *Fgf10* in tracheal design was also emphasised by *Fgf10* null embryos having truncated tracheas with disorganized rings replicating the phenotype seen in patients with tracheomalacia (Sala et al., 2011). As SMGs form between the tracheal cartilage rings, we wanted to test whether reduced gland numbers in the *Fgf10* +/- is a secondary defect to abnormal cartilage patterning. Using whole mount Alcian Blue staining, it was observed that while ring arrangements differed in all WT and *Fgf10* +/- specimens irrespective of genotype, no apparent difference of cartilage phenotype was seen between WT and *Fgf10* +/- littermates (Figure 5.6).

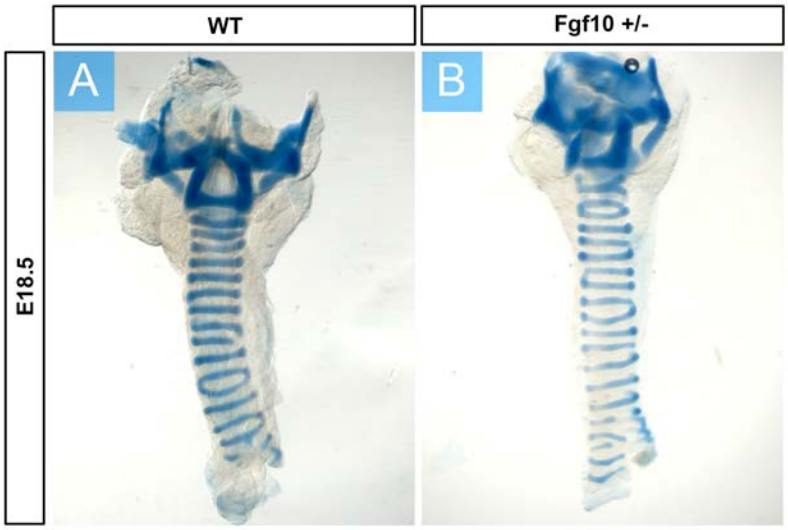

Figure 5.6 Cartilage ring staining with Alcian Blue of WT and *Fgf10* +/- embryonic tracheas.
E18.5 cartilage ring organization varied in both WT and *Fgf10* +/- however all rings showed normal patterning in both genotypes.

5.3.5 SMG Buds are Found in Fgf10 -/- Tracheas

Having observed that tracheal SMGs bud as early as E18.5 (see section 5.3.1), we were able to look at bud initiation in *Fgf10 -/-* mice, which die at birth due to lung agenesis (Min et al., 1998; Sekine et al., 1999). A litter of *Fgf10* mutant pups were collected on P0 yielding *Fgf10 -/-* (n=4), *Fgf10 +/-* (n=2) and *Fgf10* WT (n=3). Analysis of the anterior tracheal SMGs in these specimens demonstrated that glands had already budded, elongated, cavitated and commenced branching in WT animals (Figure 5.7 A, A'). The development observed in these specimens was more advanced than those previously described in CD1 animals at P0 (see section 5.3.1), showing how rapid gland morphogenesis can be, even by a few hours. Similar stages of development were seen in *Fgf10 +/-* littermates however gland development appeared delayed and branching of the formed glands clearly reduced (Figure 5.7 B, B'). Interestingly, gland buds were found in all *Fgf10 -/-* specimens investigated (Figure 5.7, C,C'). This result indicates that *Fgf10* expression is not required for initial epithelial gland bud specification however it is required for subsequent bud elongation and branching.

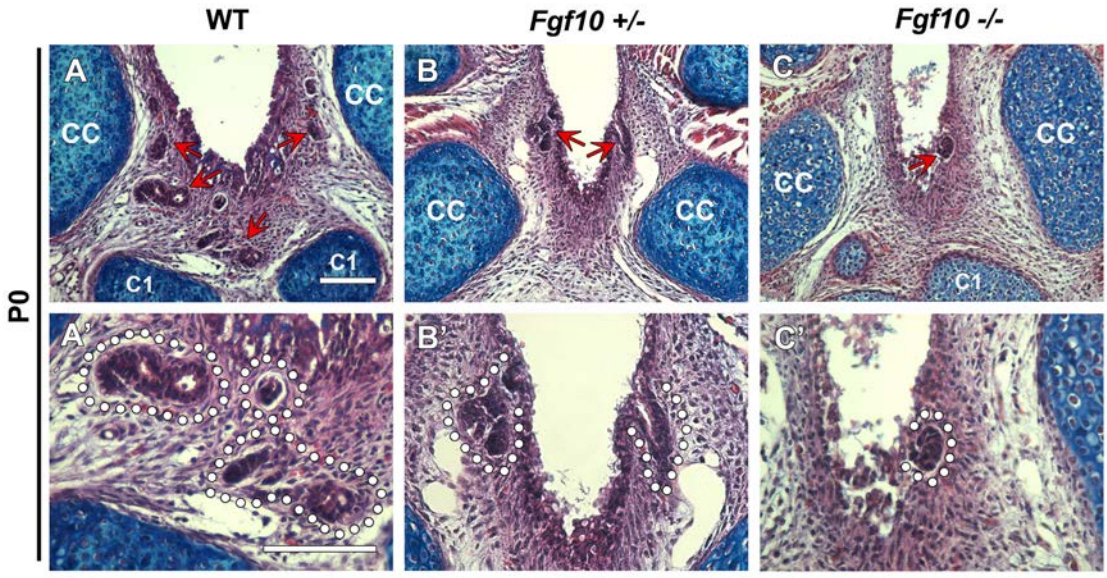

Figure 5.7 P0 tracheal SMG phenotype in *Fgf10* mutant mice.
(**A, A'**) WT animals collected showed SMGs reach lumen formation and branching stages in the ventral trachea. (**B, B'**) *Fgf10 +/-* littermates showed SMGs form lumens, however branching of the formed glands was reduced. (**C, C'**) Gland buds were found in *Fgf10 -/-* littermates however they had not elongated from the respiratory epithelium. Scale bar=100μm.

5.3.6 Fgf10 +/- Adult Mice Have a Reduction in Tracheal SMG Openings

Previous experiments have used the application of mineral oil to the mucosal tracheal surface to investigate SMG fluid secretion (Joo et al., 2001; Ianowski et al., 2007). As a reduction in anterior SMGs was observed in *Fgf10* +/- adults, we wanted to investigate if this defect in branching reduced the amount of mucus secreted into the airway lumen in heterozygous animals compared to their WT littermates. Consecutive images taken of tracheal tissue during mucus production analysis were examined and the amount of mucus bubbles present between CC and C2 were counted. Each bubble represented the presence of a gland opening. Results elucidated that the amount of bubbles was significantly reduced in *Fgf10* +/- animals ($p=0.0000379$) indicating a severe decrease in the amount of functional glands within the mesenchyme of the trachea between the anterior cartilage rings in *Fgf10* +/- adults (Figure 5.8 A-C).

5.3.7 Overall Mucus Secretion is Reduced in the Fgf10 +/- Anterior Trachea

Following analysis of the number of mucus bubbles present in the anterior tracheal samples, area, circumference and feret diameter of each mucus bubble was measured. No significant difference in measurements between WT and *Fgf10* +/- animals were observed (area $p=0.6268$; circumference $p=0.6954$; ferret diameter $p=0.7487$) (Figure 5.9 A-C). This indicates that each functional gland present in heterozygous animals produces the same amount of mucus as WT glands.

To elucidate the overall amount of mucus being secreted within the entire anterior trachea, the areas of each bubble were collected and added. This was significantly reduced in the *Fgf10* +/- adults ($p=0.0007$) (Figure 5.9 D) indicating that there is a decrease in the amount of mucus within the tracheal lumen of heterozygotes compared to WT littermates.

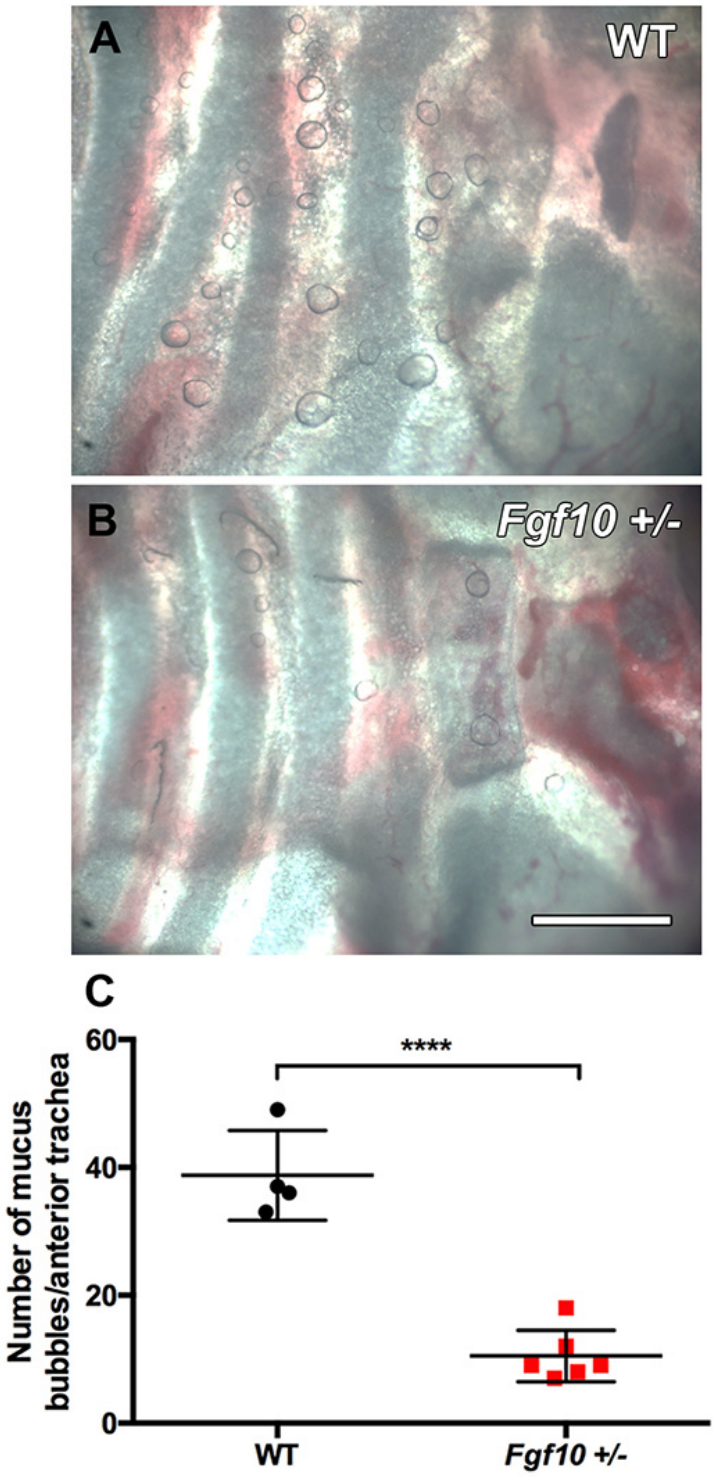

Figure 5.8 Mucus secretion analysis from WT and *Fgf10* +/- tracheal SMGs.
(A) Visualisation of functional gland openings in WT anterior tracheal tissue by mucus bubble production. **(B)** A significant decrease in the amount of mucus bubbles was observed in *Fgf10* +/- littermates. **(C)** Graphical representation of the number of mucus bubbles counted, showing a significant reduction in *Fgf10*+/- (n=6) animals compared to their WT (n=4) littermates. Scale bar = 500μm.

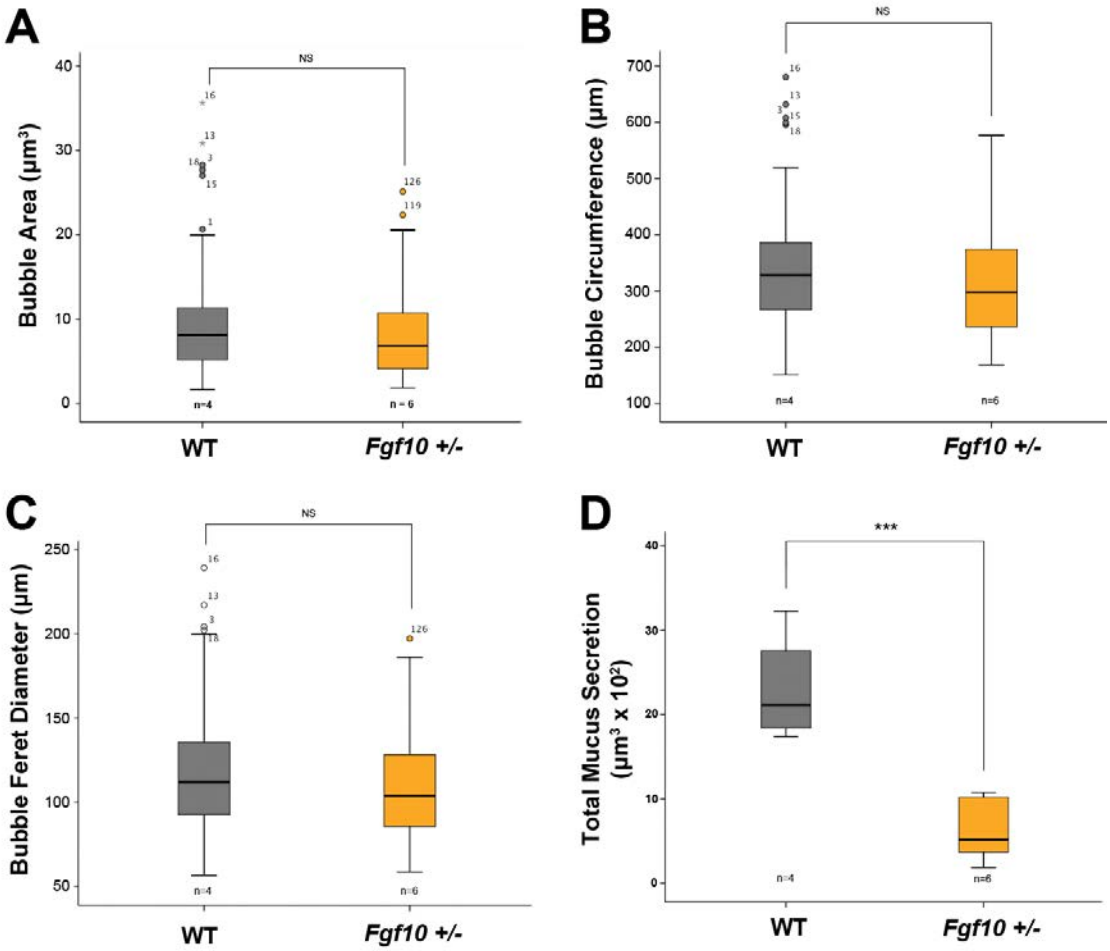

Figure 5.9 Single mucus bubble analysis and overall tracheal mucus secretion. Individual mucus bubble area (A), circumference (B) and feret diameter (C) analysis showed no significant difference in bubble sizes between WT and *Fgf10 +/-* adults indicating similar volumes of mucus secreted per functional gland. Summing up the areas of all bubbles was carried out to give a representation in the total amount of mucus secreted per anterior trachea with a significant reduction seen in *Fgf10 +/-* compared to WT littermates (D).

5.3.8 Ova-Alexa488 Transepithelial Transport

Following the results of the oil experiment analysis, showing that *Fgf10 +/-* mice produce less mucus into their airway lumens, we hypothesised that this reduction in mucus secretion would hinder the mucin-rich barrier function of these animals. To test this, WT and *Fgf10 +/-* animals were intranasally administered with OVA-Alexa488 and lung tissue was collected six hours later. We hypothesised that if *Fgf10+/-* animals had a significant decrease in mucus within their airways, this would render the epithelial barrier more permeable to OVA and a greater amount of AlexaFluor488 labelled OVA would reach the lung tissue, compared to WT littermates. A general trend was seen with an increase in positive cells found in the lungs of *Fgf10 +/-* adults however this was not significant when compared to WT littermates (p=0.1831).

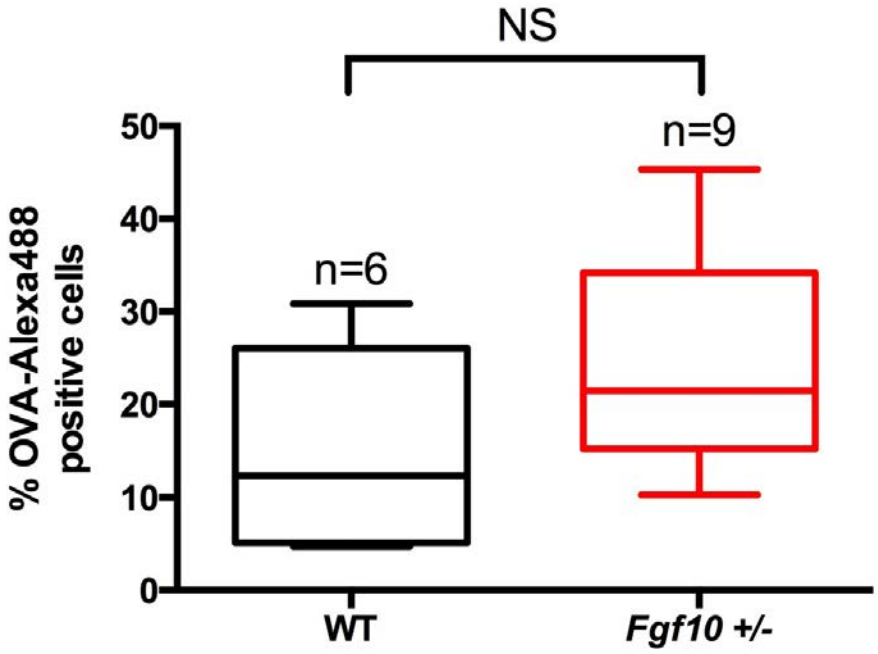

Figure 5.10 OVA-Alexa488 positive cells (%) found in the lung tissue of mice 6 hours after inoculation with OVA-Alexa488 and TNF-a

The treatment of 6-9 week old adult WT and *Fgf10 +/-* mice showed a slight increase in the number of OVA-TNFα positive cells found in *Fgf10+/-* lung tissue, however this increase was not significant compared to WT littermates.

5.3.9 Inoculation of 625µg of HDM Causes an Airway Inflammatory Response

Following the results of the OVA-Alexa488 inoculation results, it was considered that this exposure method should be used to target the inflammatory response in the animals, as opposed to directly testing the mucociliary barrier function. In light of this, we then turned to the inoculation of a more environmentally relevant allergen, house dust mite (HDM). Previous studies have specifically administered HDM extract to induce an IgE mediated allergic response (Johnson et al., 2004; Saglani et al., 2009). We employed the use of whole house dust mites however, as this would test both the particle clearance potential of the mucociliary barrier as well as immunological sensitization to the allergen. As whole HDM inoculation has not been done before in an animal model, we administered CD1 mice for three weeks with different concentrations of HDM (25µg, 125µg and 625µg) to delineate the most suitable level of whole mites required to induce inflammatory responses. Analysis of lung tissue, trachea epithelium and BAL fluid showed that the highest concentration used, 625µg of HDM, gave the most significant results (Figure 5.11 and Figure 5.12). No significant differences were seen in lung weight or any inflammatory cell levels in animals treated with 25µg (Figure 5.11). An increasing trend of T-cell and eosinophil count, as well as lung weight was observed in animals given 125µg of HDM compared to adult PBS control however these results were not statistically significant (Figure 5.11). Analysis of BAL fluid from mice exposed to 625µg of HDM delineated that eosinophil count showed an increase compared to controls however was not statistically significant ($p=0.1017$). T-cell count was significantly higher ($p=0.0449$) and also lung weights indicated inflammation with a significant increase in weight ($p=0.0171$) compared to PBS controls (Figure 5.11). Neutrophil and macrophage/dendritic cell count was not significantly different in 625µg-exposed animals. Considering the results collected from the lung weight and BAL analysis, tracheal epithelium and lung tissue from those inoculated with 625µg of HDM were stained with H&E and Alcian Blue, and analysed histologically. Investigation of alveolar lung samples showed accumulation of inflammatory infiltrate in lungs of those inoculated with HDM compared to PBS controls (Figure 5.12 A and C, white arrows). While phenotype of tracheal SMGs did not show any noticeable differences, some areas of the respiratory epithelium of the trachea appeared hyperplastic in those inoculated with HDM (Figure 5.12 B and D, black arrows).

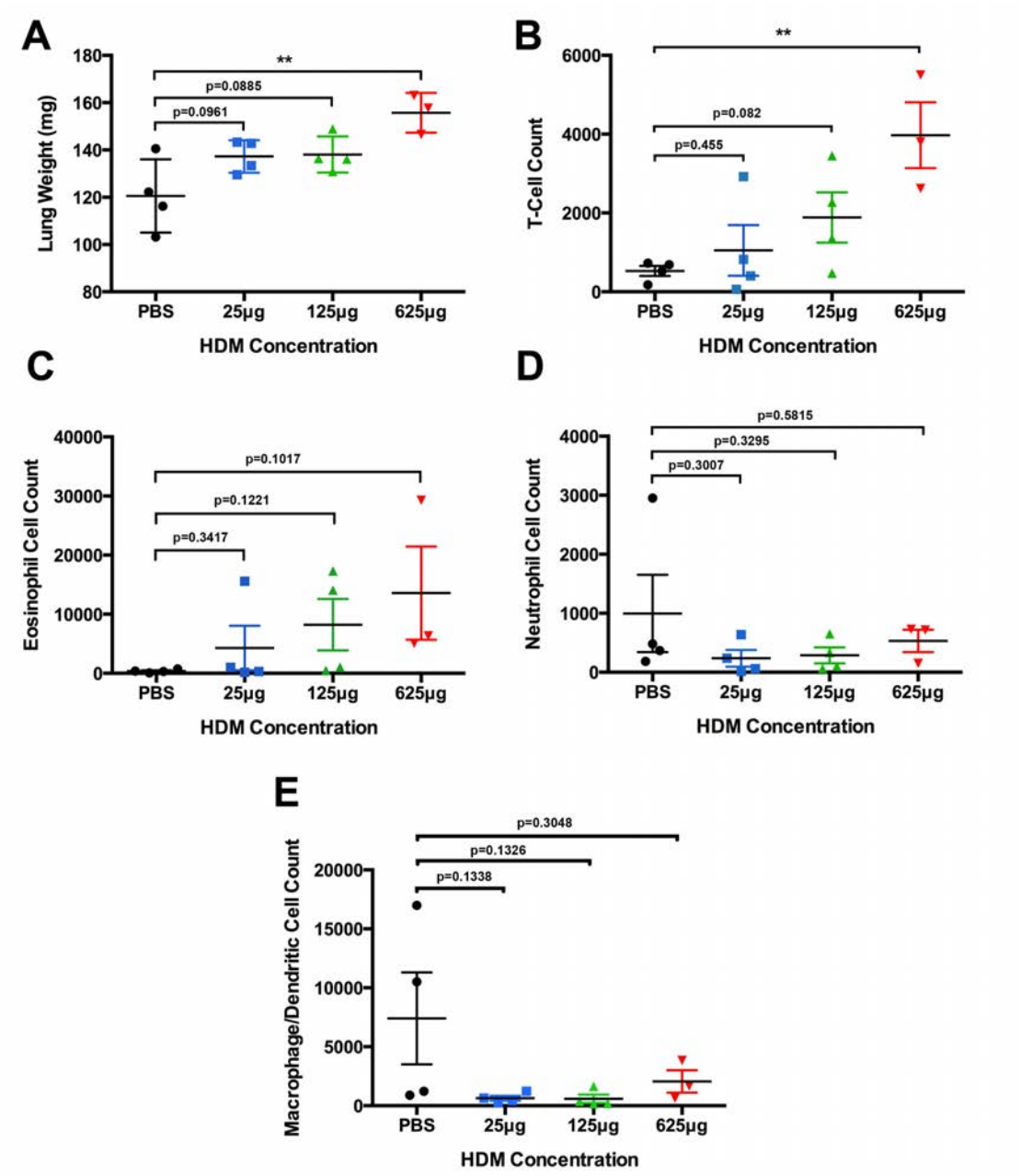

Figure 5.11 Lung inflammation and BAL inflammatory cell analysis following three weeks of whole HDM inoculations.
(A) Lung weight after 25µg and 125µg inoculations was not significantly different to PBS controls. Lung weight did increase significantly in animals exposed to 625µg of HDM. **(B)** T-Cell count was significantly higher in BAL fluid collected from mice inoculated with 625µg of HDM compared to PBS control, however was not significantly different in those inoculated with 25µg or 125µg of HDM. Eosinophil **(C)**, neutrophil **(D)** or macrophage/dendritic cell **(E)** counts were not significantly different in any of the inoculated animals when compared to PBS control.

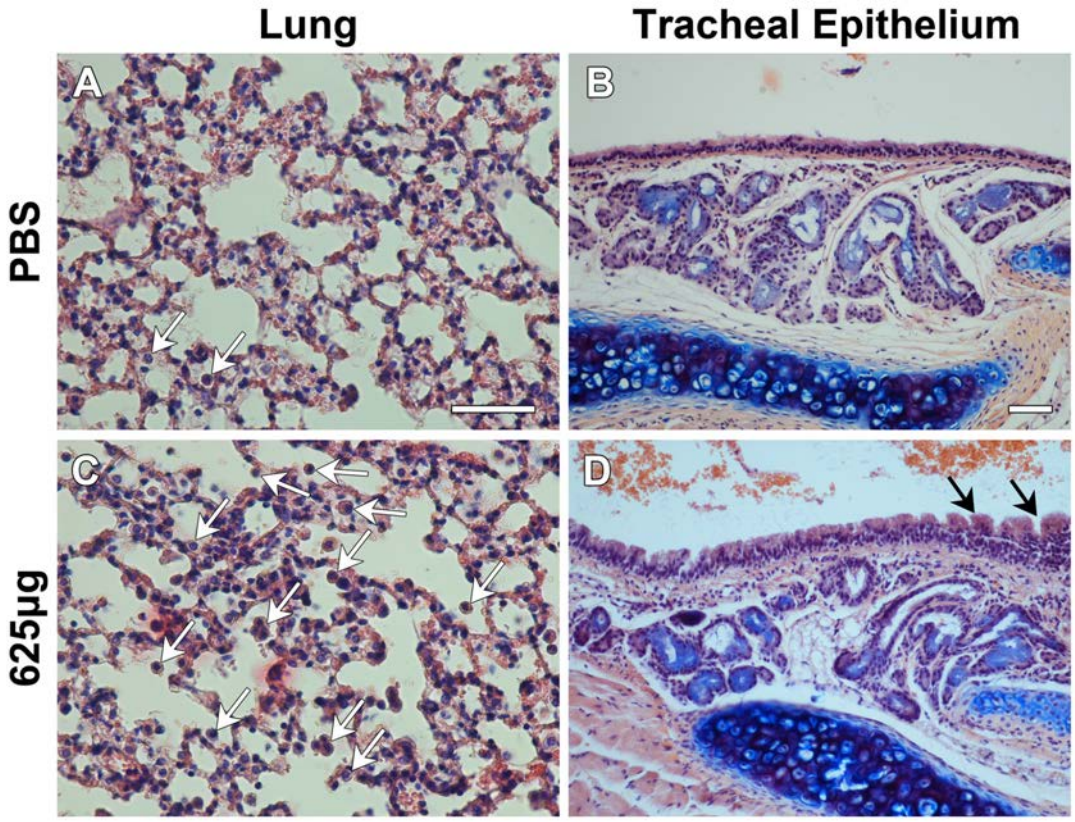

Figure 5.12 Histological analysis of lung and tracheal tissue following three weeks of different HDM inoculations.
(A) Lung tissue of PBS treated animals showing an odd inflammatory cell within alveoli. (B) Normal respiratory epithelium found in the trachea of PBS controls. (C) Tissue of HDM treated mice shows apparent inflammatory infiltrate throughout the lungs. (D) Respiratory epithelium of HDM treated mice appears swollen and possibly hyperplastic in some areas. Scale bar = 50µm.

5.3.10 Inoculation of HDM may Cause Airway Hyperplasia in Fgf10 +/-

When whole HDMs were used at the high concentration of 625µg, CD1 mice occasionally had problems inhaling the inoculant, as particles would block their nasal channels. To overcome this, when the experiment was repeated on *Fgf10* mutant mice and their WT littermates, HDM were sonicated in short 2 second bursts for approximately 10 seconds using a Vibra-Cell™ ultrasonic processor. This short sonication allowed HDM to be broken up into smaller particles to aid in inhalation of the high concentration. HDM particles were then aliquoted into suitable volumes for each inoculation procedure and stored at -20°C. Sonication was carried out by Dr. Alistair Noble. Respiratory challenge of adult male and female *Fgf10* WT (n=7) and

Fgf10 +/- (n=7) mice with 625µg of sonicated HDM was then carried out under the same conditions as CD1 mice, along with control mice inoculated with PBS (n=2 CD1 + n=2 *Fgf10* WT).

Interestingly, analysis of lung weight and BAL fluid showed no significant difference between WT and *Fgf10* +/- HDM treated animals (Figure 5.13 A-E). Furthermore, no significant difference was observed between the WT HDM treated and WT and CD1 PBS controls (Figure 5.13 A-E). A similar result was observed between controls and *Fgf10* +/- treated animals, however T-cell (p=0.038) and macrophage/dendritic cell counts (p=0.0066) were significantly higher in the treated heterozygous groups compared to PBS controls (Figure 5.13 A-E). In comparison to this, histological analysis of lung tissue did show an obvious increase in inflammatory infiltrate in those inoculated with HDM compared to PBS controls (Figure 5.13 F-H, white arrows). Histologically it was difficult to determine if inflammation was more severe in lungs of HDM treated *Fgf10* +/- animals compared to their HDM-treated WT littermates (Figure 5.13 G and H, white arrows).

The anterior epithelium of the WT PBS inoculated animals (n=2) did show slight tufts of epithelium however not substantial enough to consider irregular (Figure 5.14 A and D). The posterior epithelium of the WT control group was identified as regular (Figure 5.14 G). Analysis of tracheal respiratory epithelium showed noticeable differences between WT HDM-treated (n=3) and *Fgf10* +/- HDM treated (n=3) animals. The epithelium appeared regular in the anterior of WT inoculated tracheas close to the cricoid cartilage (Figure 5.14 B and E) while in the same location in *Fgf10* +/- treated animals the epithelium appeared irregular and assumed to be hyperplastic (Figure 5.14 C and F). Moving further posterior within the trachea areas of possible epithelial hyperplasia were seen in WT treated animals (Figure 5.14 H) as well as in the *Fgf10* +/- mice (Figure 5.14 I).

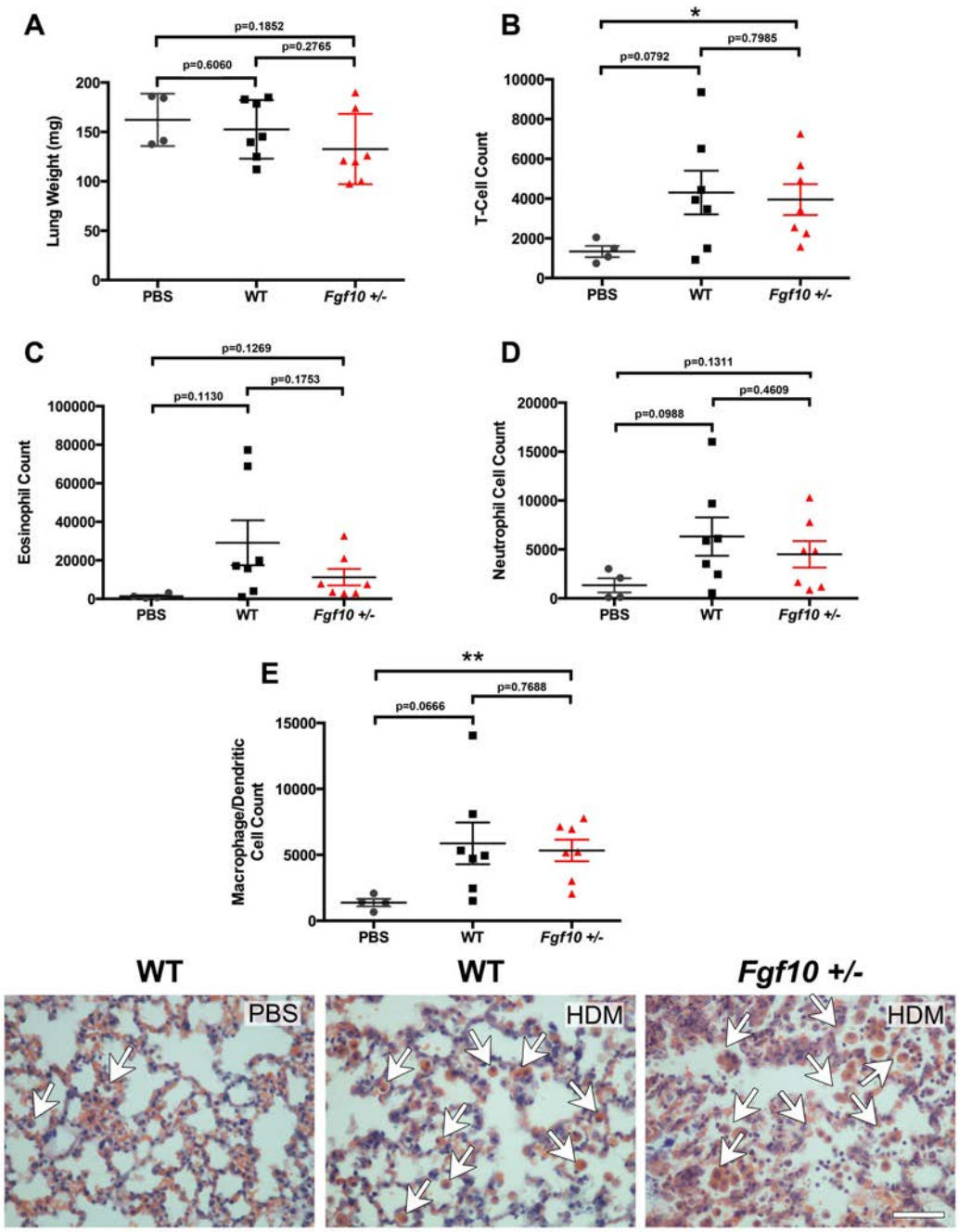

Figure 5.13 Lung inflammation and BAL inflammatory cell analysis of WT and *Fgf10+/-* adult mice following three weeks of 625µg HDM inoculations.
(A) Lung weight showed no significant difference between animals treated with HDM and those treated with PBS only. (B) A general trend of increasing T-cell count was observed in WTs treated with HDM, and a further significant increase in HDM-treated *Fgf10 +/-* mice, compared to PBS controls. Difference between both treated groups was not significant. (C-D) Eosinophil and neutrophil counts showed no significant differences between any of the groups. (E) No significant difference in macrophage/dendritic cell count was observed between control and WT treated animals, or between both treated groups, however, a significant difference between controls and *Fgf10 +/-* treated mice was observed. (F-H) Analysis of lung tissue shows inflammatory infiltrate (white arrows) in alveoli of WT and *Fgf10 +/-* HDM treated animals, while PBS treated lungs are healthy. Scale bar = 50µm.

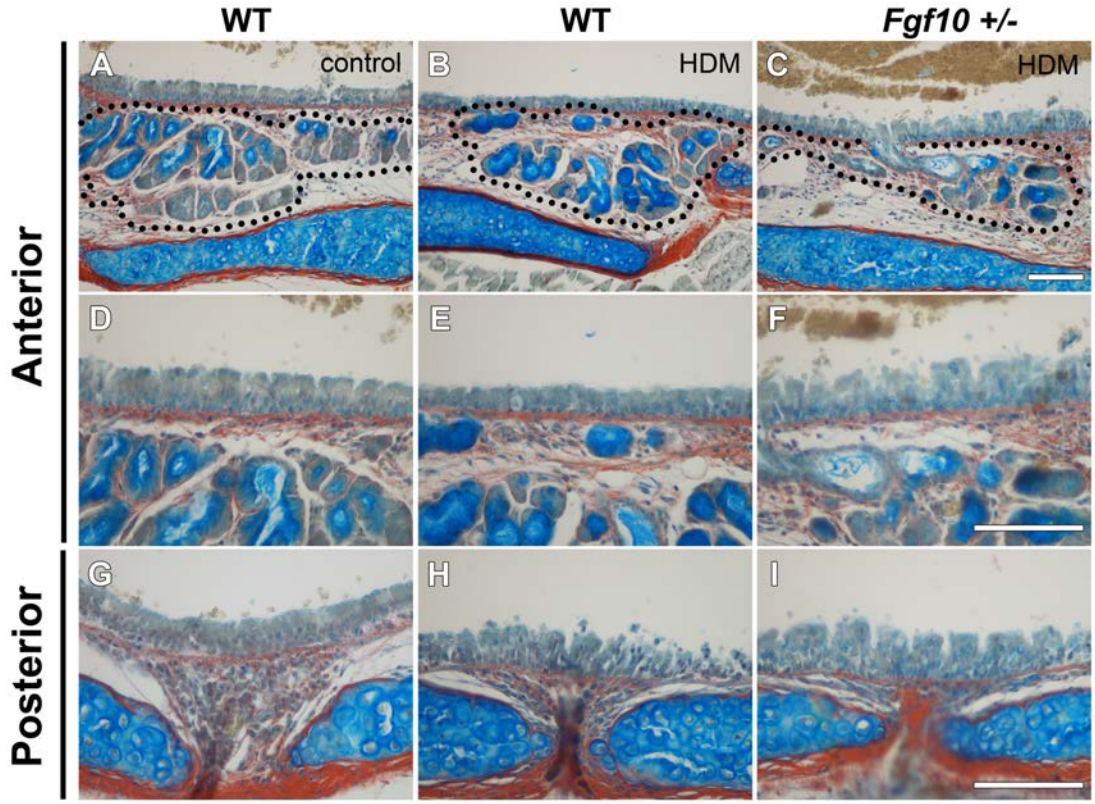

Figure 5.14 Tracheal epithelium analysis of WT and *Fgf10 +/-* adults following HDM inoculations.

(A-F) Anterior trachea of control and HDM treated animals showing SMG and respiratory epithelium. WT PBS inoculated animals show slightly tufted yet regular epithelium (A and D). WT HDM-treated mice show regular neat epithelium anteriorly (B and E) while *Fgf10 +/-* HDM-treated animals appear to have irregular hyperplastic epithelium (C and F). (G-I) The posterior epithelium was regular in all control animals (G), but showed possible hyperplasia in areas in WT HDM-treated (H) and in *Fgf10 +/-* HDM-treated (I). Scale bar=100μm.

5.4 Discussion

5.4.1 Normal Tracheal SMG Development Begins at E18.5

Previous reports have indicated that SMG development in the mouse begins at P2 (Rawlins and Hogan, 2005). Using the CD1 strain of mouse, anterior SMG gland analysis in our study elucidated that tracheal SMGs initiate as early as E18.5 in the ventral mesenchyme adjacent to the cricoid cartilage. At P0 it was recognised that glands had progressed from their early bud initiation stage to elongation through the underlying mesenchyme and the primary stages of lumen formation and branching. Images in the previous report suggest gland bud initiation was uncovered at P2 in the more dorsolateral walls of the trachea, which would agree with our investigation (Rawlins and Hogan, 2005). It must be emphasised, however, that gland development does begin first in the ventral mesenchymal wall and then as postnatal development continues, gland bud initiation progresses more dorsolaterally, and then posteriorly between the cartilage rings. Other studies have also delineated that the development and distribution of the SMGs can depend on genetic background (Borthwick et al., 1999; Innes and Dorin, 2001). Different inbred strains of mice show different posterior extensions of the SMGs between cartilage rings, while the Cystic Fibrosis mouse model has an increase in posterior extension with mutants showing glands as far as the eighth cartilage ring compared to the fourth ring in WT littermates (Borthwick et al., 1999; Innes and Dorin, 2001). This dichotomous patterning however should not impede the mouse as a model of SMG development as the glands still show homologous cellular composition and structure compared to those within the upper and lower airways of humans (Borthwick et al., 1999; Finkbeiner, 1999).

Developmental stages outlined in this study also emphasise homology between the tracheobronchial glands of mice and other animals. Unlike the nasal glands that develop for approximately two days as a long gland duct, followed by the branching of a distal gland (outlined in *Chapter 3*), the tracheal SMGs bud, elongate with a short stem, cavitate and begin branching. This developmental mechanism is similar to that seen in the branching of both the major and minor salivary glands, however in these structures gland it has been reported that branching occurs before lumen formation (Melnick and Jaskoll, 2000; Teshima et al., 2011).

5.4.2 Tracheal SMG Development and Distribution is Altered in Fgf10 +/- Mice

Considering the variable SMG distribution patterns seen in different strains of mice, we analysed the anterior SMGs and their posterior extension in *Fgf10 +/-* adults. Rawlins & Hogan (2005) had already delineated that anterior SMGs were reduced and their posterior extension impeded in *Fgf10 +/-* adult mice compared to their WT littermates, and our analysis concluded the same phenotype. It must be mentioned that although the severity of branching reduction in the anterior SMGs did show variation, all *Fgf10 +/-* glands were smaller than WT counterparts. Variation in localisation of the glands was also observed between *Fgf10 +/-* littermates but all showed reduced posterior extension of the glands. While *Fgf10 +/-* mice have lost functional expression of one of two of their copies of *Fgf10,* this does not necessarily mean that precisely 50% of FGF10 protein is synthesized. From *in vitro* manipulation studies in culture, it is understood that branching organs are extremely sensitive to fluctuations in protein levels. Different concentrations of protein can induce branching organs to develop with slightly different phenotypes (Steinberg et al., 2005). Many post-transcriptional aspects are tightly controlled before protein is synthesized (e.g RNA processing, RNA stability, translation and protein stability) meaning that proteome levels do not exactly reflect mRNA levels, and that protein concentrations can fluctuate (Vogel and Marcotte, 2012). In WTs, the effect of this does not influence phenotype however as protein expression may always be above a threshold required for normal gland development. In *Fgf10 +/-* animals however, some heterozygous mice may express proteins at a concentration above a threshold level that does not induce as severe a phenotype as other mutant littermates, whose overall protein production is severely reduced. This fluctuation in protein expression may induce variation in phenotype of the glands in *Fgf10 +/-* mice. It would then be expected that a defective phenotype could lead to a reduction in mucous secreted by these glands and negatively effect the mucin-rich protective barrier of the airways of *Fgf10 +/-* mice. Furthermore, variable expression of clinical symptoms are seen within patients who suffer from LADD syndrome, similar to the varying phenotypes observed in *Fgf10 +/-* mice (Thompson, Pembrey, and J. Graham, 1985; Rohmann et al., 2006). This again suggests that heterozygosity of *Fgf10* may lead to differences in protein levels and thus phenotypic variation.

As a previous report has shown that the mesenchymal localisation of *Fgf10*, and its epithelial receptor *Fgfr2b*, play a critical role in tracheal cartilage patterning (Sala et al., 2011), we wanted to rule out a possible influence of abnormal cartilage ring structure as an influence on the branching of *Fgf10* +/- glands. By cartilaginous preparation using whole mount Alcian Blue staining, it was clarified that *Fgf10* +/- embryonic tracheas at E18.5 show no disorganization or patterning defects in the tracheal cartilage rings. This supports the hypothesis that *Fgf10* plays a role in the mesenchymal-epithelial interactions involved in branching morphogenesis of the epithelial SMGs and that the observed gland phenotype is not a secondary effect of a cartilaginous defect.

5.4.3 Fgf10 -/- Mouse Pups Develop SMG Buds

Considering the initiation of ventral tracheal SMGs at E18.5 in our mouse line, this gave us an opportunity to collect *Fgf10* -/- pups at P0, along with their WT and *Fgf10* +/- littermates, just after birth. Interestingly, gland buds were found in the ventral and slightly more dorsal anterior positions in the *Fgf10* -/- specimens collected. Out of four mutants analysed, all had gland buds detected in ventral and some dorsolateral planes of the trachea. This result concluded that *Fgf10* is not required for the initiation of the epithelial gland primordia or the outgrowth of the initial gland bud. Alternatively it is possible that *Fgf10* plays a role in these early processes during normal gland development however in the *Fgf10* -/- mouse other *Fgfs* may compensate.

At P0, reduction in branching was also observed in *Fgf10* +/- pups at this early stage of gland developmental. At P0 the ventral glands of WT animals had reached the lumen formation stage and are undergoing clefting and branching. *Fgf10* +/- animals also showed glands had elongated into the underlying mesenchyme and formed lumens however the amount of gland branches was evidently reduced. This phenotype mirrors that reported for submandibular salivary gland (SMDG), where the gland does not progress passed the initial bud stage in *Fgf10* -/- mice, and branching is reduced leading to aplastic glands in the *Fgf10* +/- mouse (Jaskoll et al., 2005 and *Chapter 5*). This altered SMG development is similar to the aplastic lacrimal and salivary gland phenotypes observed in those that suffer from both ALSG and LADD syndrome (Milunsky et al., 2006; Shams et al., 2007; Entesarian et al., 2007). While no reports

have stated any pulmonary defects in patients with ALSG or LADD syndrome, it is quite likely that the airway SMGs would show aplasia and that this phenotype could possibly give rise to mucociliary deficiencies in those that suffer from these autosomal dominant diseases.

5.4.4 Fgf10 +/- Adults Release Less Mucus Into Their Airways due to a Reduction in SMGs

Previous studies have exploited the use of mineral oil to visualise gland mucus production in rodents and sheep (Joo et al., 2001; Ianowski et al., 2007). We adapted these protocols to allow functional tests of mucus secretion in mice. The protocol used was effective and reproducible.

The reduction in number of mucus bubbles produced was significant and could easily be observed with the naked eye. The number of bubbles counted in WT tracheal tissue averaged at 39 while in *Fgf10* +/- the mean bubble number was 11, with one heterozygous specimen producing only 7 bubbles. Analysis revealed that there was over a 50% reduction seen in all *Fgf10* +/- specimens investigated compared to their WT littermates and almost a 75% decrease in the most severe cases. As it was difficult to elucidate if there was a decrease in the amount of glands, as well as a decrease in branching, through histological means of adult tissue, this result demonstrates that there are fewer functional glands between the anterior cartilage rings in *Fgf10* +/- adult tracheas.

Previous studies have used volume and the equation $V = 4/3\ \pi r^2$ to represent mucus production, assuming spherical shape of each bubble (Joo et al., 2001; Ianowski et al., 2007). As no bubbles followed an exact spherical shape the measurement of one single radius was found not to be an accurate representation of secretion therefore area of each bubble was chosen to study. Results of this analysis concluded that bubbles were not significantly larger in the WT specimens compared to their *Fgf10* +/- littermates. This was supported by additional investigation of bubble circumference and bubble feret diameter not showing any significant difference. These results indicate that the functional glands within *Fgf10* +/- animals may undergo the same amount of branching as WT littermates, and therefore produce bubbles of the same size. The largest bubbles however were identified in the WT

specimens suggesting larger glands were present in WTs, however due to the greater number of glands within WTs of all different sizes, difference between those and their *Fgf10 +/-* littermates was not significant. Furthermore, our histological analysis of early gland development within WT and *Fgf10+/-,* showed early reduction of branching in heterozygous animals, indicating that measurement of mucus bubble production may not be an ideal representation of gland size. Considering this, total mucus bubble areas were accumulated per specimen to give an overall representation of the amount of mucus released into the anterior trachea. This result concluded a significant decrease in overall mucus released into the airway lumen in *Fgf10 +/-* animals. As only the anterior glands were included in the study, an even greater difference would be assumed if all mucus bubbles extending posteriorly in WT animals were calculated.

Our analysis of *Fgf10 +/-* tracheal SMGs above, as well as our histological analysis in *Chapter 4* indicating *Fgf10 +/-* also have hypoplastic nasal glands, suggest that these mutant mice secrete less mucus into their airway lumens. We hypothesised that trans-epithelial transport of allergens from the airway lumen into lung tissue may be increased in mice that have reduced mucous levels. Our results indicate that there was a general trend of increasing fraction of lung cells that had taken up the OVA conjugate in *Fgf10 +/-* animals compared to their WT littermates, however this difference was not statistically significant. On reflection we concluded that use of a soluble protein allergen was not ideal to answer the question of reduced mucociliary clearance.

Considering this, we decided to expose mice to whole HDM. Using whole mites, we hypothesised that while their allergens would induce an immune response in administered animals, their physical nature would also act as a damaging inhalant, and mucociliary function would be tested by the ability to remove these particles away from the lungs. Analysis of BAL collected from exposed CD1 adults using FACS showed that all HDM inoculations triggered a response represented by an increase in lung weight, indicating lung inflammation, and increased T-cell and eosinophil cell counts. These responses however were only statistically significant from administration of the highest concentration, 625μg, of HDM used. Analysis of

both lung and tracheal epithelium supported this conclusion, as inflammatory infiltrate was evident in the lung parenchyma of those induced with 625μg of HDM as well as possible hyperplasia of the respiratory epithelium in certain areas of the trachea. Considering this it was decided that 625μg of HDM in 30μl of PBS was the most suitable inoculation to analyse the inflammatory and tissue response in the WT and *Fgf10* +/- animals. During administration of CD1 animals however in the test experiment, it was observed that inhalation rates of this high concentration was not consistent. HDM was seen to collect in the small nostrils of the mice and sneezing was periodically observed. Although this may not hinder the effectiveness of the experiment due to the overall experimental length of three weeks, and repetitive inoculations every three days, it was decided to sonicate the HDM to produce smaller mite particles for inhalation of WT and *Fgf10* +/- animals. Sonication was successful and inoculant was inhaled more easily throughout the period of three weeks.

Analysis of lung weight following three-week administration saw no significant difference between WT and *Fgf10* +/- inoculated littermates. Comparison to PBS administered WTs also showed no significant difference. It must be mentioned however that this study was hindered by the general small litter size of the *Fgf10* +/- mice. This therefore required the addition of age matched CD1 mice to act as WT PBS controls (n=2) to make up sufficient numbers for the study. Although these two mice were born on the exact same day as the other *Fgf10* litters (taken from a *Fgf10* +/- and *Fgf10* +/- mating) used for HDM analysis, by the end of the three-week experiment they were considerably larger and lung weights considerably heavier than PBS controls from the *Fgf10* litter. While this characteristic should not affect other analysis, it may influence the fact that lung weight is not a reliable inflammatory indicator. Furthermore, although the lung weight analysis concluded no significant differences between all groups, histological examination of the lung parenchyma saw apparent inflammatory infiltrate within both WT and *Fgf10* +/- HDM treated tissue. This suggests that the exposure to HDM did in fact cause inflammatory responses.

T-cell count did show an increasing trend from WT PBS controls to WT HDM inoculated and then again in *Fgf10* +/- HDM inoculated, with only heterozygous treated animals showing a significant increase compared to controls. Furthermore,

there was no difference within eosinophil count between each group. Although no differences in inflammatory responses were observed between WT and *Fgf10* +/- HDM inoculated animals, interestingly the PBS control WT animals showed no significant differences in T-cell count compared to WT treated, and no significant difference in eosinophil counts compared to both treated groups. Considering the satisfactory allergen response seen in CD1 animals exposed to HDM and the well established knowledge that HDM is a significant allergen causing inflammatory cell infiltrate, the results collected indicate that this experiment may not be an ideal representation of the effects of HDM administration. This result may be due to the potential loss of the soluble allergenic protein of the HDM by sonication.

Interestingly, increased numbers of macrophage/dendritic cells were evident in the WT and *Fgf10* +/- HDM inoculated groups, compared to controls, with the difference between heterozygous treated animals and controls being significant. Three types of macrophages are present within lung tissue; bronchial macrophages (BMs), interstitial macrophages (IMs) and alveolar macrophages (AMs) (Balhara and Gounni, 2012). Recent studies have emphasised the role of these cells in preventing allergic asthma symptoms and maintaining lung homeostasis through their two primary roles of allergen recognition and presentation, and phagocytosis (Careau et al., 2010; Bang et al., 2011; Lauzon-Joset et al., 2014). It is recognised that the BMs and IMs function in antigen presentation to induce an adaptive immune response (Gong et al., 1994; Moniuszko et al., 2007; Bedoret et al., 2009) while evidence shows that AMs, which are those collected in BAL fluid, are poor APCs (Lipscomb et al., 1986; Chelen et al., 1995). It has been established that there is tight self-regulation of the AM populations to remain quiescent in normal situations and release very little cytokines to prevent collateral damage of fragile lung tissue (Holt, 1978). Therefore it is considered that the increasing trend observed in macrophages in the HDM inoculated groups in this study primarily represents AM recruitment to carry out a phagocytic role of HDM particles, as opposed to an influx of macrophages recruited for antigen recognition. Histological analysis of lung parenchyma additionally shows aggregations of inflammatory cell infiltrate suggesting localised areas of phagocytosis, possibly more so in *Fgf10* +/- animals compared to WT inoculated individuals.

Neutrophil count also showed a trend in increasing numbers in WT and *Fgf10* +/- inoculated animals compared to PBS controls. The principal function of neutrophils is also phagocytosis (Nordenfelt and Tapper, 2011). Neutrophil count showed a marked increase in WTs, however, the increase was less marked in the *Fgf10* +/- mice exposed to HDM. As macrophages function in ingestion and eradication of dead neutrophils (Savill et al., 1989), the high number of macrophages in *Fgf10* +/- HDM exposed specimens could explain why neutrophils are slightly reduced in the heterozygous animals compared to WT HDM exposed animals.

Papillary epithelial projections can be used to identify the development of epithelial hyperplasia (Sells et al., 2007). Considering this, it appears that these epithelial projections are present in the anterior trachea of *Fgf10* +/- exposed to HDM compared to a smooth epithelium present in HDM inoculated WT littermates. Moving more posterior down the trachea it appeared that possible hyperplasia occurred in the epithelium of both inoculated groups. Using rodents as models to study the effect of toxic inhalants, it has been shown that exposure to HDM (Johnson et al., 2004; Saglani et al., 2009), industrial chemicals (Nyska et al., 2005), cigarette smoke (Mebratu et al., 2011) and other air pollutants (Harkema et al., 1999) gives rise to respiratory epithelium hyperplasia. A potential metaplasia increasing the ratio of mucus cells to serous may also have occurred in both WT and *Fgf10* +/- inoculated animals however this is difficult to delineate conclusively using histological methods alone. It is also problematic to compare rates of metaplasia between WT and *Fgf10* +/- animals due to the decreased size of *Fgf10* mutant glands. Additionally, it has been shown that exposure to HDM can alter epithelial functionality and lead to the secretion of enzymes that target adhesion molecules and cause mucosal damage (Roche et al., 1997). Considering this, investigation into adhesion markers of the tracheal epithelium, such as E-cadherin, could be carried out to delineate it epithelial damage is more severe in *Fgf10* +/- exposed to HDM compared to WT littermates.

To conclude, exposure to sonicated HDM is not an ideal model for mucociliary clearance functionality of WT and *Fgf10* +/- adult mice, and application of whole HDM inoculation is more effective. It is therefore suggested that if this experiment was repeated, 125μg doses of whole HDM should be used. While this concentration

did not give statistically significant results when used on CD1 animals, it did cause inflammatory response with rising levels of T-cell and eosinophil counts. Application of a weaker dose may also elucidate mucociliary differences between WT and *Fgf10* +/- animals, as a high dose of 625μg may have masked these effects. Furthermore, 125μg of whole HDM was easily inhaled by young adult mice. Other experimental models could also be employed. For example, Hua et al. (2010) used planar gamma scintigraphy to optimally investigate nasal mucociliary clearance non-invasively in a mouse model. After isoflurane anaesthetization, mice were intranasally inoculated with radioactive particles. Using a planar gamma camera, timed retention and mucociliary clearance of radioactive particles within the nasal cavity was measured (Hua et al., 2010). This method could be applied to investigate clearance abilities in *Fgf10* +/- mice, especially in the nasal region where, in *Chapter 4,* we showed that nasal gland hypoplasia is evident.

6.1 Introduction

6.1.1 Mammalian Salivary Glands

As mentioned in *Chapter* 1, humans and mice have three major paired salivary glands in the oral cavity that produce 90% of total saliva secretion (Tucker, 2007). The major salivary glands are derived from the oral ectoderm and neural crest derived mesenchyme (Rothova et al., 2012; Jaskoll et al., 2003). The parotid gland (PG), the largest of the salivary glands, is located at the back of the mouth in front and below the ear between the upper and lower jaws (Figure 6.1). This gland is made up of serous acini exclusively and secretes saliva via the Stenson's duct, which opens into the oral cavity via the cheek. The submandibular gland (SMDG), consisting of a mix of serous and mucous acini, and the sublingual gland (SLG), predominantly made up of mucous acini, lie beneath the tongue and excrete their secretions via ducts which open into the floor of the mouth (Figure 6.1). In humans, the SMDG produces 70% of total saliva secretion and expels saliva via the Wharton's duct (Miletich, 2010). The SLG excretes via the Bartholin's duct, which is seen to open close to the SMG duct, but can also expel saliva through 8-20 smaller excretory ducts, called the ducts of Rivinus, that open out beneath the tongue (Miletich, 2010) (Figure 6.1). The remaining 10% of saliva is produced by the minor salivary glands which are located in the tongue, palate, cheeks and lips (Hand et al., 1999).

6.1.2 Importance of Saliva

The salivary glands have evolved to carry out an important function in maintaining oralpharyngeal health. The many functions of saliva include providing lubrication for digestion and speech, producing digestive enzymes and anti-microbials, buffering the pH of the mouth, as well as a protective function to the oral and oesophageal mucosa (Pedersen et al., 2002). A reduction in saliva leads to xerostomia, or dry mouth, an oral symptom that can seriously impinge the quality of life in human patients. This hyposalivation leads to problems such as mastication difficulties, halitosis, deficiency of taste and a high incidence of dental caries and candida infections. There are many reported biological driving factors that lead to xerostomia. The highest incidence of dry mouth is observed in people over the age of 65, reaching approximately 30% (Ship et al., 2002). It is not believed, however, that salivary gland dysfunction is concomitant of ageing, rather it is a side effect from prescription medications or an

outcome of a number of systemic diseases such as Sjögren's Syndrome (OMIM 270150) (Ship et al., 1995, 2002; Gupta et al., 2006; Zalewska et al., 2013). Sjögren's Syndrome (SS) is a chronic autoimmune inflammatory disease targeting the exocrine glands changing both the quality and quantity of secretion produced. It has a prevalence of 3-4% in the United Kingdom and up to 3.1 million adult sufferers in the United States with 90% of patients being female (Thomas et al., 1998; Helmick et al., 2008). Primary SS, where the disorder occurs alone, primarily affects the salivary and lacrimal glands while secondary SS arises along with other systemic connective tissue diseases such as rheumatoid arthritis (Peri et al., 2012). The prevalence of xerostomia is also common in patients with head and neck cancers, who are treated by radiation therapy and also administered chemotherapeutic drugs, which both lead to damage of the salivary glands and hyposalivation (Chambers et al., 2004).

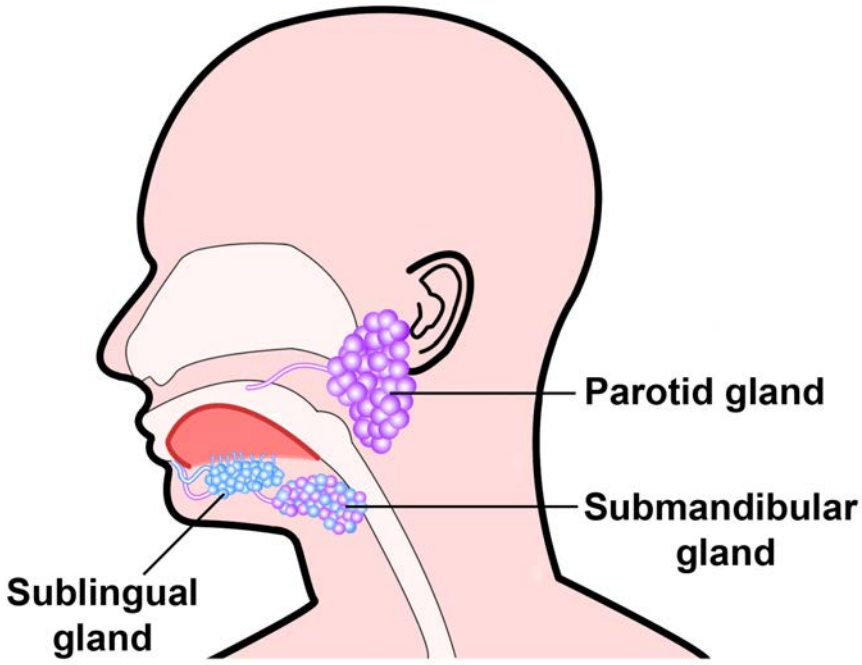

Figure 6.1 Location of the major salivary glands in humans.
The parotid gland (PG), made up of serous acini, is located in front of the ear between the upper and lower jaws. Its duct opens out into the cheek. The sublingual (SLG) and submandibular glands (SMDG) lie beneath the tongue with their ducts opening into the floor of the mouth. The SLG, consisting of mucus acini, also has an array of smaller ducts that open into the bottom of the tongue. The SMDG is made up of both mucous and serous acini.

6.1.3 Fgf10 and Salivary Gland Development

As described in *Chapter* 1, human autosomal dominant mutations in *FGF10* or its receptor *FGFR2b*, lead to Lacrimo Auriculo Dento Digital (LADD) syndrome (OMIM 149730), or the milder Aplasia of Lacrimal and Salivary Glands (ALSG) (OMIM 180920). These syndromes are characterised by hypoplasia, aplasia or atresia of both the lacrimal and salivary systems (Milunsky et al., 2006; Shams et al., 2007). Due to these phenotypes, human LADD or ALSG patients suffer from severe xerostomia. The mouse SMDG has provided a valuable model for investigating gland development and research shows it requires the interaction between mesenchymal *Fgf10* and its epithelial receptor *Fgfr2b* for successful branching morphogenesis (Ohuchi et al., 2000). As outlined in *Chapter 1*, knockout of *Fgf10,* or its receptor, leads to complete aplasia of the major salivary glands, which arrest at the epithelial thickening stage (Jaskoll et al. 2005). These mice however are perinatal lethal as they also lack lungs (Min et al., 1998; Sekine et al., 1999). In viable *Fgf10 +/-* mouse pups at P0, SMDGs are present but have fewer ducts and terminal buds (Jaskoll et al. 2005). Another study investigated *Fgf10 +/-* adult salivary glands and concluded they were hypoplastic compared to WTs yet the histology of the SMDG and SLG were similar to WT counterparts (Entesarian et al. 2005). This study by Entesarian et al. (2005) however only investigated two *Fgf10 +/-* adults and a more thorough investigation using a larger number of samples should be carried out to delineate a true difference in salivary gland phenotype.

6.1.4 The Need for a Model of Xerostomia

Animal models are indispensable tools for delineating the underlying aetiology of diseases and their contribution to biomedical discoveries has been invaluable. Our advanced knowledge of the mouse genome and the physiological similarities shared with humans makes the mouse an important mammalian model in uncovering the pathogenesis of many diseases. Murine models of xerostomia, such as the non-obese diabetic mouse (NOD), have been generated and extensively researched, however the dry mouth phenotype in these mice is a result of autoimmune exocrinopathy and therefore the xerostomia is a secondary effect of the underlying autoimmune disease (Humphreys-Beher, 1996; Lavoie et al., 2011; Lee et al., 2012). While these autoimmune models are beneficial, an animal model of dry mouth without any

underlying disease is necessary to examine the effect of dry mouth in otherwise healthy individuals.

6.1.5 Aims of Study

- To delineate the exact phenotype of SMDG and SLGs in the adult *Fgf10 +/-* mouse.
- Elucidate if this defect affects the functionality of the glands and compromises saliva secretion.

6.2 Materials and Methods

6.2.1 P14 and Adult Salivary Gland Weight Analysis

At postnatal day (P)14 WT and *Fgf10* +/- littermates were culled by exposure to CO_2 gas. Animals of this age were chosen as sexual dimorphism in salivary glands does not arise until P15 (Gresik, 1975). Mice were weighed and the SMDG and SLG glands were dissected together. Excess fat surrounding the glands was removed. Glands were dried using an air stream and weighed immediately. Glands were then fixed in 4% paraformaldehyde in PBS (PFA) at 4°C overnight and processed for histological analysis. The same process was adopted for measuring the weight of adult (7-10 weeks) salivary glands from WT and *Fgf10* +/- littermates.

6.2.2 Adult Salivary Gland Function Tests

Salivary gland function tests were primarily carried out by Prof. Gordon Proctor (Mucosal Biology and Salivary Division, Dental Institute, King's College London) while I accompanied. WT and *Fgf10* +/- adult littermates were put under mild anaesthetic (ketamine 80mg/kg; xylazine 16mg/kg) by peritoneal injection. Mice were weighed and positioned under a light microscope. An incision was made and a thin tube inserted into the trachea to facilitate breathing. Mice were then subcutaneously injected with a low dose of pilocarpine hydrochloride (0.54-0.64 μg/g body weight, Sigma Aldrich), individual SMDG and PG ducts were cut and after 10 minutes saliva was collected at the opening of ducts at room temperature and put into pre-weighed 1.5ml eppendorf tubes kept on ice. Saliva secretion volume was calculated where 1mg = 1μl saliva. Following each procedure animals were humanely killed by one lethal dose of anaesthetic. Saliva secretion was calculated as volume of saliva per minute (μl/min).

6.2.3 Statistical Analysis

Differences in gland weight were analysed using a two-tail unpaired Student's *t-test* on WT and *Fgf10* +/- aged P14 and adults aged 7-10 weeks. Specimens used for saliva secretion tests were littermates from a range of adult ages (13-54 weeks). Data from these experiments were pooled and statistical significance was calculated using a Wilcoxon's signed rank test. Due to the variation of ages used in secretion analysis, *Fgf10* +/- saliva secretion was expressed as a ratio of secretion from a matched WT

littermate, where WT secretions equal 1. Graphs were generated using GraphPad Prism 6 software.

6.2.4 Scanning Electron Microscopy (SEM)

Female adult littermates (6 weeks old) were culled by exposure to CO_2 gas. Tongues were dissected and fixed in 2.5% glutaraldehyde in 0.15M cacodylate buffer (pH 7.2) overnight at 4°C. The following tissue preparation procedure was carried out by Dr. Gema Vizcay-Barrena (centre for Ultrastructural Imaging, King's College London). Tongues were washed in cacodylate buffer and postfixed in 1% osmium tetroxide. Tissue was then dehydrated through an ethanol series and dried using a Polaron E3000 critical point dryer. Tongues were mounted and coated with gold (Emitech K550X sputter coater). Using a Hitachi S-3500N scanning electron microscope (SEM) the surface mucosa of the tongue was analysed. Images were taken of specific temporal regions of different papillae of the tongue. All images were taken with the microscope set at 10kV in high vacuum mode.

6.3 Results

6.3.1 A Reduction in Fgf10 does not Affect the Gross Morphology of the Gland at the Histological Level

To investigate a sex-independent affect of loss of *Fgf10* on salivary gland morphology, we analysed glands at P14. At this age, sex hormones have not been released and sexual dimorphism is not evident (Gresik, 1975, 1994). In agreement with this, no obvious histological differences were seen between male and female WT animals at P14 (Figure 6.2 A-D). No obvious difference in histology was evident between *Fgf10* WT and +/- littermates at P14 (**Figure 6.3** A-D). In *Fgf10 +/-* glands, the numbers of ducts and acini appeared similar to WTs, however the overall size of gland lobes appeared smaller (**Figure 6.3** A-B).

6.3.2 Fgf10 +/- Animals Show Reduced Salivary Gland Weight at P14

Given the lack of a change in histology, we moved to assess whether there was a weight difference between WT and *Fgf10 +/-* groups at P14. Comparison of WT and *Fgf10 +/-* gland weight showed a significant difference, with smaller glands observed in heterozygous animals (**Figure 6.3**, E). These results indicate that loss of function of one copy of *Fgf10* leads to a reduction in size of salivary glands at an early postnatal age with the affect of this phenotype being independent of sex.

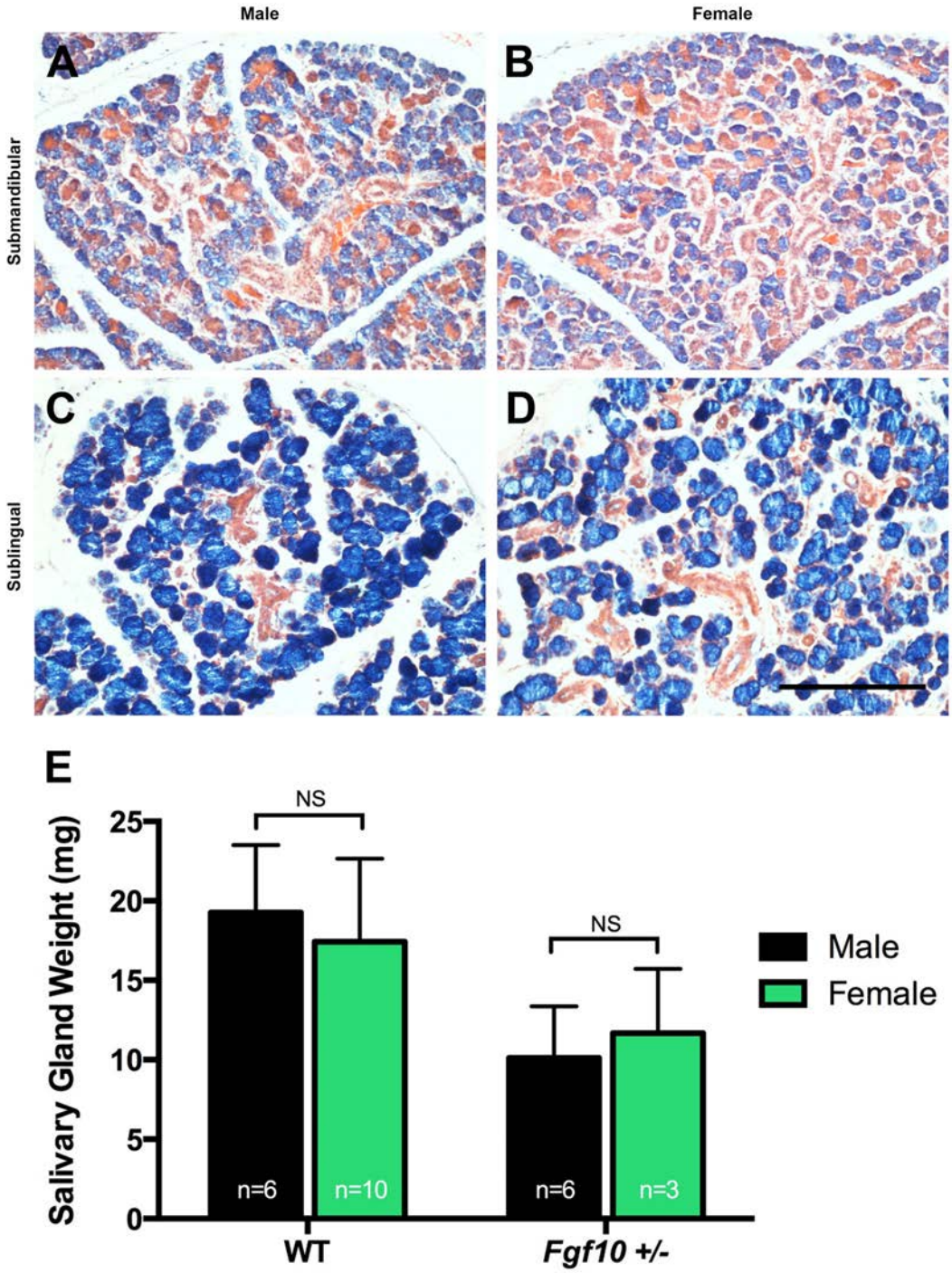

Figure 6.2 No sexual dimorphism is observed in SMG and SLGs aged P14.
No obvious morphological differences were noted in either SMDG (A, B) or SLGs (C, D) between both sexes. (E) No significant difference was seen between male and female salivary gland (SMG + SLG) weight in both WT and *Fgf10* +/- animals at P14. Scale bar = 200μM.

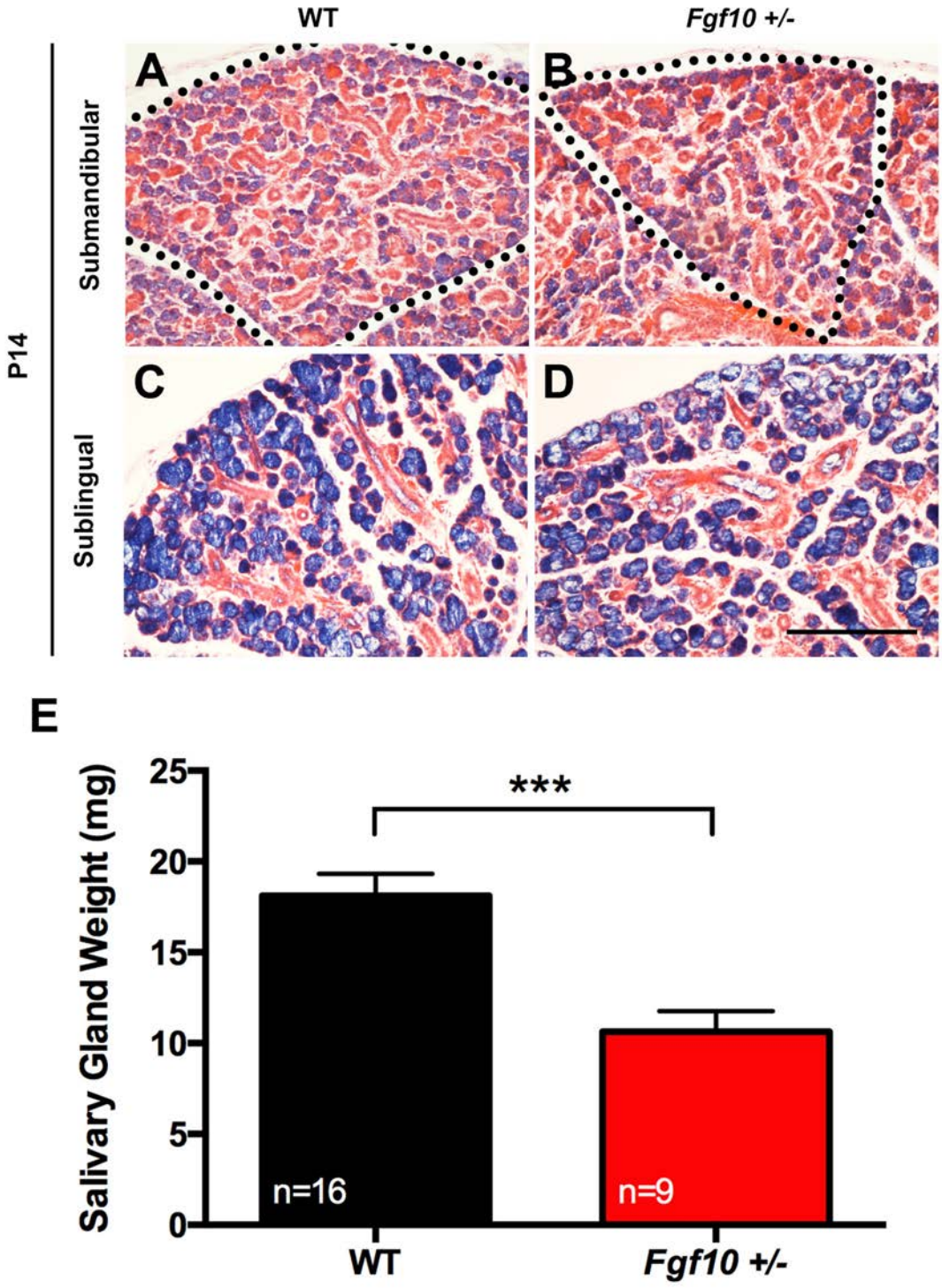

Figure 6.3 Comparison of WT and *Fgf10* +/- salivary glands at P14.
(A-D) General duct and acini arrangements of WT and *Fgf10* +/- SMG and SLGs appeared normal at P14. A reduction in size was seen in glandular lobes in *Fgf10* +/- animals compared to WT littermates (black dotted line) (A-B). (E) At P14 combined *Fgf10* +/- SMGs and SLGs weighed significantly less compared to WT littermates. Scale bar = 200μM. A-D shows glands from female specimens. *** $p<0.001$.

6.3.3 Adult Fgf10 +/- Animals Have Reduced Salivary Gland Weight

We further investigated SMDG and SLGs in littermates aged between 7-10 weeks to delineate if glands remained smaller throughout adult life. Smaller glandular lobes were observed in *Fgf10* +/- glands compared to WT littermates (Figure 6.4, A-B). No morphological differences were seen between adult WT and *Fgf10* +/- littermates at a histological level (Figure 6.4, C-F). Using salivary gland weight analysis, a significant difference in weight of WT and *Fgf10* +/- glands was observed in both adult females and males, with smaller glands found in *Fgf10* +/- animals (Figure 6.4, G). No significant difference was seen in body weight between WT and *Fgf10* +/- littermates (males p=0.5, females p=0.2), therefore a reduction in overall body weight was excluded as a factor influencing the salivary gland phenotype.

As expected a significant difference was seen between adult female and male glands in both genotypes, with males having considerably larger glands to females, due to having larger and more prevalent granular convoluted tubule (GCT) cells than those observed in females (Figure 6.4 and Figure 6.5). The larger and more numerous GCT cells is reflected functionally as GCTs are the location of amylase activity in postnatal and adult mice, which has been shown to be increased in males (Gresik, 1975).

6.3.4 Adult Salivary Gland Secretion is Severely Reduced in Fgf10 +/- Mice

Human patients with ALSG or LADD syndrome have severe dryness of mouth due to aplasia of the major salivary glands (Wiedemann and Drescher, 1986; Rohmann et al., 2006). We therefore wanted to test whether the smaller size of the salivary glands in *Fgf10* +/- mice lead to a reduction in salivary output. Saliva was collected from WT and *Fgf10* +/- littermates after inoculation with pilocarpine. As predicted from gland weight, *Fgf10* +/- animals showed a significant reduction in saliva flow compared to their WT littermates from both the SMDG and PG (Figure 6.6). Our results collectively suggest that the hyposalivation observed in *Fgf10* +/- adults is due to the reduction in size of each gland as opposed to a morphological defect at a cellular level.

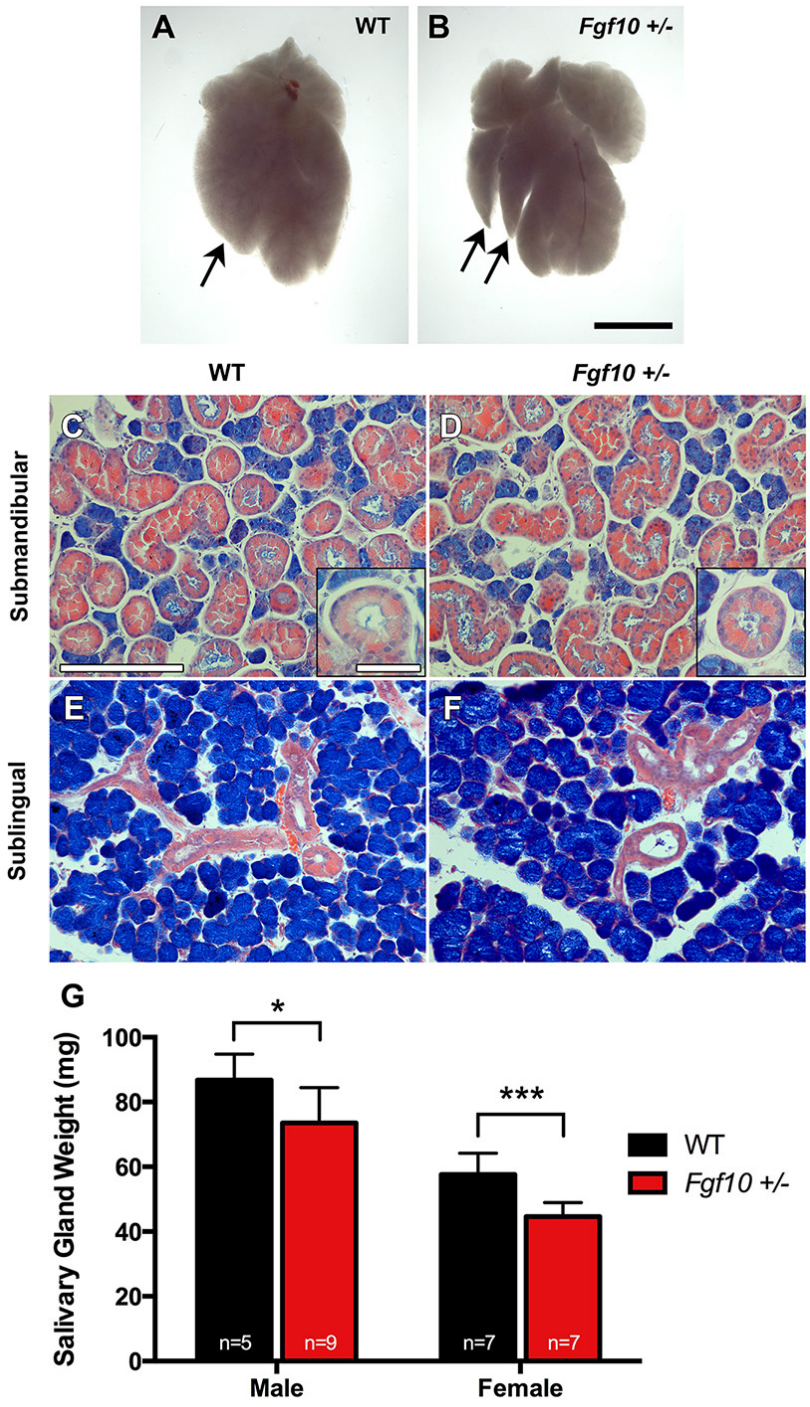

Figure 6.4 Comparison of adult salivary glands.
(A-B) Smaller gland lobes are observed in *Fgf10* +/- adult SMDGs (arrows)(scale bar=3mm). (C-F) Male glands; no histological differences are noted between WT and *Fgf10* +/- SMGs (C, D) SLGs (E, F), and GCTs (inset images C, D). (G) Male and female *Fgf10* +/- adult salivary glands show a significant decrease in weight compared to WT littermates. C-F scale bar=200μm, inset scale bar=50μm. * $p<0.05$, *** $p<0.001$.

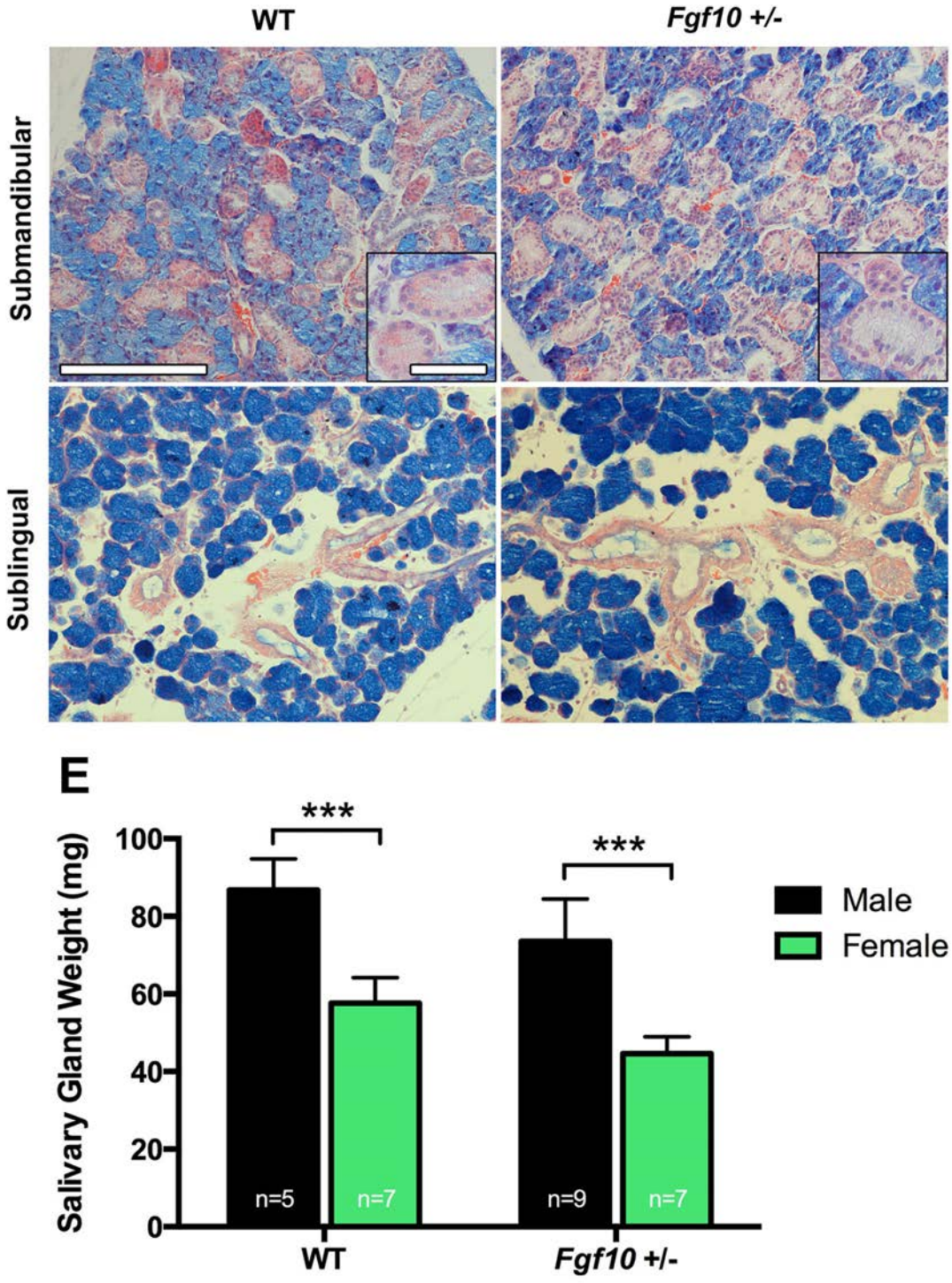

Figure 6.5 Comparison of male and female adult salivary glands.
(A-D) No morphological differences were seen in female WT and *Fgf10* +/- SMGs (A-B) and SLGs (C-D). GCTs are smaller in female adult glands (inset images A-B) than those seen in male glands (Figure 6.4). A-D scale bar=200μm, inset scale bar=50μm. (E) A significant difference is seen between male and female salivary gland weight in WT and *Fgf10* +/- groups. *** $p<0.001$.

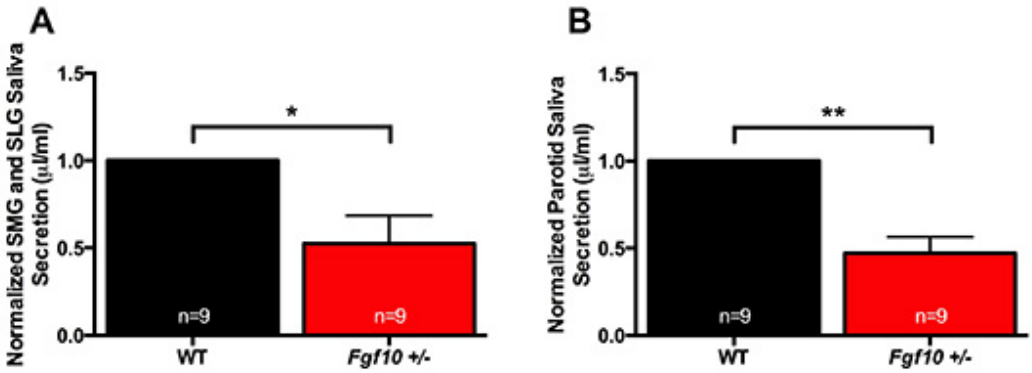

Figure 6.6 Saliva secretion from the (A) SMDG and (B) PGs.
Flow rate was significantly reduced in heterozygous adults compared to WT littermates. Saliva secretion is collected from the gland duct openings and is measured as microliter of saliva produced in 10 minutes after pilocarpine stimulation (µl/min). Graph shows secretion rates of *Fgf10 +/-* animals normalized against WT secretion rate where WT secretion = 1. Data is expressed as mean ± SEM. * $p<0.05$, ** $p<0.01$.

6.3.5 Reduction in Salivary Pellicle on the Tongue in Fgf10 +/- Mice

To further investigate the reduction of saliva flow in *Fgf10 +/-* adults, we analysed the mucosa of adult tongue papillae (10 weeks) using scanning electron microscopy. In order to assess the thickness of the salivary pellicle, we used HCl to remove mucus from the oral surface. In WT animals, sheets of mucus were observed coating the tongue, particularly in the posterior region covering the Circumvallate Papillae (CVP) and fillifom papillae. In contrast, the *Fgf10 +/-* tongues showed no mucus on the oral surface. This suggests that HCl treatment is sufficient to remove the saliva on *Fgf10 +/-* tongues however the thicker saliva pellicle in WT animals is only partially removed and sheets of saliva remain. The *Fgf10 +/-* tongues, did, however, display a healthy lawn of filliform papillae similar to their WT littermates, at this age.

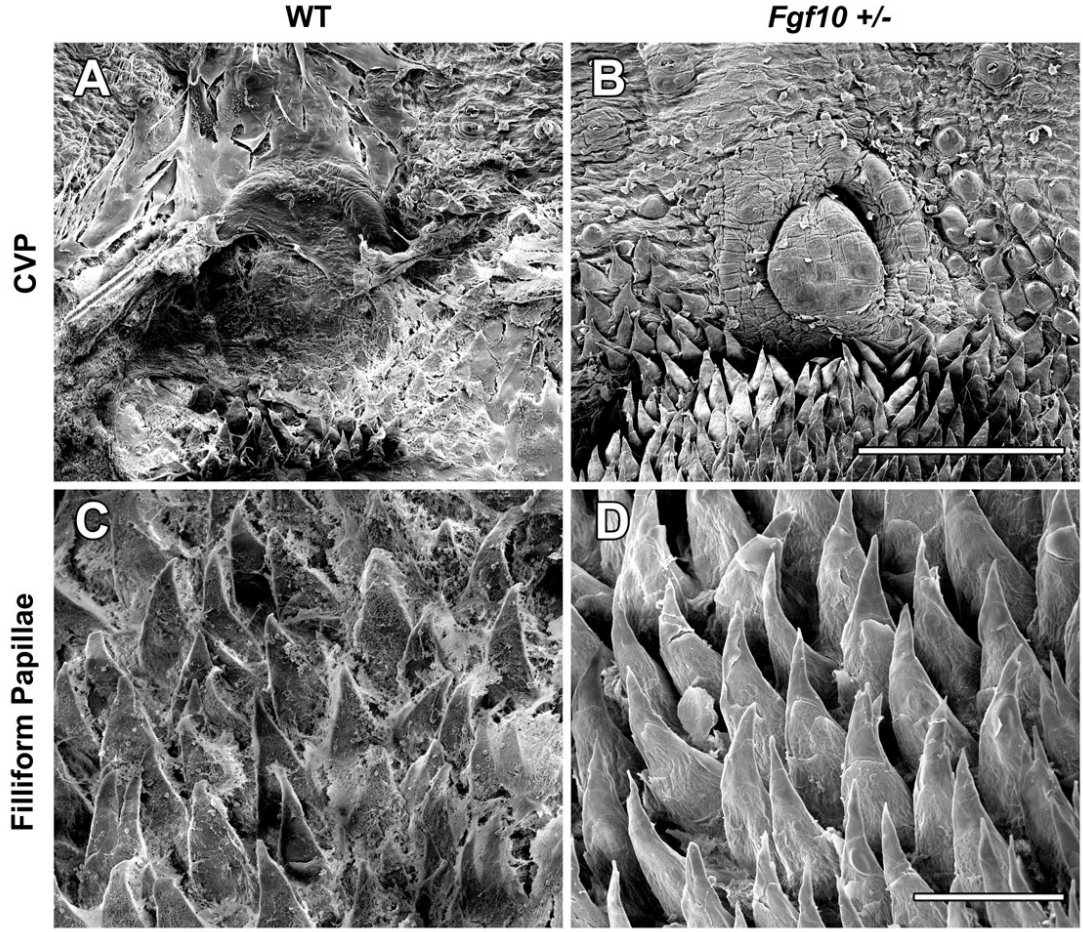

Figure 6.7 Scanning electron microscopy of 10 week old adult female tongues. WT animals retained what appeared to be sheets of mucus covering the posterior CVP (A) and filliform papillae (C) while no mucus remained on *Fgf10 +/-* tongues following HCl treatment (B, D). A and B scale bar = 500μm. C and D scale bar = 100μm.

6.4 Discussion

6.4.1 Loss of Fgf10 Leads to Defective Salivary Gland Function

In our study we show that adult *Fgf10* +/- mice have a significant reduction in saliva flow compared to control animals. Previous work has emphasised the important role of *Fgf10* in salivary gland development, with the *Fgf10* knockout mouse showing absence of the major salivary glands at birth (De Moerlooze et al. 2000; Jaskoll et al. 2005; Ohuchi et al. 2000). Additionally *Fgf10* +/- mice have reduced terminal buds and ducts at P0 (Jaskoll et al. 2005) while another study, albeit using only two samples, reported that adult *Fgf10* +/- SMDG and SLGs show normal histology (Entesarian et al. 2005). Our histological analysis concludes that there is no obvious structural differences between *Fgf10* +/- and WT adult major salivary glands. A significant difference in gland weight was observed however; with heterozygous animals showing approximately a 23% decrease in gland weight in females and a 15% decrease in males.

As first described in *Chapter* 1, *Fgf10* expression is not required for budding of the SMDG from the oral epithelium however it is imperative for the successional branching. Addition of exogenous FGF10 peptide to developing SMDGs increases epithelial cell proliferation and the number of branches compared to control glands (Jaskoll et al. 2005). In our analysis of adult gland histology, no signs of altered differentiation were seen in *Fgf10* +/- glands however smaller salivary gland lobes were observed. This indicates that a reduction in epithelial branching may occur in *Fgf10* +/- glands leading to shorter branches and thus smaller lobes. Therefore we suggest that the hyposalivation observed in *Fgf10* +/- adult mice is due to the reduction in weight and size of the salivary glands caused by a defect in early salivary gland patterning.

6.4.2 Fgf10 Function is Independent of Sex

It is well established that there is a significant sexual dimorphism in mature rodent salivary glands. Structural differences are most prominently seen in the granular GCT cells, which appear larger and more numerous in adult male mice, and the intercalated duct cells which appear more granulated in adult female mice (Lacassagne, 1940; Gresik, 1966). These cellular differences are androgen-dependant and begin to take shape at P15, with the development of GCT cells, and complete sexual dimorphism is

evident at P20 (Lacassagne, 1940; Gresik, 1975). To rule out any influence of sex on the *Fgf10* phenotype, we analysed weight and cytology of glands at P14 in male and female mice. Our results support previous reports as no weight or structural differences were seen between the sexes at this stage in WT mice. While histology of *Fgf10 +/-* salivary glands at P14 appeared normal, whole weights of mutant glands were significantly reduced.

Adult female glands are significantly smaller than male glands by age 7 weeks and GCT cells are less prominent. In both sexes, *Fgf10 +/-* glands are significantly smaller than WT littermates, with decrease in size being more significant in females. As both WT and *Fgf10 +/-* male glands develop to be much larger, and a secondary influence of androgens on salivary gland size is occurring, this may explain why the decrease in weight may be less notable compared to female heterozygotes.

This data supports the hypothesis that *Fgf10* heterozygosity is causing defective embryological salivary gland development, giving rise to a phenotype that is not rescued during postnatal development and adulthood.

6.4.3 Adult Fgf10 +/- Mice as a Model for Xerostomia

Xerostomia can be caused by a severe reduction in saliva production or a change in saliva composition produced by the salivary glands. Human studies investigating the affect of radiation therapy on head and neck cancers have shown that treatment gives rise to severe xerostomia and dysphagia (Epstein et al., 1999; Logemann et al., 2001). Our studies investigated the salivary gland cytology and function in postnatal and adult *Fgf10 +/-* mice with mutant glands showing an overall reduction in weight as well as evident hyposalivation. When 10 week old adult tongues were treated with hydrochloric acid to remove saliva from the surface mucosa, WT tongues maintained sheets of mucus covering their tongue papillae while no mucus remained on *Fgf10 +/-* tongues, indicating a thicker saliva pellicle is produced in WT animals. No evident defect in the tongue papillae was observed in *Fgf10 +/-* animals as might be expected as a consequence of dry mouth. This may be due, however, to the age restriction of animals investigated and the consequence of increased oral dryness may only be observed in older specimens. Considering the salivary gland phenotype observed in *Fgf10 +/-* adult mice, we propose it as a new mouse model of xerostomia. Further

research is encouraged to investigate the effects this hyposalivation has on the oral mucosa of *Fgf10 +/-* adult mice. Ogawa et al. (2013) visualised saliva secretion within the oral cavity by applying fluorescent sodium test paper to the tongues of mice, and observed diffusion rates of fluorescent dye within the mouth over 80 minutes. Healthy mice, as well as those implanted with functional bioengineered salivary glands, showed diffusion of fluorescence throughout the oral cavity while little fluorescence spread in the mouth of mice with deficient salivary glands (Ogawa et al., 2013). A similar protocol could be carried out on WT and *Fgf10 +/-* adult mice to compare salivary diffusion and cleansing ability. Furthermore, it is established that xerostomia causes imbalances in oral bioflora and increased bacterial infections, such as *Candida albicans* and dental caries associated organisms (Navazesh et al. 1995; Turner & Ship 2007). Buccal swabs could be taken from both WT and *Fgf10* +/- and bacterial propagation compared. Due to the hyposalivation phenotype reported in this chapter, we hypothesise that higher plated bacterial colonies would grow from *Fgf10 +/-* animals compared to WT littermates.

In conclusion, further investigation using the *Fgf10 +/-* adult mouse as a model of xerostomia will contribute to our understanding of this life-debilitating symptom and help in salivary gland regeneration studies and sialagogue treatment.

Many organs, such as the mammalian lung, kidney, pancreas, salivary gland, lacrimal gland, prostrate and mammary glands, adopt similar methods of bud induction, stalk elongation and branching morphogenesis. While the formation of these organs involves tightly regulated epithelial-mesenchymal interactions, tissue-specific mechanisms are recruited to shape each structure. The main aim of this thesis was to establish a detailed description of the developmental journey of both the anterior nasal and the tracheal submucosal respiratory glands (SMGs). Interest and investigation has been lacking in recent times as to how these imperative glands form and function, regardless of their crucial role in respiratory disease. It was our goal to uncover the role played by FGF signalling in shaping these organs and attempt to entice further research into understanding respiratory gland development.

7.1 The Respiratory SMGs as a Model of Development

The SMGs of the upper and lower airways function in producing a mucin rich secretion that filters air and protects delicate pulmonary organs from airborne pathogens. Although, it is believed, that all these SMGs share the same role, this thesis has emphasised that differential methods of development are recruited by subsets of these glands. Among the anterior nasal glands, the Steno's gland first develops at E12.5 by invaginating and extending as a long duct with a preformed lumen, similar to the development seen in the lacrimal gland of the eye (Makarenkova et al., 2000). In contrast, the lateral nasal glands (LNGs) and the medial nasal glands (MNGs) bud and extend as long solid cords of epithelial cells which undergo lumen formation succeeding stalk elongation. This similar mechanism is seen in the submandibular salivary gland (SMDG), as outlined in *Chapters 1*, *3* and *6*, as well as the prostrate. Interestingly in these organs, canalization of the epithelial stalks occurs following the induction of branching (Thomson and Marker, 2006; Miletich, 2010), however it was observed in our study that lumen formation within the LNGs and MNGs initiated before the branching of their distal glands. This early canalization was also observed before branching commenced in the tracheal SMGs, however these glands do not have a long stalk elongation stage, and rather adopt a structure with a short main duct, similar to that of the SMDGs and the prostate. Finally, the maxillary sinus gland (MSG) has no stalk elongation stage and its tubules with preformed lumens simply branch immediately from the sinus epithelium, allowing it to directly

secrete its mucus into the cavity. This method of development with a preformed lumen, similar to that seen in the Steno's gland, is also observed in the lung, as endodermal lung buds branch and extend with preformed lumens (Bellusci, Grindley, et al., 1997). Considering these contrasting developmental mechanisms, we propose the respiratory SMGs as ideal models to study bud induction, stalk elongation and branching morphogenesis.

7.1.1 The Anterior Nasal SMGs as a Model of Gland Budding and Stalk Elongation

Chapter 3 describes in detail the stages of anterior nasal gland development and demonstrates that the Steno's gland, LNGs and MNGs form long ducts that branch with distal glands. The reasoning for this could be to maximise the use of available space within the nasal region. The nose is a complicated structure with weaving concha and meatuses, increasing mucosal surface area to humidify and filter air. Large glands have evolved to develop in available mesenchymal spaces distal to the nostrils. The development of a long duct allows the secretion of the gland fluid close to the nares so air can be moistened and humidified from the earliest areas of the respiratory tree. Considering this developmental method, the nasal SMGs provide a model for investigating the cellular and molecular processes that are involved with gland budding and stalk elongation. In this study, we investigated the role of *Fgf10* in controlling nasal gland development and observed noticeable differences in the function of this growth factor for early budding and stalk elongation. Results showed that *Fgf10* is essential for the invagination and elongation of the Steno's gland, while the extension of MNG and LNGs, is independent of FGF10 signalling (Figure 7.1). This suggests that FGF10 signalling may be required to act as both a mitogen and a chemo-attractant for the indentation of the respiratory epithelial lip to form a duct with a preformed lumen, however other paracrine factors are needed for the invagination of a solid bud of cells. In the case of the MNGs, it appears that FGF7 is needed for their duct elongation (Figure 7.1, B), based on their absence in the *Fgfr2b* null mouse and the localisation of *Fgf7* mRNA in the nasal septum where these glands develop. The LNGs however appear to develop independent of FGFR2b signalling as their ducts are present in *Fgfr2b* -/-. Based on the findings of Grüneberg (1971), it may be that these glands require Eda signalling for their bud outgrowth and duct elongation (Figure 7.1, C).

Further investigation is required to elucidate other signalling molecules and pathways involved in SMG bud induction and development. Using the culture method established in *Chapter* 3, nasal SMG development can be manipulated in future studies and molecular signals involved in forming these organs can be elucidated. It must be emphasised however that signalling factors involved in development may be heterogeneous among these glands, and each subset of SMGs must be analysed as separate entities.

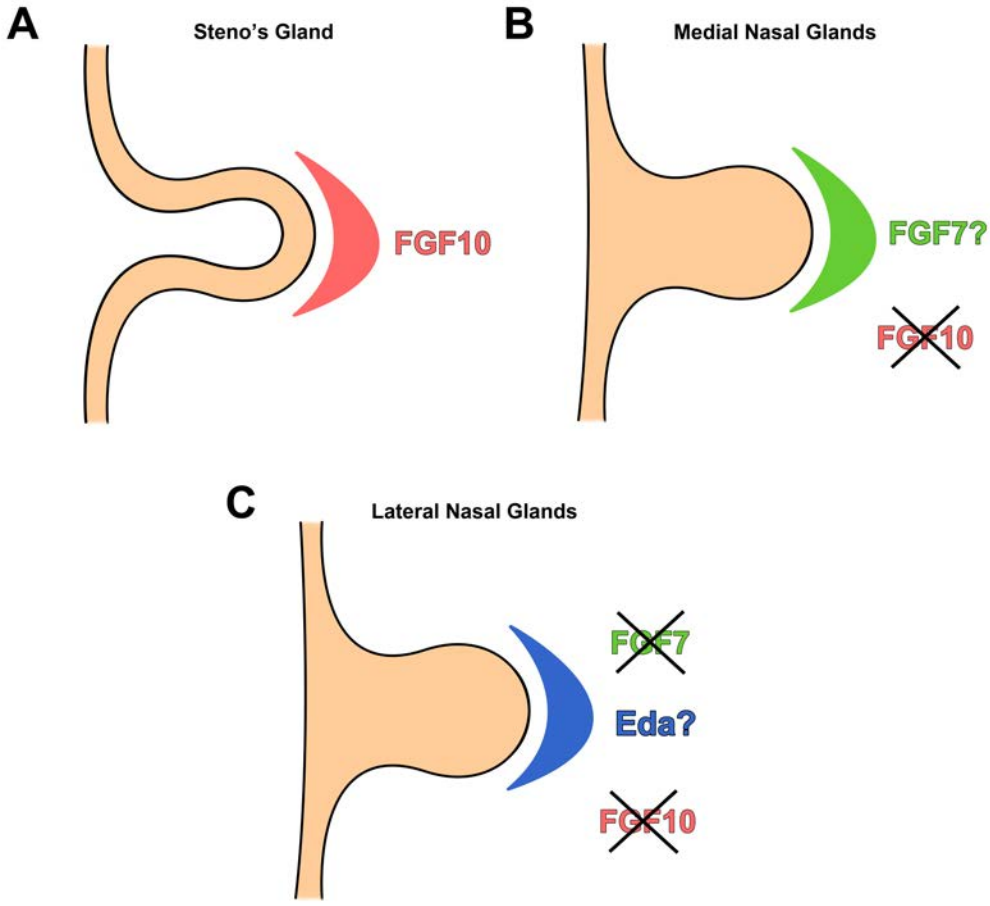

Figure 7.1 Possible mesenchymal paracrine factors required for anterior nasal gland outgrowth.
(A) Steno's gland bud induction requires FGF10 to act possibly as a mitogen or chemo-attractant for duct outgrowth. (B) Expression patterns of *Fgf7* and the absence of the MNGs in the *Fgfr2b* knockout mouse indicate FGF7 may act as a chemoattractant for MNG duct outgrowth and elongation. (C) The LNG ducts develop in the *Fgfr2b* knockout mouse ruling out the dependence of FGF7 or FGF10 for their outgrowth. Other paracrine factors involved in other signalling pathways are more critical for their development, with previous research suggesting Eda signalling.

7.1.2 The Role of Fgf10 in SMG Branching Morphogenesis

As mentioned continuously in this thesis, *Fgf10* is known to be a critical player in branching morphogenesis of a number of structures with supporting evidence seen in the lung and salivary glands. In accordance with every other aspect of branching morphogenesis, there are important differences in the role of *Fgf10* depending on the branching structure. In terms of the respiratory SMGs however, although their bud and duct elongation stages recruit different mechanisms for successful development, the branching of all respiratory SMGs seems to be *Fgf10* dependent. From *in situ* hybridisation analysis, *Fgf10* is expressed throughout the mesenchyme surrounding all branching nasal glands. During branch formation in the lung, *Fgf10* expressing cells are located in two spaced groups, leading to the bifurcation of elongating epithelial stalks, attracting each branch to each FGF10 source. No localised expression of *Fgf10* was seen in the mesenchyme of the nasal glands, however clefting epithelial branches may be attracted to areas of high *Fgf10* expression that may not be seen using *in situ* hybridisation on tissue sections (Figure 7.2). *Fgfr2* expression, as well as *Spry1* and *Pea3* expression within the distal epithelial buds, further supports the requirement of FGF10 signalling in nasal gland branching morphogenesis. Using *in situ* hybridisation methods, the expression of both *Fgfr2* and *Spry1* appears more widespread in the gland bud epithelial cells than that of *Pea3*, suggesting that nuclear transcription factor activation is only occurring in the peripheral bud cells (Figure 7.2). A similar role for *Fgf10* is assumed in the tracheal SMGs, as tracheal epithelial buds are present in the *Fgf10 -/-* mouse at birth, yet they do not continue to elongation and branching stages similar to their WT littermates. Furthermore, branching of extended glands in the *Fgf10* +/- P0 mouse is reduced and this phenotype is not rescued in adults. Using the tracheal SMG oil experiment, we demonstrated that this developmental defect has an effect on function of the gland in adult life, with mucus secretion being significantly reduced in *Fgf10 +/-* animals. Additionally, our analysis of salivary gland dysplasia further highlights the requirement of *Fgf10* in the branching of the SMDG and the influence loss of *Fgf10* expression has on saliva output.

While our work primarily focused on the influence of mesenchymal *Fgf10* on the outgrowth and branching of the respiratory glands, epithelial factors are also assumed to be critical in regulating gland development. For example epithelial Sonic hedgehog

(Shh) has been reported to tightly control branching of both lungs and SMDGs (Bellusci, Furuta, et al., 1997; Pepicelli et al., 1998; Jaskoll et al., 2004). During branching stages of lung development, *Shh* is upregulated in distal lung epithelium and increases cell proliferation in the extending branches (Bellusci, Furuta, et al., 1997). Upregulation of *Shh* in the lung, was followed by down regulation of mesenchymal *Fgf10,* indicating a possible inhibitory role for *Shh* (Bellusci, Furuta, et al., 1997). Furthermore, in the *Shh* -/-, mouse, lungs fail to develop due to lack of outgrowth and branching, however differentiation of bronchiole epithelium and alveolar sacs is observed, indicating that *Shh* is not required for cellular differentiation (Pepicelli et al., 1998). In the developing SMDG, *Shh* is again similarly localised to ducts of the SMDGS as well as terminal end buds (Jaskoll et al., 2004). Interestingly, in the *Shh -/-* mouse at E18.5, an undifferentiated dysplastic gland forms, indicating that during SMDG development *Shh* is required for gland growth and cellular differentiation (Jaskoll et al., 2004). Spatial expression of *Shh* within these epithelial structures leads to inhibition of *Fgf10* in inter-branching zones, and thus gives rise to focal expression of *Fgf10* in the adjacent mesenchyme (Chuang and McMahon, 2003). Investigation into the expression, role, and possible interaction of *Shh* with *Fgf10* during development of the different subsets of respiratory glands should help uncover the role played by this signalling molecule during branching morphogenesis (Figure 7.2).

Another possible FGF10 antagonist during respiratory gland development could be Bone morphogenetic protein 4 (BMP4). In lung development, *Bmp4* is expressed in the ventral mesenchyme during early stages of lung induction however it is highly expressed in the distal gland buds at later branching stages (Weaver et al., 1999). It has been suggested that *Bmp4* and *Fgf10* play complimentary roles during lung branching morphogenesis, with initial mesenchymal *Fgf10* expression indirectly inducing *Bmp4* expression in the lung endoderm, which is followed by high levels of *Bmp4* within the lung bud epithelium antagonizing *Fgf10* (Weaver et al., 2000). This inhibition of *Fgf10* allows the extension of one single bud as opposed to the development of numerous end buds. A new bud is formed when *Fgf10* expression shifts to an area adjacent to lung epithelium low in *Bmp4* expression (Weaver et al., 2000). An antagonizing role of *Bmp4* is also supported by the inability of lung buds to grow towards an FGF10 source *in vitro* when exogenous BMP4 protein is applied

(Weaver et al., 2000). During SMDG development, *Bmp4* is mesenchymally expressed (Hoffman et al., 2002). Similarly to the lung, BMP4 inhibits gland budding during *in vitro* SMDG investigation, with glands cultured with BMP4 showing similar phenotypes to those incubated with FGF inhibitor SU5402 (Hoffman et al., 2002). Furthermore, when SMDGs are cultured with BMP antagonist sFRP1, branching of SMDGs is induced with a 26% increase observed in the amount of gland buds in treated glands compared to controls (Patel et al., 2011). *Bmp4* has also been shown to be expressed in the mesenchyme surrounding budding and branching tracheal respiratory SMGs (Rawlins and Hogan, 2005). This data collectively poses interesting questions for the role and regulatory functions of *Bmp4* in branching morphogenesis. Whether these functions are conserved during respiratory SMG development, or even heterogeneous among these glands must be elucidated.

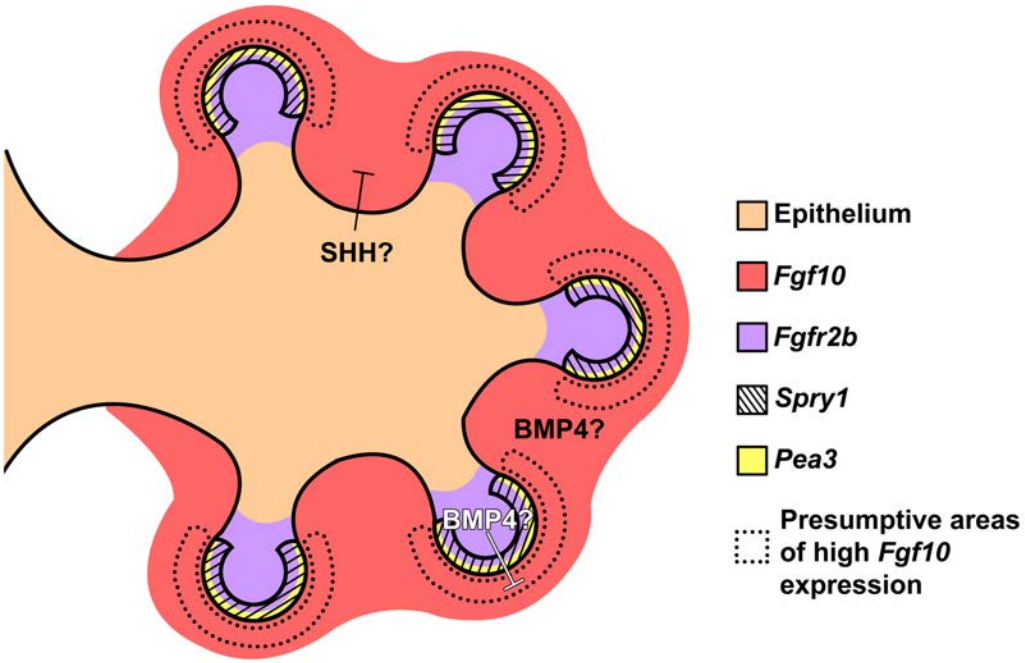

Figure 7.2 Schematic representation of the main findings of this thesis on anterior nasal gland branching morphogenesis and proposed signalling network interactions based on the findings of others.

During branching morphogenesis of all the respiratory glands, *Fgf10* is expressed all throughout the mesenchyme surrounding the forming end buds. Based on previous work on lung morphogenesis (Bellusci, Grindley, et al., 1997), it is hypothesised that high concentrations of *Fgf10* are localised to the mesenchyme adjacent to extending buds (dotted sections), allowing *Fgf10* expression to stimulate cell proliferation and cell migration towards a localised source. This FGF10 activity on the end buds is supported by *Fgfr2b* expression identified within the gland bud epithelial cells, along with downstream targets of FGF signalling *Spry1* and *Pea3*. While *Spry1* expression is seen in peripheral bud cells, *Pea3* expression is more restricted to the outermost distal cells. This indicates that the FGF10 signal is stimulating intracellular responses in the *Spry1* positive cells, however is only leading to a nuclear translocation of this signal and transcription factor activation in the *Pea3* positive cells. Thus, changes in cellular behaviour only occur in these outermost distal epithelial cells.

Collecting data reported during lung (Bellusci, Furuta, et al., 1997; Pepicelli et al., 1998) and SMDG (Jaskoll et al., 2004) branching morphogenesis, it is hypothesised that *Shh* may be expressed within the SMG gland epithelium, and may also play a *Fgf10* inhibitory role to prevent new bud outgrowth in all epithelial areas exposed to mesenchymal FGF10, and thus control the patterning of the outgrowth of existing branches.

Furthermore, *Bmp4* may also play a role in patterning the branching gland epithelium. *Bmp4* expression may be induced in the gland epithelial buds, similar to the developing lung (Weaver et al., 1999), or may be expressed in the surrounding mesenchyme, as seen during SMDG development (Hoffman et al., 2002). Mesenchymal *Bmp4* expression has already been elucidated during tracheal SMG development (Rawlins and Hogan, 2005) however must be investigated during anterior nasal gland development. The interaction between *Bmp4* and *Fgf10* needs to also be addressed, and delineated this is similar to that seen during lung and SMDG development (Weaver et al., 2000; Hoffman et al., 2002; Patel et al., 2011).

7.2 Lumen Formation in the SMGs

In order for a branched organ to successfully carry out its function of transporting either a liquid or a gas, tightly controlled tubule formation must occur (Iruela-Arispe and Beitel, 2013). An array of tubulogenesis methods are adopted in different branched organs, but more interestingly these diverse mechanisms are seen within the anterior nasal glands alone. The Steno's gland, as well as the MSG, has preformed lumens during ductal elongation and branching, respectively. This means that these glands provide a model system for investigation into cellular behaviours and interactions as it is assumed changes to cell-to-cell adhesion and apical-basal polarity of cells is required in order for the respiratory epithelium to invaginate and develop this way. In contrast, the LNGs and the MNGs form as epithelial buds and elongate as solid cords of cells that at a later stage cavitate and form hollow tubes. These glands provide a model system to investigate the cell behaviours involved in delayed lumen formation.

Research is on-going into the mechanisms underlying cavitation of solid epithelial tubes. Some studies have suggested that programmed cell death along with polarization of luminal cells shape out hollows in mammary and salivary gland ducts (Humphreys-Beher, 1996; Jaskoll et al., 1998; Wells and Patel, 2010). From our analysis of the nasal SMGs, apoptosis, by the detection of activated Caspase-3, does not seem to be required for normal tubulogenesis within the LNGs and MNGs. More recent studies demonstrated that ductal cavitation is independent of cell death and relies on vasoactive intestinal peptide (VIP)-dependent neuronal signals that are required for lumen formation and lumen expansion (Nedvetsky et al., 2014). In this study it was proposed that there were four main stages of tubule formation in the developing SMDG (Nedvetsky et al., 2014). The first step involves the proliferation of already differentiated luminal cells, which can be identified with the marker cytokeratin 19 (K19) at E13. Between E13-E13.5 these K19+ cells aggregate along the midline of the epithelial stalk and subcellular mechanisms lead to the polarization of these cells, allowing them to reorganise and form small spaces within the stalk (Nedvetsky et al., 2014). These microlumena then fuse to form one single lumen. The final stage is then characterized by expansion of this lumen to form a hollow tube (Nedvetsky et al., 2014).

Our work suggests that lumen formation within the LNGs and MNGs may also employ this method of lumen formation and rely on neuronal factors due to the close proximity of nerves during all stages of their development. These recent revelations strike up interesting questions about how contiguous lumens form within solid epithelial ducts and we believe the LNGs and MNGS will provide another model system to investigate the cellular and molecular mechanisms required for tube formation. Application of the tight junction marker Zona occluding-1 (ZO1) could be applied to developing LNGs and MNGs to elucidate if these glands follow a similar mechanism to that observed in the SMDG, where first microlumena form within solid epithelial cords and fusion of these spaces create a continuous lumen. Additionally, using the culture method established in *Chapter 3*, exogenous addition and inhibition of neurotrophic factors such as neurturin and neurotransmitters, specifically VIP, to developing anterior nasal glands will help delineate the necessity of the nerve supply, observed in our study, for their development and tubule formation. Furthermore, although the timing of the stalk elongation stage is shorter, tracheal SMGS also originate as solid epithelial buds that undergo lumen formation. Therefore, investigation could also be carried out with these glands of the lower airway to uncover if similar mechanisms are involved or if differential processes occur.

7.3 The Future of SMG Research

Although research is improving our understanding of numerous respiratory diseases, we must not ignore that one of the primary causes of pulmonary obstruction and infection is mucus blockage of the airway tubes. Due to the pivotal involvement of the SMGs in producing mucus, their form and function should be at the forefront of investigation. Before we uncover the developmental errors that occur in those that suffer from respiratory disease however, it is imperative we understand the coordinated activities of signalling pathways and complex tissue interactions that are required to pattern functional respiratory glands and delineate if SMG development influences gland secretion and contributes to airway disease. We hope, that the work of this thesis will provide an aid for future research in identifying patterns of respiratory gland development and help stimulate future investigation into the mechanisms involved in shaping these structures, in the hopes of understanding and tackling the causes of respiratory disease.

References

Aikawa, T. et al. (1992) Marked goblet cell hyperplasia with mucus accumulation in the airways of patients who died of severe acute asthma attack. *Chest*. 101 (4), 916–921.

Albert, R. et al. (2000) Error and attack tolerance of complex networks. *Nature*. 406 (6794), 378–382.

Alfaqeeh, S. A. & Tucker, A. S. (2013) The slice culture method for following development of tooth germs in explant culture. *Journal of Visualised Experiments : JoVE*. 13 (81), e50824.

Andrew, D. J. & Ewald, A. J. (2010) Morphogenesis of epithelial tubes: Insights into tube formation, elongation, and elaboration. *Developmental Biology*. 341 (1), 34–55.

Arce, L. et al. (2006) Diversity of LEF/TCF action in development and disease. *Oncogene*. 25 (57), 7492–7504.

Arlian, L. G. et al. (2002) Dust mite allergens: ecology and distribution. *Current Allergy and Asthma Reports*. 2 (5), 401–411.

Bafico, A. et al. (2001) Novel mechanism of Wnt signalling inhibition mediated by Dickkopf-1 interaction with LRP6/Arrow. *Nature Cell Biology*. 3683–686.

Baker, P. & Schroeder, T. (1967) Cytoplasmic filaments and morphogenetic movement in the amphibian neural tube. *Developmental Biology*. 432450.

Balhara, J. & Gounni, a S. (2012) The alveolar macrophages in asthma: a double-edged sword. *Mucosal immunology*. [Online] 5 (6), 605–609.

Ballard, S. T. & Spadafora, D. (2007) Fluid secretion by submucosal glands of the tracheobronchial airways. *Respiratory physiology & neurobiology*. [Online] 159 (3), 271–277.

Bang, B. R. et al. (2011) Alveolar macrophages modulate allergic inflammation in a murine model of asthma. *Experimental & Molecular Medicine*. 43 (5), 275–280.

Barclay, A. N. (2003) Membrane proteins with immunoglobulin-like domains—a master superfamily of interaction molecules. *Seminars in Immunology*. 15 (4), 215–223.

Barnes, P. J. et al. (1998) Inflammatory mediators of asthma: an update. *Pharmacological Reviews*. 50 (4), 515–596.

Barnes, P. J. (2004) Mediators of Chronic Obstructive Pulmonary Disease. *Pharmacological Reviews*. 56 (4), 515–548.

Barrientos, S. et al. (2008) Growth factors and cytokines in wound healing. *Wound Repair and Regeneration*. 16 (5), 585–601.

Basbaum, C. et al. (1990) The Serous Cell. *Annual Review of Physiology*. 52, 97–113.

Bast, T. (1924) The maxillary sinus of the dog, with special reference to certain new structures, probably sensory in nature. *American Journal of Anatomy*. 33 (3), 449–483.

Baur, X. et al. (2012) Bronchial asthma and COPD due to irritants in the workplace - an evidence-based approach. *Journal of Occupational Medicine & Toxicology*. 7 (1), 19.

Bedoret, D. et al. (2009) Lung interstitial macrophages alter dendritic cell functions to prevent airway allergy in mice. *The Journal of Clinical Investigation*. 119 (12), 3723–3738.

Bellusci, S., Grindley, J., et al. (1997) Fibroblast growth factor 10 (FGF10) and branching morphogenesis in the embryonic mouse lung. *Development*. 124 (23), 4867–4878.

Bellusci, S., Furuta, Y., et al. (1997) Involvement of Sonic hedgehog (Shh) in mouse embryonic lung growth and morphogenesis. *Development*. 124 (1), 53–63.

Bojsen-Moller, F. (1967) Topography and development of anterior nasal glands in pigs. *Journal of Anatomy*. 101 (Pt 2), 321–331.

Bojsen-Moller, F. (1964) Topography of the nasal glands in rats and some other mammals. *The Anatomical Record*. 15011–24.

Borghese, E. (1950) The development in vitro of the submandibular and sublingual glands of Mus musculus. *Journal of Anatomy*. 84 (3), 287–302.

Borthwick, D. W. et al. (2001) Evidence for stem-cell niches in the tracheal epithelium. *American Journal of Respiratory Cell and Molecular Biology*. 24 (6), 662–670.

Borthwick, D. W. et al. (1999) Murine submucosal glands are clonally derived and show a cystic fibrosis gene-dependent distribution pattern. *American Journal of Respiratory Cell and Molecular Biology*. 20 (6), 1181–1189.

Bradding, P. et al. (1994) Interleukin-4, -5, and -6 and tumor necrosis factor-alpha in normal and asthmatic airways: evidence for the human mast cell as a source of these cytokines. *American Journal of Respiratory Cell and Molecular Biology*. 10 (5), 471–480.

Brightling, C. et al. (2008) Targeting TNF- α: A novel therapeutic approach for asthma. *Journal of Allergy and Clinical Immunology*. 121 (1), 5–12.

Broman, I. (1921) Über die Entwicklung der konstanten grösseren Nasennebenhöhlendrüsen der Nagetiere. *Z. Anat. Entwickl. Gesch.* 60439–60586.

Brunner, H. (1942) Nasal Glands. *Archives of Otolaryngology*. 35 (2), 183–209.

Burgess, W. et al. (1990) Characterization and cDNA cloning of phospholipase C-gamma , a major substrate for heparin-binding growth factor 1 (acidic fibroblast growth factor)-activated tyrosine kinase. *Molecular & Cellular Biology*. 10 (9), 4770–4777.

Burri, P. H. & Moschopulos, M. (1992) Structural analysis of fetal rat lung development. *The Anatomical Record*. 234 (3), 399–418.

Butler, D. G. (2002) Hypertonic fluids are secreted by medial and lateral segments in duck (Anas platyrhynchos) nasal salt glands. *The Journal of Physiology*. 540 (3), 1039–1046.

Cardoso, W. V et al. (1997) FGF-1 and FGF-7 induce distinct patterns of growth and differentiation in embryonic lung epithelium. *Developmental Dynamics*. 208 (3), 398–405.

Cardoso, W. V & Lü, J. (2006) Regulation of early lung morphogenesis: questions, facts and controversies. *Development*. 133 (9), 1611–1624.

Careau, E. et al. (2010) Alveolar macrophages reduce airway hyperresponsiveness and modulate cytokine levels. *Experimental Lung Research*. 36 (5), 255–261.

Carreira, a C. et al. (2014) Bone morphogenetic proteins: facts, challenges, and future perspectives. *Journal of Dental Research*. 93 (4), 335–345.

Chambers, M. S. et al. (2004) Radiation-induced xerostomia in patients with head and neck cancer: pathogenesis, impact on quality of life, and management. *Head Neck*. 26 (9), 796–807.

Chelen, C. et al. (1995) Human alveolar macrophages present antigen ineffectively due to defective expression of B7 costimulatory cell surface molecules. *Journal of Clinical Investigation*. 95 (March), 1415–1421.

Chipuk, J. E. et al. (2004) Direct activation of Bax by p53 mediates mitochondrial membrane permeabilization and apoptosis. *Science*. 303 (February), 1010–1014.

Chotteau-Lelievre, A. et al. (2003) PEA3 transcription factors are expressed in tissues undergoing branching morphogenesis and promote formation of duct-like structures by mammary epithelial cells in vitro. *Developmental Biology*. 259241–257.

Chotteau-Lelièvre, A. et al. (1997) Differential expression patterns of the PEA3 group transcription factors through murine embryonic development. *Oncogene*. 15 (8), 937–952.

Chua, K. et al. (1988) Sequence analysis of cDNA coding for a major house dust allergen Der p 1. Homology with cysteine proteases. *The Journal of Experimental Medicine*. 16, 7175–7182.

Chuang, P.-T. & McMahon, A. P. (2003) Branching morphogenesis of the lung: new molecular insights into an old problem. *Trends in Cell Biology*. 13 (2), 86–91.

Clark, D. C. (1999) Esophageal atresia and tracheoesophageal fistula. American Family Physician. 59 (4), 910–916.

Clayton, E. et al. (2007) A single type of progenitor cell maintains normal epidermis. *Nature*. 446, 185–189.

Cohn, L. et al. (1997) Induction of airway mucus production by T helper 2 (Th2) cells: a critical role for interleukin 4 in cell recruitment but not mucus production. *The Journal of Experimental Medicine*. 186 (10), 1737–1747.

Cole, B. B. et al. (2010) Tracheal basal cells: a facultative progenitor cell pool. *The American Journal of Pathology*. 177 (1), 362–376.

Crackower, M. et al. (1998) Assignment of mouse Fibroblast Growth Factor 10 (Fgf10) gene to the telomeric region of chromosome 13. *Genomics*. 248, 247–248.

Crews, C. M. et al. (1992) The primary structure of MEK, a protein kinase that phosphorylates the ERK gene product. *Science*. 258 (5081), 478–480.

Cuschieri, A. & Bannister, L. H. (1974) Some histochemical observations on the mucosubstances of the nasal glands in the mouse. *Histochemical Journal*. 6 (5), 543–558.

Davidson, G. et al. (2005) Casein kinase 1 gamma couples Wnt receptor activation to cytoplasmic signal transduction. *Nature*. 438, 867–872.

Dean, C. H. et al. (2005) Canonical Wnt signaling negatively regulates branching morphogenesis of the lung and lacrimal gland. *Developmental Biology*. 286 (1), 270–286.

Dikic, I. & Giordano, S. (2003) Negative receptor signalling. *Current Opinion in Cell Biology*. 15 (2), 128–135.

Döffinger, R. et al. (2001) X-linked anhidrotic ectodermal dysplasia with immunodeficiency is caused by impaired NF-kappaB signaling. *Nature Genetics*. 27 (3), 277–285.

Doupe, D. P. et al. (2012) A single progenitor population switches behavior to maintain and repair esophageal epithelium. *Science*. 337, 091–1093.

Driskell, R. R. et al. (2004) Wnt-responsive element controls Lef-1 promoter expression during submucosal gland morphogenesis. *American Journal of Physiology Lung Cellular and Molecular Physiology*. 287 (4), L752–63.

Driskell, R. R. et al. (2007) Wnt3a regulates Lef-1 expression during airway submucosal gland morphogenesis. *Developmental Biology*. 305 (1), 90–102.

Duan, D. et al. (1998) Lef1 transcription factor expression defines airway progenitor cell targets for in utero gene therapy of submucosal gland in cystic fibrosis. *American Journal of Respiratory Cell and Molecular Biology*. 18 (6), 750–758.

Duan, D. et al. (1999) Submucosal gland development in the airway is controlled by lymphoid enhancer binding factor 1 (LEF1). *Development.* 126 (20), 4441–4453.

Eastman, Q. & Grosschedl, R. (1999) Regulation of LEF-1/TCF transcription factors by Wnt and other signals. *Current Opinion in Cell Biology*. 11 (2), 233–240.

Eblaghie, M. C. et al. (2006) Evidence that autocrine signaling through Bmpr1a regulates the proliferation, survival and morphogenetic behavior of distal lung epithelial cells. *Developmental Biology*. 291, 67–82.

El-Gohary, Y. et al. (2010) Congenital anomalies of the esophagus. *Seminars in Pediatric Surgery*. 19, 186–193.

Emoto, H. et al. (1997) Structure and expression of human Fibroblast Growth Factor-10. *Journal of Biological Chemistry*. 272 (37), 23191–23194.

Engelhardt, J. F. et al. (1992) Submucosal glands are the predominant site of CFTR expression in the human bronchus. *Nature Genetics*. 2 (3), 240–248.

Entesarian, M. et al. (2007) FGF10 missense mutations in aplasia of lacrimal and salivary glands (ALSG). *European Journal of Human Genetics.* 15 (3), 379–382.

Entesarian, M. et al. (2005) Mutations in the gene encoding fibroblast growth factor 10 are associated with aplasia of lacrimal and salivary glands. *Nature Genetics.* 37 (2), 125–127.

Epstein, J. B. et al. (1999) Quality of life and oral function following radiotherapy for head and neck cancer. *Head & Neck*. 21 (1), 1–11.

Ettensohn, C. a (1985) Mechanisms of epithelial invagination. *The Quarterly Review of Biology*. 60 (3), 289–307.

Faham, S. et al. (1996) Heparin structure and interactions with basic Fibroblast Growth Factor. *Science*. 271, 1116–1120.

Ferreira, J. N. & Hoffman, M. P. (2013) Interactions between developing nerves and salivary glands. *Organogenesis*. 9 (3), 199–205.

Finkbeiner, W. E. (1999) Physiology and pathology of tracheobronchial glands. *Respiration Physiology*. 118 (2-3), 77–83.

Fitzgerald, M. & Ryan, D. (2011) Cystic fibrosis and anaesthesia. *Continuing Education in Anaesthesia, Critical Care & Pain*. 11 (6), 204–209.

Freeman, J. a (1962) Fine structure of the goblet cell mucous secretory process. *The Anatomical Record*. 144, 341–357.

Frisch, D. (1967) Ultrastructure of the mouse olfactory mucosa. *American Journal of Anatomy*. 121 (1), 87–120.

Fuchs, E. (1983) Evolution and complexity of the genes encoding the keratins of human epidermal cells. *Journal of Investigative Dermatology*. 81, 141s–144s.

Fürthauer, M. et al. (2002) Sef is a feedback-induced antagonist of Ras/MAPK-mediated FGF signalling. *Nature Cell Biology*. 4 (2), 170–174.

Gardner, A. M. et al. (1994) MEK-1 phosphorylation by MEK kinase, Raf, and mitogen-activated protein kinase: analysis of phosphopeptides and regulation of activity. *Molecular Biology of the Cell*. 5, 193–201.

Van Genderen, C. et al. (1994) Development of several organs that require inductive epithelial-mesenchymal interactions is impaired in LEF-1-deficient mice. *Genes & Development*. 8 (22), 2691–2703.

Germain, R. N. (1994) MHC-dependent antigen processing and peptide presentation: providing ligands for T lymphocyte activation. *Cell*. 76 (2), 287–299.

Getchell, M. L. & Getchell, T. V (1992) Fine structural aspects of secretion and extrinsic innervation in the olfactory mucosa. *Microscopy Research and Technique*. 23 (2), 111–127.

Gilmore, T. D. (2006) Introduction to NF-kappaB: players, pathways, perspectives. *Oncogene*. 25 (51), 6680–6684.

Glazer, L. & Shilo, B. Z. (1991) The Drosophila FGF-R homolog is expressed in the embryonic tracheal system and appears to be required for directed tracheal cell extension. *Genes & Development*. 5 (4), 697–705.

Gong, J. L. et al. (1994) Interstitial lung macrophages interact with dendritic cells to present antigenic peptides derived from particulate antigens to T cells. *Immunology*. 81 (3), 343–351.

Gospodarowicz, D. (1975) Purification of a Fibroblast Growth Factor from bovine pituitary. *Journal of Biological Chemistry*. 250 (7), 2515–2520.

Green, D. R. & Reed, J. C. (1998) Mitochondria and Apoptosis. *Science*. 281 (5381), 1309–1312.

Greene, W. & Thomas, W. (1992) IgE binding structures of the major house dust mite allergen DER P I. *Molecular Immunology*. 29 (2), 257-262.

Gresik, E. W. (1966) A previously unreported cell type in female mouse submandibular glands. *Journal of Cellular Biology.* 31, 144a.

Gresik, E. W. (1994) The granular convoluted tubule (GCT) cell of rodent submandibular glands. *Microscopy Research and Technique*. 27 (1), 1–24.

Gresik, E. W. (1975) The postnatal development of the sexually dimorphic duct system and of amylase activity in the submandibular glands of mice. *Cell and Tissue Research*. 157 (3), 411–422.

Gross, E. a et al. (1982) Comparative morphometry of the nasal cavity in rats and mice. *Journal of Anatomy*. 135 (Pt 1), 83–88.

Grüneberg, H. (1971) The glandular aspects of the tabby syndrome in the mouse. *Journal of Embryology and Experimental Morphology*. 25 (1), 1–19.

Gumbiner, B. (1992) Epithelial Morphogenesis. *Cell*. 69, 365–367.

Guo, L. et al. (1996) Keratinocyte growth factor is required for hair development but not for wound healing. *Genes and Development*. 10 (2), 165–175.

Gupta, A. et al. (2006) Hyposalivation in elderly patients. *J of the Canadian Dental Association.* 72 (9), 841–846.

Hacohen, N. et al. (1998) Sprouty encodes a novel antagonist of FGF signaling that patterns apical branching of the Drosophila airways. *Cell*. 92 (2), 253–263.

Hanafusa, H. et al. (2002) Sprouty1 and Sprouty2 provide a control mechanism for the Ras/MAPK signalling pathway. *Nature Cell Biology*. 4 (11), 850–858.

Hand, A. R. et al. (1999) Morphological features of the minor salivary glands. *Archives of Oral Biology*. 44 Suppl 1S3–10.

Harkema, J. R. et al. (1999) Long-lasting effects of chronic ozone exposure on rat nasal epithelium. *American Journal of Respiratory Cell and Molecular Biology*. 20, 517–529.

He, X. et al. (2004) LDL receptor-related proteins 5 and 6 in Wnt/beta-catenin signaling: arrows point the way. *Development*. 131 (8), 1663–1677.

Headon, D. J. & Overbeek, P. a (1999) Involvement of a novel Tnf receptor homologue in hair follicle induction. *Nature Genetics*. 22 (4), 370–374.

Helmick, C. G. et al. (2008) Estimates of the prevalence of arthritis and other rheumatic conditions in the United States. Part I. *Arthritis & Rheumatology*. 58 (1), 15–25.

Hoffman, M. et al. (2002) Gene expression profiles of mouse submandibular gland development: FGFR1 regulates branching morphogenesis in vitro through BMP- and FGF-dependent mechanisms. *Development*. 129 (24), 5767–5778.

Hogan, B. L. (1996) Bone morphogenetic proteins: multifunctional regulators of vertebrate development. *Genes & Development*. 10 (13), 1580–1594.

Hogan, B. L. M. & Kolodziej, P. a (2002) Organogenesis: molecular mechanisms of tubulogenesis. *Nature Reviews. Genetics*. 3 (7), 513–523.

Hogg, N. a et al. (1983) Lumen formation in the developing mouse mammary gland. *Journal of Embryology and Experimental Morphology*. 73, 39–57.

Hollister, D. W. et al. (1973) The lacrimo-auriculo-dento-digital syndrome. *The Journal of Pediatrics*. 83 (3), 438–444.

Holt, P. G. et al. (1981) Inhibition of specific IgE responses in mice by pre-exposure to inhaled antigen. *Immunology*. 42 (3), 409–417.

Holt, P. G. (1978) Inhibitory activity of unstimulated alveolar macrophages on T-lymphocyte blastogenic response. *The American Review of Respiratory Disease*. 118 (4), 791–793.

Hong, K. et al. (2004) In vivo differentiation potential of tracheal basal cells: evidence for multipotent and unipotent subpopulations. *American Journal of Physiology Lung Cellular and Molecular Physiology*. 286 (4), 643–649.

Hua, X. et al. (2010) Noninvasive real-time measurement of nasal mucociliary clearance in mice by pinhole gamma scintigraphy. *Journal of Applied.* 108 (1), 189–196.

Humphreys, R. C. et al. (1996) Apoptosis in the terminal endbud of the murine mammary gland: a mechanism of ductal morphogenesis. *Development*. 122 (12), 4013–4022.

Humphreys-Beher, M. G. (1996) Animal models for autoimmune disease-associated xerostomia and xerophthalmia. *Advances in Dental Research*. 10 (1), 73–75.

Hurle, J. M. et al. (1996) Morphology and significance of programmed cell death in the developing limb bud of the vertebrate embryo. *Microscopy Research and Technique*. 34, 236–246.

Ianowski, J. P. et al. (2007) Mucus secretion by single tracheal submucosal glands from normal and cystic fibrosis transmembrane conductance regulator knockout mice. *The Journal of Physiology*.580 (Pt 1), 301–314.

Innes, B. a. & Dorin, J. R. (2001) Submucosal gland distribution in the mouse has a genetic determination localised on Chromosome 9. *Mammalian Genome*. 12 (2), 124–128.

Ioannides, A. S. et al. (2002) Dorsoventral patterning in oesophageal atresia with tracheo-oesophageal fistula: Evidence from a new mouse model. *Journal of Pediatric Surgery*. 37 (2), 185–191.

Iruela-Arispe, M. L. & Beitel, G. J. (2013) Tubulogenesis. *Development.* 140 (14), 2851–2855.

Isaac, D. D. & Andrew, D. J. (1996) Tubulogenesis in Drosophila: a requirement for the trachealess gene product. *Genes & Development*. 10 (1), 103–117.

Itoh, N. & Nagata, S. (1993) A novel protein domain required for apoptosis. *The Journal of Biological Chemistry*. 268 (15), 10932–10937.

Janknecht, R. (1996) Analysis of the ERK-stimulated ETS transcription factor ER81. *Molecular and Cellular Biology*. 16 (4), 1550–1556.

Janson, C. et al. (2001) The European Community Respiratory Health Survey: what are the main results so far? *European Respiratory Journal*. 18 (3), 598–611.

Jarecki, J. et al. (1999) Oxygen regulation of airway branching in Drosophila is mediated by branchless FGF. *Cell*. 99 (2), 211–220.

Jaskoll, T. et al. (2003) Ectodysplasin receptor-mediated signaling is essential for embryonic submandibular salivary gland development. *Anatomical Reord Part A: Discoveries in Molecular Cellular and Evolutionary Biology.* 271 (2), 322–331.

Jaskoll, T. et al. (2005) FGF10/FGFR2b signaling plays essential roles during in vivo embryonic submandibular salivary gland morphogenesis. *BMC Developmental Biology*. 5, 11.

Jaskoll, T. et al. (1998) Mouse submandibular gland mucin: embryo-specific mRNA and protein species. *Mechanisms of Development*. 74 (1-2), 179–183.

Jaskoll, T. et al. (2004) Sonic hedgehog signaling plays an essential role during embryonic salivary gland epithelial branching morphogenesis. *Developmental Dynamics*. 229 (4), 722–732.

Jaskoll, T. & Melnick, M. (2006) Embryonic salivary gland branching morphogenesis. In Davies J.A (ed.) *Branching Morphogenesis*. Springer. 160–175.

Jaskoll, T. & Melnick, M. (1999) Submandibular gland morphogenesis: stage-specific expression of TGF-alpha/EGF, IGF, TGF-beta, TNF, and IL-6 signal transduction in normal embryonic mice and the phenotypic effects of TGF-beta2, TGF-beta3, and EGF-r null mutations. *The Anatomical Record*. 256 (3), 252–268.

Jeong, H. et al. (2000) The large-scale organization of metabolic networks. *Nature*. 407 (6804), 651–654.

Jiang, G. & Hunter, T. (1999) Receptor signalling: When dimerization is not enough. *Current Biology*. 9 (15), R568–71.

Johnson, D. E. et al. (1990) Diverse Forms of a Receptor for Acidic and Basic Fibroblast Growth Factors. *Molecular and Cellular Biology*. 10 (9), 4728–4736.

Johnson, J. R. et al. (2004) Continuous exposure to house dust mite elicits chronic airway inflammation and structural remodeling. *American Journal of Respiratory and Critical Care Medicine*. 169, 378–385.

Joo, N. S. et al. (2001) Optical method for quantifying rates of mucus secretion from single submucosal glands. *American Journal of Physiology Lung Cellular and Molecular Physiology*. 281 (2), L458–468.

Kalinina, J. et al. (2012) The alternatively spliced acid box region plays a key role in FGF Receptor autoinhibition. *Structure*. 20 (1), 77–88.

Kammandel, B. et al. (1999) Distinct cis-essential modules direct the time-space pattern of the Pax6 gene activity. *Developmental Biology*. 205 (1), 79–97.

Kerem, B. et al. (1989) Identification of the Cystic Fibrosis Gene: Genetic Analysis. *Science*. 245 (4922), 1073–1080.

Kerjaschki, D. (1974) The anterior medial gland in the mouse nasal septum: an uncommon type of epithelium with abundant innervation. *Journal of Ultrastructure Research*. 46 (3), 466–482.

Kerman, B. E. et al. (2006) From fate to function: the Drosophila trachea and salivary gland as models for tubulogenesis. *Differentiation*. 74 (7), 326–348.

Keswani, S. G. et al. (2011) Submucosal gland development in the human fetal trachea xenograft model: implications for fetal gene therapy. *Journal of Pediatric Surgery*. 46 (1), 33–38.

Kim, C. F. (2007) Paving the road for lung stem cell biology : bronchioalveolar stem cells and other putative distal lung stem cells. *American Journal of Physiology Lung Cellular and Molecular Physiology*. (2), 1092–1098.

Kirsch, T. et al. (2000) Crystal structure of the BMP-2 – BRIA ectodomain complex. *Nature Structural & Molecular Biology*. 7 (6), 492–496.

Kishigami, S. & Mishina, Y. (2005) BMP signaling and early embryonic patterning. *Cytokine & Growth Factor Reviews*. 16 (3), 265–278.

Klockars, M. & Reitamo, S. (1975) Tissue distribution of lysozyme in man. *Journal of Histochemistry & Cytochemistry*. 23 (12), 932-940.

Knox, S. et al. (2010) Parasympathetic innervation maintains epithelial progenitor cells during salivary organogenesis. *Science*. 329 (5999), 1645–1647.

Komiya, Y. & Habas, R. (2008) Wnt signal transduction pathways. *Organogenesis.* 4 (2), 68–75.

Kouhara, H. et al. (1997) A lipid-anchored Grb2-binding protein that links FGF-receptor activation to the Ras/MAPK signaling pathway. *Cell*. 89 (5), 693–702.

Koyama, N. et al. (2008) Signaling pathways activated by epidermal growth factor receptor or fibroblast growth factor receptor differentially regulate branching morphogenesis in fetal mouse submandibular glands. *Development, Growth and Differentiation*. 50 (7), 565–576.

Kramer, S. et al. (1999) Sprouty: a common antagonist of FGF and EGF signaling pathways in Drosophila. *Development*. 126, 2515–2525.

Kresch, M. J. et al. (1998) Ontogeny of apoptosis during lung development. *Pediatric research*. 43, 426–431.

Kumar, R. K. et al. (2008) The "classical" ovalbumin challenge model of asthma in mice. *Current Drug Targets*. 9, 485–494.

Lacassagne, A. (1940) Dimorphisme sexuel de la glande sous-maxillaire chez la souris. *C. R. Soe. Diol.* 133, 180–181.

Lanner, F. & Rossant, J. (2010) The role of FGF/Erk signaling in pluripotent cells. *Development.* 137 (20), 3351–3360.

De Launoit, Y. et al. (1997) Structure – Function Relationships of the PEA3 Group of Ets-Related Transcription Factors. *Biochemical and Molecular Medicine*. 61, 127–135.

Lauzon-Joset, J.-F. et al. (2014) Dysregulation of alveolar macrophages unleashes dendritic cell-mediated mechanisms of allergic airway inflammation. *Mucosal Immunology*. 7 (1), 155–164.

Lavoie, T. N. et al. (2011) Current concepts: mouse models of Sjögren's syndrome. *Journal of Biomedicine & Biotechnology*. 549107.

LeBleu, V. S. et al. (2007) Structure and function of basement membranes. *Experimental Biology and Medicine.* 232 (9), 1121–1129.

Lee, B. H. et al. (2012) Animal models in autoimmune diseases: lessons learned from mouse models for Sjögren's syndrome. *Clinical Reviews in Allergy &Immunology*. 42 (1), 35–44.

Lee, P. L. et al. (1989) Purification and complementary DNA cloning of a receptor for basic fibroblast growth factor. *Science.* 245 (4913), 57–60.

Lee, T. et al. (1996) Regulated Breathless receptor tyrosine kinase activity required to pattern cell migration and branching in the Drosophila tracheal system. *Genes & Development*. 10 (22), 2912–2921.

Leevers, S. et al. (1994) Requirement for Ras in Raf activation is overcome by targeting Raf to the plasma membrane. *Nature*. 369, 411–414.

Lersch, R. & Fuchs, E. (1988) Sequence and Expression of a Type II Keratin, K5, in Human Epidermal Cells. *Molecular and Cellular Biology*. 8 (1), 486–493.

Li, E. & Hristova, K. (2010) Receptor tyrosine kinase transmembrane domains. Function, dimer structure and dimerization energetics. *Cell Adhesion and Migration*. 4 (2), 249–254.

Li, P. et al. (1997) Cytochrome c and dATP-dependent formation of Apaf-1/caspase-9 complex initiates an apoptotic protease cascade. *Cell*. 91 (4), 479–489.

Li, Y. et al. (2008) Bmp4 is required for tracheal formation: a novel mouse model for tracheal agenesis. *Developmental Biology*. 322 (1), 145–155.

Lipscomb, M. et al. (1986) Human alveolar macrophages: HLA-DR-positive macrophages that are poor stimulators of a primary mixed leukocyte reaction. *Journal of Immunology*. 136 (2), 497–504.

Liu, C. et al. (2002) Control of beta-catenin phosphorylation/degradation by a dual-kinase mechanism. *Cell*. 108 (6), 837–847.

Liu, Y. et al. (2003) Role for ETS domain transcription factors Pea3/Erm in mouse lung development. *Developmental Biology*. 261 (1), 10–24.

Logemann, J. A. et al. (2001) Effects of xerostomia on perception and performance of swallow function. *Head & Neck*. 23 (4), 317–321.

Lombaert, I. et al. (2011) Salivary gland progenitor cell biology provides a rationale for therapeutic salivary gland regeneration. *Oral Diseases*. 17 (5), 445–449.

Loo, B. M. et al. (2001) Binding of heparin/heparan sulfate to fibroblast growth factor receptor 4. *Journal of Biological Chemistry*. 276 (20), 16868–16876.

Lowe, L. a et al. (2005) Wheeze phenotypes and lung function in preschool children. *American Journal of Respiratory and Critical Care Medicine*. 171 (3), 231–237.

Mailleux, A. A. et al. (2001) Evidence that SPROUTY2 functions as an inhibitor of mouse embryonic lung growth and morphogenesis. *Mechanisms of Development*. 102 (1-2), 81–94.

Makarenkova, H. P. et al. (2000) FGF10 is an inducer and Pax6 a competence factor for lacrimal gland development. *Development*. 127 (12), 2563–2572.

Mannino, D. M. & Buist, a S. (2007) Global burden of COPD: risk factors, prevalence, and future trends. *Lancet*. 370 (9589), 765–773.

Mao, J. et al. (2001) Low-density lipoprotein receptor-related protein-5 binds to Axin and regulates the canonical Wnt signaling pathway. *Molecular Cell*. 7, 801–809.

Martín-Belmonte, F. & Yu, W. (2008) Cell Polarity Dynamics Controls the Mechanism of Lumen Formation in Epithelial Morphogenesis. *Current Biology*. 18 (7), 507–513.

Martinez, F. et al. (1995) Asthma and wheezing in the first six years of life. *The New England Journal of Medicine*. 332 (3), 133–138.

Massagué, J. et al. (1994) The TGF-β family and its composite receptors. *Trends in Cell Biology*. 4, 172–178.

Masson, P. L. et al. (1966) Immunohistochemical localisation and bacteriostatic properties of an iron-binding protein from bronchial mucus. *Thorax*. 21 (6), 538–544.

Mason I. J et al. (1994) FGF-7 (keratinocyte growth factor) expression during mouse development suggests roles in myogenesis, forebrain regionialisation and epithelial-mesenchymal interactions. *Mechanisms of Development.* 45(1):15-30

Mebratu, Y. A. et al. (2011) Cigarette smoke suppresses Bik to cause epithelial cell hyperplasia and mucous cell metaplasia. *American Journal of Respiratory and Critical Care Medicine*. 183, 1531–1538.

Melnick, M. & Jaskoll, T. (2000) Mouse Submandibular Gland Morphogenesis: a Paradigm for Embryonic Signal Processing. *Critical Reviews in Oral Biology & Medicine*. 11 (2), 199–215.

Metcalfe, D. D. et al. (1997) Mast cells. *Physiological Reviews*. 77, 1033–1079.

Metzger, R. et al. (2008) The Branching Program of Mouse Lung Development. *Nature*. 453 (7196), 745–750.

Meyer, T. N. et al. (2004) Spatiotemporal regulation of morphogenetic molecules during in vitro branching of the isolated ureteric bud: toward a model of branching through budding in the developing kidney. *Developmental Biology*. 275 (1), 44–67.

Meyrick, B. et al. (1969) A reconstruction of the duct system and secretory tubules of the human bronchial submucosal gland. *Thorax*. 24 (6), 729–736.

Meyrick, B. & Reid, L. (1970) Ultrastructure of cells in the human bronchial submucosal glands. *Journal of Anatomy*. 107 (Pt 2), 281–299.

Michael, M. et al. (1994) Embryonic Development of the Olfactory Organ in Mice. *Qatar University Science*. 14 (2), 338–346.

Miki, T. et al. (1992) Determination of ligand-binding specificity by alternative splicing: two distinct growth factor receptors encoded by a single gene. *Proceedings of the National Academy of Sciences of the United States of America*. 89 (1), 246–250.

Miletich, I. (2010) Introduction to salivary glands: structure, function and embryonic development. In Tucker A.S & Miletich I. (eds.) *Salivary Glands. Development, Adaptations and Disease.* Frontiers in Oral Biology. Basel, Karger. 14, 1–20.

Milián, E. & Díaz, A. M. (2004) Allergy to house dust mites and asthma. *Puerto Rico Health Sciences Journal*. 23 (1), 47–57.

Miller, L.-A. D. et al. (2004) Role of Sonic hedgehog in patterning of tracheal-bronchial cartilage and the peripheral lung. *Developmental Dynamics.* 231 (1), 57–71.

Milunsky, J. et al. (1990) Agenesis or hypoplasia of major salivary and lacrimal glands. *American Journal of Medical Genetics*. 37, 371–374.

Milunsky, J. M. et al. (2006) LADD syndrome is caused by FGF10 mutations. *Clinical Genetics*. 69 (4), 349–354.

Min, H. et al. (1998) Fgf-10 is required for both limb and lung development and exhibits striking functional similarity to Drosophila branchless. *Genes & Development*. 12 (20), 3156–3161.

Minowada G. et al. (1999) Vertebrate Sprouty genes are induced by FGF signaling and can cause chondrodysplasia when overexpressed. *Development.* 126:4465-4475

Miyazono, K. et al. (2010) Bone morphogenetic protein receptors and signal transduction. *Journal of Biochemistry*. 147 (1), 35–51.

Moe, H. & Bojsen-moller, F. (1971) The Fine Structure of the Lateral Nasal Gland (Steno's Gland) of the Rat. *Journal of Ultrastructure Research*. 36 (1-2), 127–148.

De Moerlooze, L. et al. (2000) An important role for the IIIb isoform of fibroblast growth factor receptor 2 (FGFR2) in mesenchymal-epithelial signalling during mouse organogenesis. *Development*. 127 (3), 483–492.

Mohammadi, M. et al. (1991) A tyrosine-phosphorylated carboxy-terminal peptide of the fibroblast growth factor receptor (Flg) is a binding site for the SH2 domain of phospholipase C-gamma. *Molecular and Cellular Biology*. 11 (10), 5068–5078.

Moniuszko, M. et al. (2007) Bronchial macrophages in asthmatics reveal decreased CD 16 expression and substantial levels of receptors for IL-10, but not IL-4 and IL-7. *Folia Histochemica et Cytobiologica*. 45, 181–189.

Morlon, A. et al. (2005) TAB2, TRAF6 and TAK1 are involved in NF-kappaB activation induced by the TNF-receptor, Edar and its adaptator Edaradd. *Human Molecular Genetics*. 14 (23), 3751–3757.

Mowry, R. W. (1956) Alcian blue techniques for the histochemical study of acidic carbohydrates. *Journal of Histochemistry & Cytochemistry*. 4, 403.

Myat, M. M. & Andrew, D. J. (2000) Organ shape in the Drosophila salivary gland is controlled by regulated, sequential internalization of the primordia. *Development.* 127 (4), 679–691.

Navazesh, M. et al. (1995) Relationship between salivary flow rates and Candida albicans counts. *Oral Surgery, Oral Medicine, Oral Pathology, Oral Radiology, and Endodontics*. 80 (3), 284–288.

Nedvetsky, P. I. et al. (2014) Parasympathetic Innervation Regulates Tubulogenesis in the Developing Salivary Gland. *Developmental Cell*. 30 (4), 449–462.

Ng, A. N. Y. et al. (2005) Formation of the digestive system in zebrafish: III. Intestinal epithelium morphogenesis. *Developmental Biology*. 286 (1), 114–135.

Nials, A. T. & Uddin, S. (2008) Mouse models of allergic asthma: acute and chronic allergen challenge. *Disease Models & Mechanisms*. 1, 213–220.

Nordenfelt, P. & Tapper, H. (2011) Phagosome dynamics during phagocytosis by neutrophils. *Journal of Leukocyte Biology*. 90 (2), 271–284.

Nyska, A. et al. (2005) Olfactory epithelial metaplasia and hyperplasia in female Harlan Sprague-Dawley rats following chronic treatment with polychlorinated biphenyls. *Toxicologic Pathology*. 33 (3), 371–377.

Oeckinghaus, A. & Ghosh, S. (2009) The NF-kappaB family of transcription factors and its regulation. *Cold Spring Harbor Perspectives in Biology*. 1 (4), a000034.

Ogawa, M. et al. (2013) Functional salivary gland regeneration by transplantation of a bioengineered organ germ. *Nature Communications*. 4, 2498.

Ohuchi, H. et al. (2000) FGF10 acts as a major ligand for FGF receptor 2 IIIb in mouse multi-organ development. *Biochemical and Biophysical Research Communications*. 277 (3), 643–649.

Ohuchi, H. et al. (1997) The mesenchymal factor, FGF10, initiates and maintains the outgrowth of the chick limb bud through interaction with FGF8, an apical ectodermal factor. *Development*. 124 (11), 2235–2244.

Oliver, A. et al. (2000) High Frequency of Hypermutable Pseudomonas aeruginosa in Cystic Fibrosis Lung Infection. *Science*. 288 (5469), 1251–1253.

Olsen, S. K. et al. (2003) Fibroblast growth factor (FGF) homologous factors share structural but not functional homology with FGFs. *The Journal of Biological Chemistry*. 278 (36), 34226–34236.

Ong, S. H. et al. (2001) Stimulation of phosphatidylinositol 3-kinase by fibroblast growth factor receptors is mediated by coordinated recruitment. *PNAS*. 98 (11), 6074–6079.

Oppenheimer, E. & Esterly, J. (1975) Pathology of cystic fibrosis: review of the literature and comparison with 146 autopsied cases. In Rosenberg H.S & Bolande R.P (eds.) *Perspectives in Pediatric Pathology*. Yearbook Medical Publishers. Chicago, USA. 2, 241–278.

Ordoñez, C. L. et al. (2001) Mild and moderate asthma is associated with airway goblet cell hyperplasia and abnormalities in mucin gene expression. *American Journal of Respiratory and Critical Care Medicine*. 163 (2), 517–523.

Ornitz, D. & Itoh, N. (2001) Fibroblast growth factors. *Genome Biology*. 2 (3), 1–12.

Ornitz, D. M. et al. (1996) Receptor Specificity of the Fibroblast Growth Factor Family. *Journal of Biological Chemistry*. 271 (25), 15292–15297.

Ornoy, A. et al. (1987) Pathological confirmation of cystic fibrosis in the fetus following prenatal diagnosis. *American Journal of Medical Genetics*. [Online] 28935–947.

Orr-Urtreger, A. et al. (1993) Developmental Localisation of the Splicing Alternatives of Fibroblast Growth Factor Receptor-2 (FGFR2). *Developmental Biology.* 158 (2), 475–486.

Paratore, C. et al. (2002) The Role of the Ets Domain Transcription Factor Erm in Modulating Differentiation of Neural Crest Stem Cells. *Developmental Biology*. 250 (1), 168–180.

Park, W. Y. et al. (1998) FGF-10 is a chemotactic factor for distal epithelial buds during lung development. *Developmental Biology*. 201 (2), 125–134.

Patel, N. et al. (2011) Coordination of epithelial branching and salivary gland lumen formation by Wnt and FGF signals. *Developmental Biology*. 358 (1), 156–167.

Pavlov, I. (1906) The Scientific Investigation of the Psychical Faculties or Processes in the Higher Animals. *Science*. 24 (620), 613–619.

Pedersen, A. M. et al. (2002) Saliva and gastrointestinal functions of taste, mastication, swallowing and digestion. *Oral Diseases*. 8 (3), 117–129.

Pepicelli, C. V et al. (1998) Sonic hedgehog regulates branching morphogenesis in the mammalian lung. *Current Biology*. 8 (19), 1083–1086.

Peri, Y. et al. (2012) Sjogren's syndrome, the old and the new. *Best Practice and Research Clinical Rheumatolgy*. 26 (1), 105–117.

Peterka, M. et al. (2002) Body Weight in Mouse Embryos Specifies Staging of Tooth Development. *Connective Tissue Research*. 43, 186–190.

Peters, K. et al. (1994) Targeted expression of a dominant negative FGF receptor blocks branching morphogenesis and epithelial differentiation of the mouse lung. *The EMBO Journal.* 13 (14), 3296-3301.

Peters, K. G. et al. (1992) Two FGF receptor genes are differentially expressed in epithelial and mesenchymal tissues during limb formation and organogenesis in the mouse. *Development.* 114 (1), 233–243.

Pierre, S. et al. (2011) Understanding SOS (Son of Sevenless). *Biochemical Pharmacology*. 82 (9), 1049–1056.

Popp, J. & Martin, J. (1984) Surface Topography and Distribution of Cell Types in the Rat Nasal Respiratory Epithelium: Scanning Electron Microscopic Observations. *American Journal of Anatomy*. 436, 425–436.

Porter, a G. & Jänicke, R. U. (1999) Emerging roles of caspase-3 in apoptosis. *Cell Death and Differentiation*. 6 (2), 99–104.

Prescott, E. et al. (1995) Chronic mucus hypersecretion in COPD and death from pulmonary infection. *European Respiratory Journal*. 8 (8), 1333–1338.

Proctor, G. B. & Carpenter, G. H. (2007) Regulation of salivary gland function by autonomic nerves. *Autonomic Neuroscience.* 133 (1), 3–18.

Purves, D. et al. (2004) The Olfactory Epithelium and Olfactory Receptor Neurons. In Purves D, Augustine G.J, et al. *Neuroscience*. Sinauer Associates, Inc. Sunderland, MA. 3, 337–370.

Pye, D. a. & Gallagher, J. T. (1999) Monomer Complexes of Basic Fibroblast Growth Factor and Heparan Sulfate Oligosaccharides Are the Minimal Functional Unit for Cell Activation. *Journal of Biological Chemistry*. 274 (19), 13456–13461.

Rawlins, E. et al. (2009) The Role of Scgb1a1+ Clara Cells in the Long-Term Maintenance and Repair of Lung Airway, but Not Alveolar, Epithelium. *Cell Stem Cell*. 4 (6), 525–534.

Rawlins, E. L. et al. (2007) Lung development and repair: contribution of the ciliated lineage. *Proceedings of the National Academy of Sciences of the United States of America*. 104 (2), 410–417.

Rawlins, E. L. & Hogan, B. L. M. (2006) Epithelial stem cells of the lung: privileged few or opportunities for many? *Development*. 133 (13), 2455–2465.

Rawlins, E. L. & Hogan, B. L. M. (2005) Intercellular growth factor signaling and the development of mouse tracheal submucosal glands. *Developmental Dynamics.* 233 (4), 1378–1385.

Razvi, S. et al. (2009) Respiratory microbiology of patients with cystic fibrosis in the United States, 1995 to 2005. *Chest*. 136 (6), 1554–1560.

Reed, J. C. (1997) Cytochrome c: can't live with it--can't live without it. *Cell*. 91 (5), 559–562.

Reich, A. et al. (1999) Sprouty is a general inhibitor of receptor tyrosine kinase signaling. *Development*. 126, 4139–4147.

Reid, L. (1960) Measurement of the bronchial mucous gland layer: a diagnostic yardstick in chronic bronchitis. *Thorax*. 15, 132–141.

Remy, P. & Baltzinger, M. (2000) The Ets-transcription factor family in embryonic development: lessons from the amphibian and bird. *Oncogene*. 19 (55), 6417–6431.

Rentrop, M. et al. (1986) Differential localisation of distinct keratin mRNA-species in mouse tongue epithelium by in situ hybridisation with specific cDNA probes. *The Journal of Cell Biology*. 103 (6 Pt 2), 2583–2591.

Riordan, J. R. et al. (1989) Identification of the cystic fibrosis gene: cloning and characterization of complementary DNA. *Science.* 245 (4922), 1066–1073.

Rishikaysh, P. et al. (2014) Signaling involved in hair follicle morphogenesis and development. *International Journal of Molecular Sciences*. 15 (1), 1647–1670.

Roche, N. et al. (1997) Allergic and nonallergic interactions between house dust mite allergens and airway mucosa. *The European Respiratory Journal*. 10 (3), 719–726.

Rock, J. R. et al. (2010) Airway basal stem cells: a perspective on their roles in epithelial homeostasis and remodeling. *Disease Models & Mechanisms*. 3 (9-10), 545–556.

Rock, J. R. et al. (2009) Basal cells as stem cells of the mouse trachea and human airway epithelium. *Proceedings of the National Academy of Sciences of the United States of America*. 106 (31), 12771–12775.

Rodriguez-Pinto, D. (2005) B cells as antigen presenting cells. *Cellular Immunol*ogy. 238 (2), 67–75.

Rogers, D. (2007) Physiology of Airway Mucus Secretion and Pathophysiology of Hypersecretion. *Respiratory Care*. 52 (9), 1134–1149.

Rogers, D. F. (2008) Airway Mucus Hypersecretion in Asthma and COPD: Not the Same?. In Barnes P. et al. (eds.) *Asthma and COPD. Basic Mechanisms and Clinical Management*. Academic Press Inc. 2, 211–223.

Rogers, D. F. (2004) Airway mucus hypersecretion in asthma: an undervalued pathology? *Current Opinion in Pharmacology*. 4 (3), 241–250.

Rohmann, E. et al. (2006) Mutations in different components of FGF signaling in LADD syndrome. *Nature Genetics*. 38 (4), 414–417.

Romagnani, S. (1991) Type 1 T helper and type 2 T helper cells: Functions, regulation and role in protection and disease. *International Journal of Clinical and Laboratory Research*. 21, 152–158.

Rommens, J. et al. (1989) Identification of the Cystic Fibrosis Gene: Chromosome Walking and Jumping. *Science*. 245, 1059–1065.

Rothova, M. et al. (2012) Lineage tracing of the endoderm during oral development. *Developmental Dynamics.* 241 (7), 1183–1191.

Rowe, S. M. et al. (2005) Cystic fibrosis. *The New England Journal of Medicine*. 352 (19), 1992–2001.

Saetta, M. & Turato, G. (1997) Inflammatory Cells in the Bronchial Glands of Smokers with Chronic Bronchitis. *American Journal of Respiratory and Critical Care Medicine*. 156, 1633–1639.

Saglani, S. et al. (2009) Pathophysiological Features of Asthma Develop in Parallel in House Dust Mite – Exposed Neonatal Mice. *American Journal of Respiratory Cell and Molecular Biology.* 41 (3), 281–289.

Sala, F. G. et al. (2011) FGF10 controls the patterning of the tracheal cartilage rings via Shh. *Development.* 138, 273–282.

Samakovlis, C. et al. (1996) Development of the Drosophila tracheal system occurs by a series of morphologically distinct but genetically coupled branching events. *Development.* 122 (5), 1395–1407.

Sasaki, A. et al. (2003) Mammalian Sprouty4 suppresses Ras-independent ERK activation by binding to Raf1. *Nature Cell Biology*. 5 (5), 427–432.

Sato, M. & Kornberg, T. B. (2002) FGF is an essential mitogen and chemoattractant for the air sacs of the drosophila tracheal system. *Developmental Cell*. 3 (2), 195–207.

Savill, J. et al. (1989) Macrophage Phagocytosis of Aging Neutrophils in Inflammation. *Journal of Clinical Investigation*. 83, 865–875.

Schlessinger, J. (2000) Cell Signaling by Receptor Tyrosine Kinases. *Cell*. 103, 211–225.

Schlessinger, J. (1988) Signal transduction by allosteric receptor oligomerization. *Trends in Biochemical Sciences*. 13, 443–447.

Schuler, M. et al. (2000) p53 Induces Apoptosis by Caspase Activation through Mitochondrial Cytochrome c Release. *Journal of Biological Chemistry*. 275 (10), 7337–7342.

Schweizer, J. et al. (1988) The intermediate filament system of the keratinizing mouse forestomach epithelium: coexpression of keratins of internal squamous epithelia and of epidermal keratins in differentiating cells. *Cell and Tissue Research*. 253 (1), 221–229.

Seaton, A. et al. (1995) Particulate air pollution and acute health effects. *The Lancet*. 345, 176–178. August 2014).

Sedgwick, J. & Holt, P. (1983) Induction of IgE-isotype specific tolerance by passive antigenic stimulation of the respiratory mucosa. *Immunology*. 50, 625–630.

Sekine, K. et al. (1999) Fgf10 is essential for limb and lung formation. *Nature Genetics*. 21 (1), 138–141.

Sells, D. M. et al. (2007) Respiratory tract lesions in noninhalation studies. *Toxicologic Pathology*. 35, 170–177.

Semënov, M. V. et al. (2001) Head inducer dickkopf-1 is a ligand for Wnt coreceptor LRP6. *Current Biology*. 11, 951–961.

Serafin, W. & Austen, K. (1987) Mediators of Immediate Hypersensitivity Reactions. *The New England Journal of Medicine*. 317, 30–34.

Shams, I. et al. (2007) Lacrimo-auriculo-dento-digital syndrome is caused by reduced activity of the fibroblast growth factor 10 (FGF10)-FGF receptor 2 signaling pathway. *Molecular and Cellular Biology*. 27 (19), 6903–6912.

Sharrocks, A. D. et al. (1997) The ETS-domain transcription factor family. *The International Journal of Biochemistry & Cell Biology*. 29 (12), 1371–1387.

Sheehan, J. K. et al. (1995) Analysis of respiratory mucus glycoproteins in asthma: a detailed study from a patient who died in status asthmaticus. *American Journal of Respiratory Cell and Molecular Biology*. 13, 748–756.

Shen, M. M. et al. (2008) Progenitor cells for the prostate epithelium: roles in development, regeneration, and cancer. *Cold Spring Harbor Symposia on Quantitative Biology*. 73, 529–538.

Shiang, E. & Holmes, L. (1977) The lacrimal-auriculo-dento-digital syndrome. *Pediatrics*. 59, 927–930.

Ship, J. A. et al. (1995) Longitudinal analysis of parotid and submandibular salivary flow rates in healthy, different-aged adults. *The Journals of Gerontology Series A: Biological Sciences and Medical Sciences.* 50 (5), M285–9.

Ship, J. A. et al. (2002) Xerostomia and the geriatric patient. *Journal of the American Geriatrics Society*. 50 (3), 535–543.

Smythe, W. R. et al. (2000) Bilateral sequential lung transplant for ectodermal dysplasia. *The Annals of Thoracic Surgery*. 70, 654–656.

Spivak-Kroizman, T. et al. (1994) Heparin-Induced Oligomerization of FGF Molecule Is Responsible for FGF Receptor Dimerization, Activation, and Cell Proliferation. *Cell*. 79, 1015–1024.

Srivastava, A. et al. (1997) The Tabby phenotype is caused by mutation in a mouse homologue of the EDA gene that reveals novel mouse and human exons and encodes a protein (ectodysplasin-A) with collagenous domains. *Proceedings of the National Academy of Sciences of the United States of America*. 94 (24), 13069–13074.

Stanier, P. & Pauws, E. (2012) Development of the lip and palate: FGF signalling. In Cobourne M.T (ed.) *Cleft Lip and Palate.* Frontiers of Oral Biology. Basel, Karger. 16, 1671–80.

Steinberg, Z. et al. (2005) FGFR2b signaling regulates ex vivo submandibular gland epithelial cell proliferation and branching morphogenesis. *Development.* 132 (6), 1223–1234.

Steinman, R. (1991) The dendritic cell system and its role in immunogenecity. *Annual Review of Immunology*. 9, 271–296.

Stone, K. D. et al. (2010) IgE, mast cells, basophils, and eosinophils. *Journal of Allergy and Clinical Immunology*. 125, S73-S80.

Sturgess, J. & Imrie, J. (1982) Quantitative evaluation of the development of tracheal submucosal glands in infants with cystic fibrosis and control infants. *The American Journal of Pathology*. 106 (3), 303–311.

Sun, P. et al. (2010) Cytokeratin expression during mouse embryonic and early postnatal mammary gland development. *Histochemistry and Cell Biology*. 133 (2), 213–221.

Sun, X. et al. (1999) Targeted disruption of Fgf8 causes failure of cell migration in the gastrulating mouse embryo. *Genes & Development*. 13, 1834–1846.

Sutherland, D. et al. (1996) branchless encodes a Drosophila FGF homolog that controls tracheal cell migration and the pattern of branching. *Cell*. 87 (6), 1091–1101.

Tefft, J. D. et al. (1999) Conserved function of mSpry-2, a murine homolog of Drosophila sprouty, which negatively modulates respiratory organogenesis. *Current Biology.* 9 (4), 219–222.

Teshima, T. H. N. et al. (2011) Development of human minor salivary glands: expression of mucins according to stage of morphogenesis. *Journal of Anatomy*. 219 (3), 410–417.

Theiler, K. (1989) *The House Mouse. Atlas of Embryonic Development.* Springer-Verlag. New York.

Thesleff, I. (2003) Epithelial-mesenchymal signalling regulating tooth morphogenesis. *Journal of Cell Science*. 116 (9), 1647–1648.

Thomas, E. et al. (1998) Sjogren's syndrome: a community-based study of prevalence and impact. *British Journal of Rheumatology*. 37 (10), 1069–1076.

Thomas, P. S. et al. (1995) Tumor necrosis factor-alpha increases airway responsiveness and sputum neutrophilia in normal human subjects. *American Journal of Respiratory and Critical Care Medicine.* 152, 76–80.

Thomas, P. S. (2001) Tumour necrosis factor-alpha: the role of this multifunctional cytokine in asthma. *Immunology and Cell biology*. 79 (2), 132–140.

Thomas, P. S. & Heywood, G. (2002) Effects of inhaled tumour necrosis factor alpha in subjects with mild asthma. *Thorax.* 57, 774–778.

Thomas, W. R. et al. (2002) Characterization and immunobiology of house dust mite allergens. *International Archives of Allergy and Immunology*. 129 (1), 1–18.

Thompson, E., Pembrey, M. & Graham, J. M. (1985) Phenotypic variation in LADD syndrome. *Journal of Medical Genetics*. 22 (5), 382–385.

Thompson, E., Pembrey, M. & Graham, J. (1985) Phenotypic variation in LADD syndrome. *Journal of Medical Genetics*. 22, 382–385.

Thomson, A. A. & Marker, P. C. (2006) Branching morphogenesis in the prostate gland and seminal vesicles. *Differentiation.* 74, 382–392.

Thurlbeck, W. et al. (1961) Development and distribution of mucous glands in the foetal human trachea. *British Journal of Diseases of the Chest*. 55, 54–64.

Tomkinson, A. et al. (2001) Temporal association between airway hyperresponsiveness and airway eosinophilia in ovalbumin-sensitized mice. *American Journal of Respiratory and Critical Care Medicine*. 163, 721–730.

Tovey, E. et al. (1981) Mite faeces are a major source of house dust allergen. *Nature*. 289, 592–593.

Tsang, M. & Dawid, I. B. (2004) Promotion and attenuation of FGF signaling through the Ras-MAPK pathway. *Science's STKE: Signal Transduction Knowledge Environment*. 2004 (228), pe17.

Tsuboi, R. et al. (1990) Correlation of cell migration, cell invasion, receptor number, proteinase production, and basic fibroblast growth factor levels in endothelial cells. *The Journal of Cell Biology*. 110 (2), 511–517.

Tucker, A. S. (2007) Salivary gland development. *Seminars in Cell and Developmental Biology*. 18 (2), 237–244.

Turner, M. D. & Ship, J. A. (2007) Dry Mouth and Its Effects on the Oral Health of Elderly People. *Journal of the American Dental Association*. 138, 15S–20S.

Unanue, E. R. (1984) Antigen-presenting function of the macrophage. *Annual Review of Immunology*. 2, 395–428.

Vainikka, S. et al. (1992) Fibroblast Growth Factor Receptor-4 shows novel features in genomic structure, ligand binding and signald transduction. *The EMBO Journal.* 1 (12), 4273–4280.

Vankeerberghen, A. et al. (2002) The cystic fibrosis transmembrane conductance regulator: an intriguing protein with pleiotropic functions. *Journal of Cystic Fibrosis*. 1, 13–29.

Vidić, B. (1971) The prenatal morphogenesis of the lateral nasal wall in the rat (Mus rattus). *Journal of Morphology*. 133 (3), 303–317.

Vidić, B. & Greditzer, H. G. (1971) The histochemical and microscopical differentiation of the respiratory glands around the maxillary sinus of the rat. *The American Journal of Anatomy*. 132 (4), 491–513.

Vogel, C. & Marcotte, E. M. (2012) Insights into the regulation of protein abundance from proteomic and transcriptomic analyses. *Nature Reviews. Genetics*. 13 (4), 227–232.

Walker, J. et al. (2008) Diverse Roles of E-Cadherin in the Morphogenesis of the Submandibular Gland: Insights Into the Formation of Acinar and Ductal Structures. *Developmental Dynamics*. 237 (11), 3128–3141.

Wallace, K. N. & Pack, M. (2003) Unique and conserved aspects of gut development in zebrafish. *Developmental Biology*. 255 (1), 12–29.

Wallingford, J. B. & Habas, R. (2005) The developmental biology of Dishevelled: an enigmatic protein governing cell fate and cell polarity. *Development.* 132, 4421–4436.

Walsh, D. W. et al. (2010) Extracellular BMP-antagonist regulation in development and disease: tied up in knots. *Trends in Cell Biology*. 20 (5), 244–256.

Warburton, D. et al. (2005) Molecular mechanisms of early lung specification and branching morphogenesis. *Pediatric Research*. 57 (5 Pt 2), 26R–37R.

Wasylyk, B. et al. (1998) Ets transcription factors: nuclear effectors of the Ras-MAP-kinase signaling pathway. *Trends in Biochemical Sciences*. 23 (6), 213–216.

Watson, D. K. et al. (1988) Mammalian ets-1 and ets-2 genes encode highly conserved proteins. *PNAS*. 85 (21), 7862–7866.

Weaver, M. et al. (1999) Bmp signaling regulates proximal-distal differentiation of endoderm in mouse lung development. *Development*. 126, 4005–4015.

Weaver, M. et al. (2000) Bmp4 and Fgf10 play opposing roles during lung bud morphogenesis. *Development*. 127, 2695–2704.

Weinstein, M. et al. (1998) FGFR-3 and FGFR-4 function cooperatively to direct alveogenesis in the murine lung. *Development*. 125 (18), 3615–3623.

Wells, K. L. et al. (2013) Dynamic relationship of the epithelium and mesenchyme during salivary gland initiation: the role of Fgf10. *Biology Open*. 2 (10), 981–989.

Wells, K. L. & Patel, N. (2010) Lumen formation in salivary gland development. In Tucker A.S & Miletich I. (eds.) *Salivary Glands. Development, Adaptations and Disease.* Frontiers in Oral Biology. Basel, Karger. 78–89.

Wells, U. & Widdicombe, J. G. (1986) Lateral Nasal Gland Secretion In The Anaesthetized Dog. *The Journal of Physiology*. 374, 359–374.

Werner, S. (1998) Keratinocyte growth factor: a unique player in epithelial repair processes. *Cytokine & Growth Factor Reviews*. 9 (2), 153–165.

Whitman, M. (1998) Smads and early developmental signaling by the TGFbeta superfamily. *Genes & Development*. 12 (16), 2445–2462.

Wiedemann, H. R. (1997) Salivary gland disorders and heredity. *American Journal of Medical Genetics*. 68 (2), 222–224.

Wiedemann, H. R. & Drescher, J. (1986) LADD syndrome: report of new cases and review of the clinical spectrum. *European Journal of Pediatrics*. 144 (6), 579–582.

Wine, J. J. & Joo, N. S. (2004) Submucosal glands and airway defense. *Proceedings of the American Thoracic Society*. 1 (1), 47–53.

Wrana, J. et al. (1994) Mechanism of activation of the TGF-β receptor. *Nature*. 370, 341–347.

Xiao, H. (2013) The Importance of Bronchial Epithelial Junction Integrity in Asthma. *Journal of Allergy & Therapy*. S11, 10–13.

Xin et al. (1992) Molecular cloning and characterization of PEA3, a new member of the Ets oncogene family that is differentially expressed in mouse embryonic cells. *Genes and Development.* 6:481-496.

Yamasaki, M. et al. (1996) Structure and Expression of the Rat mRNA Encoding a Novel Member of the Fibroblast Growth Factor Family. *Journal of Biological Chemistry*. 271 (27), 15918–15921.

Yanagita, M. (2005) BMP antagonists: their roles in development and involvement in pathophysiology. *Cytokine & Growth Factor Reviews*. 16 (3), 309–317.

Yayon, A. et al. (1992) A confined variable region confers ligand specificity on fibroblast growth factor receptors: implications for the origin of the immunoglobulin fold. *The EMBO Journal.* 1 (5), 1885–1890.

Ying, S. et al. (1991) TNF alpha mRNA expression in allergic inflammation. *Clinical and Experimental Allergy.* 21 (6), 745–750.

Yordy, J. S. & Muise-Helmericks, R. C. (2000) Signal transduction and the Ets family of transcription factors. *Oncogene*. 19 (55), 6503–6513.

Yusoff, P. et al. (2002) Sprouty2 inhibits the Ras/MAP kinase pathway by inhibiting the activation of Raf. *The Journal of Biological Chemistry* 277 (5), 3195–3201.

Zalewska, A. et al. (2013) Rheumatoid arthritis patients with xerostomia have reduced production of key salivary constituents. *Oral Surgery, Oral Medicine, Oral Pathology and Oral Radiology.* 115 (4), 483–490.

Zeng, X. et al. (2005) A dual-kinase mechanism for Wnt co-receptor phosphorylation and activation. *Nature*. 438, 873–877.

Zhang, S. et al. (2001) Expression of Sprouty genes 1, 2 and 4 during mouse organogenesis. *Mechanisms of Development*. 109 (2), 367–370.

Zhao, G.-Q. (2003) Consequences of knocking out BMP signaling in the mouse. *Genesis.* 35 (1), 43–56.

Zhao, J. et al. (2013) Th17 responses in chronic allergic airway inflammation abrogate regulatory T-cell-mediated tolerance and contribute to airway remodeling. *Mucosal Immunology*.

Zou, H. et al. (1999) An APAF-1 Cytochrome c Multimeric Complex Is a Functional Apoptosome That Activates Procaspase-9. *Journal of Biological Chemistry*. 274 (17), 11549–11556.